The Role of Visco-elasticity on the Crack Growth Behaviour of Rubber

by

Katsuhiko Tsunoda

A thesis submitted to the University of London
for the degree of Doctor of Philosophy

Materials Department
Queen Mary
University of London
Mile End Road
London E1 4NS

May 2001

Abstract

This thesis concerns crack growth phenomena in rubber. It is widely known that a relationship exists between the magnitude of the stored energy release rate available to drive a crack, called the tearing energy (T), and the resultant crack growth rate. For rubbers this basic relationship is said to be a characteristic of the material. The magnitude of T is related to both the visco-elastic losses and the crack tip diameter (d). However the actual size of d and its relationship with the visco-elastic losses is not clear. This thesis examines the crack growth behaviour in relation to d and the visco-elastic losses for a wide range of rubbers, whose visco-elastic properties are altered either by swelling in a liquid, altering the test temperature or the cross-link density and by the incorporation of fillers. Static, constant T, crack growth tests were carried out. These revealed that two different crack growth processes exist. For the fast crack growth process, T is determined by variations in the visco-elastic losses alone. For the slow crack growth process, T is determined by variations in both the visco-elastic losses and d. It is proposed here that the factors, which alter d, are associated with cavitation ahead of the crack tip for unfilled materials and with strength anisotropy for carbon black filled materials.

In cyclic crack growth tests, the crack growth per cycle, dc/dn, can be considered to result from the sum of time and cyclic dependent crack growth components. For the first time, the detailed magnitudes of the contribution of each of these components to dc/dn have been determined, for a wide range of materials and mechanisms responsible for this behaviour are postulated. Also crack growth tests, both static and cyclic, were extended to very large extensions. Lastly this investigation revealed that the tensile strength for both crystallising and non-crystallising rubber can be predicted using the tearing energy concept for a variety of loading regimes.

To my parents, my wife Yuko

and my son Ryoei

Acknowledgements

The present work was sponsored by Bridgestone Corporation, Japan

I would like to express my sincere gratitude to my supervisors, Dr. James Busfield, Professor Craig Davies, and Professor Alan Thomas, for their guidance, tremendous help, and encouragement throughout the course of this programme.

I would also like to express my cordial gratitude and appreciation to Dr. Yoshihide Fukahori for his suggestion, comments, and encouragement throughout this programme.

I would express my gratitude to my colleagues at Queen Mary, University of London, especially Christian Ratsimba, Chudej Deeprasertkul and Ken Yamaguchi, for their friendly help, suggestion and support. I would also like to thank to staff and technicians in the Materials Department and Engineering Faculty for their help, especially Tony Otten.

Finally, special thanks go to my family and friends for their continuous support and encouragement throughout this study.

List of contents

List of figures

Chapter Two

Chapter Three

Chapter Four

Chapter Five

Chapter Six

Chapter Seven

List of tables

Chapter Two

Chapter Three

Chapter Six

Chapter Seven

List of Symbols

English Alphabet

A_t	Crack growth constant in fatigue crack growth (in region II)
A_o	Unstrained cross-sectional area of the specimen
a_T	Shift factor in the WLF relationship
B	Crack growth constant in fatigue crack growth (in region III)
B_S	Static crack growth constant
b	Number of active bonds per unit volume
C_1	Material constant
$C_{1\cdot chem.}$	Material constant measured from the swelling method
$C_{1\cdot dry}$	Material constant in the unswollen state
$C_{1\cdot phys}$	Material constant measured from the stress-strain behaviour
C_2	Material constant
C_{W1}	WLF parameter
C_{W2}	WLF parameter
c	Crack length
c_o	Initial crack length
c_1	crack length
c_{total}	Total crack length
D	Diameter of the high strain region ahead of a crack
d	diameter of the crack tip or effective crack tip diameter
d_b	Crack tip diameter at rupture
d_o	Minimum possible crack tip diameter
dc/dn	Crack growth per cycle
$dc/dn_{\_cycle}$	cyclic dependent component of crack growth per cycle
$dc/dn_{\_time}$	Time dependent component of crack growth per cycle
$dc\ dt$	Crack growth rate
E	Tensile modulus or Young's modulus
E''	Dynamic loss modulus
E'	Dynamic storage modulus

e	Rate of elongation or strain rate
$\dot{e}$	Corrected rate of elongation
F	Force
F_A, F_B	Forces applied in region A and B for the split test specimen
f	Cyclic frequency applied in cyclic crack growth measurement
G	Strain energy release rate
G_c	Critical strain energy release rate
G_S	Shear modulus of rubber
G''	Shear loss modulus
G'	Shear storage modulus
H_z	Frequency of cyclic loading
h	Thickness of the specimen
I	Moment of inertia of the oscillating beam
I_1,I_2	Strain invariant
J_b	Bond rupture energy
K_s	Constant for tensile strength in the swollen state
k	Constant in the expression of the tearing energy in simple extension
k_D	Scaling factor used for determining the relationship between D and d
k_f	Characteristic constant for a filler
k_z	Rate constant in fatigue crack growth due to ozone
L	Total energy loss during crack growth
L_X	Distance from the crack tip
L_X'	Distance from the crack tip to show a peak σ_{XX}
l_o	Unstrained height of the pure shear test specimen
l_o'	Unstrained height of the pre-strained pure shear test specimen
l_s	Unstrained half length of the specimen used in dynamic property measurement
M_c	Number average molar mass between cross-links
$M_{c\ mech}$	Number average molar mass between cross-links from a mechanical test
$M_{c\ chem}$	Number average molar mass between cross-links from a swelling test
M_o	Mass of the rubber specimen
$M_{r\ net}$	Mass of the rubber network

M_{tf}	Total mass of the mix formulation
N	Number of cycles to break (fatigue life)
$[O_3]$	Ozone concentration
P	Pressure
P_c	Critical pressure
P_c'	Critical pressure to open cavities under tri-axial stresses
R	Gas constant
R_a	Aspect extension ratio ($\lambda/\lambda_{\text{-pre-strain}}$)
R_z	Crack growth rate in cyclic crack growth (in region I)
r	Crack growth rate or tear rate
r_c	Critical crack growth rate
r_d	Distance between the centre of the oscillating beam and specimen
r_o	Original radius of the micro void in rubber
r_t	Radius of a semi circle which represents the model of the crack tip
r_1	Radius of the cavity ahead of a crack
S	Rate of grip separation in the trouser tear test
T	Tearing energy
T_c	Critical tearing energy
T_o	Threshold tear strength
$T_{.max}$	Maximum tearing energy during cyclic loading
$T_{.min}$	Minimum tearing energy during cyclic loading
T_u	Unit value of $1.0 J.m^{-2}$ for making T/T_u dimensionless
t	time
U	Elastic stored energy
V_{CB}	Volume fraction of carbon black
V_r	Volume fraction of rubber
$V_{r\,net}$	Volume fraction of rubber network
V_{solv}	Volume fraction of swelling liquid
W	Elastic stored energy density
W_b	Elastic stored energy density to break
W_h	Hysteresis energy density
W_{ht}	Hysteresis energy density at the crack tip
W_o	Minimum possible elastic stored energy density

W_S	Elastic stored energy density after pre-strain
W_t	Elastic stored energy density at the crack tip or suitable average of W_α
W_α	Elastic stored energy density at the crack tip at an angular distance α from the pole
w	Total width of the specimen
w'	Total width of the pre-strained specimen
w_r	Weight of the rubber specimen
w_w	Weight of the rubber specimen in water

Greek Alphabet

Φ	Reduced stress
Λ	Logarithmic decrement
α	Angular distance of the semicircle representing the model of a crack tip
α_S	Angle between the clamps for an angles test specimen
β	Crack growth exponent in fatigue crack growth (in region II)
β_S	Static crack growth constant
χ	Interaction parameter between a rubber and a swelling liquid
δ	Loss angle or differencing symbol
μ	Number of monomer units between cross-links
λ	Extension ratio
λ_A, λ_B	Extension ratios applied in region A and B for the split test specimen
λ_b	Extension ratio at break
$(\lambda_b)_s$	Extension ratio at break in the swollen state
λ_1, λ_2, λ_3	Principle extension ratios
γ	Surface energy
γ_P	Extra surface energy arising from the energy dissipation around the crack tip
ν	Poison's ratio
ν_{act}	Actual cross-link density
ν_{chem}	Total cross-link density measured by the swelling method
ν_{chem}	Total cross-link density measured from the stress-strain behaviour
θ	Temperature
θ_g	Glass transition temperature
θ_s	Reference temperature in the WLF relationship
θ_D	The angular displacement of the beam
θ_{Do}	The initial angular displacement of the beam
ρ_r	Density of a rubber
ρ_w	Density of water
σ	Engineering stress

σ_b	Tensile strength at break
σ_b'	Corrected tensile strength at break
σ_{XX}	Principle stress in the X direction
σ_{YY}	Principle stress in the Y direction
σ_{ZZ}	Principle stress in the Z direction
τ	Loading time of an element ahead of the crack tip
ω	Angular frequency of the oscillating beam
ξ	Length of a molar unit

Abbreviations

CR	Chloroprene rubber
DBA	Dibutyl Adipate
EPDM	Ethylene propylene diene monomer
IR	cis 1-4 polyisoprene
NBR	Nitryl butadiene rubber
NR	Natural rubber – cis 1-4 polyisoprene
SBR	Styrene butadiene rubber
phr	Parts per hundred of rubber by mass

Chapter One

General Introduction

1-1. Background of this study

Rubber materials exhibit a range of unusual physical properties, such as large strain elasticity, incompressibility, internal damping and high strength. As a result rubbers are now used in a wide range of different commercial applications, such as tyres, automotive components, conveyer belts, rubber tracks, hoses, sports goods and medical products. In general, the life of these rubber products is determined by fracture processes that occur in the bulk of the rubber rather than due to a general degradation of the physical properties. Therefore, how to develop or design more durable or higher strength rubber materials and how to predict precisely the life of products manufactured from rubber is of the utmost concern for research engineers working for rubber product manufacturers.

In addition market requirements for rubber products are getting more demanding. In particular, a reduction in energy consumption is becoming more important reflecting environmental concerns, particularly in European countries. If you examine the case of a tyre, an increased durability, expressed as a higher cutting resistance and/or a higher abrasion resistance, is required at the same time as a lower energy consumption, effected by a lower rolling resistance. However, these design requirements are difficult to achieve simultaneously as with increasing visco-elastic losses the strength properties in the rubber are increased whereas with decreasing visco-elastic losses the energy consumption is decreased.

Much research has been undertaken in an attempt to understand the fracture in rubber. This work has, for example, identified the important role of visco-elastic losses in determining the strength. However, there are still a lot of unknown areas to investigate. To meet the more demanding and sophisticated market requirements and to improve the material design methodologies, much more research must still be carried out. Therefore, the work in this thesis was initiated in order to enhance the understanding of the fracture mechanics of rubber.

1-2. Structure of this thesis

This thesis is composed of a number of chapters. In **Chapter 2**, the relevant literatures on the fracture mechanics of rubber are summarised. In particular work relating to the visco-elastic losses and crack tip size effects under a variety of loading regimes is discussed in order to support the research undertaken in this study.

In **Chapter 3** the experimental methods used to characterise the rubber materials and liquid used in this study are described. One of the principle aims of this study is to investigate the role of internal viscosity (visco-elastic losses) in the crack growth behaviour of rubber. The cross-link density, M_c, has a significant effect on the visco-elastic losses. The magnitude of M_c can be determined from both a measure of the stress-strain behaviour and also using an equilibrium swelling method. The dynamic behaviour of rubber can be measured in a variety of ways. A free vibration technique is adopted here as it is a sensitive technique for measuring the behaviour of materials with low visco-elastic losses. The dynamic loss modulus, E'', is measured as it is a direct measure of the internal viscosity of the material. Therefore, the techniques used to measure both the cross-link density and the dynamic mechanical properties are present.

Chapter 4 describes the crack growth behaviour measured using the trouser tear test, conducted at a constant rate of grip separation for strain crystallising rubbers, NR and IR and for an effectively non-crystallising rubber, SBR, with various degrees of swelling and test temperatures. The effect of resulting changes in the visco-elastic loss on crack growth behaviour is hence investigated. The resulting magnitude of tearing energy necessary to drive a crack is compared with the dynamic loss modulus measured in chapter 3.

Chapter 5 describes the crack growth behaviour measured using a constant tearing energy test carried out over a wide range of crack growth rates, covering eight orders of magnitude. The detailed mechanisms and the role of both the visco-elastic losses and the effective crack tip diameter in determining the magnitude of T and hence the crack growth behaviour are examined. Cavitation ahead of the advancing crack tip and strength anisotropy are presented as possible mechanisms for crack tip blunting. These are the mechanisms that increase the crack tip diameter and therefore increase the strength of a rubber.

Chapter 6 describes how the cyclic crack growth behaviour changes for rubbers with widely different visco-elastic properties. Two different elements of cyclic crack growth identified as time dependent and cyclic are considered. The mechanisms responsible for time dependent and cyclic crack growth are explored utilising measurements of the effect of frequency on cyclic crack growth and utilising the constant tearing energy test results obtained in chapter 5.

In **Chapter 7** the mechanisms associated with tensile failure are explored in terms of changes in the visco-elastic losses affected by changing the extent of swelling and the temperature of the test. An attempt to predict the tensile strength for both NR and SBR utilising the tearing energy concept and the crack growth measurements made earlier is discussed for a variety of different loading regimes.

And finally in **Chapter 8** a summary of the significant results obtained in this work together with proposed suggestions for future work are presented.

Chapter Two

Relevant literature survey

2-1. General introduction on the fracture mechanics

The history of fracture mechanics dates back to the 1920s when Griffith[1] first proposed that the strength of any real solid material is governed by the distributions of flaws and that failure initiates from the largest of them. Though the Griffith theory describes the behaviour of sharp tip cracks in linear, perfectly elastic materials, it has been shown to provide an excellent framework for interpreting the failure of polymers. The Griffith theory is the earliest statement of what has come to be known as linear elastic fracture mechanics (LEFM).

2-1-1. Energy balance approach

Griffith based his theory of fracture on two ideas. First, he considered that fracture produced new surface area and postulated that for fracture to occur the increase in energy required in producing the new surface must be balanced by a decrease in the elastically stored energy. Secondly, to explain the large discrepancy between the measured strength of materials and that predicted by theoretical considerations, Griffith proposed that large stress concentrations existed in the specimen in the region of the small inherent sharp cracks. Fracture thus occurred due to the propagation of those cracks, which originated at pre-existing flaws. Griffith concluded that the energy criterion for fracture was given as

$$-\frac{1}{h}\left(\frac{\mathrm{d}U}{\mathrm{d}c}\right) \geq 2\gamma \qquad (2\text{-}1)$$

where U is the elastic stored energy in the specimen, h is the thickness, c is the crack length and γ is the surface energy. The quantity $1/h(\mathrm{d}U\,\mathrm{d}c)$ is called the energy release rate and is generally given the symbol G. The above criterion means that fracture occurs when the energy change per unit of crack propagation is greater than

the surface energy. For an ideal perfectly elastic material, the strain energy release rate G would be equal to 2γ as

$$G = 2\gamma \tag{2-2}$$

where γ is the surface energy. However, experimental results showed that the required energy was much higher than this surface energy, due to the existence of energy dissipation processes, such as plastic deformation or yielding. Orowan[2] and Irwin[3] suggested that the criterion for crack growth should be modified as

$$G \geq 2\gamma + \gamma_p \tag{2-3}$$

where γ_p is the extra surface energy term which arises from the energy dissipation process around the crack tip. This modification introduced the critical value, G_c including all the energy dissipation process. Generally, it is assumed that crack propagation occurs when G reaches a critical value G_c as

$$G \geq G_c \tag{2-4}$$

Following the Griffith theory, other fracture mechanics approaches were developed, such as the stress intensity factor by Irwin[4] and the J-contour integral by Rice[5][6] for some materials and in certain circumstances these approaches are seen to be an improvement on the Griffith theory. However, they still have restrictions in that they can only work well for elastic deformations. Therefore, for a visco-elastic material, such as rubber, another approach has to be used.

2-2. *Fracture mechanics of rubber*

2-2-1. Tearing energy concept

The first successful application of fracture mechanics to rubber was the tearing energy concept proposed by Rivlin and Thomas[7]. During the fracture of rubber, irreversible processes occur in the high-strain region of the crack tip leading to energy dissipation. The tearing energy (T) was hence defined as the total energy

required to create new fracture surfaces by the crack growth process. Thus the tearing energy (T) was given as

$$T = -\frac{1}{h}\left(\frac{\partial U}{\partial c}\right)_l \tag{2-5}$$

where U is the elastic stored energy density in the test piece, h is the thickness of the specimen and c is the crack length. The suffix, l, indicates that the applied forces do not move, and hence external forces do no work. Hence, the criterion for the onset of crack growth is written as

$$T \geq T_c \tag{2-6}$$

where T_c is the critical tearing energy. The tearing energy hence takes into account not only the surface energy but also the associated energy losses. This energy dissipation process could be the sudden relaxation of small regions of the highly strained rubber at the crack tip where crack growth takes place. The magnitude of this energy dissipation would depend on strain and the physical properties of the material. In the region where crack growth takes place, the rubber would reach a limiting extensibility, which is a characteristic of the material itself. It was postulated that this energy dissipation process would depend only on the physical properties of the material and not on the test piece geometry.

The validity of this tearing energy concept has been established by many workers[8][9] and figure 2-1 illustrates the measured relationship between tearing energy, T, and the crack growth rate, r, for unfilled SBR tested under steady crack growth conditions using a variety of test piece geometries. It can be seen that the results are consistent with a single relationship, independent of test piece geometry, as implied by the tearing energy concept. The magnitude of the tearing energies obtained, ranged from 1.0 $kJ.m^{-2}$ to 100 $kJ.m^{-2}$. These values substantially exceeded the surface energy, which is about 0.1 $J.m^{-2}$ for many materials. This clearly implies that the energy dissipation process plays a major role in the crack growth of any rubber and was the major factor determining strength. Figure 2-2 illustrates the five different shaped test pieces used to measure T values in figure 2-1. In each case, T can be calculated from easily measurable applied forces or displacements, which makes them convenient for experimental investigation.

For the simple extension test piece, commonly known as a trouser test piece, the tearing energy is given as[7]

$$T = \frac{2F\lambda}{h} - wW \tag{2-7}$$

where F is the applied tearing force, λ is the extension ratio in the legs, h is the specimen thickness in the unstrained state, w is the total width of the test piece and W is the elastic stored energy density in the legs of the test piece that are in simple extension. A useful approximation is obtained when the legs of that test piece are not extensible, for example, by using wider test piece legs so that $\lambda \cong 1$ and $W=0$, then equation 2-7 can be reduced to

$$T = \frac{2F}{h} \tag{2-8}$$

For the pure shear test piece, the tearing energy is given as[7]

$$T = Wl_0 \tag{2-9}$$

where W is the elastic stored energy density in the region of the test piece which is subjected to the pure shear state and l_0 is the unstrained distance between the two parallel clamps.

For the split tear test piece, the tearing energy is given as[8][9]

$$T = \frac{F_A \lambda_A \sin\beta}{h} + \frac{F_B(\lambda_A \cos\beta - \lambda_B)}{h} - w(W_A - W_B) \tag{2-10}$$

where λ_A, λ_B and W_A, W_B are the extension ratios and elastic stored energy densities in the regions A and B respectively, $\tan\beta$ is $=F_A/F_B$, and w is the width.

For the angled test piece, the tearing energy is given as[8][9]

$$T = \frac{2F}{h}\sin\alpha_S \tag{2-11}$$

where F and h have the same meaning as in equation (2-7) and α_S is the angle between the clamps.

For the tensile strip, edge crack, test piece, the tearing energy is given as[7]

$$T = 2kWc \tag{2-12}$$

where W is the elastic stored energy density in the bulk of the material at large strains, c is the crack length, and k departs from the classical value of π being given approximately as

$$k \approx \frac{\pi}{\sqrt{\lambda}} \tag{2-13}$$

where λ is the extension ratio[10].

2-2-2. *Effective tip diameter*

Thomas[11] extended the tearing energy concept by considering the strain concentration at the crack tip. Modelling the crack as a parallel-sided slit terminated with a semi-circular crack tip, he showed that the tearing energy is approximately related to the effective crack tip diameter using the following arguments.

The shape of the crack tip is taken to be a parallel slit terminated by a semi-circle as illustrated in figure 2-3. It can be seen that the system loses the elastic stored energy per unit volume present in the shaded area when the crack of length c is increased by an amount of Δc referred to the unstrained state. The amount of this energy loss, ΔU, is given as

$$-\Delta U = \int_{-\frac{\pi}{2}}^{+\frac{\pi}{2}} W_\alpha \Delta c h r_t \cos\alpha \mathrm{d}\alpha \tag{2-14}$$

where W_α is the elastic stored energy per unit volume of the rubber at the crack tip at an angular distance α from the pole, h is the thickness of the specimen and r_t is the radius of the semi-circle. Thus gives

$$T = -\frac{1}{h}\left(\frac{\mathrm{d}U}{\mathrm{d}c}\right)_l = r_t \int_{-\frac{\pi}{2}}^{+\frac{\pi}{2}} W_\alpha \cos\alpha \mathrm{d}\alpha = W_t 2r_t = W_t d \tag{2-15}$$

where W_t is a suitable average of W_α and d is the diameter of the model crack tip. Thomas[11] verified this crack tip concept comparing the magnitudes of T calculated from equation (2-15), which concerns the strain energy present at the crack tip and the crack tip diameter and from equation (2-7) using trouser test specimen, which concerns applied forces to the system. Clearly the good agreement found between the two methods of calculating the tearing energy is illustrated in figure 2-4.

If the test piece were extended to tensile rupture, W_t in equation (2-15) represents the work to break per unit volume of rubber, W_b, and equation (2-15) becomes

$$T = W_b d_b \text{ or } W_b = \frac{T}{d_b} \tag{2-16}$$

where d_b is the diameter of the strained crack tip that results in a tensile rupture. Thomas verified this relationship experimentally by measuring the tearing energy of test pieces having model tip diameters in the range of 1mm to 3mm. He found T/d_b to be fairly constant and approximately equal to the work to break (W_b) in tensile tests.

Greensmith[12] made further progress by comparing the tearing energy for crack growth at various rates with the values of W_b measured in tension on test pieces extended at various rates. He expressed the results by plotting T/d and W_b against the reciprocal of time, t^{-1}, taken in extending the test piece to breaking point as shown in figure 2-5 for an unfilled and a filled SBR. In both cases, T/d and W_b are comparable in magnitude and showed a similar dependence on time, except that T/d was consistently higher than W_b. The flaw theory of tensile strength was employed to account for this phenomenon[11]. It is known that the tensile strength decreases as the volume of the test piece increases[13]. This results from there being more and larger flaws present in a large test piece than in a small one as a matter of a probability. In addition, in a crack growth test the volume at the crack tip, which is highly strained, is much smaller than in a tensile strength test specimen. Hence, in crack growth there may be an apparent somewhat greater strength and energy adsorption per unit volume than is anticipated from a tensile strength test even if it tested at the same extension rate.

Following Greensmith's work, much research has been carried out to investigate the effect of the crack tip diameter on the crack growth behaviour[14-17]. Gent and Henry[14] measured the crack growth behaviour by employing a special crack growth specimen, designed to restrict possible deviations of the growing crack from a planar path and thus placing an upper bound upon the magnitude of tip diameter, d as shown in figure 2-6. Special specimens were produced by sticking parallel flexible metal strips to thin rubber sheets at various spacing in the range of 0.01cm to 3cm and by testing the specimens over a wide range of crack growth rates and temperatures. The experimental results showing the relationship between the

measured tearing energy and the crack growth rates are shown in figure 2-7 with only the results from specimens of gap width 0.3cm and 0.01cm being shown.

The results for the wide gap test specimens were similar in magnitude to those obtained by other workers[18] using non-restricted test pieces of a similar vulcanizate. The results for the narrow gap test pieces were virtually identical at high temperatures. However, at low temperatures the wide gap test pieces showed substantially higher values of tearing energy. This was attributed to a significant increase in crack tip diameter, to values exceeding 0.01cm.

Lake and Yeoh[15][16] investigated the effect of crack tip sharpness on crack growth behaviour by carrying out cutting experiments employing a sharp razor blade. From observations of the roughness of fracture surfaces, the crack tip diameter is estimated to lie normally in the range of 0.1mm to 1mm, instead of the minimum possible values of about 10-20nm. However, the razor blade reduced the effective crack tip diameter greatly to about 100nm. Greensmith[12] found that the mean crack tip diameter depended on crack growth rate and temperature. On the other hand, in the cutting process the crack tip diameter was determined by the diameter of the blade tip. The results indicated that the tearing energy obtained in this cutting experiment was substantially unchanged over a wide range of cutting speeds in contrast to the tearing energy required for crack growth, which increased greatly as the crack growth rate increased. Thus, it was suggested that the intrinsic strength of rubber appeared to be relatively unaffected by crack growth rate and temperature over a wide range, but that the crack tip diameter must be a strong function of crack growth rate and temperature, presumably as a result of the crack tip deviation on a microscopic scale.

Thomas[19] also proposed that the effective tip diameter was related to the magnitude of the tearing energy, by considering the hysteretic energy loss in the high strain region ahead of the advancing crack tip and the diameter of this high strain region. As the crack grows an element ahead of the crack tip goes through a strain cycle as it passes through the high strain region around the crack tip (figure 2-8). If the crack grows by Δc a volume of material $\Delta c.h.D$, where h is the thickness of the specimen and D is the diameter of this high strain region, is taken through this cycle. If the hysteretic energy loss per unit volume in this region is W_{ht}, then the total energy loss, L, is given as

$$L = \Delta c.h.D.W_{ht} \tag{2-17}$$

This energy loss or work done must be provided by a reduction in the elastic stored energy in the bulk of the material. If this reduction in elastic stored energy for crack growth of Δc is ΔU, then $\Delta U=L$ and

$$\Delta U = \Delta c.h.D.W_{ht} \tag{2-18}$$

hence the tearing energy is given as

$$T = \frac{1}{h}\left(\frac{\Delta U}{\Delta c}\right) = D.W_{ht} \tag{2-19}$$

The diameter of the high strain region ahead of the advancing crack tip, D, would scale with the crack tip diameter, d, as

$$D = k_D d \tag{2-20}$$

where k_D is the scaling factor. Hence, we finally have

$$T = k_D d W_{ht} \tag{2-21}$$

The value of L must be measured at the relevant frequency. If it is assumed that the extent of the high strain region in the direction of growth is similar in magnitude to that in the transverse direction, then the time of loading, τ, is given by

$$\tau = \frac{D}{r} \tag{2-22}$$

where r is the velocity of crack growth. The equivalent frequency is given approximately by (τ/2), and thus the rate dependence of the tearing energy parallels the frequency dependence of W_{ht}.

2-2-3. Threshold tearing energy (T_o)

It has already been illustrated that an irreversible energy dissipation processes occurs in the highly strained region around a crack tip when crack growth take place. When these energy dissipation processes can be minimised under certain conditions, the rubber vulcanizate shows a minimum tearing energy[20-22]. This minimum tearing energy has been termed the threshold tearing energy, T_o. Generally, this threshold tearing energy can be determined experimentally at low crack growth rates, at high

temperatures and when the material is highly swollen with a low viscosity liquid as illustrated in figures 2-9.

This threshold tearing limit was first observed by Lake and Thomas[23] in cyclic crack growth tests. They defined T_0 as the minimum tearing energy at which cyclic crack growth could take place. At a tearing energy of less than T_0 crack growth was solely attributed to chemical attack by ozone. A more detailed discussion of cyclic crack growth behaviour is given later in section 2-4.

Lake and Thomas[23] found the magnitude of T_0 to be more or less similar for a wide range of rubbers, including both crystallising and non-crystallising rubbers, even though their other strength properties, such as tensile strength and tear strength, were widely different. This magnitude of T_0 for a range of rubbers was around 50 $J.m^{-2}$, suggesting that it could be related solely to the strength of the chemical bonds in the main polymer chains. The magnitude of T_0 can be calculated from the molecular structure of rubber and the strength of primary chemical bonds as follows. A schematic diagram considering a number of molecular chains lying across the plane of crack propagation is shown in figure 2-10. This plane will be crossed by the molecular chains, whose end points (cross-links) lie on opposite sides of the plane as illustrated. In order for the crack to propagate, all such chains must be broken. If the chains were essentially straight, as is approximately the case at rupture, then the forces are transmitted primarily by the cross-links and each bond in the backbone chain would be subject to the same force. Lake and Thomas[23] assumed that the tip diameter of the advancing crack, d, had the minimum possible value, d_0, for rubber, when the elastic stored energy, W, had the minimum possible value, W_0, which was determined by the bond strength. Thus, on a molecular scale equation 2-15 becomes

$$T_0 = W_0 d_0 \qquad (2\text{-}23)$$

where W_0 is the minimum possible strain energy density at the tip and d_0 is the minimum possible tip diameter of the crack, which is the smallest and sharpest possible. However, in case of the rubber, it is impossible for this to be of atomic dimensions due to its structure and it must be of the order of the distance between adjacent cross-links in the unstrained state. An estimation of the minimum energy required for crack propagation can be made using equation 2-23, if it is assumed that the tip diameter has its smallest possible value, d_0, given as

$$d_o \cong \xi\mu^{1\,2} \tag{2-24}$$

where ξ is the length of a monomer unit and μ is the number of monomer units between cross-links[24]. Putting the elastic stored energy density at the crack tip as bJ_b, where b is the number of active bonds per unit volume and J_b is the bond rupture energy and putting this and equation 2-24 into 2-23 gives

$$T_o \cong bJ_b\xi\mu^{1\,2} \tag{2-25}$$

The value of T_o calculated using this theory was about 25 $J.m^{-2}$, whereas the value measured experimentally was about 50 $J.m^{-2}$, higher by a factor of 2. Considering the uncertainties in the approximations and the assumptions of the theory, the agreement between theory and experiment can be regarded as very good.

The effect of polymer type and the magnitude of degree of cross-linking on T_o are found to be broadly in accord with the theory, as is the absence of temperature dependence or dependence on the degree of swelling with solvents. Cross-link types are found to have some effect, with poly-sulphidic cross-links tending to yield higher T_o values than mono- or di- sulphidic, perhaps because of their tendency to break more easily under stress and to reform two new cross-links in the deformed shape. This process effectively increases the magnitudes of μ.

The uniqueness of this theory is that, just like Grffith's theory, it relates fracture to molecular parameters. Indeed, T_o would be the surface energy (2γ), if the irreversible processes of energy dissipation were negligible and intermolecular separation only was involved.

2-3. Crack growth behaviour

2-3-1. Types of crack growth

Crack growth consists of two general types. These will be referred to as steady and stick-slip, respectively[18]. The most convenient way to distinguish the two types of crack growth behaviour is to carry out crack growth measurement at a constant rate of grip separation test using a trouser test piece, where the fluctuations of force with rate reflect the nature of the crack growth process. In the case of steady crack growth, the force and crack growth rate remain essentially constant (figure 2-11 (a), (b)) or show only small fluctuations with time. The appearance of the fracture surface depends on the degree of fluctuation reflecting the nature of the crack growth process. If the fluctuations are relatively small, a smooth fracture surface or regularly rough with a relatively straight crack path is produced. In case of stick-slip behaviour, crack growth does not propagate continuously (curve (c)). Two fracture surface types appear on an irregular surface, a combination of smooth and rough. The rough surface corresponds to the stick period where the crack growth process appears suspended and the smooth surface corresponds to the crack growing. Knotty crack growth is one kind of stick-slip crack growth (curve (d)), where the crack starts to propagate across the direction of extension but halts and tends to grow at right angles, along the line of stretching in either or both directions for a short distance before resuming the main line of crack growth. In this mode, the crack deviates under increasing force, until new crack growth occurs ahead and the force drops abruptly. The reason for this knotty crack growth is thought to be associated with the development of an anisotropic zone perpendicular to the direction of the crack. This zone forms barriers in the path of crack growth and results in the deviation of the crack growth.

2-3-2. Effect of variables on crack growth in rubber

2-3-2-1. Effect of crack growth rate and temperature

The magnitude of the tearing energy is not constant due to irreversible energy loss processes. The magnitude depends on both the crack growth rate and the

temperature. The effect of crack growth rate and temperature are illustrated on the 3 dimensional plots of tearing energy, crack growth rate, and temperature shown in figure 2-12 for unfilled SBR, NR and FT black filled SBR[25].

In case of the unfilled SBR, figure 2-12(a), the tearing energy increases with increasing crack growth rate and decreasing temperature. This reflects the dominant influence of the visco-elastic energy dissipation. In case of the strain crystallising rubber NR, figure 2-12(b), the dependence of tearing energy on crack growth rate and temperature becomes less marked. This has been associated with strain-crystallisation, whose effect on crack growth behaviour outweighs the effect of the viscous component. The high tearing energy observed in NR, over a wide range of crack growth rates and temperatures could be associated with the high energy losses resulting from the heat of strain crystallisation. In case of the carbon black filled SBR, figure 2-12(c), a flat plateau is observed at low crack growth rates and at low temperatures. This flat plateau represents a large increase in the tearing energy over the unfilled material and is associated with knotty crack growth. Outside of this region, where knotty crack growth does not occur, the carbon black loading causes only a small increase in tearing energy compared to that for unfilled SBR. This suggests that the development of knotty crack growth depends on not only crack growth rate but also on temperature. This plot also indicates a complex crack growth phenomenon in reinforced rubbers, which involves two opposing processes, associated with visco-elastic energy dissipation and strength anisotropy. Even in the presence of carbon black, the crack growth behaviour is governed principally by visco-elastic effects, hence the tearing energy increases with increasing crack growth rate as shown in figure 2-12(a). However, in the presence of carbon black the tearing energy tends to decrease with increasing crack growth rate due to the extent of strength anisotropy. The observed dependence of tearing energy on crack growth rate and temperature represents the balance, which is struck between these two opposing processes.

2-3-2-2. Time–temperature superposition principle

In the absence of crystallisation or the presence of filler particles, the mechanical energy loss (hysteresis) is predominantly associated with visco-elastic

effects. The magnitude of the energy dissipation is determined by the internal viscosity of the material. Under these conditions, the rubber behaviour can be described using the time temperature superposition principal. This internal viscosity is highly dependent on temperature and its temperature dependence may be described by considering the flow viscosity. The internal viscosity and flow viscosity of rubbers are not equivalent, but the flow viscosity may be readily measured and reflects the mobility of the segments constituting the polymer molecules. Williams, Landel and Ferry[26] developed an equation, which rationalises the temperature dependence of viscosity for glass-forming liquids. The well-known equation (WLF equation) is given as

$$\log a_T = \frac{-C_{W1}(\theta - \theta_S)}{C_{W2} + \theta - \theta_S} \tag{2-26}$$

where θ_S is a reference temperature, usually taken as θ_g+50°C, θ is the temperature of measurement, θ_g is the glass transition temperature of the rubber, and a_T is the shift factor. The WLF equation may also be derived from the semi-empirical Doolittle equation[27][28], which relates the viscosity of a liquid to the free volume, the volume available for segmental motion. The amount of free volume increases as temperature increases and thus the segmental mobility increases and the viscosity decreases. Furthermore, amorphous polymers have similar thermal expansion coefficients and their viscosities are all in reasonable agreement with equation 2-26 up to the temperatures of about θ_g+100°C. In the WLF equation the constants C_{W1} and C_{W2} were originally thought to be universal constants, having values of 17.4 and 51.6 (K) respectively, but they have been found to vary somewhat from polymer to polymer, as shown in table 2-1[29]. In a cross-linked rubber the internal viscosity is still related to the rearrangement of molecular chains and is directly related to segmental mobility. It varies with temperature in the same manner as for uncross-linked rubbers and its temperature dependence can be described by the WLF equation.

Mullins[30] found that the WLF equation could be used to describe the dependence of the tearing energy of amorphous rubber on crack growth rate and temperature, as illustrated by the master curve shown in figure 2-13.

Kadir and Thomas[31] also showed that tearing energy data, for a range of rubbers with cracks growing in the smooth fracture surface region, could be

superimposed using the WLF equation as shown in figure 2-14. However, it was found that to obtain such a master curve, the reference temperature, θ_S, had to be θ_g+20°C, 30°C lower than the usual reference temperature. This was considered to be due to the fact that the glass transition temperature might be altered in the high strain region ahead the crack tip due to rate effects or the presence of a hydrostatic stress component.

Mullins[32] presented strong evidence for a relationship between the tearing energy of amorphous rubber and the energy dissipation processes. He compared the values of critical tearing energy obtained for six different amorphous elastomers, three SBR materials with low styrene content with the range of θ_g from -72°C to -78°C and three butadiene-acrylonitorile copolymers with the range of θ_g from -30°C to -50°C, with energy dissipation by viscous processes, in the form of the shear loss modulus as shown in figure 2-15. It was proposed that the magnitude of the tearing energy is equal for all unfilled amorphous rubber under conditions of equal segmental mobility, and that the dependence of tearing energy on temperature and crack growth rate arises solely from corresponding changes in segmental mobility. Thus, internal energy dissipation determines the tearing energy of such amorphous rubbers, with a greater energy dissipation resulting in a greater tearing energy.

2-3-2-3. Effect of cross-linking system

The tearing energy of an unfilled rubber depends on the nature of the backbone, the molar mass and the concentration and nature of the cross-links. Different vulcanising systems can produce widely different strengths for the same polymer backbone, even when compared at similar degrees of cross-linking. Brown, Porter and Thomas[34] investigated the effect of vulcanising system on the tearing energy for mono-sulphide, poly-sulphide and peroxide cross-linked systems. Their data is shown in figure 2-16 where the shear modulus is used to reflect the cross-link concentration. The tearing energy decreased with increasing shear modulus for each of the three vulcanising systems. The observed ranking of the strength was poly-sulphide > mono-sulphide > peroxide system. This decreasing order of strength seemed to follow an increase in the bond strength of the cross-link. Mechanically

weak cross-links presumably re-distributed local stresses in the network by breaking and reforming during the deformation[33]. It is assumed that the poly-sulphidic cross-links break before the main backbone chain under the high stresses around the crack tip resulting in higher strength for the poly-sulphidic cross-links than for C-C cross-links.

2-3-3. Cavitation and related fracture

2-3-3-1. Intrinsic flaw sizes

The mechanisms whereby micro-voids and cracks are initiated in rubbers are not clearly established. The initiation sites may arise from accidental scratches or nicks in the moulded or cut surfaces but, as Gent[35] has commented, even if such flaws are carefully prevented, for example by moulding against polished glass surfaces, the breaking strength of the rubber is not increased dramatically. Thus, it appears that other sources of flaws such as dirt and dust particles must inevitably be present. Apart from such foreign bodies the common assumption that the cross-links are uniformly distributed is not necessarily true and local fluctuations will occur within the material. This kind of feature will give rise to local inhomogeneity in the material, which may act as micro-void initiation sites. An estimation of the size of intrinsic flaws present in rubber can be obtained by using equation 2-12 for tensile strip specimen, and taking the value of T to be the threshold tearing energy, T_0. This reveals that the intrinsic flaw sizes are equivalent to edge crack lengths, c_0, of between 25 to 50μm. It is interesting that between these limits the value of c_0 appears independent of the particular rubber and of the detailed compound formulations, although these factors greatly affect the strength. However, as Gent[36] has commented, the value of c_0 is the depth of an edge crack equivalent in stress concentrating power to natural flaws which may be smaller and sharper, or larger and blunter, than those calculated for edge cracks.

2-3-3-2. *Initiation under tri-axial stresses*

An area, where the mechanism and mechanics of microvoid growth, leading to crack initiation and propagation, have been studied is the failure of rubber under the action of tri-axial tensile stresses. When a thin disc of rubber is bonded between rigid end plates and subjected to an applied uni-axial tension, tri-axial tension develops within the rubber layer due to the incompressibility of rubber. Indeed, if the value of Poisson's ratio, ν, of rubber is 0.5, the stress state of the rubber layer is assumed to be in hydrostatic tension. Gent and Lindley[37] using this type of test piece with various SBR and NR compounds found that small cracks were initiated in the rubber at relatively low applied stresses and strain levels and that the point of initial fracture was clearly marked by a point of inflexion in the stress-strain curve. The initiated cracks then propagated at relatively greater applied stresses than for the initiation stage. Gent *et al*[38][39] modelled these observations using a small spherical micro void within a block of rubber which expanded elastically from its original radius, r_o, to a new radius, λr_o, under the action of an inflating pressure, P, as shown schematically in figure 2-17. From the theory of large elastic deformations, the relationship for the inflating pressure, P, is given as

$$\frac{P}{E} = \frac{\left(5 - 4\lambda^{-1} - \lambda^{-4}\right)}{6} \tag{2-27}$$

where E is Young's modulus and λ is the extension ratio of the radius given as

$$\lambda = \frac{r_1}{r_o} \tag{2-28}$$

Equation 2-27 does not involve the value of the radius, r_1, and it predicts that at a critical pressure, P_c, of $5E/6$, any small void will grow to infinite size. In reality, of cause, the original void will form an internal crack when the wall extension reaches the fracture strain of the rubber and crack growth will be developed. Thus, the pressure for crack initiation, P_c, is given as

$$P_c = \frac{5}{6}E \tag{2-29}$$

It has been suggested that when the volume under the dilatational stress, $P=(\sigma_{XX}+\sigma_{YY}+\sigma_{ZZ})$ 3, is small, the critical pressure for crack initiation is much larger

than the predicted value given in equation (2-29)[39]. This was considered to be due to the extra effect of surface energy and a modified criterion, given as the following equation was suggested.

$$P_c = \frac{5}{6}E + \frac{2\gamma}{r_o} \tag{2-30}$$

where γ is the surface energy. This implied that the second term, related to surface energy, is dominated when the size of cavity was relatively small.

Rubber is commonly found to undergo internal cavitation under the conditions of tri-axial tension as shown in figure 2-18. This phenomenon must therefore be regarded as a consequence of an elastic instability of pre-existing cavities too small to be readily detected. It does not involve the fracture energy because it is principally a transformation of potential energy from one strained state to another. In consequence, the critical stress given in equation (2-30) does not depend on the strength of the rubber but only on its elastic modulus. Cavitation stresses in bonded rubber blocks under tension (figure 2-19)[37] and near rigid inclusions (figure 2-20,-21)[40] at points where a tri-axial tension is generated are found to be accurately proportional to the Young's modulus E and largely independent of the strength of the rubber, in accordance with the dominant role of elasticity rather than a rupture criterion.

If the precursor cavities are extremely small, less than about 0.1 μm in radius, their surface energy becomes a significant additional restraint for expansion. As shown in figure 2-22, the tri-axial tension necessary for cavity expansion is then considerably greater[39]. Thus, if elastomers could be prepared without any micro-cavities, they would be much more resistant to cavitation.

2-3-4. Static, constant T, crack growth behaviour

2-3-4-1. Effect of crack growth rate

Thomas[8] suggested that a discrepancy existed in the tearing energy against rate relationship obtained from static, constant T, crack growth measurements when compared with constant rate of grip separation measurements. He compared static crack growth behaviour obtained by employing a pure shear test geometry with

constant rate of grip separation test obtained using a simple extension test geometry (trouser test specimen) as shown in figure 2-23.

There is approximate agreement between constant rate of grip separation behaviour and static crack growth behaviour at rates of less than about 10^{-2} cm.s^{-1}. However, above this critical rate, r_c, there is marked disagreement between the crack growth behaviour in these two tests; static crack growth behaviour giving much higher rates for a given tearing energy. The manner of static crack growth undergoes a fairly abrupt change at r_c. At lower crack growth rates, r fluctuates somewhat, but it is rarely more than three times the average. Above r_c, the rate fluctuates between low values (-10^{-2} cm.s^{-1}) and much higher values (1 to 10cm.s^{-1}), and the crack growth has a "stick-slip" behaviour. The average crack growth rate observed in this region is governed by the relative times that crack growth spends in the "stick" or "slip" states. The appearance of the torn surfaces correlates with these rate changes. Below r_c, the fracture surfaces are rough and irregular, but above in the "slip" regions they are much smoother, and in "stick" regions they are rough. The large fluctuations in crack growth rate, which were observed for static crack growth measurements above r_c, suggests that the discrepancy between these and the constant rate of grip separation results may arise from the different averaging processes.

Kadir and Thomas[31] carried out a further investigation on the effect of rate on static crack growth behaviour for a non-crystallising elastomer. They found a tearing energy, T, against crack growth rate, r, relationship, which could be schematically represented, as shown in figure 2-24, where the static crack growth behaviour can be divided into three regions.

In the low crack growth rate region-A at a rates of less than about 0.1 mm.s^{-1} for SBR the cracks grow in a relatively steady manner where the appearance of the surface is rough. In the intermediate region-B of stick-slip, very large changes in instantaneous rate are observed between the "stick" and "slip" states. Here the average value of crack growth rate has little significance as it depends strongly on how much time is spent in a stick or slip mode, this seems to be governed largely by chance. In contrast, at fast crack growth rate region-C at a rate of more than about 10 mm.s^{-1}, crack growth occurs at a remarkably constant rate. The fracture surface in this region is very smooth, reminiscent of a glassy fracture surface. Kadir and Thomas determined this tearing energy against crack growth rate relationship for

four different materials, BR, NR, SBR and NBR as shown in figure 2-25. It is worth noting that the critical rate, at the transition from the rough surface region to the stick-slip region, for unfilled SBR is observed at the same rate as was observed by Thomas[8] previously. Thus, crack growth rate and the associated nature of the fracture surface are reproducible features of static crack growth behaviour.

2-3-4-2. Effect of the specimen thickness

As was described in the previous section, the magnitude of the tearing energy is not constant for a particular material but depends strongly on both the crack growth rate and the temperature due to the viscous work component. Kadir and Thomas[31] showed that the thickness of the specimen could also have an effect on the crack growth behaviour and thought that this effect was associated with the scale of behaviour at the crack tip. The roughness developed on the fracture surface was of the order of a few tenths of a millimetre in scale. If the thickness of the specimen was also of this order, then it might be expected that the scale of the roughness, and hence the crack growth behaviour, would be influenced by the thickness. The measured effect of the thickness of the specimen is shown in figure 2-26 employing two different test piece thicknesses.

In the smooth surface region (fast crack growth rates), no thickness effect was found, but a significant effect was seen in the rough and stick-slip regions. This was interpreted as showing that in the smooth surface region a sharp crack tip was produced, but the development of the full potential roughness was inhibited by the thickness limitation in the rough and stick-slip regions. The results of a more detailed study of the thickness effect in these regions are shown in figure 2-27[31]. The thickness has the most significant effect when the thickness is less than 1mm, consistent with the observed magnitude of the roughness.

2-3-4-3. Effect of the pressure

The abrupt change in crack growth behaviour and fracture surface appearance as a function of crack growth rate in static crack growth behaviour is described in the

previous section. A possible explanation for this behaviour is the role of hydrostatic (tri-axial) tension in rubbers (section 2-3-3-2). Under hydrostatic tension, rubber cavitates, and the necessary stress is of the order of the Young's modulus. Just ahead of a crack, high tensile stresses must be developed locally to rupture the primary chemical bonds. The resulting hydrostatic tension ahead of the crack tip could be large enough to produce cavitation, which may be a possible source of the roughness development on the fracture surface. However, when the crack propagates very rapidly, the rate of extension at the crack tip will be very high, assumed to be of the order of $10^8 s^{-1}$[31]. This will almost certainly be rapid enough to increase the magnitude of the elastic modulus substantially and it is postulated that the fracture of the rubber chains could now occur before cavitation takes place. Measurements of high-speed crack propagation in a bursting balloon[41] support the suggestion that the modulus of the rubber in the neighbourhood of the crack tip is very high and that this results from the visco-elastic increase in modulus with increasing rate of extension.

Imposition of an external hydrostatic pressure would suppress cavitation and hence influence the crack growth behaviour. Lake *et al.*[42] investigated this effect. They measured the static crack growth behaviour of a non-crystallising rubber immersed in a non-swelling liquid at various pressures. The resulting effect of pressure on the crack growth rate for unfilled SBR is illustrated in figure 2-28.

A strong dependence of crack growth rate, r, on pressure was observed, r changing by about three orders of magnitude over the range studied. Results for different T values showed essentially a parallel relationship on this semi-logarithmic plot. However, figure 2-29 shows photomicrographs of fracture surfaces (for the same T value) at widely different pressures and it is apparent that there is no significant change in appearance. Therefore it cannot be argued from these experimental results that the hydrostatic pressure produces any appreciable change in fracture surface roughness, as might have been expected if cavitation were being suppressed.

Thus, the effect of pressure in this work seems to be largely associated with the corresponding change in the θ_g. Their results, hence, provide no evidence that cavitation process plays as important part in the crack growth process, but they are not sufficiently conclusive for this possibility to be ruled out.

2-3-4-4. Effect of the oxygen

As well as the energy dissipative processes that are strongly dependent on temperature and crack growth rate and which are known to be the major contributors to the strength of rubber, the presence or absence of air is known to have an effect on the crack growth process. In *vacuo*, the mechanical fatigue life of a NR vulcanizate was found to be increased by a factor of 10 compared to failure in air[43]. Similarly, the crack growth rate under intermittently applied loads was found to be reduced by a factor of 3-4 in *vacuo*[44] and for a carbon black filled NR vulcanizate in nitrogen by a similar but somewhat smaller factor of 1.8[45]. Also, the tensile strength of an SBR vulcanizate at high temperature was found to be increased in *vacuo* by a surprisingly large amount, about 45% on average[46]. Thus, there is some information on the effect of oxygen on the strength of rubber, however there is relatively little quantitative information available on the effect of oxygen concentration. Gent *et al.*[47][48] investigated the effect of oxygen on the static crack growth behaviour for an unfilled SBR over a wide range of atmospheric pressure as illustrated in figure 2-30 and 2-31. In all cases, the crack growth rate was lower at low air pressure by a constant factor, independent of the tearing energy. Thus, removing air completely has the same proportionate effect at slow and fast crack growth rates. The major changes occurred at pressures of between 0.001 and 1 atmospheres, and over this range linear logarithmic relationships as shown in figure 2-31 were observed of the same slope. The effect of atmospheric pressure appeared to be independent of the level of stress. The compound with C-C cross-links was least affected by atmospheric pressure, the one with mainly mono-sulphide cross-links was more strongly affected and the compound with mainly poly-sulphide cross-links was most strongly affected. These tendencies are consistent with the known susceptibility of these materials to oxidation[48].

2-4. Cyclic crack growth behaviour

2-4-1. Cyclic crack initiation

The initiation of mechanical cyclic cracks in rubber is due to the presence of inhomogeneities, or irregularities that result in highly localised stress concentrations on loading. Compounded rubbers contain various additives such as curatives, process aids, and fillers, resulting in various degrees of inhomogeneity on a microscopic scale, probably of the order of 10μm in size, depending on the particular additives. Rubber without those additives may contain gel particles, micro-voids and roughness at cut or moulded edges, which can also act as sites for crack initiation. Lake[49] estimated that the effective initial flaw size would be about 25μm for natural rubber. The presence of ozone also gives rise to cracks on the surface when tensile stresses are present.

When observing a cyclic fracture surface, it can sometimes be divided into three regions associated with crack initiation, crack growth, and catastrophic failure[50]. However, generally speaking, there is no sharp distinction between the crack initiation and the crack propagation regions. When a rubber component is subjected to repeated stresses, a certain time passes before visible cyclic cracks appear. Whether this induction time should be considered as a part of the crack initiation process or as a part of the crack propagation process is still being debated in the literature. It appears that what matters in practise is how fast an initial flaw of a certain size will propagate under given loading conditions and crack initiation should be tackled as a crack propagation process. With laboratory test pieces, the random process of crack initiation from natural flaws is avoided by pre-cracking the specimen. This leads to more reproducible results, since the sensitivity to defects that are not an inherent property of the material is eliminated. Thus, the focus in fracture mechanics is shifted to cyclic crack growth and away from the crack initiation processes.

2-4-2. Cyclic crack growth behaviour

It is well known that the relationship between the crack growth per cycle, dc/dn, and tearing energy, T, is a characteristic of a material because the relationship is independent of the test piece geometry as illustrated in figure 2-32[51]. In case of cyclic crack growth measurement, it is generally found that the extent of crack growth during each loading cycle is determined by the maximum tearing energy during the cycle. Furthermore it is not much influenced by the way in which this maximum tearing energy is reached even for a relatively viscous material[51][52][53]. Thus, crack growth per cycle may be represented by an equation given as

$$\frac{dc}{dn} = f(T) \tag{2-31}$$

where c is the crack length, n is the number of cycles, and T is the maximum tearing energy during a cycle. In case of the figure 2-33, the relationship between crack growth per cycle and tearing energy is given as

$$\frac{dc}{dn} = B\left(\frac{T}{T_u}\right)^{\beta} \tag{2-32}$$

where B and β are material's constants and T_u=1.0J.m^{-2} and is included to make T/T_u dimensionless.

The relationship between crack growth per cycle and tearing energy over a wide range of tearing energy for unfilled NR and SBR is illustrated in figure 2-33. The data can be represented by four regions.

In region I the tearing energy, T, is less than the threshold tearing energy T_o and hence no mechanical crack growth occurs. T_o is the mechanical fatigue limit. Below T_o, crack growth is caused by ozone degradation and the rate equation takes the form

$$\frac{dc}{dn} = k_z[O_3] = R_z \tag{2-33}$$

where k_z is the rate constant due to ozone, $[O_3]$ is the ozone concentration and R_z is the crack growth rate, which is independent of the tearing energy. The chemical reaction between ozone and carbon-carbon double bonds, which are present in the backbone of natural and various olefin rubbers, is rapid and results in molecular

scission. Ozone will attack rubbers above a critical tensile stress, which corresponds to strain energy of about 0.1 J/m^2 for unprotected NR and SBR compounds.

In the region II, crack growth is dependent on both ozone attack and mechanical factors in an approximately additive and linear fashion. Hence;

$$\frac{dc}{dn} = R_z + A_t(T - T_o) \tag{2-34}$$

where A_t is a crack growth constant for region II.

In the region III, the power law dependency between crack growth rate and T has been found for many rubbers as well as for non-rubbery materials. Thus;

$$\frac{dc}{dn} = B\left(\frac{T}{T_u}\right)^{\beta} \tag{2-32}$$

where B and β are constants, characteristic of region III. For natural rubber β is about 2, and for SBR, β is about 4. In general, β lies between 2 and 6 for most rubber vulcanizates, depending mainly on the rubber and to a lesser extent on secondary factors such as compounding ingredients.

In the region IV, dc/dn approaches the velocity of elastic waves in rubber, about 50 m.s^{-1}. Thus;

$$T = T_c \tag{2-35}$$

where T_c is the critical tearing energy, where catastrophic tearing takes place.

2-4-3. Mechanical limit for cyclic crack growth

As was mentioned in the previous section, it has been found that at a tearing energy of less than T_o, the threshold value, the crack growth rate is extremely slow (virtually a constant rate in region I in figure 2-33). At a T value less of than T_o, mechanical crack growth is absent and ozone attack is the only mechanism for crack growth. The existence of T_o means that if this tearing energy value is not exceeded during cyclic loading then the cyclic life will be virtually infinite in the absence of ozone attack. Thus, rubber can exhibit a mechanical fatigue limit for cyclic crack growth like other materials such as metals. The tensile strain e_o corresponding to T_o is called the "mechanical cyclic limit" for a particular rubber. The e_o for natural

rubber and for the most synthetic rubbers examined to data lies within the range 65 to 95% (figure 2-34). Therefore, for tensile strains below about 65% strain the fatigue life is virtually infinite[54]. The magnitude of e_0 is extremely important since most rubber components subject to repeated loading are designed to work below it. However, in a component of complex geometry and loading, it is not easy to determine the actual magnitude of local strains and it is hence not easy to determine whether the working conditions are below T_0.

2-4-4. Cyclic life determination

A theoretical S-N curve can be predicted from the cyclic crack growth characteristics[49][55] as shown in figure 2-34. The crack growth per cycle, at tearing energies $T > T_0$, is found to be a function of T until catastrophic failure occurs at tearing energies, above the critical tearing energy, $T > T_c$.

$$\frac{dc}{dn} = f(T) \tag{2-31}$$

If the fatigue life can be defined by the number of cycles, N, required for crack growth from a crack length c_0 to c_1, then the number of cycles is given as

$$N = \int_{c_0}^{c_1} \frac{dc}{f(T)} \tag{2-36}$$

This integration can be evaluated from the relationship between tearing energy and crack length. The value of T can be calculated for particular sample dimensions and type of deformation. For example, for simple tensile extension and a specimen with an edge crack, the tearing energy is given as

$$T = 2kWc \tag{2-12}$$

As was described in the previous section, in the intermediate tearing energy region (region III), the crack growth per cycle is given as

$$\frac{dc}{dn} = B\left(\frac{T}{T_u}\right)^{\beta} \tag{2-32}$$

Substituting equation (2-12) and (2-32) into (2-31) and integrating between the initial crack length c_o to a final failure crack length c_1, the number of cycles to failure is gives as

$$N = \frac{1}{(\beta-1)B(2kW)^{\beta}}\left(\frac{1}{c_o^{\beta-1}} - \frac{1}{c_1^{\beta-1}}\right) \tag{2-37}$$

If the crack length c_1 is appreciably greater than c_o, the second term in the brackets in equation (2-37) can be neglected. Therefore, equation (2-37) can be written as

$$N = \frac{1}{(\beta-1)B(2kW)^{\beta} c_o^{\beta-1}} \tag{2-38}$$

where N is the number of cycles to failure and c_o is the equivalent crack length of the largest naturally occurring flaw that is present.

In general the fatigue life N of any rubber component can be predicted by integrating equation (2-31) as

$$N = \int_{T_i}^{T_c}\left(\frac{1}{dT/dc}\right)\frac{dT}{f(T)} \tag{2-39}$$

where T_i is the initial tearing energy which depends on the initial crack length and T_c is the catastrophic tearing energy. The validity of this approach had been examined by many workers[49][51][56][57] employing tensile specimens containing inserted cuts of various lengths. They have found that in the absence of inserted cracks the size of an inherent defect is in the range of 5 to 70μm. A rubber component initially contains a wide distribution of flaw sizes and therefore the range of initial values of tearing energy. The flaw giving the highest tearing energy will be the critical one that is responsible for the catastrophic crack growth fracture.

2-4-5. Effect of variables on cyclic crack growth behaviour

2-4-5-1. Effect of non-fully relaxing

The strain cycle to which a specimen is subjected during cyclic crack growth may or may not include zero strain. It is known that when the strain is not relaxed to zero for a part of each cycle, the crack growth per cycle decreases and the cyclic life

increases for a strain-crystallising rubber, such as NR[58][59][60]. Thomas[61] suggested that strain-crystallisation takes place at the crack tip as the stress increases and that the crystals melt as the strain decreases to zero. As a consequence increments of crack growth occur on subsequent extension before strain-crystallisation takes place. This effect of not fully relaxing the strain for an unfilled NR is illustrated in figure 2-35[58]. In this instance, with a minimum tearing energy of about 6% of the maximum, the threshold tearing energy is effectively increased and the crack growth per cycle at higher tearing energies is reduced by a factor of 10. A much smaller non-fully relaxing effect is also observed in a non-crystallising rubber, such as SBR, in part because of the occurrence of static, constant tearing energy, time dependent crack growth.

2-4-5-2. Effect of frequency

A change in cyclic frequency alters the strain rate, the number of cycles per unit time, and the time under deformation for each cycle. The effect of frequency on cyclic crack growth behaviour has been studied[52][53] and has shown distinct differences in behaviour between non-crystallising and strain-crystallising rubbers. In the case of a non-crystallising rubber, the increment of the crack growth during each cycle is considered to result from the sum of two different components; the time dependent and the cyclic crack growth component. The first depends only on the length of time of a cycle and on the maximum tearing energy. The second is related to a genuine cyclic growth phenomena and its extent depends on the exact details of both the loading and the unloading process. Significant effects of frequency have been found for non-crystallising rubbers reflecting the time dependent element of crack growth, which is superimposed on the cyclic crack growth measurement. At large frequencies, the cyclic growth component is dominant and the measured crack growth per cycle at a given tearing energy decreases by a factor of three over a range of 10 to 100 cycles per minute (cpm). However, at low frequencies, below 10cpm, the time dependent component is dominant and the overall crack growth per cycle is inversely proportional to the frequency[55].

For a strain-crystallising rubber, crack growth takes place in a stick-slip manner. Crack growth does not occur in a time dependent manner and cracks can

only propagate above a given critical applied tearing energy. Hence, the time dependent component does not dominate and cyclic frequency has very little effect on the crack growth per cycle. Very little effect of cyclic frequency on cyclic crack growth behaviour is observed over the range of 10 to 1000cpm[49]. At still lower frequencies, below 10cpm, the crack growth per cycle is virtually independent of frequency.

However, if the frequency is high, especially for thick specimens, excessive heat is generated and the predominant cause of failure is now no longer one of mechanical cyclic crack growth but rather elevated temperature degradation.

2-4-5-3. Effect of oxygen

The presence of atmospheric oxygen can influence cyclic crack growth in rubbers as illustrated in figure 2-36[55]. In-*vacuo*, the value of the tearing energy required to achieve a particular crack growth per cycle is increased by a factor of around 2. However, at higher tearing energies, the effect of oxygen is frequency dependent. At high frequencies, the crack growth per cycle is the same in air and in-*vacuo* as the time dependent crack growth component is minimized. At lower frequencies, the crack growth rate is significantly higher in air as the time dependent component dominates the crack growth behaviour. Similar effects have been found not only for NR, a strain-crystallising rubber, but also for SBR, a non-crystallising rubber[43]. It is proposed that the stress-activated oxidative processes that lead to the breakage of the polymer chains in the vicinity of the crack tip are time dependent[43]. Suitable anti-oxidants mitigate the effect of oxygen and give crack growth behaviour typically about midway between two curves shown in figure 2-36 for crack growth behaviour in air and in-*vacuo*.

2-4-5-4. Effect of temperature

The effect of temperature on cyclic crack growth is much greater for a non-crystallising rubber than for a strain-crystallising rubber[53][58][59] as illustrated in figure 2-37[52]. Lake[55] suggested that this difference in cyclic crack growth

behaviour is due to the difference in nature and extent of the high strain mechanical hysteresis. In the case of a non-crystallising rubber, such as SBR, the mechanical hysteresis is solely governed by the internal viscosity of the material as for the case of static crack growth behaviour. This internal viscosity decreases with increasing temperature[32][52]. Conversely, in case of a strain-crystallising rubber, such as NR, mechanical hysteresis at break is derived principally from the crystallisation process and is not largely affected by the temperature[36]. Hence, the crack growth behaviour of a strain-crystallising rubber is not affected as significantly by a change in temperature[62]. Figure 2-37 clearly illustrates the relative magnitude of these effects with a 10^4 fold decrease in cyclic life being observed for unfilled SBR when the temperature is raised from 0°C to 100°C, in contrast to unfilled NR, which exhibits only a four fold decrease.

2-4-5-5. Effect of vulcanising system

The effect of the type of vulcanising system on the cyclic crack growth behaviour in unfilled NR has been studied by Lake and Lindley[58][59] employing poly-sulphide, mono-sulphide and C-C cross-links. They found that the poly-sulphide system gave longer cyclic lives than the mono-sulphide and C-C cross-links by a factor of up to 2. They concluded that the superiority of the poly-sulphide cross-links is due to their labile nature, which enables them to break and reform in the strained state, hence relieving stress concentrations at the crack tip.

2-4-5-6. Effect of nature of rubber

The crack growth behaviour for different rubbers[58][59] is illustrated in figure 2-38. The power law exponent β in equation (2-32) is found to be approximately 2 for both filled and unfilled NR, a strain-crystallising rubber and approximately 4 for SBR, a non-crystallising rubber. In general, the value of β is used to represent the crack growth characteristics for each material and is said to reflect its mechanical hysteresis but such a value of β can be affected by both the strain level and the strain rate. Figure 2-39 shows a comparison of cyclic crack growth behaviour for different

rubbers plotted on the same graph and clearly no single material has the best cyclic life over the whole range of tearing energy[63]. Therefore, there is much scope in blending rubbers to develop optimised cyclic life over a wide range of tearing energy.

2-4-5-7. Effect of swelling

It has been seen that cyclic crack growth behaviour is mainly governed by energy dissipative processes with higher energy dissipation at crack tips resulting in lower crack growth per cycle. As is described in the previous section (2-2-3) the magnitude of the tearing energy, T, necessary to drive a crack at given rate approaches a minimum, threshold tearing energy, T_0, when the visco-elastic work is minimised. The magnitude of this threshold tearing energy can be determined experimentally when the rubber is highly swollen with a low viscosity liquid. It can be expected therefore that swelling would have a significant effect on cyclic crack growth behaviour. However, very limited research work had been undertaken in this area. Cho *et al*[64] investigated in a limited manner the effect of swelling on cyclic crack growth for non-crystallising SBR and NBR rubbers by comparing unswollen and equilibrium swollen state as illustrated in figure 2-40. Figure 2-41 shows the effect of "equilibrium" swelling on the cyclic crack growth behaviour for two different cross-link densities. Over the range of measured tearing energies, the measured crack growth per cycle at a given tearing energy increases with increasing the extent of swelling for both unfilled SBR and NBR. However, it seems that the crack growth per cycle is not increased by a constant factor, but depends on the magnitude of the tearing energy and on the type of rubber. In figure 2-40, the slopes do not change significantly between the dry and swollen states for both SBR and NBR rubbers, which indicates that the magnitude of the power exponent β in equation (2-32) is not altered by the swelling process. However, conclusions should not be drawn from these limited results. As is described in the previous section, for non-crystallising rubbers, the cyclic crack growth increment of each cycle is considered to result from two different components known as the time dependent and cyclic crack growth components. Therefore, significant effects of frequency have been found for non-crystallising rubbers such as SBR, reflecting the time dependent

element of crack growth. It is expected that cyclic crack growth for such a highly swollen rubber would be governed mostly by the time dependent component. The magnitude of β might hence be dependant on the extent of swelling and the cyclic frequency of the testing. However, the relative contributions of the time dependent and cyclic dependent components to the total cyclic crack growth has not been studied in unswollen materials to any great extent and for swollen materials not at all. Once the magnitudes of these contributions have been determined, then the mechanisms responsible for each component of crack growth can be speculated upon.

2-5. *Tensile strength*

2-5-1. *Effect of rates and temperature*

Smith[65] investigated the effect of rate and temperature on the tensile strength at break, σ_b, for an amorphous SBR determined in uni-axial tension. The results of this work are illustrated in figure 2-42. Here, a small correction factor (θ_g/θ) has been applied to the measured values to allow for changes in the elastic modulus with temperature. These normalised values are denoted as σ_b'. It can be seen that the experimental data form reasonably parallel curves and hence the WLF superposition principal could be applicable. The strength at a given temperature is thus equal to that at another temperature provided that the rate is adjusted by the time temperature superposition principal. The master curve for tensile strength, obtained from the data shown in figure 2-42, is given in figure 2-43. This master curve shows the form expected of a viscosity-controlled process such as segmental mobility. It rises sharply with increasing rate of elongation to a maximum value at high rates when the segments cannot move and the material behaves like a brittle glass[66].

Tensile rupture may be regarded as catastrophic crack growth at the tip of an intrinsic flaw. The success of the WLF superposition for fracture criterion and tearing energy indicates that it would also hold for tensile rupture properties. However, Bueche and Halpin[67] suggested that the rate of extension at the crack tip would be much higher than the rate in the bulk of the specimen and that this difference should be taken into account in the relationship between crack growth and tensile rupture properties.

2-5-2. *The failure envelope*

Smith[68] proposed an alternative representation for tensile rupture data for unfilled SBR over a wide range of temperatures and rates of elongation as shown in figure 2-44 using the data given in figure 2-42 and 2-43. This yielded a single curve, termed the "failure envelope", when σ_b' was plotted against λ_b, which has a characteristic parabolic shape. Rate and temperature are not shown explicitly but

decreasing the temperature or increasing the rate merely shifts the rupture point in an anticlockwise direction around the envelope.

However, it should be noted, as Smith[69][70] also suggested, that the location of the failure envelope will depend on the test method. The failure envelope obtained from constant strain rate tests would be different from that derived from cyclic tests. Also, a crystallising rubber, such as NR, which does not follow the WLF relationship over a range of rates and temperatures, would not yield a simple failure envelope.

2-5-3. Strain crystallising rubber

In strain crystallising rubbers, such as natural rubber, crystallisation will take place in the high strain regions around the crack tip and this increases the extent of energy dissipation. This strain-crystallisation is reflected in the larger values of critical tearing energy, T_c, for a natural rubber compared to values for an unfilled SBR, over a wide range of rates and temperatures when the crystallisation takes place. Also, since hysteresis arising from crystallisation is not highly dependent on rate and temperature, unlike that arising from internal viscosity or segmental mobility of the material, the tensile strength of natural rubber over this range is almost independent of rate and temperature. However, Kadir and Thomas[71] suggested that at low temperatures and high rates, crystallisation cannot develop quickly enough, and hence the value of T_c is now mainly related to the polymer's glass transition temperature, θ_g. Thomas and Whittle[72] investigated the influence of temperature on the tensile strength of natural rubber. They found an abrupt drop in tensile strength with increasing temperature, characteristic of a crystallising rubber as illustrated in figure 2-45. This effect is not observed in SBR, either unfilled or carbon black filled[12][65][73]. It was initially assumed that this critical temperature was that at which no crystallisation could take place even at the highest stresses. However, tensile failure is assumed to be due to crack growth initiated at small flaws[74][75], and the local stresses at the crack tip would be substantially greater than the bulk values. Furthermore considering the fact that the tensile strength even at high temperatures is still often much greater than the tensile strength of non-crystallising rubber, it would appear that crystallisation may still occur locally even above the critical temperature.

Thomas[75] and Bell[76] compared the variation of tensile strength with increasing temperature with the variation of tensile strength with increasing initial flaw sizes at a given temperature. Figure 2-46 shows the variation of the tensile strength for unfilled NR as a function of an artificially introduced initial crack length. An abrupt fall in tensile strength occurs at a critical crack length, and this is a qualitatively similar behaviour to that observed in the variation with temperature. Thomas[75] proposed a quantitative theory to explain this general characteristic of tensile strength as illustrated in figures 2-45 and 2-46. It is proposed that a change occurs in the mechanism of rupture from essentially a catastrophic crack growth process to a cyclic crack growth process. If the initial crack size is sufficiently small then the bulk of the test piece becomes crystalline before the crack growth can take place and catastrophic crack growth process does not occur and failure is postponed until instability due to crack growth from the initial crack takes place. In regard to the variation of tensile strength with temperature, the mechanism of tensile failure above critical temperature, θ_c, is essentially a crack growth process, the critical tear strength, T_c, at these temperatures being sufficiently low that even the small naturally occurring flaws can initiate failure before the necessary stress is reached for the body of the test piece to crystallise. Conversely at a low temperature, crystallisation in the bulk of the test piece occurs before crack growth failure and the mechanism of rupture is then like the cyclic crack growth process.

Thomas[7][8] verified this theory utilising a fracture mechanics approach. For a tensile strip test piece, if crystallisation does not occur within the bulk of the specimen, failure occurs by tearing and the energy work to break, W_b, will be given as

$$W_b = \frac{T_c}{2kc} \qquad (2\text{-}12)'$$

where T_c is the critical tearing energy and c is the initial crack length. The magnitude of the critical tearing energy can be determined from a trouser tear test. However, if the bulk of the test piece crystallises, then W_b is gives as

$$W_b = \frac{1}{4kc^{1/2}B^{1/2}} \qquad (2\text{-}40)$$

where B is the crack growth constant, normally determined by the first few cycles (about 10) of cyclic crack growth measurement. Thus, equation (2-12)' and (2-40)

would describe the tensile strength of a specimen with artificially inserted cracks over the entire range of initial crack lengths. The theoretically calculated tensile strength is compared with the experimental data in figure 2-47[76]. It shows fair agreement with the experimental results over the wide range of initial crack sizes and suggests that the modelling of the failure process is correct. Only at very small crack lengths do the theoretical predictions and the experiment results diverge as the theory predicts an infinite tensile strength as the initial crack length approaches zero, which is practically unobtainable because natural flaws will always exist in the test piece.

2-5-4. Energy dissipation and strength

The variation of tensile strength with rate and temperature in accord with the WLF equation for simple visco-elastic materials was described in the previous section. Thus, energy dissipative processes have a direct influence on the fracture behaviour of rubber. Smith[77] showed a general correlation between the tensile strength and the temperature interval, θ-θ_g, between the test temperature θ and the glass transition temperature θ_g as shown in figure 2-48 where the strength of polyurethane elastomers with values of θ_g ranging from -67 °C to -17 °C is shown. In this representation all the results fell onto a single curve, which suggested again that the segmental mobility governed the strength properties.

A more striking demonstration of the close relation between energy dissipation and tensile strength was given by Grosch *et al.*[78]. They showed a direct relationship between the inputted energy density to break, W_b and the dissipated energy on extension, hysteresis energy, W_h, as plotted in figure 2-49 on double logarithmic axis. This relationship held irrespective of the mechanism of energy loss for filled and unfilled strain crystallising and amorphous elastomers. Their empirical relationship is given as

$$W_b = 410 W_h^{1.3} \qquad (2\text{-}41)$$

with W_b and W_h being measured in $J.m^{-3}$. From this it is seen that the materials that require the most energy to rupture are precisely those in which the major part of the energy is dissipated before rupture.

2-5-5. *Effect of swelling*

A substantial decrease in tensile strength occurs on swelling for unfilled and carbon black filled strain crystallising and amorphous rubbers. Dogadkin *et al.*[79] found that for lightly swollen carbon black filled natural rubber, SBR and NBR, the changes in tensile strength and breaking elongation with the degree of swelling were dependent on the nature of the swelling liquid. Grosch *et al.*[78] measured the variation of the inputted elastic stored energy density to break as a function of extent of swelling (volume fraction of rubber, V_r) for four unfilled rubbers, NR, SBR, NBR and BR as illustrated in figure 2-50. For BR, the energy density to break decreases almost linearly with decreasing volume fraction of rubber, V_r, over a wide range of V_r. For the other three rubbers a simple linear relationship holds only for low values of V_r (highly swollen state). Above a critical value of V_r, the inputted elastic energy to break rises more rapidly and both this critical V_r and the magnitude of the deviation from linearity depend on the type of rubber. For the non-crystallising rubbers the variation of the energy density to break with swelling is related directly to the internal viscosity, which they exhibit at the test temperature. Swelling reduces intermolecular cohesion and extends the molecular network by dilatational deformation. Both effects would be expected to reduce the tensile strength and breaking elongation. Taylor[80] suggested that if the second effect only is considered, the breaking extension ratio, $(\lambda_b)_s$ would be given as

$$(\lambda_b)_s = K_s V_r^{1/3} \qquad (2\text{-}42)$$

where V_r is the volume fraction of rubber in the swollen state and K_s is a constant. The results expressing the dependence of $(\lambda_b)_s$ on swelling ratio for unfilled NR and SBR plotted as a function of $V_r^{1/3}$ are shown in figure 2-51[81]. The dependence is substantially as predicted. However at low degrees of swelling, the deviation from equation (2-42) is significant, which clearly suggests a large effect on intermolecular cohesion for small extent of swelling.

2-6. *Summary and aims of this study*

Crack growth in rubber has been successfully described utilising a fracture mechanics approach in terms of the tearing energy (equivalent to an elastic energy release rate)[7-9]. The tearing energy, T, is defined as the total energy required to create new fracture surfaces and to grow a crack at a given rate and is given by equation (2-5).

The magnitude of T for a given crack growth rate is mainly determined by the total visco-elastic work done at the crack tip. This in part is determined by the volume of material in the tip region, which is related to the crack tip diameter and increases with an increase in the crack tip diameter[11-17]. This has been confirmed by carrying out cutting experiments[15-17] and hence restricting the crack tip diameter artificially during crack growth. However general research works in this area is very limited, because of the difficulties in determining the actual crack tip diameter experimentally. The mechanism of crack tip blunting, increase in crack tip diameter with decreasing crack growth rate, could be associated with the visco-elastic behaviour of the rubber and its inherent structure, expressed as the distance between cross-links. The reasons for such effects on crack tip diameter is not at all clear. There is clearly a need for more detailed research work to clarify what determines the variation of the crack tip diameter as a function of tearing energy, crack growth rate, visco-elastic properties and chemical structure of the rubber.

Especially for non-crystallising rubbers, the magnitude of T depends on crack growth rate and temperature in a manner, which follows the visco-elastic properties (energy dissipation process) as predicted by the WLF relationship[25][26][31]. With increasing rate and decreasing temperature, visco-elastic work increases hence the magnitude of T increases. It is known that the magnitude of T approaches a minimum value, which is called as threshold tearing energy, T_o, when the visco-elastic work is minimised and the major work to be done is that to break chemical bonds[20-22]. There are a number of techniques to reduce the magnitude of visco-elastic effects, such as, increasing the extent of swelling, elevating the temperature, reducing the rate or increasing the cross-link density of the rubber. However, the swelling technique solely reduces the visco-elastic work without altering the basic chemical structure of the rubber. Therefore, the swelling technique is a rational method for investigating

crack growth behaviour as swelling to different extents makes it possible to study the effect of visco-elastic work on crack growth independently and sensitively.

It is thought that rubber can cavitate under hydrostatic tension, and that the stresses necessary for cavitation are of the order of the Young's modulus of the rubber[31][37-40]. Just ahead of an advancing crack, high stresses must be developed locally to break the primary chemical bonds. It has been suggested that a possible mechanism of crack growth is the intersection of the major crack with cavities ahead of the crack. The extent of this would be associated with the magnitude of fracture surface roughening. A limited amount of research work has been carried out on the relationship between crack growth behaviour and cavitation with changing experimental conditions, such as the pressure and the thickness of the specimen[31][42][48]. If crack growth occurs under pressure, the cavitation process will be suppressed, hence, the crack growth behaviour and the fracture surface will be affected. With decreasing the thickness of the specimen, the stresses through the thickness will be decreased due to the plane stress condition, hence crack growth behaviour and the fracture surface will also be affected. However, in spite of such experiments being carried out, evidence of cavitation playing a principal role in the crack growth process has not been confirmed conclusively.

For a non-crystallising rubber, a large discrepancy exists in the tearing energy against rate relationship obtained from static, constant T, crack growth and from constant rate of grip separation measurement[8]. Most crack growth measurements have been carried out in constant rate of grip separation test because of the experimental simplicity and time efficiency. However static, constant tearing energy, crack growth measurement is a more useful experimental technique from which to obtain fundamental and spontaneous crack growth behaviour in rubber under a given stress field. For a non-crystallising rubber, it is found that static crack growth behaviour can be represented by three regions on a plot of tearing energy against rate relationship, with clear transition points as illustrated in figure 2-24[31]. This behaviour cannot be observed in constant rate of grip separation tests. At fast crack growth rate (region-C) surfaces are very smooth, like a glassy fracture and cracks grow at a constant rate in a manner controlled by the visco-elastic behaviour of the rubber, being scaled by the WLF relationship. At low crack growth rates (region-A) the cracks grow in fairly steady manner but the fracture surface is now clearly rough.

In intermediate region (region-B) crack growth takes place in a stick-slip manner with a resultant rough and smooth surface. This abrupt change in crack growth behaviour between region-A and -C seems to be associated with a distinct change in surface roughness due to the crack tip blunting. It has been suggested that this surface roughening observed in region-A results from the intersection of the propagating major crack with growing cavities. At fast crack growth rates in region-C, it is suggested that the elastic modulus ahead of the crack tip increases substantially suppressing cavity growth. However, this process and the detailed mechanisms of static crack growth behaviour have not been fully investigated. The basis and mechanism of the transitions in crack growth behaviour needed to be evaluated.

Part of the present work was undertaken in an attempt to further this understanding of the mechanism of the transition in static crack growth behaviour as illustrated in figure 2-24, particularly in light of the cavitation concept. It was proposed to carry out crack growth experiments on a non-crystallising rubber, SBR, with widely different visco-elastic properties achieved by swelling with liquids, varying temperatures, cross-link densities and by filling with carbon black. Hence, the main purpose of this study was to investigate the effect of the magnitude of visco-elastic losses (energy dissipation) on the rough to smooth fracture surface transition and hence the crack tip behaviour. Crack growth experiments were also carried out on specimens of different thicknesses, which would have different magnitude of dilatational stresses ahead of the crack tip, with hence a different propensity to cavitate.

Cyclic crack growth behaviour can also be described in terms of the tearing energy concept[51-53]. It is well known that the relationship between the crack growth per cycle, $dc\ dn$, and the tearing energy, T, is a characteristic for a given rubber and that this relationship is independent of the test piece geometry. In the case of the representation of cyclic crack growth data, it is generally assumed that the cracks grow at the maximum tearing energy during a cycle. Furthermore, the crack growth per cycle is not much influenced by the way in which this maximum tearing energy is reached even for a relatively viscous material. The crack growth per cycle can be represented as $dc\ dn=B(T\ T_u)^{\beta}$ (equation2-32), where B and β are material constants. For most rubber vulcanizates, the value of exponent β lies between 2 and 6,

depending strongly on the type of rubber and to a lesser extent on other factors such as the cross-link density and the type of cross-link. It tends to be lower if the rubber exhibits a higher mechanical hysteresis, since cyclic crack growth is mainly governed by energy dissipative process arising from internal molecular motion and from strain-crystallisation.

As has been fully described throughout this chapter the magnitude of the tearing energy is significantly influenced by the visco-elastic properties of the rubber[20-22]. If the rubber is highly swollen with a low viscosity liquid, the magnitude of the tearing energy decreases. It is hence expected that swelling a rubber will significantly influence its cyclic crack growth behaviour. However very limited research has been carried out in this area. Therefore, in this study, an experimental investigation was carried out in an attempt to clarify the effect of swelling on cyclic crack growth behaviour.

The increment of crack growth during each cycle is considered to result from the sum of two different components; the time dependent component and the cyclic growth component[52][53]. The first depends only on the length of time of a cycle and on the maximum tearing energy. The second is genuine cyclic growth, the extent of which depends on the details of the loading and unloading process. For a non-crystallising rubber, significant effects of cyclic frequency on cyclic crack growth behaviour have been found, reflecting the time dependent element of crack growth. With increasing frequency, the measured crack growth per cycle at a given tearing energy decreases as the cyclic growth component dominates the crack growth process. However, the relative magnitude of the contribution of these two components the cyclic crack growth behaviour is unknown. The element of time dependent crack growth per cycle can be predicted using static, constant tearing energy, crack growth measurement. It should hence be possible to determine the relative contributions by utilising static crack growth measurement and cyclic crack growth measurements at different cyclic frequencies. In addition experiments on specimens swollen to different extents should help to elucidate the mechanism of cyclic crack growth for each component.

The tensile strength of rubber is also significantly influenced by the visco-elastic properties arising from mechanical hysteresis and strain induced crystallisation[65-67][71]. It has been shown that the failure of rubber is initiated from

flaws or stress raisers present in rubber. For a strain-crystallising rubber, an abrupt drop in strength as a function of initial flaw size or temperature of test is observed[75][76]. The mechanism of this abrupt fall is thought to be the change in mechanism from a catastrophic crack growth process to a cyclic crack growth process. If the rubber is highly swollen, it can be expected that this change in mechanism will be dependent on the extent of swelling as the visco-elastic losses decreases. However, the effect of swelling on tensile strength in terms of initial flaw sizes has not been investigated. Such an investigation was carried out here and the static and cyclic crack growth data were used to model the results.

Table 2-1 WLF parameters

Polymer	θ_g (K)	C_{W1}	C_{W2} (K)
Poly(1,4-butadiene)	172	11.2	60.5
Natural Rubber (cis-1.4.polyisoplene)	200	16.8	53.6
Poly-isobutylene	205	16.6	104.4
Universal Constants	-	17.4	51.6

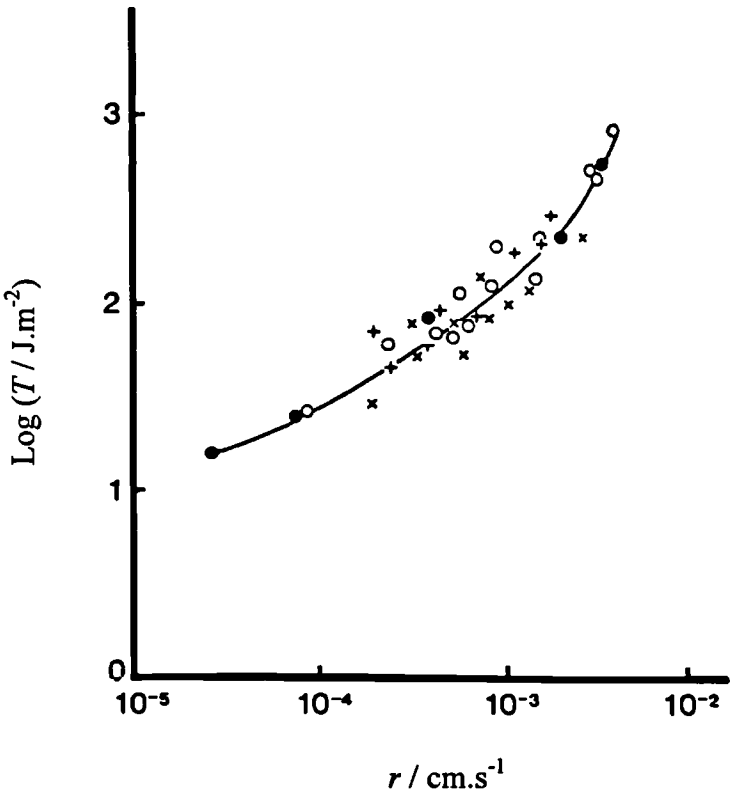

Figure 2-1. The tearing energy (T) as a function of crack growth rate (r) for an unfilled SBR using variety of test piece geometries, shown in figure 2-2 (a), (b), (c), and (d): x, simple extension (trousers); +, pure shear; o, split; •, angled[8].

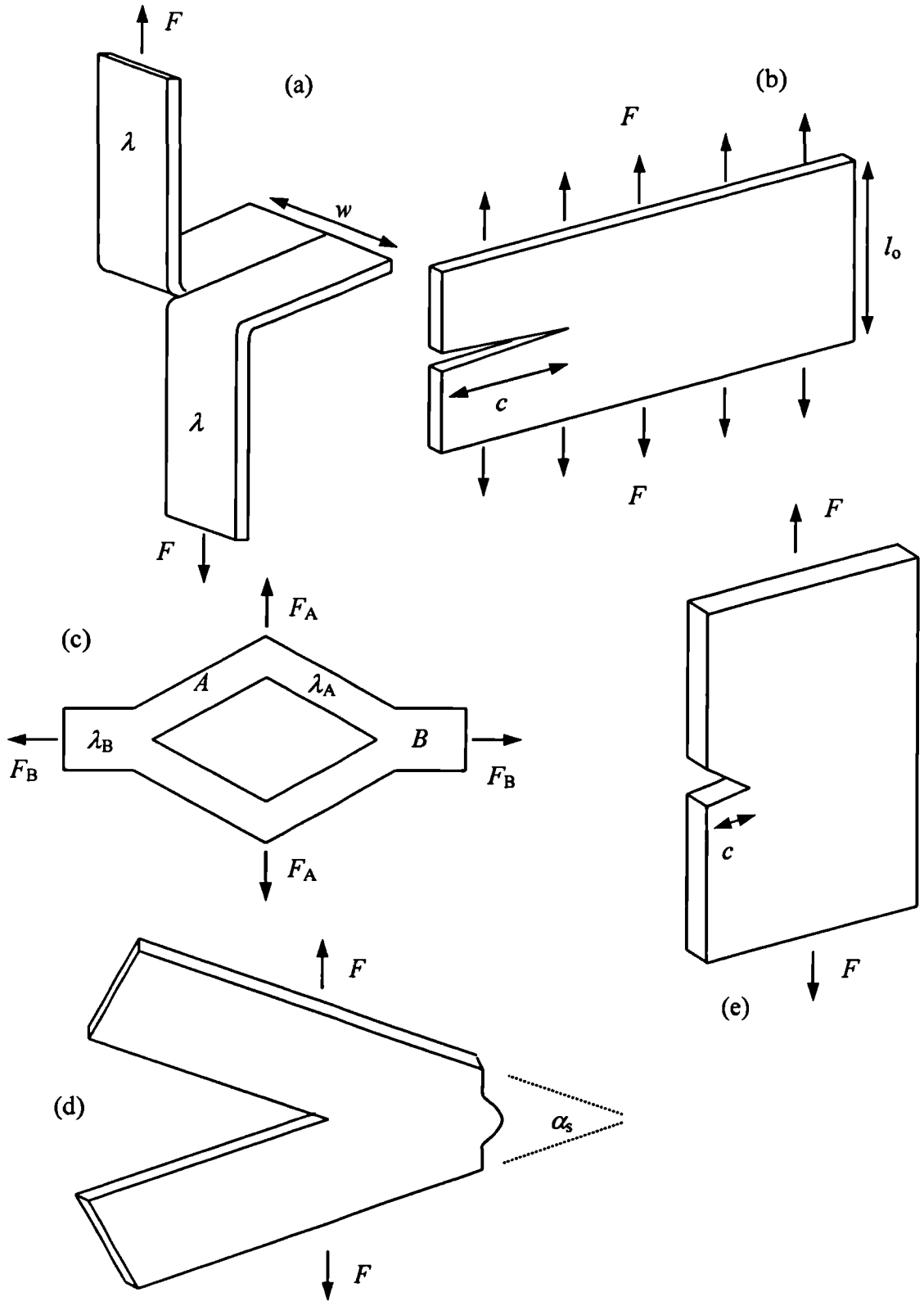

Figure 2-2. Types of test pieces for which the tearing energy for a given crack growth rate can be calculated; (a)simple extension (trouser)[7],(b) pure shear[7], (c)split[8], (d)angled[9] and (e)tensile strip (edge crack)[7].

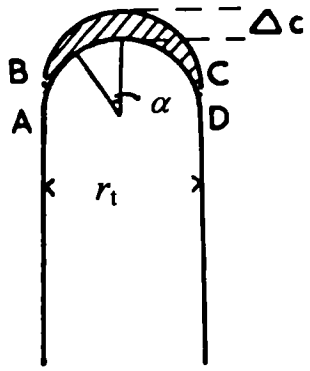

Figure 2-3. Schematic diagram for the shape of a crack tip used in equation (2-14)[11].

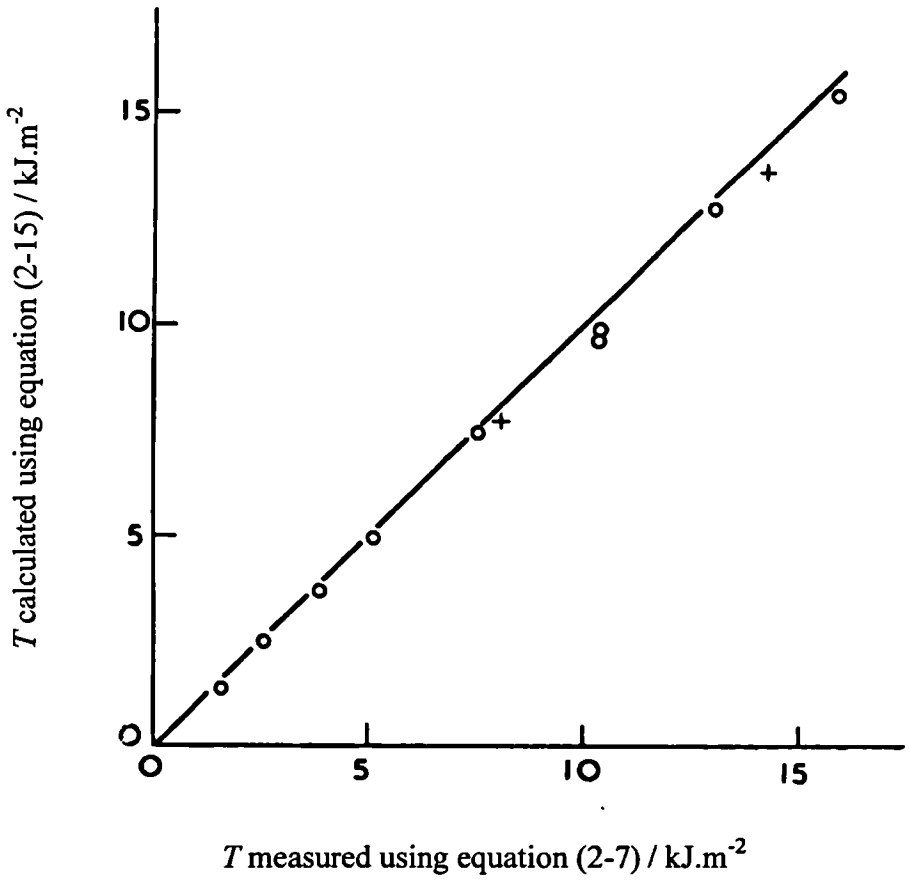

Figure 2-4. Plot of the comparison of the magnitudes of tearing energy calculated from equation (2-7) and (2-15)[11].

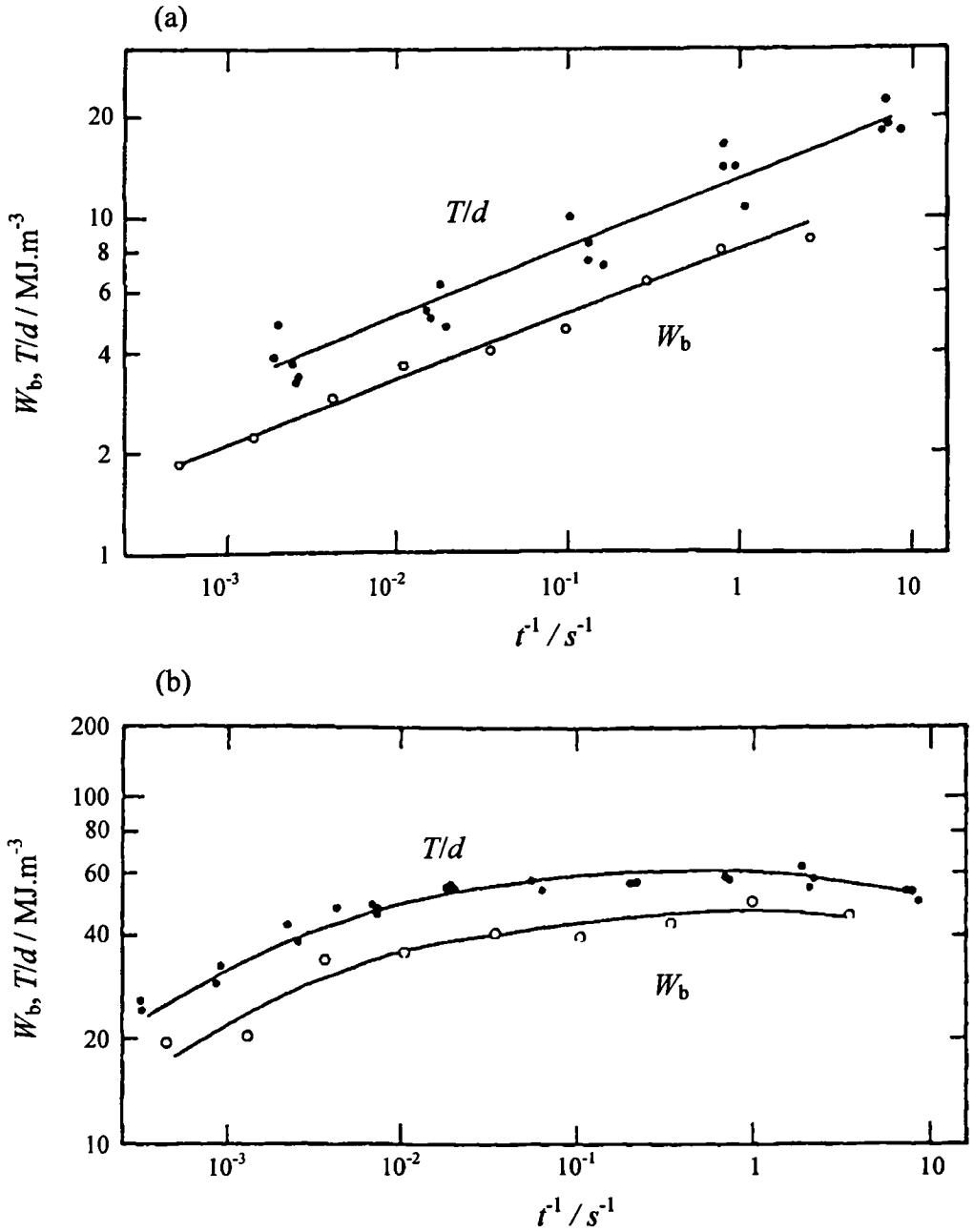

Figure 2-5. Comparison of the work to break per unit volume, W_b, and the tearing energy, T, to initiate crack growth at an incision at 25°C (a) for an unfilled SBR (b) for a SRF carbon black filled SBR[12].

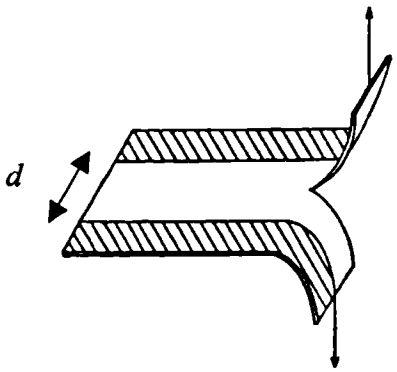

Figure 2-6. Schematic figure showing a modified trouser tear method of crack growth measurement[14].

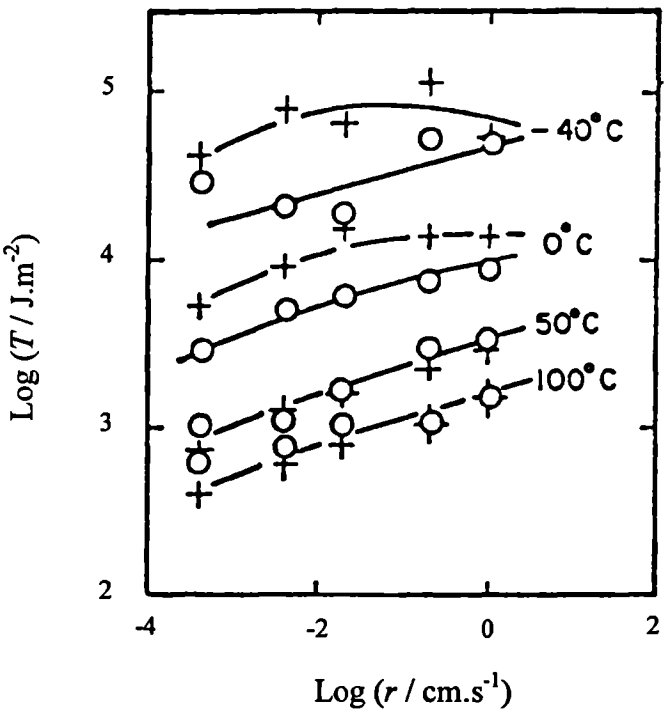

Figure 2-7. Experimental relationship for the measured tearing energy of an unfilled SBR vulcanizate as a function of crack growth rate at various temperatures. +; wide gap test piece (0.3cm), o; narrow-gap test piece (0.01cm)[14].

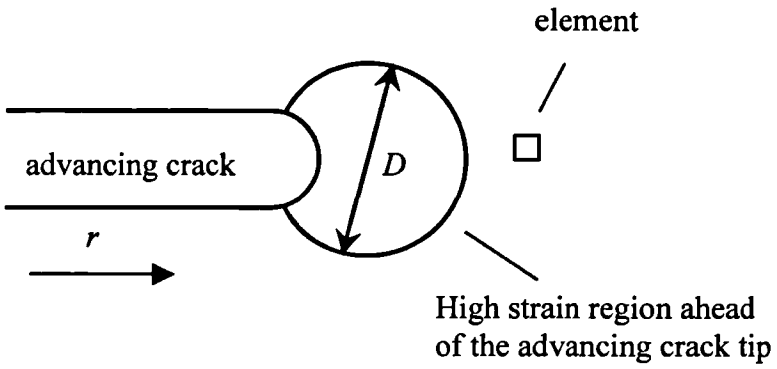

Figure 2-8. Schematic diagram illustrating the role of the high strain region ahead of an advancing crack tip.

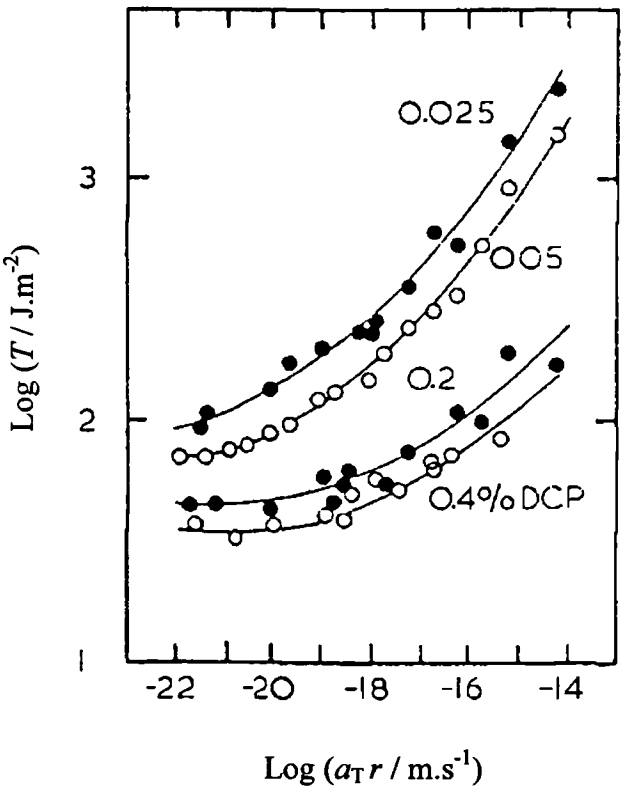

Figure 2-9(a). Tearing energy, T, as a function of effective crack growth rate, $a_T r$ at θ_g for unfilled SBR cross-linked to various extents with Dicumyl Peroxide (DCP)[21].

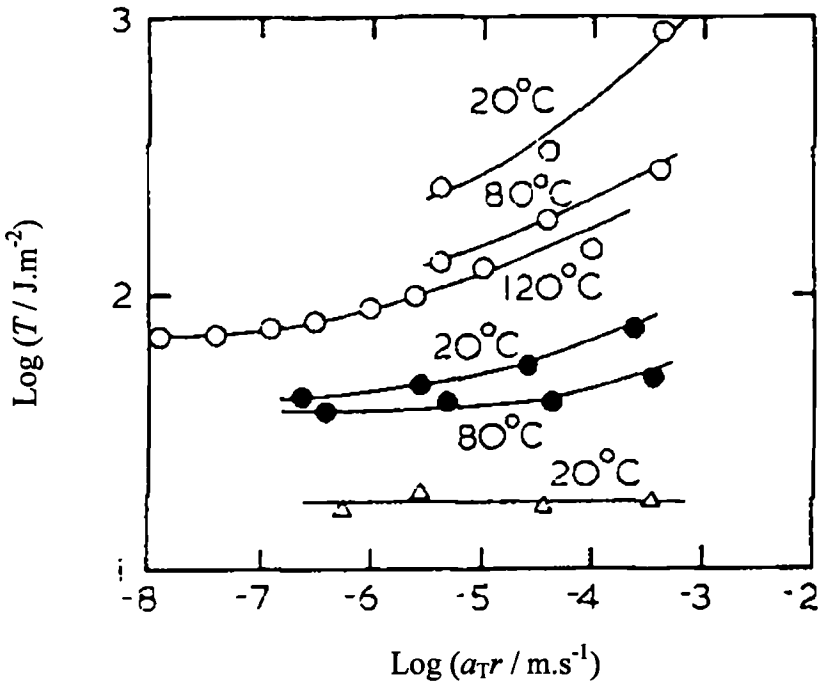

Figure 2-9(b). Effect of temperature and swelling on the tearing energy for an unfilled SBR; o, unswollen (V_r 1.00); •, swollen by Paraffin oil (V_r 0.39); Δ swollen by m-xylene (V_r 0.15)[21].

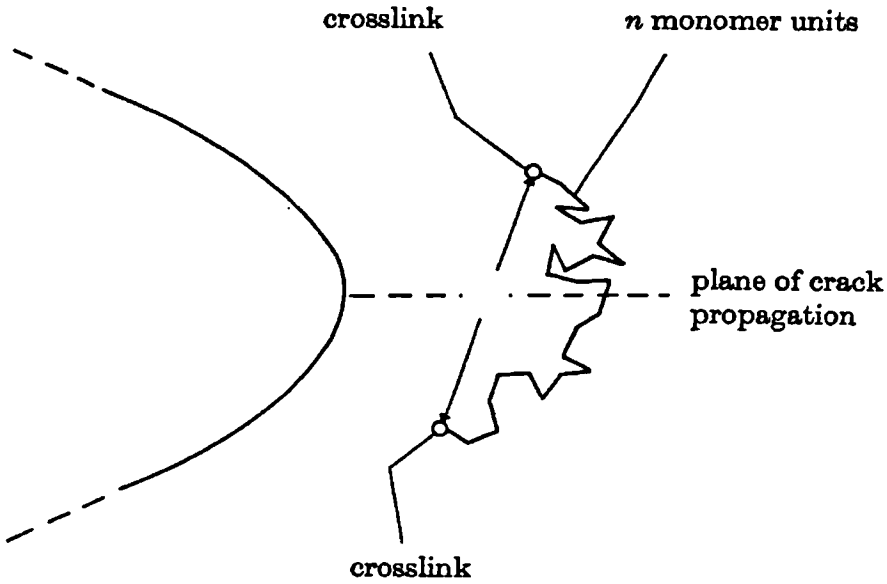

Figure 2-10 Schematic diagram showing a polymer chain lying across the plane of crack propagation[23].

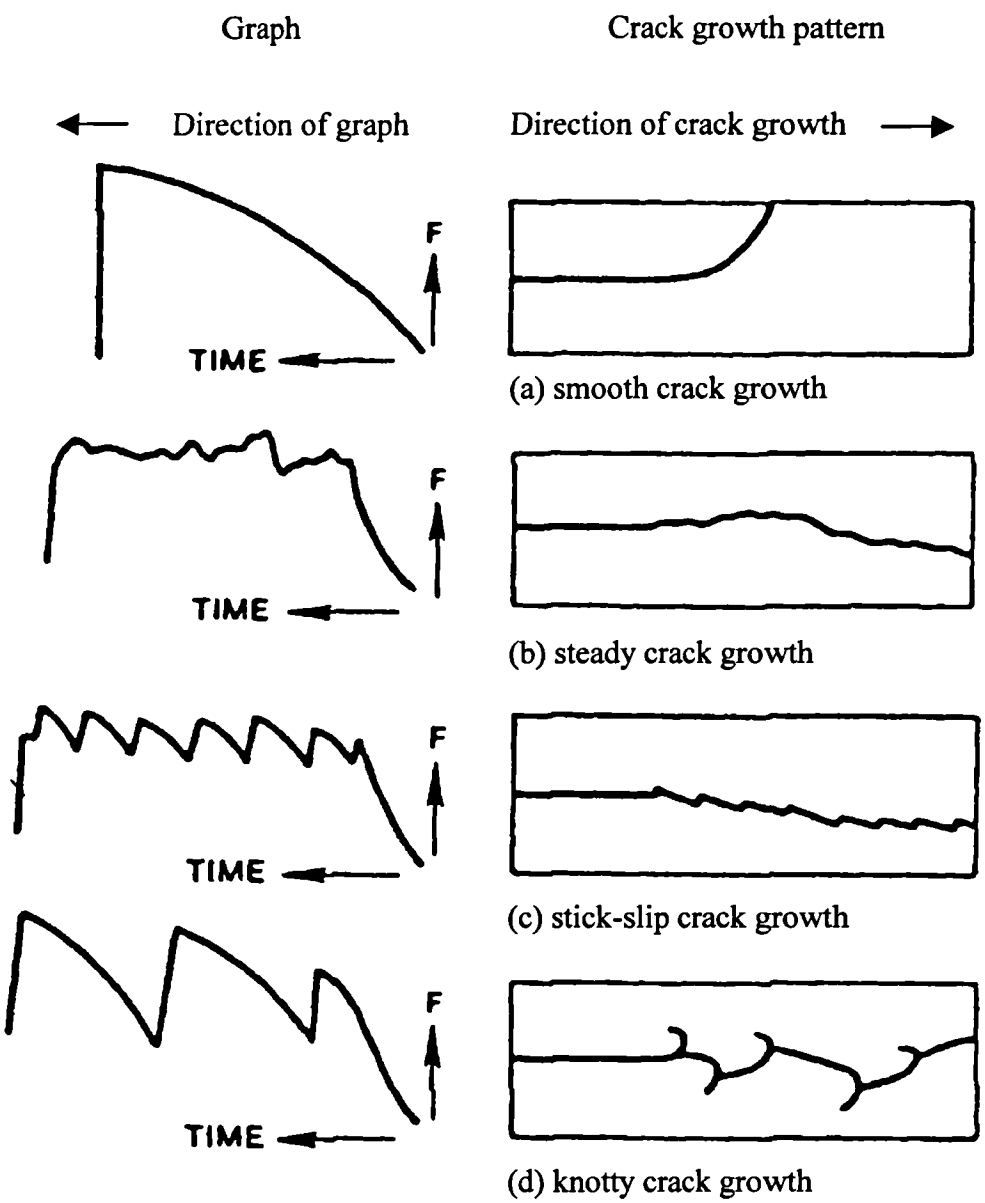

Figure 2-11. Schematic diagrams illustrating force–time relationships and crack paths for different types of crack growth.

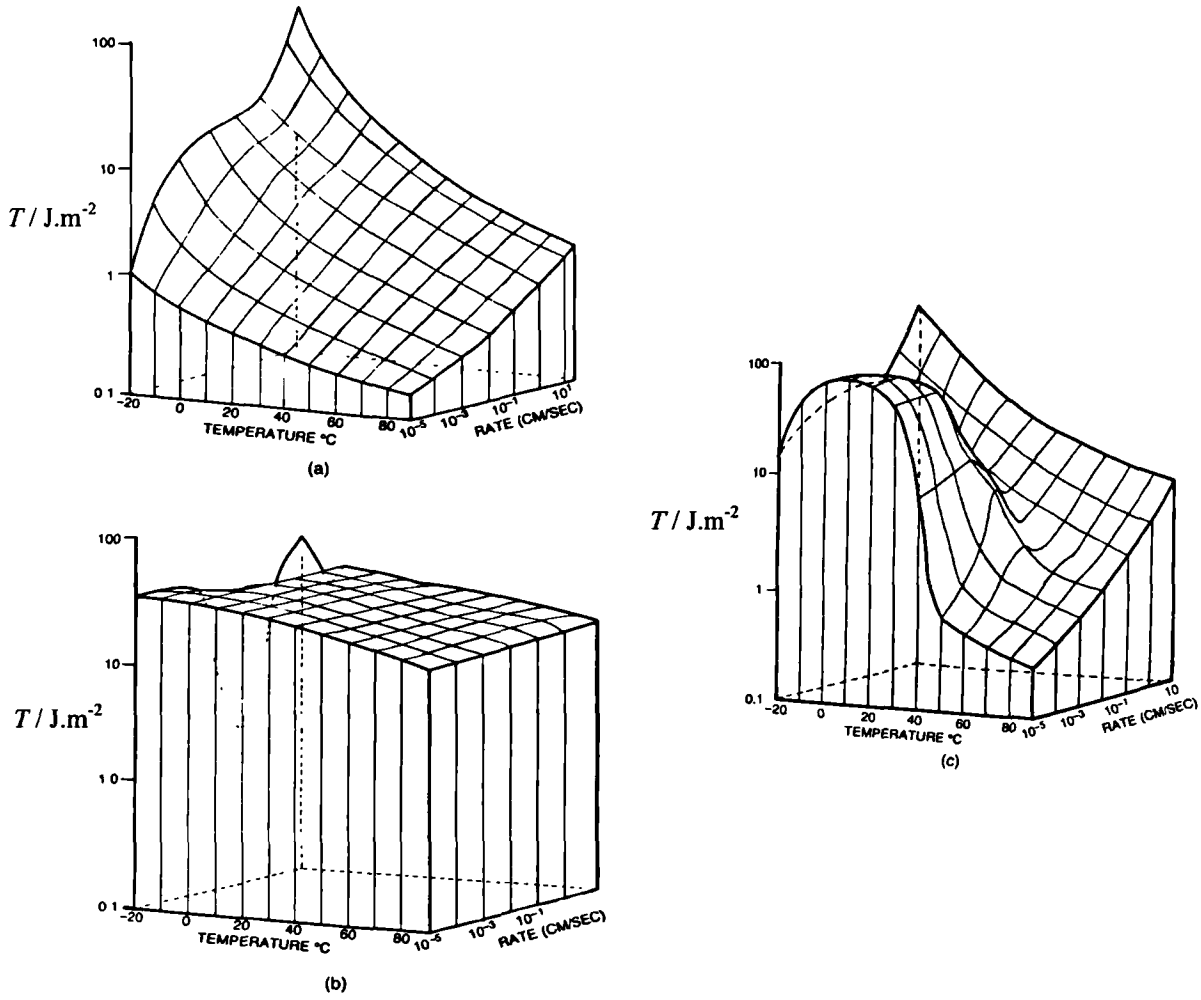

Figure 2-12. The effect of crack growth rate and temperature on tearing energy for (a) unfilled SBR, (b) unfilled NR and (c) FT black filled SBR[18].

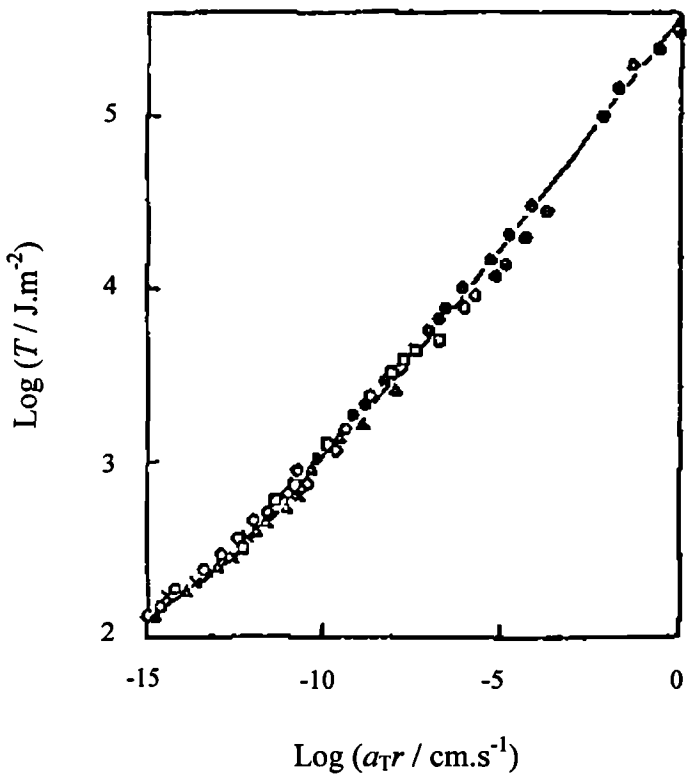

Figure 2-13. WLF master relation for the tearing energy for an unfilled SBR measured over a range of rates and temperatures[32].

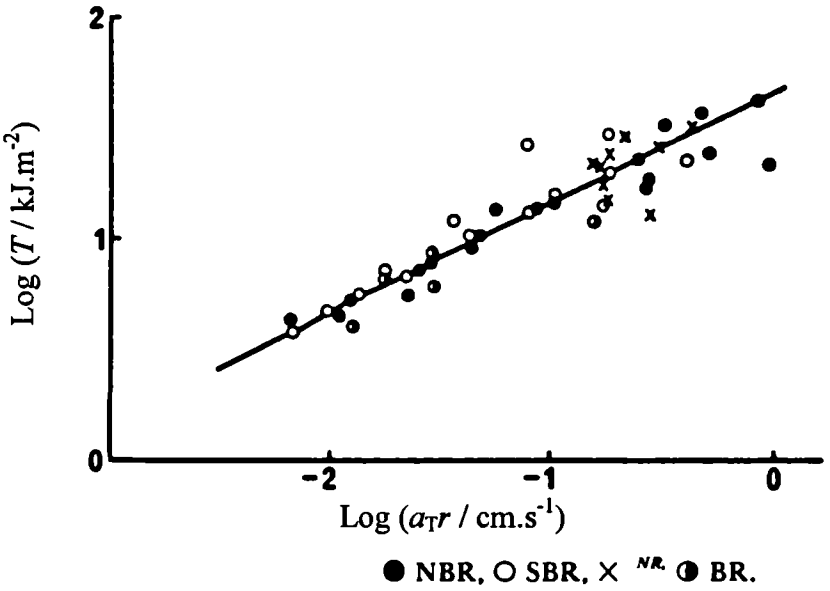

Figure 2-14. WLF master relation for the tearing energy using the data from the smooth fracture surface region for a range of materials[31].

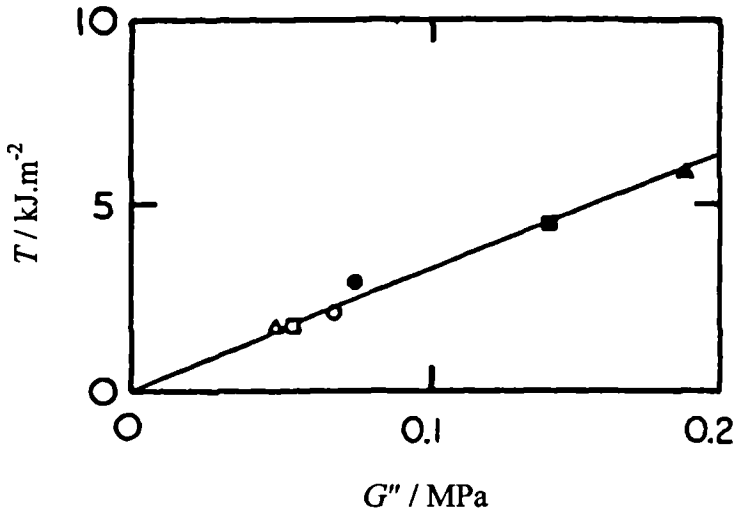

Figure 2-15. Tearing energy versus shear loss modulus for six unfilled amorphous rubbers[32].

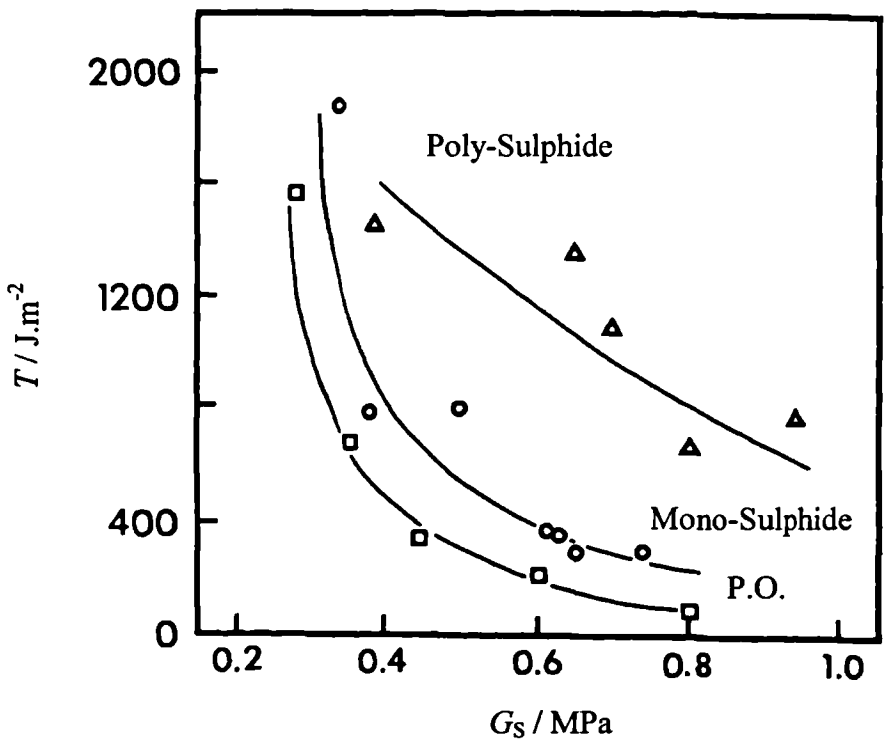

Figure 2-16. The effect of the vulcanising system and cross-link density on the crack growth behaviour for unfilled NR at a crack growth rate of $10\mu m.s^{-1}$[34].

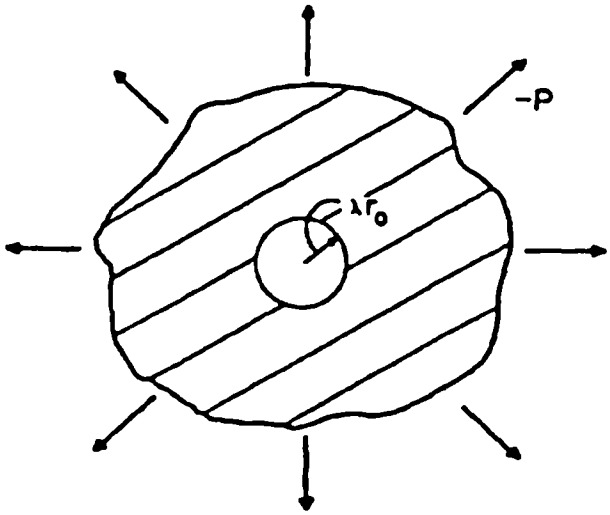

Figure 2-17. Schematic figure illustrating the expansion of a cavity under tri-axial tension.

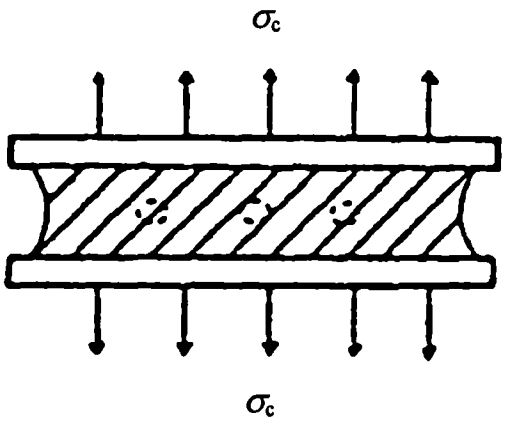

Figure 2-18. Schematic figure illustrating cavitation in a bonded block.

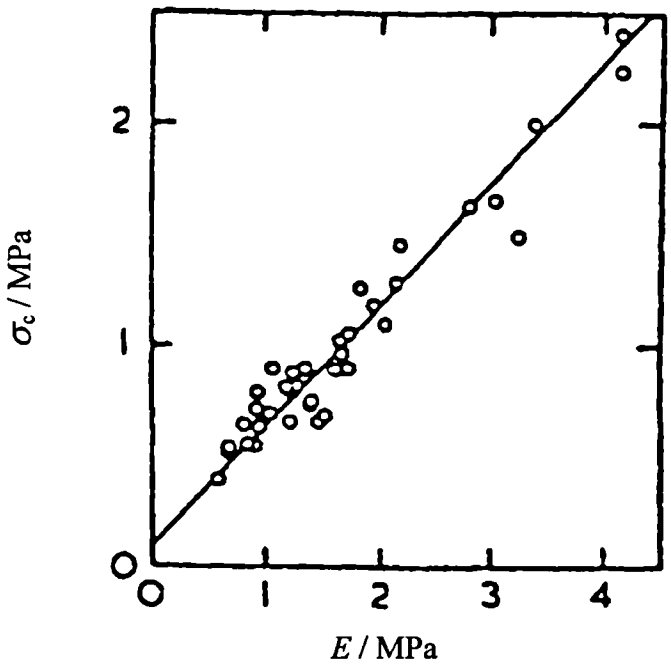

Figure 2-19. Critical applied stress for cavitation in bonded blocks versus Young's modulus[37].

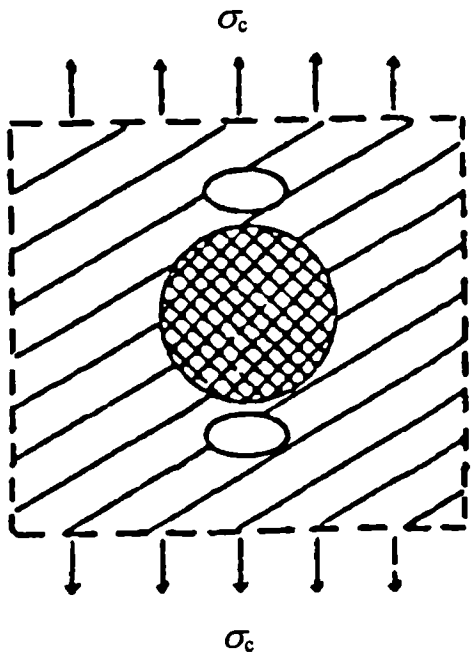

Figure 2-20. Schematic figure illustrating cavitation near a rigid inclusion.

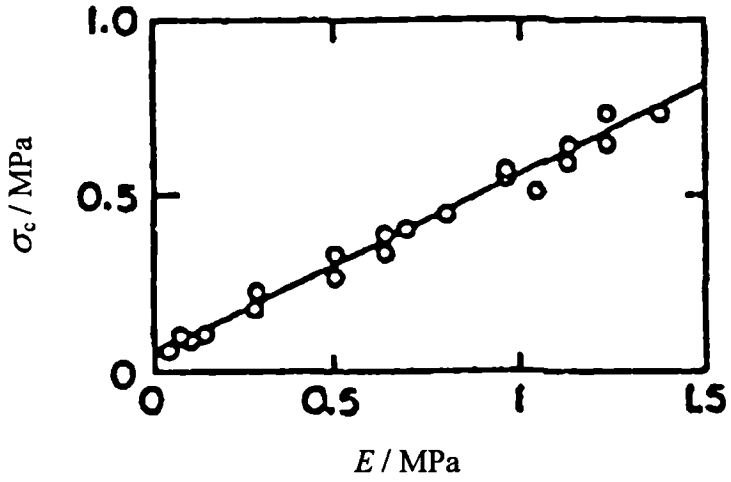

Figure 2-21. Critical applied stress for cavitation near a rigid inclusion versus Young's modulus[40].

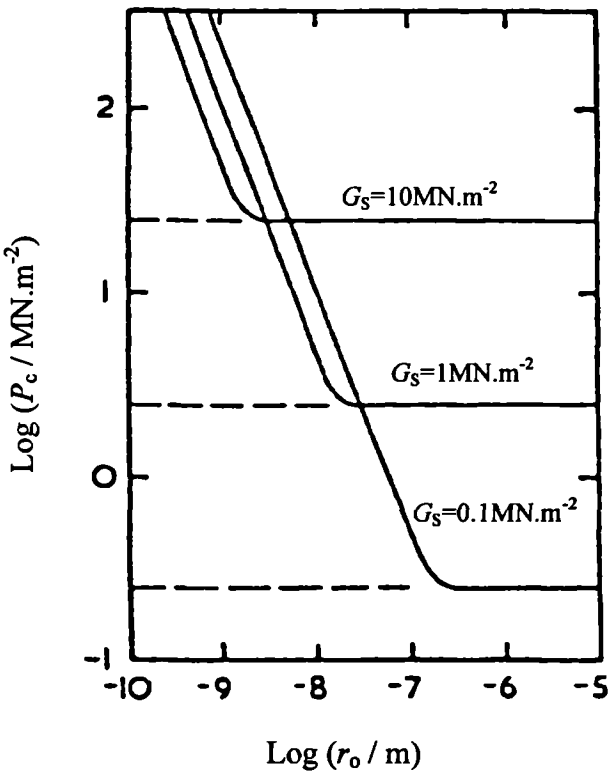

Figure 2-22. Theoretical cavitation stress P_c versus initial radius r_o of a spherical cavity for elastomers of various shear modulii G_S[39].

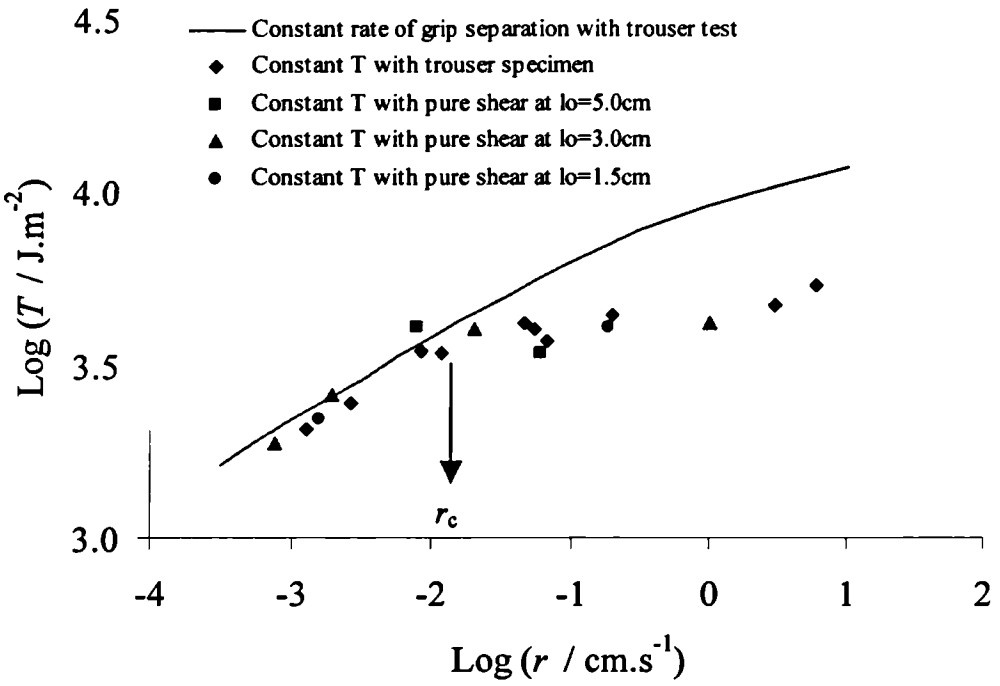

Figure 2-23. Comparison of tearing energy versus crack growth rate data from static, constant tearing energy, crack growth and constant rate of grip separation crack growth measurement[8].

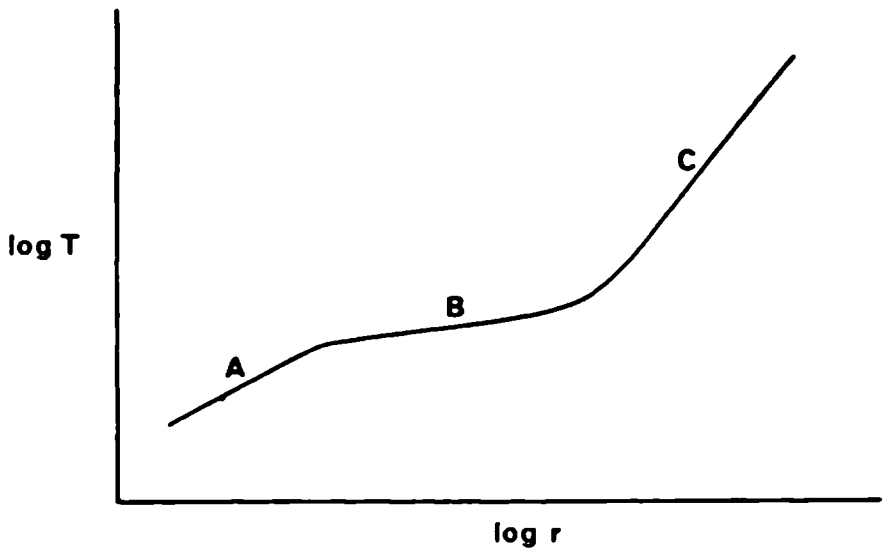

Figure 2-24. Schematic diagram illustrating a tearing energy against rate relationship. (A; rough surface, B; stick-slip behaviour, C; smooth surface)[31]

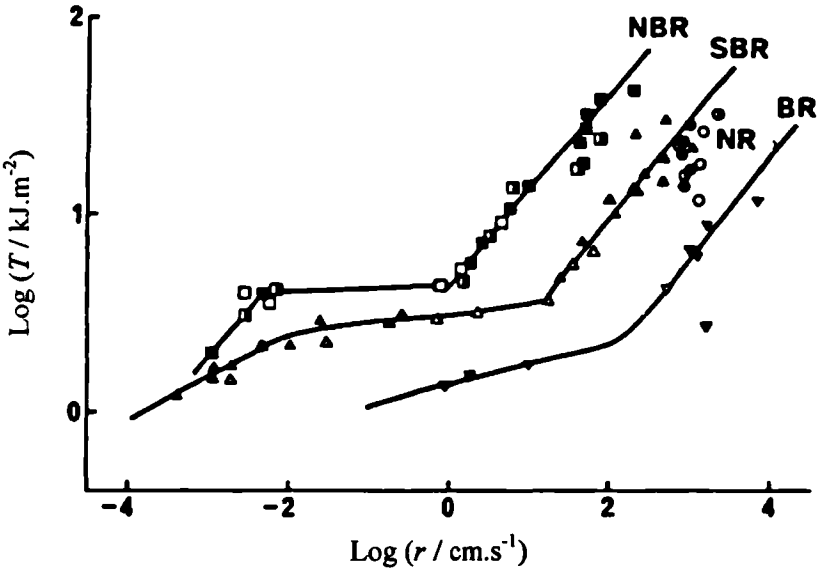

Figure 2-25 Tearing energy against rate relationship for four different rubbers determined using a pure shear test specimen in static, constant T, crack growth measurements[31].

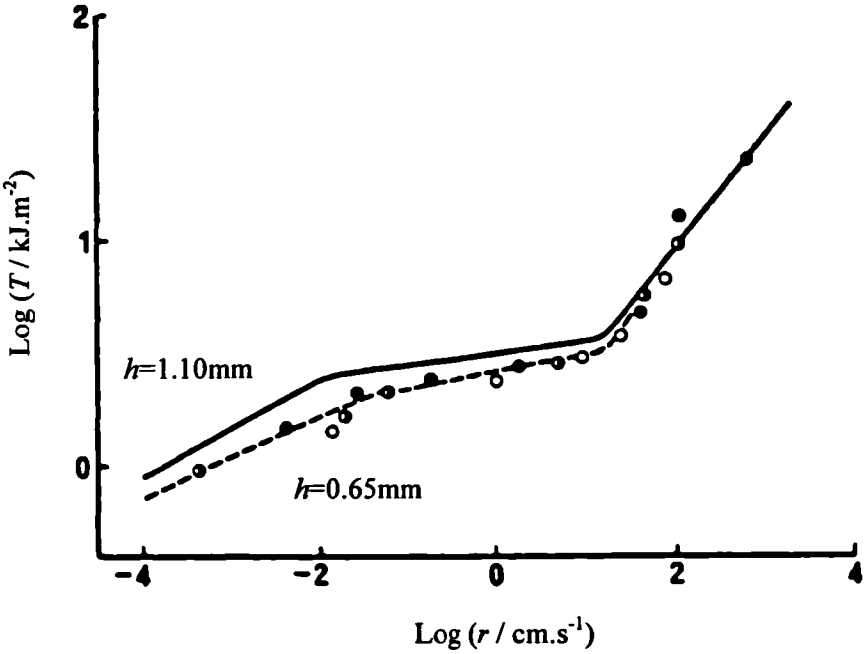

Figure 2-26 Tearing energy against rate relationship for unfilled SBR of different specimen thicknesses. The dashed curve is for test pieces of 0.65mm thickness and the full curve is for test pieces of 1.10mm thickness[31].

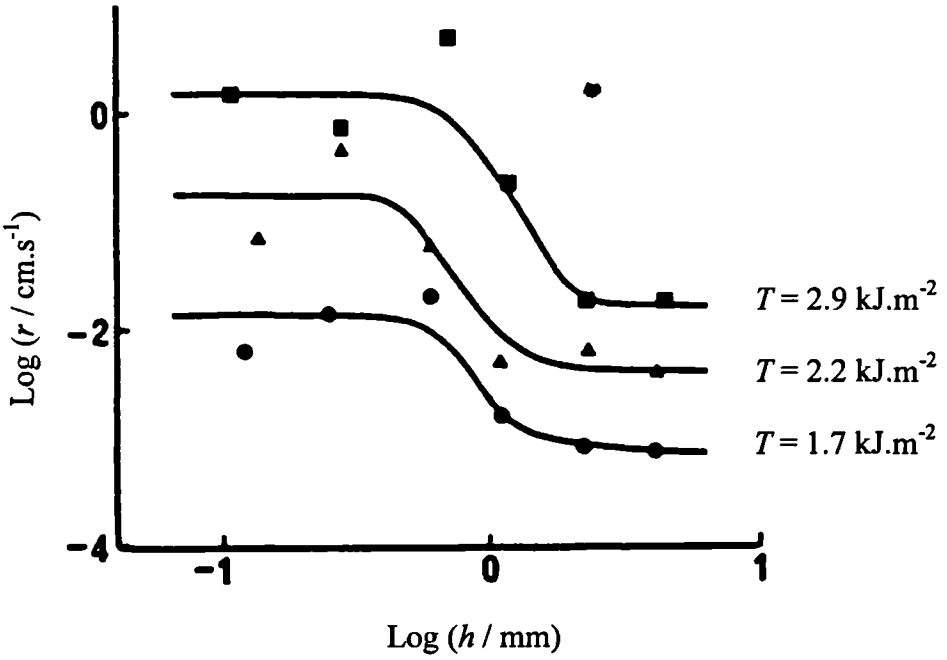

Figure 2-27. Effect of the specimen thickness on crack growth rate, r, at different tearing energies for unfilled SBR[31].

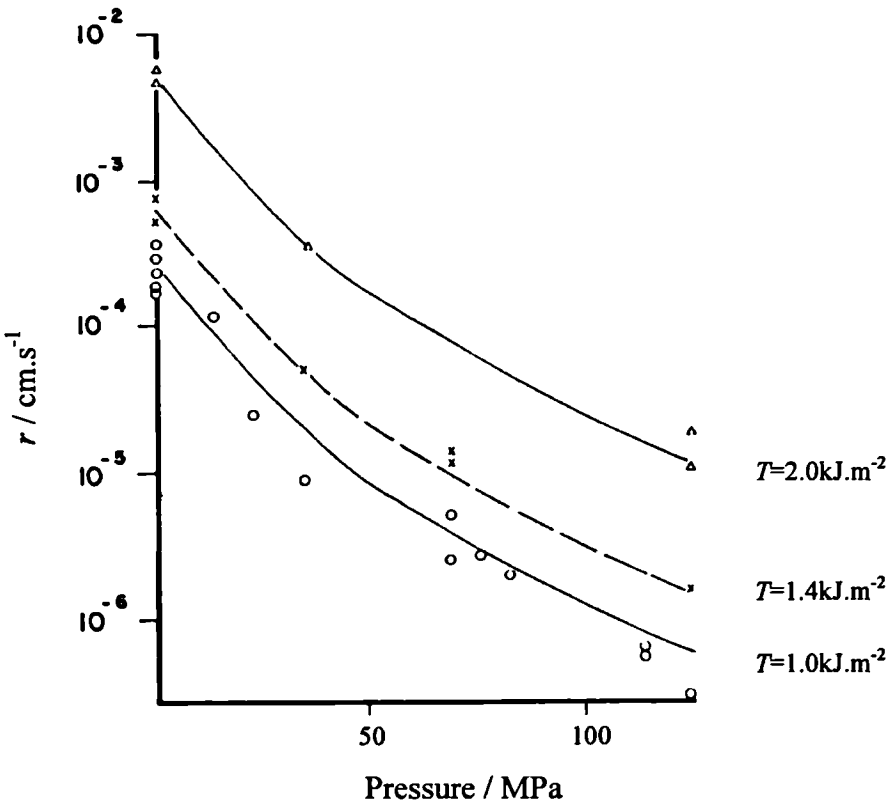

Figure 2-28. Time dependent crack growth rate, r, (logarithmic scale) versus pressure for unfilled SBR at 20°C at various T values[42].

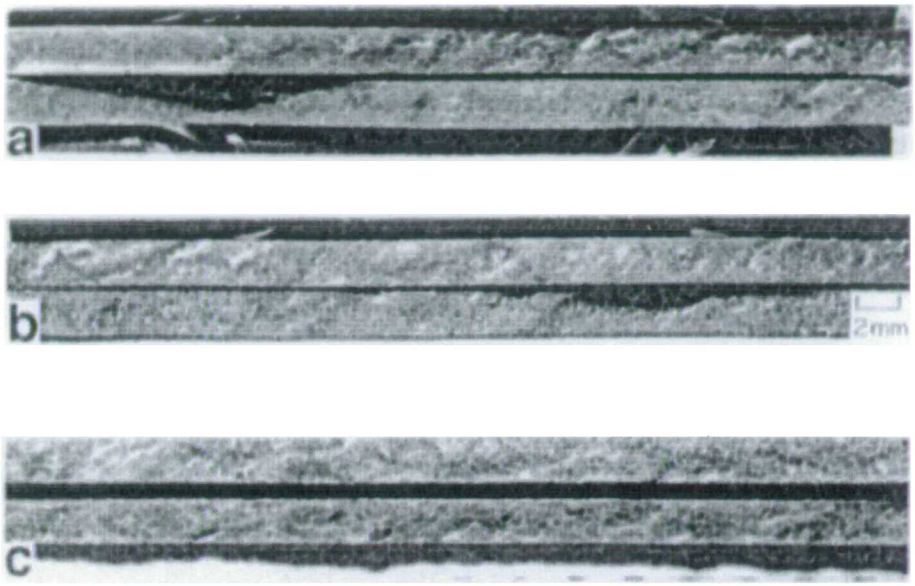

Figure 2-29. Photomicrographs of fracture surfaces for various test pressures for an unfilled SBR vulcanizate at 20°C, obtained at T=1.9kJ.m^{-2} at hydrostatic pressures of (a)0.1MPa, (b)36MPa and (c)124MPa[42].

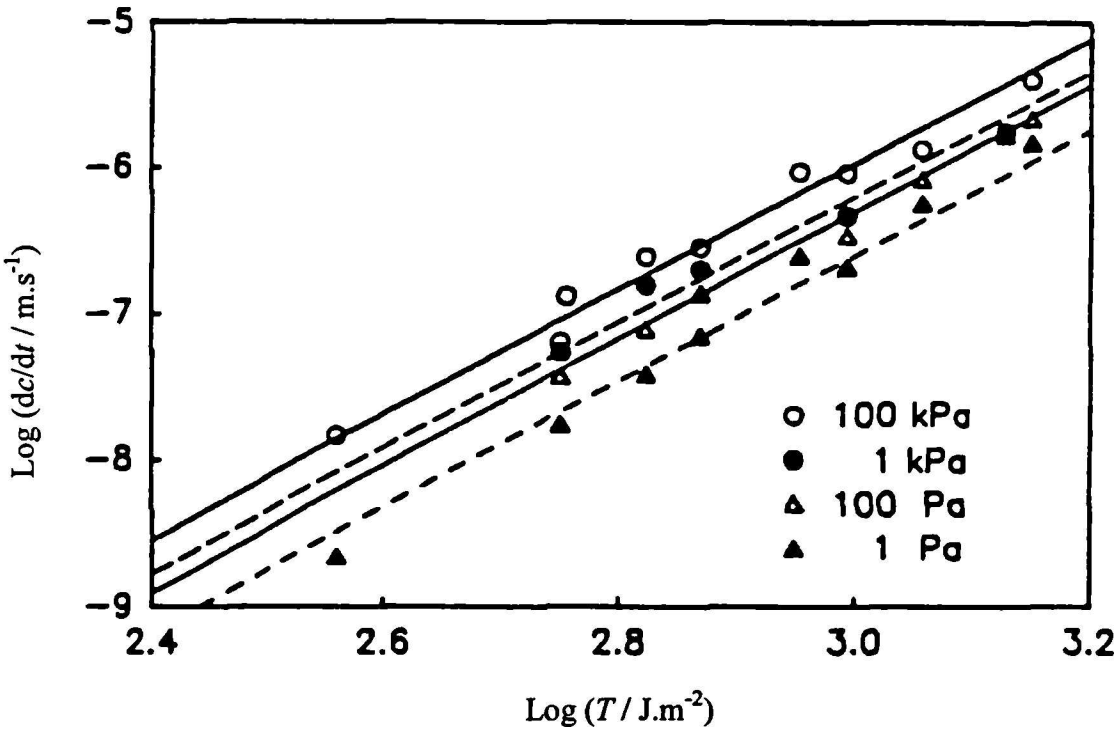

Figure 2-30. The effect of air pressure on the tearing energy against rate, dc/dt, relationship for unfilled SBR[48].

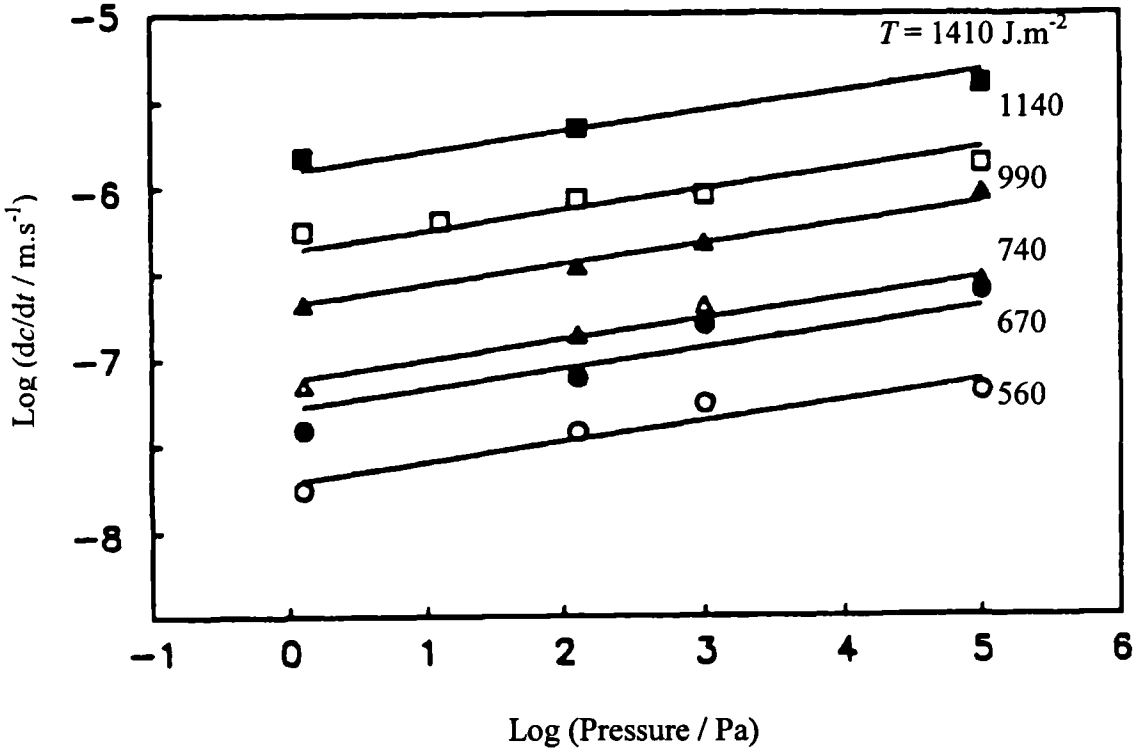

Figure 2-31. Crack growth rate against air pressure relationship for unfilled SBR at various tearing energies obtained using pure shear test specimens[48].

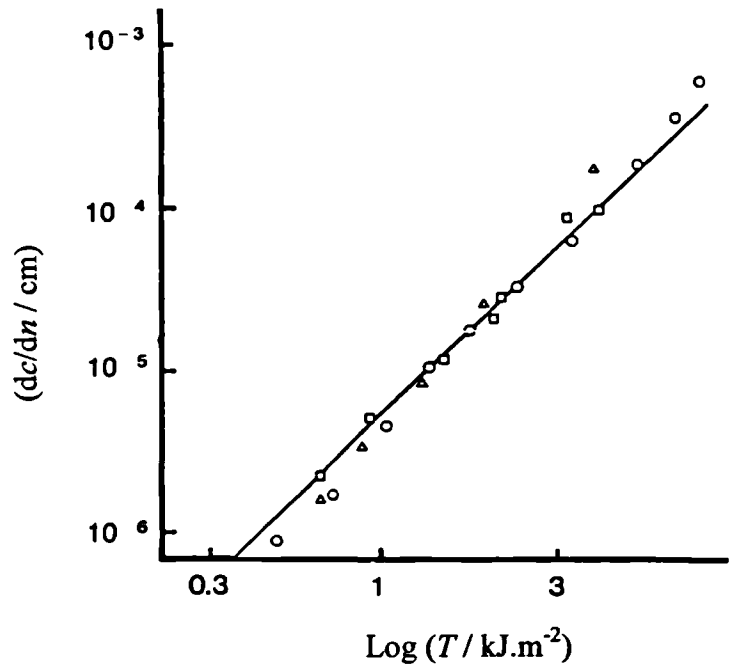

Figure 2-32. Crack growth per cycle, d*c*/d*n*, as a function of the maximum value of the tearing energy, *T*, during a cycle for an unfilled NR obtained using various test piece geometries. (□)trousers, (Δ)pure shear, (o)tensile strip with edge crack[51].

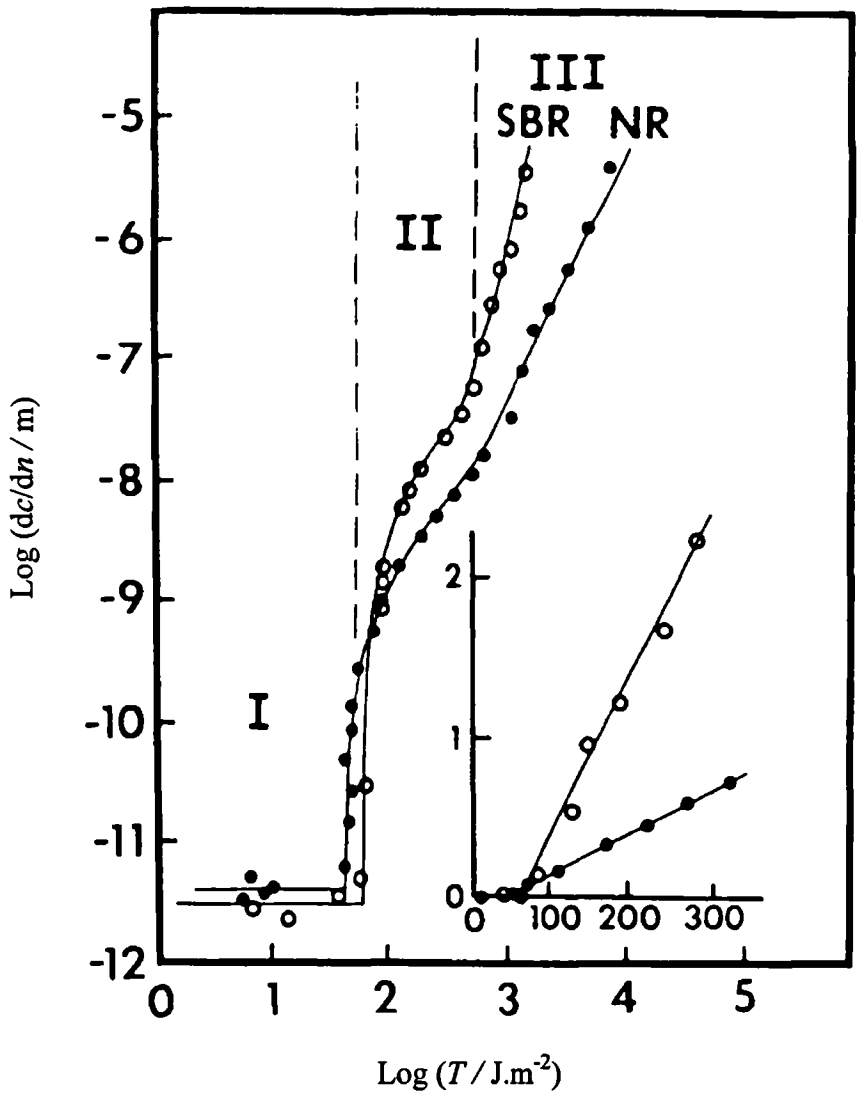

Figure 2-33. Crack growth per cycle, dc/dn, as a function of tearing energy, T, for unfilled NR (•) and SBR (o). The inset shows the region near the threshold tearing energy for mechanical fatigue, T_o, plotted on a linear scale[49].

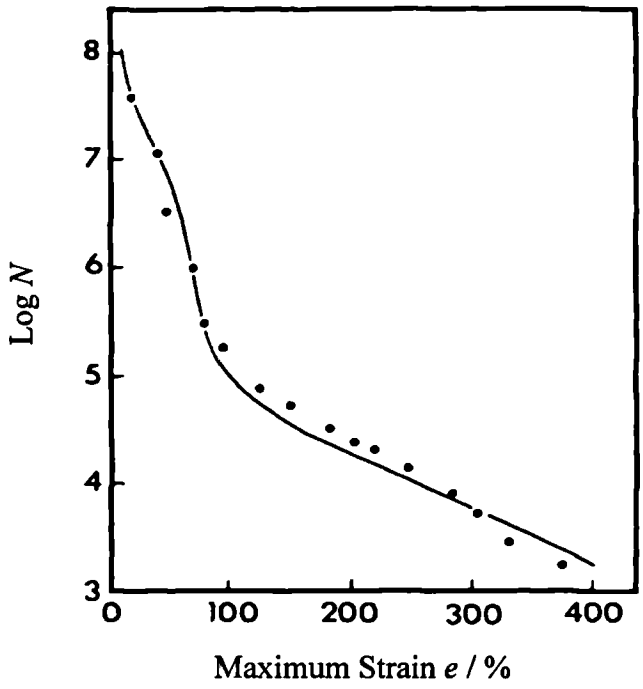

Figure 2-34. Tensile fatigue life N as a function of maximum strain e for an unfilled NR in air. The theoretical strain was derived from the crack growth characteristics, assuming a natural flaw size of 25μm[49].

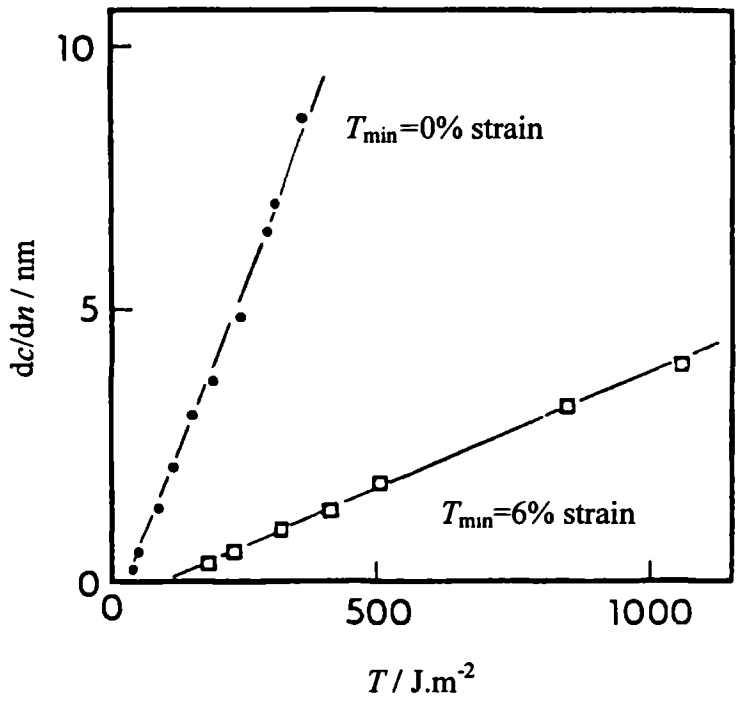

Figure 2-35 The crack growth per cycle, dc/dn, as a function of maximum tearing energy, T, for different minimum tearing energies, T_{min}. T_{min} equal to zero and T_{min} equal to about 6% of the maximum[58].

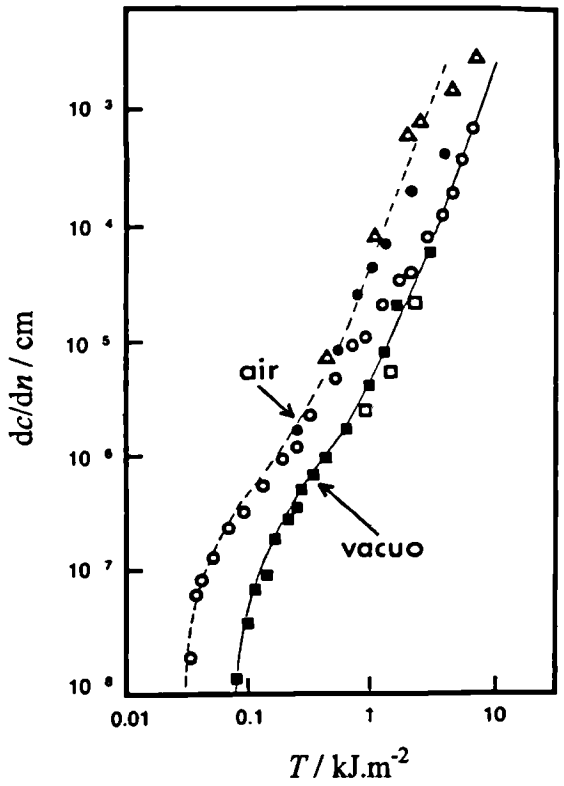

Figure 2-36. Crack growth per cycle as a function of tearing energy for unfilled NR over a wide range of frequency in air and in-*vacuo*. In air, 2Hz (o), 0.02Hz (•), 0.002Hz (Δ). In-*vacuo*, 2Hz (■), 0.02Hz (□)[55].

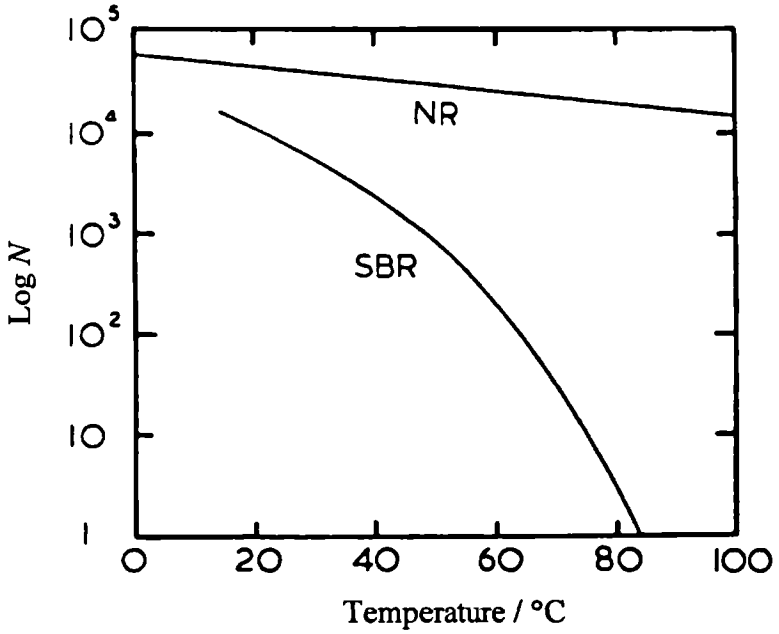

Figure 2-37. Cyclic life, *N*, as a function of temperature for unfilled NR and SBR determined using tensile test specimens[52].

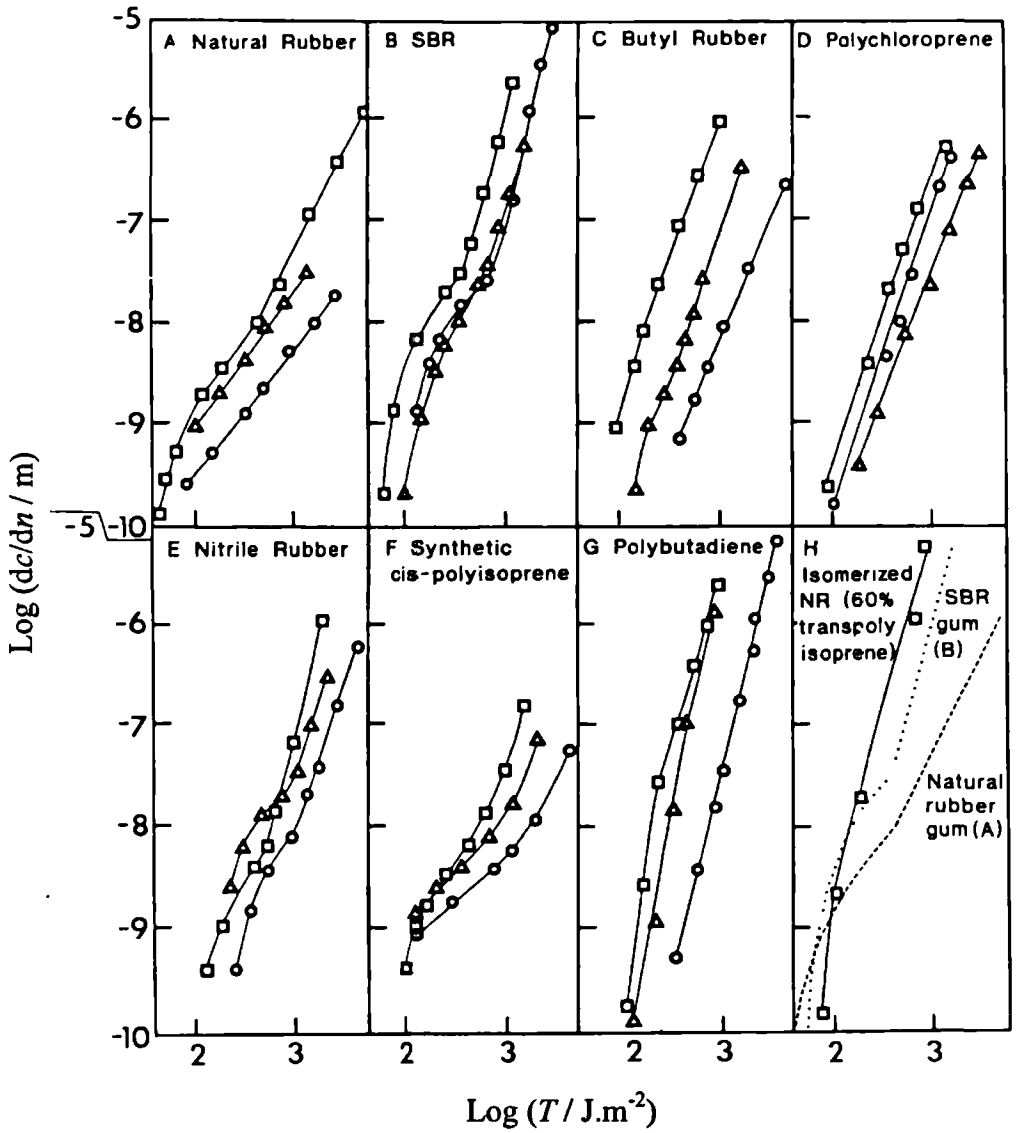

Figure 2-38. Crack growth per cycle versus tearing energy for different rubbers, unfilled (□), 50phr MT black filled (Δ) and 50phr HAF black filled (o) measured at room temperature[59].

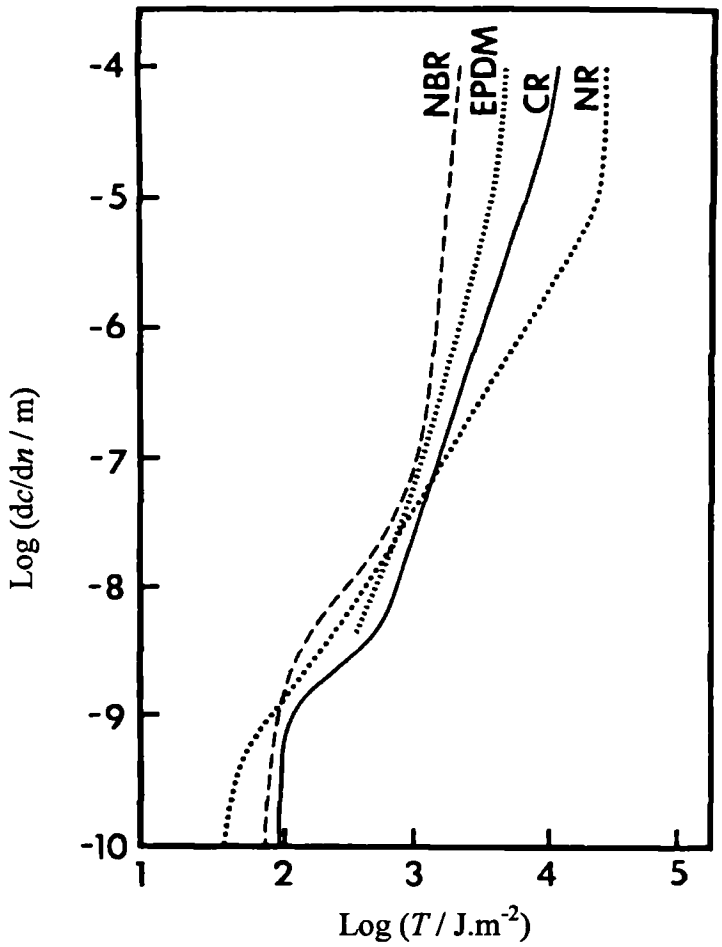

Figure 2-39. Crack growth per cycle versus tearing energy for different rubbers plotted on the same scale measured at room temperature[63].

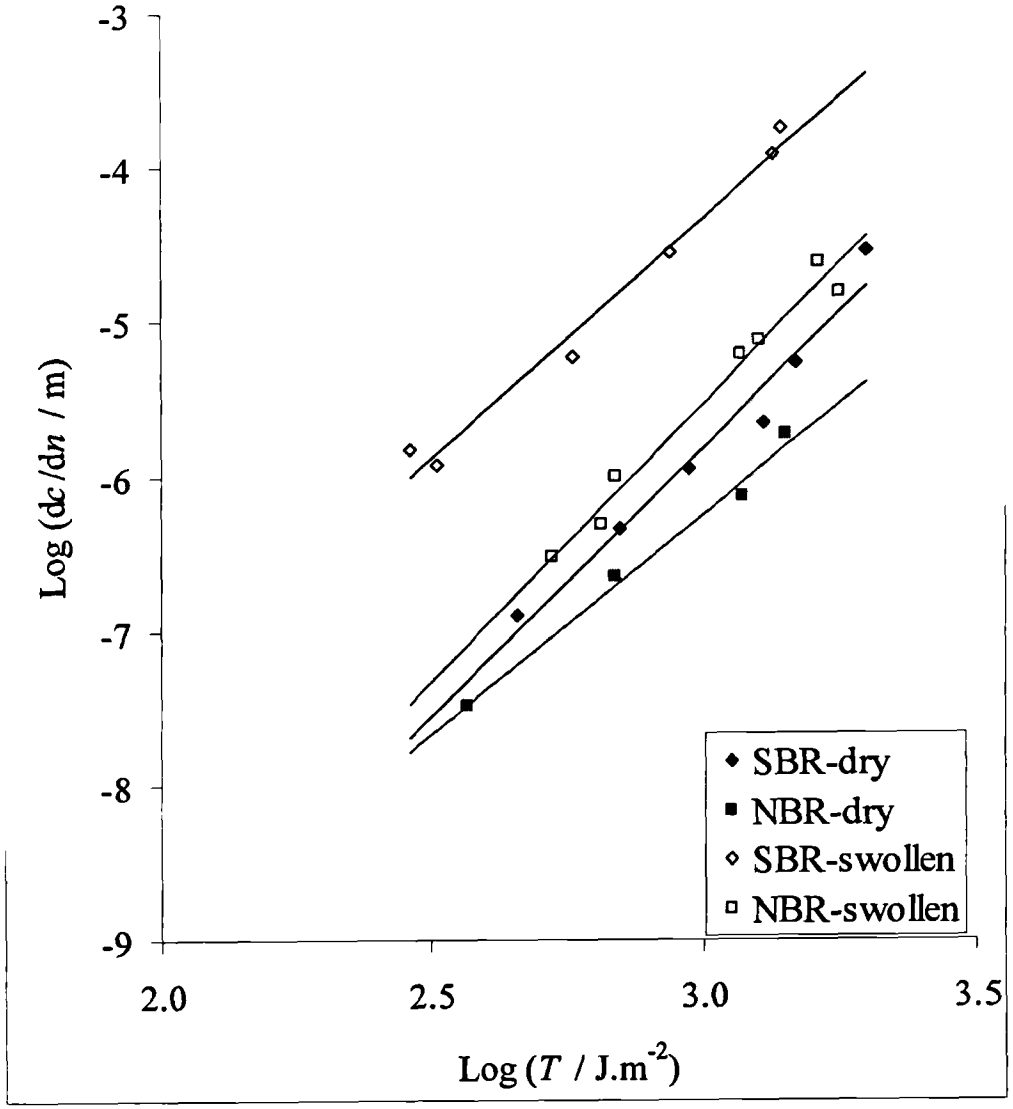

Figure 2-40. The effect of swelling on cyclic crack growth behaviour for unfilled SBR and NBR for pure shear test specimens. The SBR-swollen was swollen to V_r=0.50 and the NBR-swollen was swollen to V_r=0.69[64].

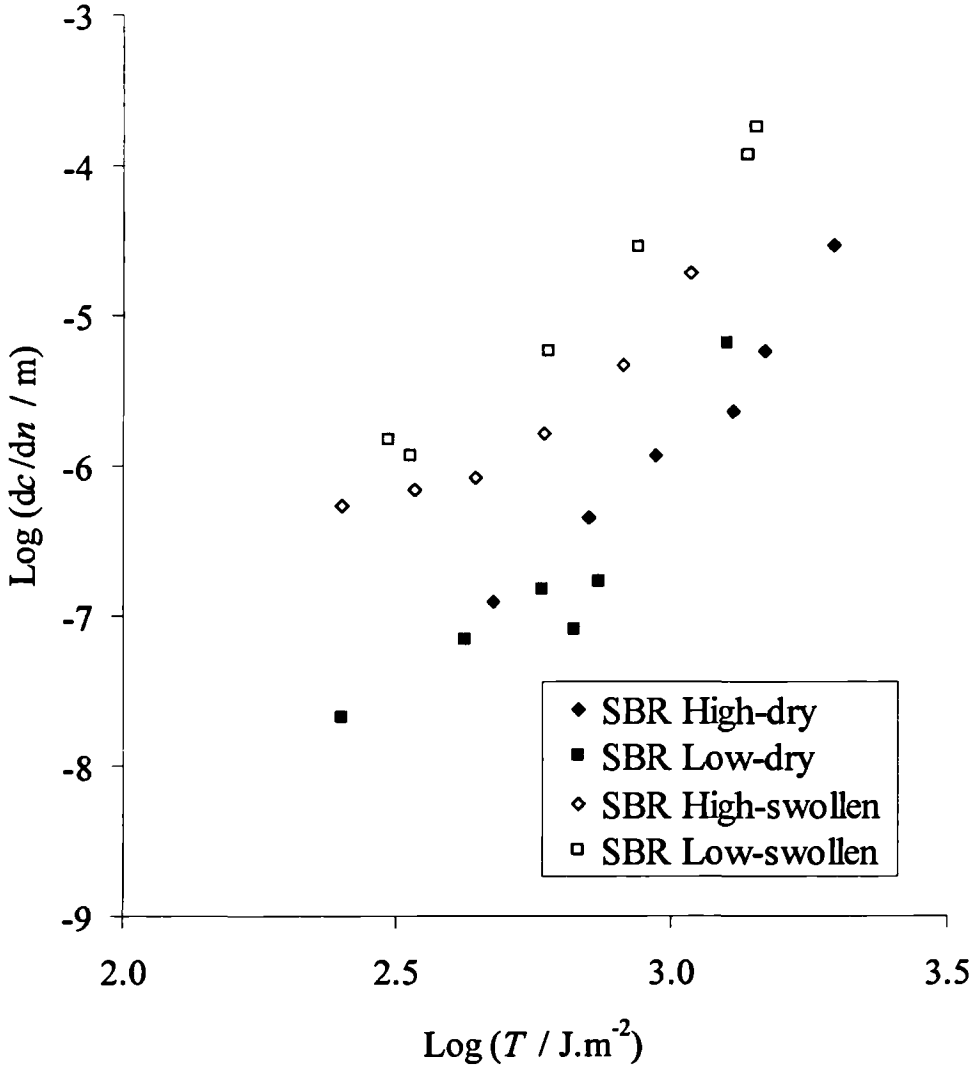

Figure 2-41. The effect of swelling on the cyclic crack growth behaviour for unfilled SBR of different cross-link densities. High cross-link density SBR was swollen to V_r=0.56 and the low cross-link density SBR was swollen to V_r=0.50[64].

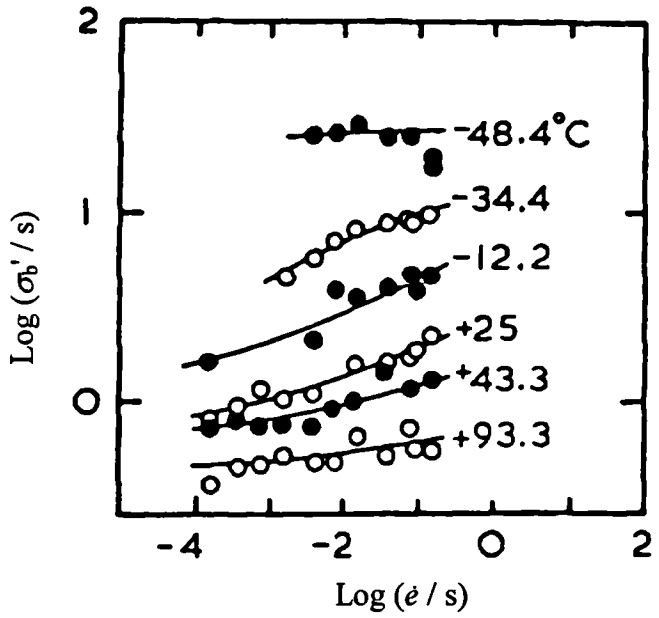

Figure 2-42. Tensile strength σ_b' versus rate of elongation $\dot{e}$ for an unfilled SBR[65].

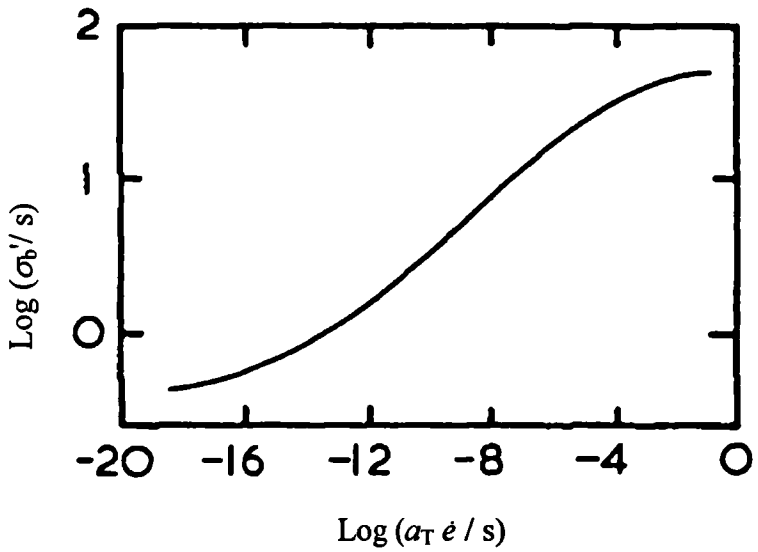

Figure 2-43 Master relation for breaking stress σ_b' as a function of rate of elongation, e, reduced to θ_g using the WLF equation[65].

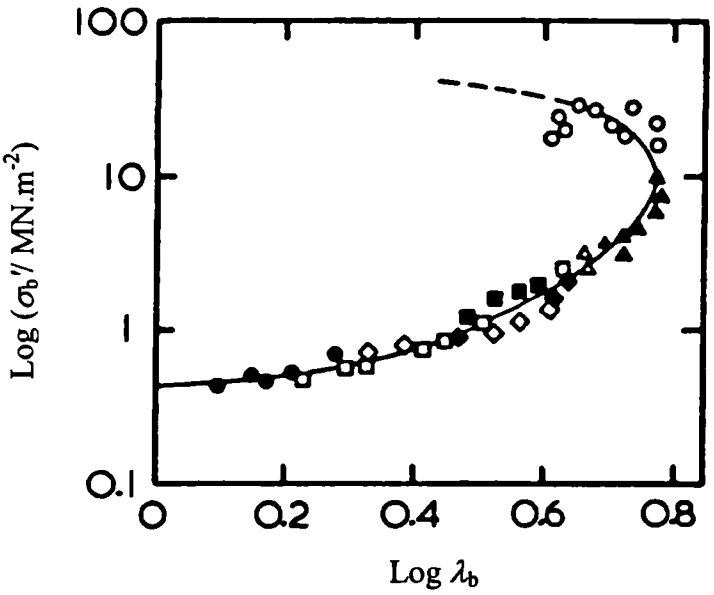

Figure 2-44. The failure envelope for an unfilled SBR determined at various rates and temperatures, as indicated in figure 2-42 and 2-43[68].

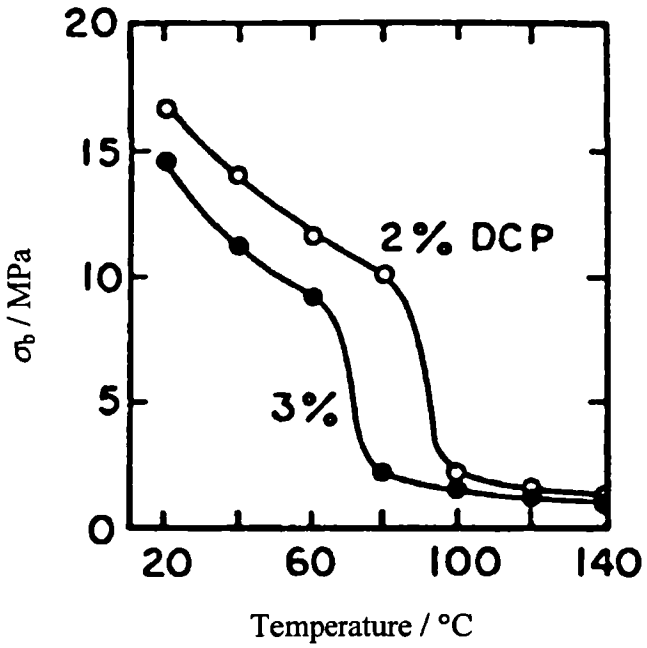

Figure 2-45. The dependence of the tensile strength on temperature for a natural rubber cross-linked with Dicumyl peroxide[72].

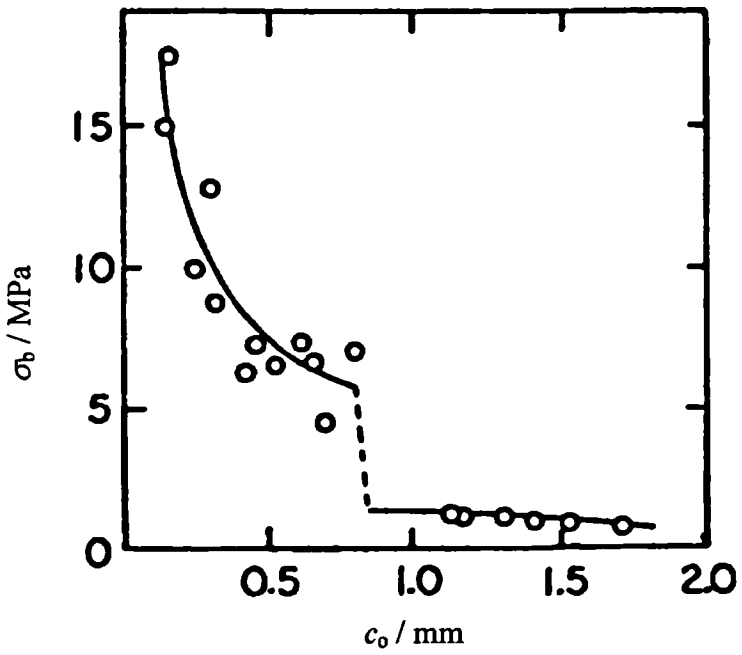

Figure 2-46 The tensile strength, σ_b, of an unfilled NR cross-linked with 2% dicumyl peroxide as a function of artificially introduced crack length, c_0, at room temperature[72]

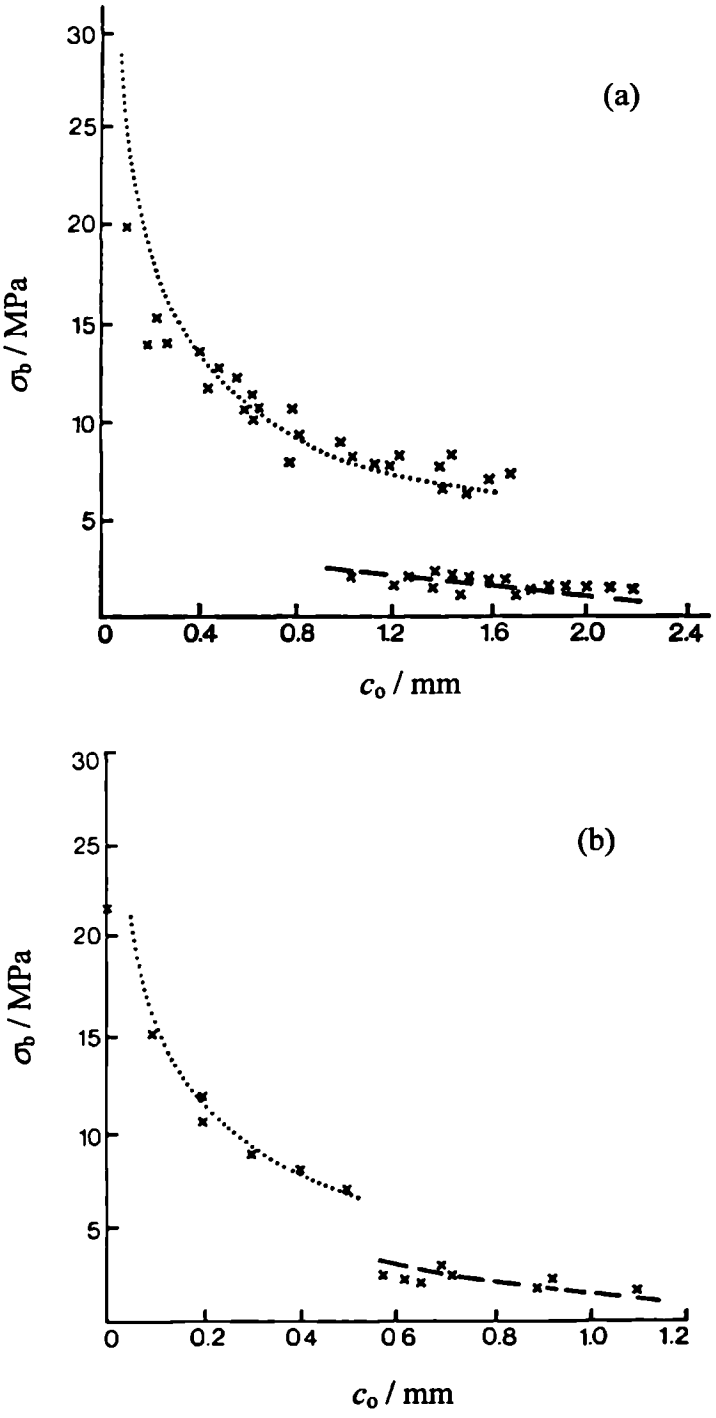

Figure 2-47. Tensile strength, σ_b, as a function of initial crack length, c_o. The dotted line is the value theoretically calculated using equation (2-40) (for the condition of strain crystallisation of the bulk of the specimen) and the dashed line is the value calculated using the equation (2-12)' (for the condition of no crystallisation of the bulk of the specimen); (a) at 23°C, and (b) at 60°C[76].

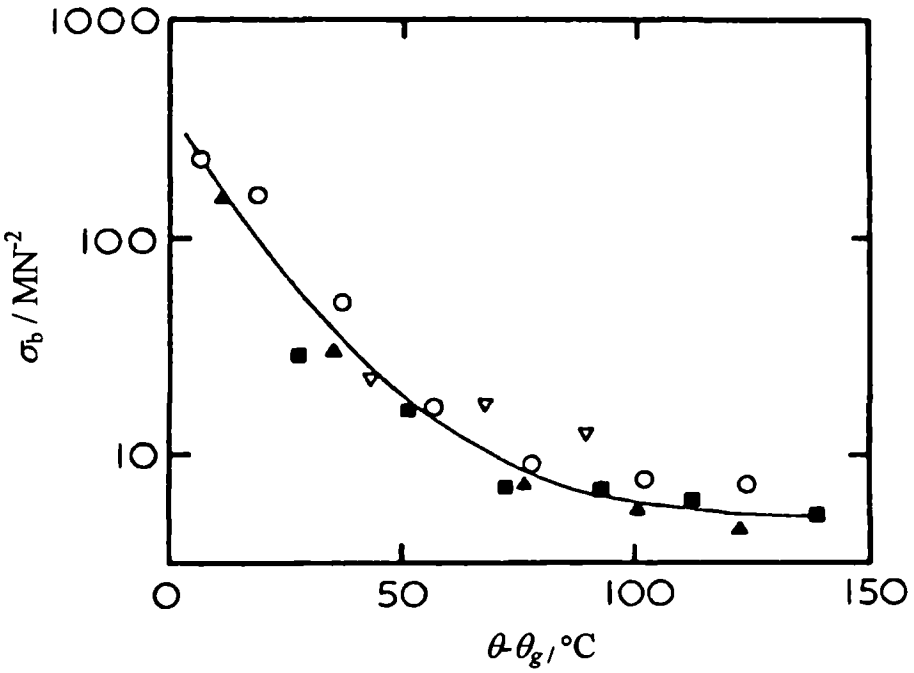

Figure 2-48. Tensile strength as a function of temperature interval θ-θ_g, for polyurethane elastomers over a wide range of θ_g from -67°C to -17°C[77].

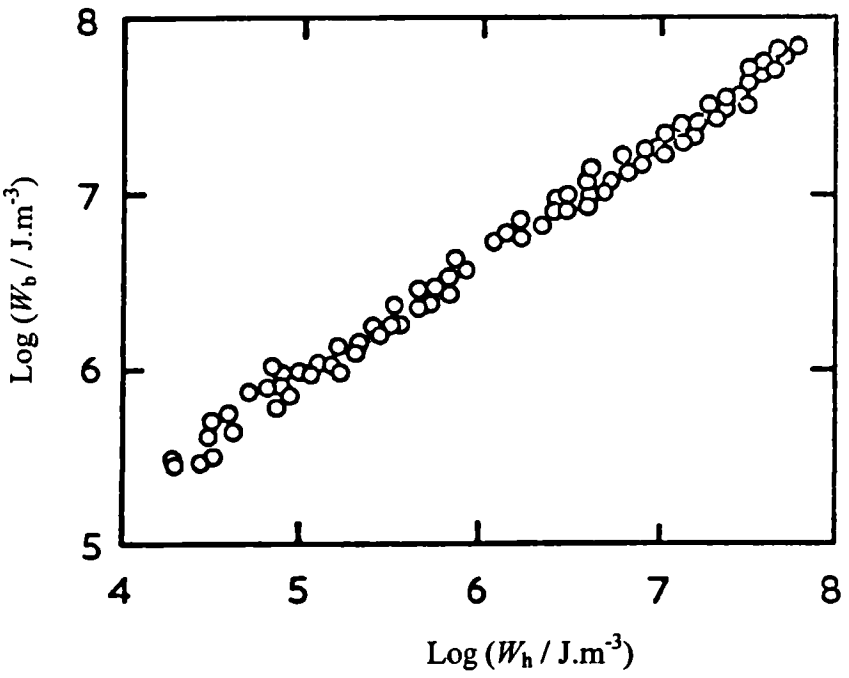

Figure 2-49. Inputted energy density to break, W_b, as a function of dissipated energy on extending to the breaking elongation, W_h[78].

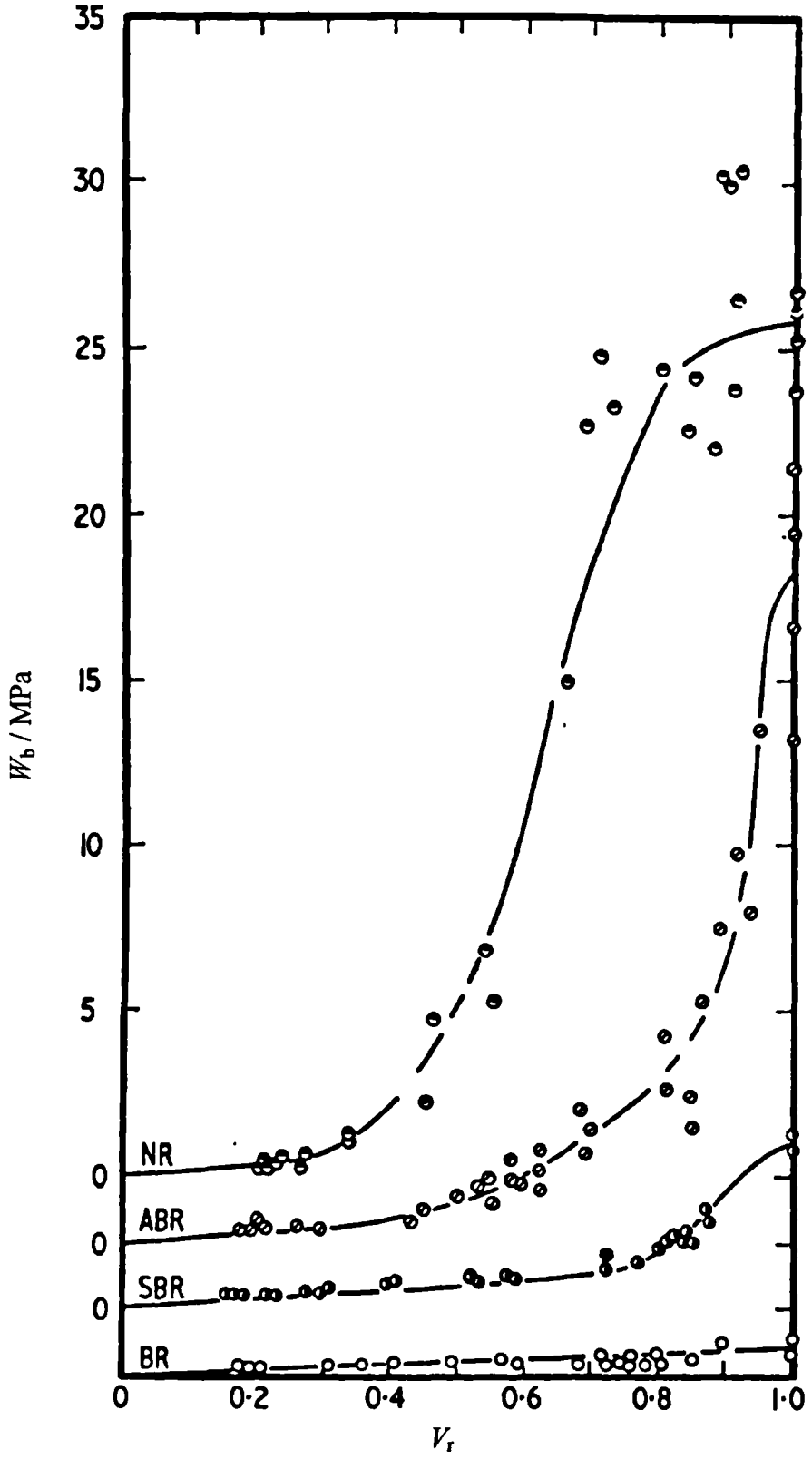

Figure 2-50. Inputted energy density to break as a function of volume fraction of rubber, V_r, for four unfilled elastomers[78].

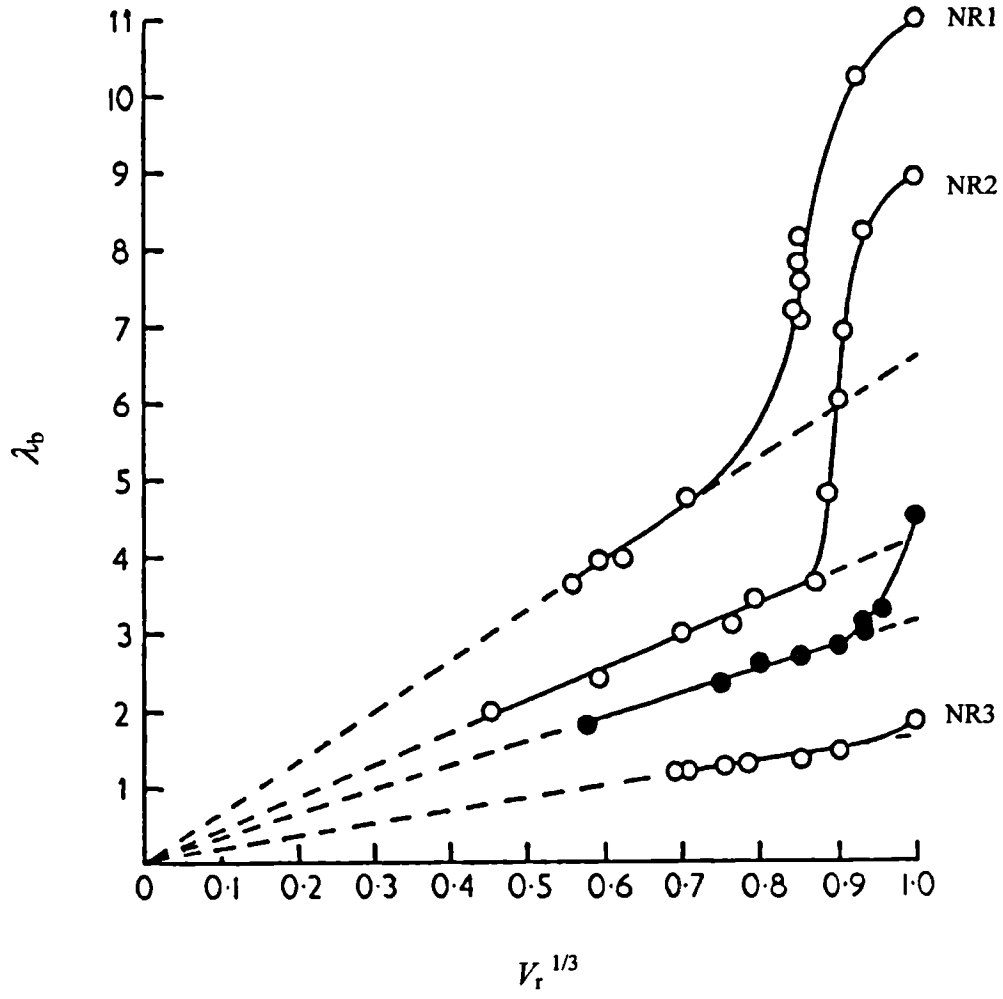

Figure 2-51. Extension ratio at break, λ_b, as a function of $V_r^{1/3}$ for three different unfilled NR compounds(o), whose cross-link density increases from NR1 to NR3, and SBR(•)[81].

Chapter Three

Characterisation of materials used in this study

3-1. Introduction

As was discussed in section 2-6, the principle aim of this study is generally to investigate the role of energy dissipative processes in crack growth and fracture of rubber under static and cyclic loading. In this chapter the rubbers and liquids to be used in this study are identified and the methods used to characterise them are described. The experimental methodologies and test methods for crack growth studies are discussed in chapters – 4, 5, 6, and 7 where the results are also presented.

As was shown in section 2-2-2, the tearing energy, T, necessary for crack propagation at a given rate can be represented as

$$T = W_{ht} k_D d \tag{3-1}$$

where W_{ht} is the hysteretic energy loss per unit volume at the crack tip, k_D is a scaling factor, and d is the effective crack tip diameter. This representation clearly indicates that the visco-elastic loss (energy dissipation process) plays a significant role in determining the magnitude of T and hence the crack growth behaviour. Therefore the visco-elastic behaviour and factors, which alter such behaviour for each material, must be studied.

The cross-link density, M_c, has a significant effect on the visco-elastic losses in rubbers. Here, the magnitudes of M_c are determined from both the material constant, C_1, which is determined from stress-strain measurements and by the swelling method[82][83][84]. The dynamic loss modulus, E'', is a direct measure of the internal viscosity of a polymeric material. It is measured here for swollen and unswollen materials of a range of cross-link densities, using dynamic mechanical property measurements.

3-2. Rubber

A rubber consists of long flexible chain-like molecules, which are inter-connected at various points by cross-links to form a loose molecular network. At temperatures above the glass transition temperature, each elementary network chain undergoes rapid Brownian motion between a large number of possible conformations by rotating about single valance bonds in the chain backbone. Under stress, the chains are forced into conformations, which are less probable than those in the undeformed state. Energy is stored and retractive forces are exerted primarily because of this reduction in conformational entropy, rather than due to an increase in internal energy. This results in the most important characteristic of a rubber, its ability to undergo large deformation and to return to its original shape in a reversible manner.

Styrene-Butadiene Rubber (SBR) is a random copolymer of styrene and butadiene. SBR is a synthetic rubber, made by free radical emulsion polymerisation or anionically in solution. The most commonly used SBR and the one mainly used in this study, consists of 23.5% styrene and 76.5% butadiene, which has a glass transition temperature, θ_g, of approximately –55°C. A diagram illustrating the structure of repeat units is given in figure 3-1. SBR is known as an essentially non-strain crystallising rubber, as under a large strain, little crystallisation takes place. This feature results in significant differences between the mechanical properties of NR (a strain crystallising rubber) and SBR.

Natural Rubber, NR, is a product coagulated from the latex of the rubber tree. NR consists of approximately 100% cis-1.4 poly-isoprene and has a glass transition temperature, θ_g, of approximately –70°C. A diagram illustrating the structure of the repeat units is given in figure 3-1. Isoprene Rubber, IR, is a synthetic rubber equivalent to natural rubber with almost the same chemical structure, 94 to 98% of cis-1.4 poly-isoprene and 6 to 2% of trans-3.4 poly-isoprene. IR can be made with a higher purity than NR as it is free from contaminants, such as proteins, that are present in NR. Both NR and IR are well known as strain-crystallising rubbers. Under large strains these rubbers exhibit extremely high strengths and fatigue resistance.

3-3. Rubber compounding and formulations

The rubber mainly used in this study was Styrene-butadiene rubber, SBR. The SBR rubber compounds were cross-linked to various extents using either sulphur or peroxide curing system. A peroxide system produces simple carbon-carbon cross-links and a network whose topological structure is close to ideal. Carbon black was also employed to vary the energy dissipative process of the material. Only one type of carbon black, high abrasion furnace (HAF N330) was used in this study to avoid complications due to the effects of variable size and structure of the carbon black on the mechanical properties. HAF particles have an average diameter of about 26 to 30nm according to the ASTM classification. The formulations for all the SBR compounds made are given in table 3-1.

Natural rubber, NR, and synthetic cis 1.4 poly-isoprene rubber, IR, were employed in this study to investigate the role of stain crystallisation in the strength of rubbers. These strain-crystallising rubbers were cross-linked using a sulphur curing system providing conventional sulphur cross-links. The formulations for NR and IR compounds are given in table 3-2.

The rubber compounds were prepared by mixing utilising a two-roll mill for the unfilled rubbers and an internal mixer for the carbon black filled rubbers. The rubber sheets were prepared with a hot press at a pressure of about 20MPa. The curing temperatures and times for each compound are also listed in tables 3-1 and 3-2.

3-4. Density of rubbers

The density of the rubbers was determined by using a simple experimental technique based on Archimedes law, by weighing the specimen in air and in water. First the weight of the specimen, w_r, is measured in the air using a 4 digit electronic balance. Then, the specimen is hung in water and the weight, w_w, measured. The density of rubber is calculated using equation (3-2) as

$$\rho_r = \frac{w_r \rho_w}{w_r - w_w} \qquad (3\text{-}2)$$

where ρ_r is the density of the rubber and ρ_w is the density of water. The calculated densities for each rubber compound are also listed in tables 3-1 and 3-2.

3-5. *Cross-link density*

The cross-link density is a significant function in determining the visco-elastic properties of a rubber and hence the strength of a rubber. It is hence very important to determine the cross-link density for each material used. The cross-link density can be measured using either a stress-strain curve or a swelling technique as follows.

3-5-1. Cross-link density measurement by stress-strain curve

The total cross-link density, $\nu_{phys.}$ can be determined using tensile stress-strain curves and by utilising the Mooney-Rivlin constant $C_{1\ phys.}$[82] as

$$\nu_{phys} = \frac{2C_1}{R\theta} \tag{3-3}$$

where ν_{phys} is the physical cross-link density, C_1 is a material constant derived from the Mooney-Rivlin equation, R is the gas constant and θ is the absolute temperature. The Mooney-Rivlin equation for uni-axial extension is given as

$$\sigma = 2\left(\lambda - \frac{1}{\lambda^2}\right)\left(C_1 + C_2\frac{1}{\lambda}\right) \tag{3-4-1}$$

$$\text{which yields} \quad [\Phi] = \frac{\sigma}{2\left(\lambda - \frac{1}{\lambda^2}\right)} = C_1 + C_2\frac{1}{\lambda} \tag{3-4-2}$$

where σ is the stress, λ is the extension ratio, and C_1 and C_2 are constants[85][86]. The left hand term, $[\Phi]$ in equation (3-4-2) is known as the reduced stress. C_1 and C_2 can thus be obtained from a plot of $[\Phi]$ against λ^{-1}. It is known that the C_1 value relates to the number of chemical and physical cross-links which gives the stiffness of the rubber material and the C_2 value which relates to the number of chain entanglements. The values of ν_{phys} were obtained from the C_1 values using equation (3-3).

The stress-strain measurements presented in this section were mostly carried out at an average cross-head speed of 50mm.min^{-1} at 20°C. Tensile strip specimens, 50mm long, 10mm in width and about 1mm in thickness were used. The stress-strain behaviour and the corresponding Mooney-Rivlin plots for unfilled SBR for a wide range of cross-link densities are given in figures 3-2 and 3-3. The stress-strain behaviour and the corresponding Mooney Rivlin plots for unfilled NR (NR00-S1) and IR (IR00-S1) are given in figures 3-4 and 3-5.

The number average molar mass between cross-links ($M_{c\cdot phys}$) is given as

$$M_{c\cdot phys} = \frac{\rho_r}{\nu_{phys}} \tag{3-5}$$

where ρ_r is the density of the rubber. The results obtained for all materials are given in tables 3-1 and 3-2.

3-5-2. Cross-link density measurement by swelling

The chemical method for measuring the cross-link density is suitable for both unfilled and carbon black filled rubbers. The rubber specimen was weighed in air accurately using an electronic balance and was then immersed in a swelling solvent such as *n*-Decane. The change in weight of the rubber specimen was recorded as a function of time. The volume of the solvent absorbed can be calculated easily from the difference between the weight of swollen and unswollen specimens. The volume fraction of the rubber network in the unswollen specimen can be calculated using the following equation.

$$\nu_{r.net} = \left(\frac{M_o}{\rho_{r\,net}}\right)\left(\frac{M_{r\,net}}{M_{tf}}\right) \tag{3-6}$$

where $\nu_{r.net}$ is the volume of the rubber network, M_o is the mass of the rubber specimen, $M_{r\,net}$ is the mass of the rubber network (combination of the hydrocarbon and the sulphur), M_{tf} is the total mass of the mix formulation and $\rho_{r\,net}$ is the density of the rubber network. The value of $\rho_{r\,net}$ was 0.94g.cm^{-3} for the NR and the SBR and 0.92g.cm^{-3} for the IR used in this study. The volume fraction of rubber was then calculated using the following equation.

$$V_r = \left(\frac{V_{r.net}}{V_{r.net} + V_{solv}} \right) \tag{3-7}$$

where V_r is the volume fraction of rubber, $V_{r.net}$ is the volume of the rubber network and V_{solv} is the volume of solvent in the swollen sample. The cross-link density, ν_{chem}, is then determined using the Flory-Rehner relationship[83] as

$$\ln(1 - V_r) + V_r + \chi V_r^2 + 2\rho_{r.net} V_L \nu_{chem} (V_r)^{1/3} = 0 \tag{3-8}$$

where V_r is the volume fraction of rubber at equilibrium swelling, χ is the interaction parameter for the rubber and the swelling liquid and V_L is the molar volume of swelling liquid. The value of V_L for n-Decane is 195.2 $cm^3.mol^{-1}$. The value of χ with *n*-Decane is 0.42 for NR and IR, and 0.64 for SBR. The material constant from the equilibrium swelling method, $C_{1.chem}$, is given as

$$C_{1.chem} = \nu_{chem} R\theta \tag{3-9}$$

The results obtained from a range of cross-linked SBR materials calculated using the two methods, stress-strain curve and swelling, are compared in figure 3-6. The line in the figure denotes the equality of both quantities. In most cases, the values of $C_{1.chem}$ are larger than those for $C_{1.phys}$. This is thought to be due to the uncertainty of the origin of χ, which is usually determined to fit the magnitude of $C_{1.chem}$ to that of $C_{1.phys}$. To avoid this problem it was decided to use the stress-strain method to determine values of C_1, and hence to determine the value of M_c for all the unfilled materials. However, due to the experimental difficulties in determining the accurate C_1 values for carbon black filled materials from stress-strain measurements, C_1 values were measured for those materials using the swelling method.

In case of the carbon black filled rubber, it is known that carbon black restricts the mobility of the rubber network. Porter[84] developed an empirical relationship, which corrected the cross-link density measured by swelling in a carbon black filled rubber. The actual cross-link density, ν_{act}, for a carbon black filled rubber is given as

$$\nu_{act} = \frac{\nu_{chem.}}{1 + K_f V_{CB}} \tag{3-10}$$

where K_f is a constant characteristic of a given filler, K_f=2.6 for HAF carbon black, and V_{CB} is the volume fraction of carbon black in the rubber. The number average molar mass between cross-links ($M_{c.chem}$) is then given as

$$M_{c\,chem} = \frac{1}{2v_{act}} \tag{3-11}$$

3-6. *Swelling of rubber*

3-6-1. Characteristics of the swelling liquids

The plasticizing effect of swelling liquids on rubbers alters the effective segmental mobility of the rubber chains and this is reflected in the change in the internal viscosity. It is expected that this will also have a significant effect on the strength properties. The internal viscosity is dependent on the viscosity, chemical nature and amount of a swelling liquid. Therefore, suitable liquids are chosen on the basis of their viscosities, chemical structure and swelling ability. Dibutyl adipate (DBA) was used in this study because of its ability to swell rubbers to a large extent and because of its low viscosity. The property constants for DBA are given in table 3-3.

3-6-2. Swelling process

Specimens for testing were swollen to any achievable swelling ratio (volume fraction of rubber) in a glass dish. Typical swelling behaviour as a function of time is illustrated in figure 3-7. The time required for a through sample thickness to reach equilibrium swelling depends on the characteristics of the liquid. The absorbed liquid has to be distributed uniformly across the whole section of a sample to be tested. This was achieved by first swelling in the liquid for a given time, which resulted in a gradient of liquid concentration across the sample. The samples were then left in air for the time necessary to achieve a given equilibrated uniform swelling throughout the samples. The time used for this equilibration process was well in excess of that

necessary. The final volume fraction of rubber in any sample was determined as described in section 3-5-2.

3-6-3. Tensile stress-strain behaviour of swollen rubber

In this section the stress-strain data for unfilled SBR (SBR00-S3) and unfilled NR (NR00-S1) swollen to various extents with DBA are presented utilising the Mooney-Rivlin equation given earlier in equation (3-4). As was discussed in section 3-5-1, by considering the measured stress-strain behaviour in this way, it is possible to characterise these materials. The stress-strain behaviour and corresponding Mooney-Rivlin plots for unfilled SBR (SBR00-S3) swollen with DBA to various volume fractions of rubber are shown in figures 3-8 and 3-9. The materials constants determined, C_1 and C_2, are given in table 3-4. The stress-strain behaviour and corresponding Mooney-Rivlin plots for unfilled NR (NR00-S1) swollen with DBA to various volume fractions of rubber are shown in figures 3-10 and 3-11. The materials constants determined, C_1 and C_2, are given in table 3-5.

It can be seen that the stiffness of the rubber decreased with decreasing volume fraction of rubber (increasing extent of swelling). From figure 3-8 the values of C_1 and C_2 both decreased with decreasing volume fraction of rubber. According to the Gaussian network theory for swollen rubbers, the value of C_1 for a swollen rubber is given as

$$C_1 = C_{1.dry} V_r^{1/3} \qquad (3\text{-}12)$$

where $C_{1.dry}$ is the network parameter for the dry (unswollen) state and V_r is the volume fraction of rubber. The determined C_1 values for unfilled SBR (SBR00-S3) and unfilled NR (NR00-S1) from figures 3-9 and 3-11 are plotted as a function of volume fraction of rubber on a double logarithmic scale in figures 3-12 and 3-13. For both SBR and NR the slopes are found to be approximately 1/3. This indicated that the behaviour of the swollen network can be described by the simple statistical theory.

3-7. Dynamic mechanical properties

3-7-1. Oscillating beam apparatus

The dynamic loss modulus, E'', is a direct measure of internal energy dissipation especially for a non-strain crystallising rubber. Internal energy dissipation determines the strength of the rubber, the greater the dissipation, the greater the strength. Therefore, determining the dynamic mechanical properties of the materials used in this study is very important. A wide variety of experimental techniques have been developed for determining the dynamic mechanical properties of rubbers. The most commonly used apparatus would be a dynamic mechanical thermal analyser (DMTA). However, a DMTA type apparatus has some difficulties in measuring the dynamic properties, such as tan-δ and E'', at very small values of loss angle (tan-δ) especially for unfilled and swollen rubbers. Furthermore if tan-δ, and hence E'', were to be measured as a function of strain, it would be very difficult to carry out such measurements accurately on the very small specimens of uncertain initial length, which are normally employed in a DMTA apparatus. Due to these limitations Akutagawa[87] investigated the effect of the incorporation of low molar mass liquids on the dynamic mechanical properties for unfilled rubbers by utilising a simple oscillating beam apparatus. This technique was extended by Deeprasertkul[88] for carbon black filled rubbers. In this study, this simple oscillating beam apparatus was adopted to characterise the dynamic mechanical properties of the rubbers. A schematic diagram of this apparatus is given in figure 3-14.

A beam with end weights of a known moment of inertia was supported by a knife edge and clamped at the centre of a rubber specimen. The specimen was extended to a specified pre-strain. The beam was set in motion by switching off a small electromagnet. As the beam oscillates, the period of oscillation and the decay in the oscillation amplitude were measured using a capacitance transducer and recorded on an X-t recorder. A typical oscillating signal and the decay of amplitude is illustrated schematically in figure 3-15.

3-7-2. Calculation of the dynamic mechanical properties

The motion of the oscillating system with a rubber test specimen in a strained state can be represented using the following equation[87].

$$I\frac{\partial^2\theta_D}{\partial t^2}+2(E'+iE'')\lambda^{-2}r_d^{\,2}\frac{A_o}{l_s}\theta_D=0 \qquad (3\text{-}13)$$

where I is the moment of inertia of the beam, θ_D is the angular displacement of the beam, λ is the pre-strain extension ratio of the specimen, r_d is the distance between the centre of the beam and specimen, which is 68mm in this study, A_o is the unstrained cross sectional area of the specimen, l_s is the unstrained half length of the specimen, E' is the dynamic storage modulus and E'' is the dynamic loss modulus. If this equation (3-13) is assumed to have a solution of the form

$$\theta_D=\theta_{Do}e^{-qt}e^{i\omega t} \qquad (3\text{-}14)$$

where θ_{Do} is the initial angular displacement, ω is the angular velocity of the beam, q is a constant and t is time, then equation (3-13) can be solved to yield

$$E'=\frac{I\omega^2}{2r_d^{\,2}}\frac{l_s}{A_o}\lambda^2 \qquad (3\text{-}15)$$

and

$$E''=\frac{\Lambda}{\pi}\frac{I\omega^2}{2r_d^{\,2}}\frac{l_s}{A_o}\lambda^2 \qquad (3\text{-}16)$$

where Λ is the logarithmic decrement which can be defined as the natural logarithm of the ratio of the amplitude of two successive cycles, given as

$$\Lambda=\ln\left(\frac{X_n}{X_{n+1}}\right) \qquad (3\text{-}17)$$

where X_n is the amplitude of the n^{th} cycle and X_{n+1} is the amplitude of the following cycle. For determining the value of Λ, 6 successive cycles were used in this study. The loss tangent δ is then given as

$$\tan\delta=\frac{E''}{E'}=\frac{\Lambda}{\pi} \qquad (3\text{-}18)$$

3-7-3. Dynamic mechanical properties of rubber used in this study

3-7-3-1. Effect of swelling

The dynamic mechanical properties of both unswollen rubbers and rubbers swollen with DBA were determined for SBR00-S3, NR00-S1 and IR00-S1. The specimen dimensions were approximately 80mm in length, 5mm in width and 1mm in thickness. Rubber specimens were stretched to specific pre-strains and the dynamic properties were measured using the simple oscillating beam apparatus at room temperature monitored as 20°C ±2°C.

The measured dynamic mechanical properties as a function of pre-strain are given in figures 3-16 to 3-21. The values of the dynamic storage modulus, E', are shown in figures 3-16 to 3-18. The shape of the curves was similar to that for the unswollen rubbers. The magnitude of E' decreased with decreasing volume fraction of rubber, V_r, at a given λ. The value of E' was approximately constant at low pre-strains and showed an upturn at a certain strain, λ_{TS}. The values of the dynamic loss modulus, E'', are given in figures 3-19 to 3-21. It was seen that the form of E'' as a function of pre-strain can be divided into two regions. At low and moderate strains up to around λ=2.0 the value of E'' was approximately constant. At higher pre-strains, the magnitude of E'' increased rapidly with increasing pre-strain by a factor of two or more.

3-7-3-2. Effect of average molar mass between cross-links

The average molar mass between cross-links, M_c, was expected to strongly affect the dynamic properties and this effect was studied for unfilled SBR. The dynamic storage modulus, E', as a function of strain for materials with different M_c values is shown in figure 3-22. As is the case in figure 3-16 to 3-18, the value of E' was approximately constant at low strains up to a certain λ_{TS}. At λ greater than the strain ratios λ_{TS}, E' increased with increasing λ. The magnitude of λ_{TS} decreased with decreasing average molar mass between cross-links. The dynamic loss modulus, E'', is shown in figure 3-23. At strains greater than λ_{TD}, the magnitude of E'' increased rapidly with increasing λ. The magnitude of λ_{TD} decreased with decreasing average

molar mass between cross-links. This phenomenon was found to correlate with the observed extension ratios at which the corresponding stress-strain plots departed from the Mooney-Rivlin prediction[87]. It is suggested that both phenomena are associated with the onset of finite extensibility. In the low and moderate strain region, up to λ_{TD}, orientations of the stretched network chains will remain relatively random, while above λ_{TD} network chains will tend to orientate. At a given λ this effect will be greatest for the rubber with the shortest network chains. This could be the explanation for the observed crossover in figure 3-23, where the magnitude of E'' increased with decreasing network chain length in the largest strain region. It was found that the crossover in the relation between E'' and λ for different M_c values is observed in both non-crystallising rubber and strain-crystallising rubbers[87]. Therefore, the upturn in the curves observed in figures 3-22 and 3-23 is associated with the onset of finite extensibility rather than onset of strain crystallisation.

Table 3-1(a). Compound formulations and material properties for sulphur cured unfilled SBR used in this study.

		SBR00-S1	SBR00-S2	SBR00-S3	SBR00-S4
Styrene-butadiene rubber	SBR#1502	100.0	100.0	100.0	100.0
Carbon black (HAF)	N330	-	-	-	-
Stearic acid		2.0	2.0	2.0	2.0
Zinc oxide		5.0	5.0	5.0	5.0
Antioxidant and ozonant	6PPD (6C)	3.0	3.0	3.0	3.0
Sulphur		0.5	1.0	1.5	10.0
Accelerator	DPG*	1.3	1.3	1.3	1.3
Accelerator	MBTS**	1.0	1.0	1.0	1.0
Sp. Gr.	/g.cm^{-3}	0.987	0.989	0.991	1.030
Curing condition	at 160 °C	30min	30min	30min	30min
$M_{c\ pysc}$	/g.mol^{-1}	66428	22266	9889	1084
$M_{c\ chem}$	/g.mol^{-1}	56403	20230	10661	1926
$C_{1\ mech}$	/MPa	0.020	0.057	0.107	0.595
$C_{1\ chem}$	/MPa	0.022	0.056	0.166	1.286

* Diphenylguanidine

** Dibenzothiazylsulfide

Table 3-1(b). Compound formulations and material properties for per-oxide cured unfilled SBR used in this study.

		SBR00-P1	SBR00-P2	SBR00-P3	SBR00-P4
Styrene-butadiene rubber	SBR#1502	100.0	100.0	100.0	100.0
Peroxide	DCP***	0.1	0.3	0.5	5.0
Sp. Gr.	/g.cm^{-3}	0.940	0.940	0.940	0.940
Curing condition	at 160 °C	30min	30min	30min	30min
$M_{c\ pysc}$	/g.mol^{-1}	-	21339	9301	593
$M_{c\ chem}$	g.mol^{-1}	77890	13592	5917	862
$C_{1\ mech}$	/MPa	0.019	0.084	0.195	1.328
$C_{1\ chem}$	/MPa	-	0.054	0.125	1.955

*** Dicumyl peroxide

Table 3-1(c). Compound formulations and material properties for 10phr and 50phr carbon black filled SBR used in this study.

		SBR10 -S1	SBR10 -S2	SBR10 -S3	SBR50 -S1	SBR50 -S2	SBR50 -S3
Styrene-butadiene rubber	SBR#1502	100.0	100.0	100.0	100.0	100.0	100.0
Carbon black (HAF)	N330	10.0	10.0	10.0	50.0	50.0	50.0
Stearic acid		2.0	2.0	2.0	2.0	2.0	2.0
Zinc oxide		5.0	5.0	5.0	5.0	5.0	5.0
Antioxidant and ozonant	6PPD (6C)	3.0	3.0	3.0	3.0	3.0	3.0
Sulphur		1.5	4.0	8.0	1.5	4.0	8.0
Accelerator	DPG*	1.3	1.3	1.3	1.3	1.3	1.3
Accelerator	MBTS**	1.0	1.0	1.0	1.0	1.0	1.0
Sp. Gr.	/g.cm^{-3}	0.987	0.989	0.991	1.030	1.065	1.181
Curing condition	at 160 °C	30min	30min	30min	30mın	15min	15min
$M_{c\ chem}$	/g.mol^{-1}	10275	3624	1715	7615	3116	1919
$C_{1\ chem}$	/MPa	0.122	0.349	0.748	0.185	0.454	0.744

Table 3-2. Compound formulations for unfilled NR and IR used in this study.

		NR00-S1	IR00-S1
Natural rubber	SMR CV60	100.0	-
cis-1.4 Isoprene rubber	JSR IR#2200	-	100.0
Stearic acid		2.0	2.0
Zinc oxide		5.0	5.0
Antioxidant and ozonant	6PPD (6C)	3.0	3.0
Sulphur		1.5	1.5
Accelerator	DPG*	-	0.2
Accelerator	CBS****	1.5	1.5
Sp. Gr.	/g.cm^{-3}		
Curing condition	at 160 °C	20min	25min
$M_{c\ pysc}$	/g.mol^{-1}	8551	7094
$C_{1\ mech}$	/MPa	0.134	0.161

**** N-Cyclohexyl-2-benzothiazyl-sulfenamide

Table 3-3. Liquid parameters used in this study.

Index	Liquid	M_w	Density /g.cm^{-3}	Viscosity /Pa.s at 20 °C	V_L /cm^3.mol^{-1}
DBA	Dibutyl adipate	258.4	0.962	0.038	268.4

Table 3-4. Experimentally measured material constants for unswollen and swollen SBR (SBR00-S3) with DBA.

	C_1 / MPa	C_2 / MPa
V_r 1.00	0.1447	0.1438
V_r 0.88	0.1404	0.1202
V_r 0.76	0.1302	0.0808
V_r 0.61	0.1159	0.0607
V_r 0.41	0.1053	0.0153

Table 3-5. Experimentally measured material constants for unswollen and swollen NR (NR00-S1) with DBA.

	C_1 / MPa	C_2 / MPa
V_r 1.00	0.1339	0.0979
V_r 0.90	0.1267	0.0791
V_r 0.78	0.1247	0.0574
V_r 0.57	0.1098	0.0355
V_r 0.40	0.1010	0.0101

(A) SBR

M=54 (Butadiene unit) *M*=105 (Styrene unit)

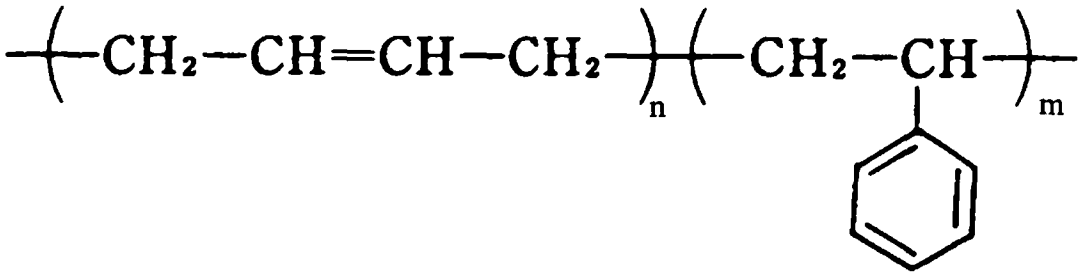

(B) NR *M*=68

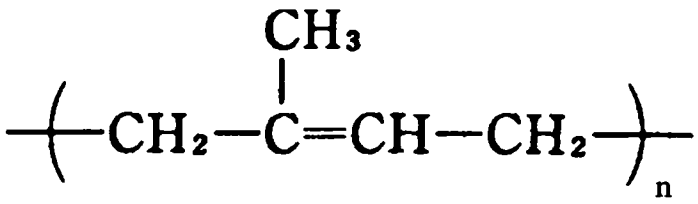

Figure 3-1. Chemical structure of rubbers; (A) Styrene-butadiene rubber (SBR), (B) cis-1.4 poly-isoprene rubber (NR and IR), with the relative molar mass of the repeat units, *M*.

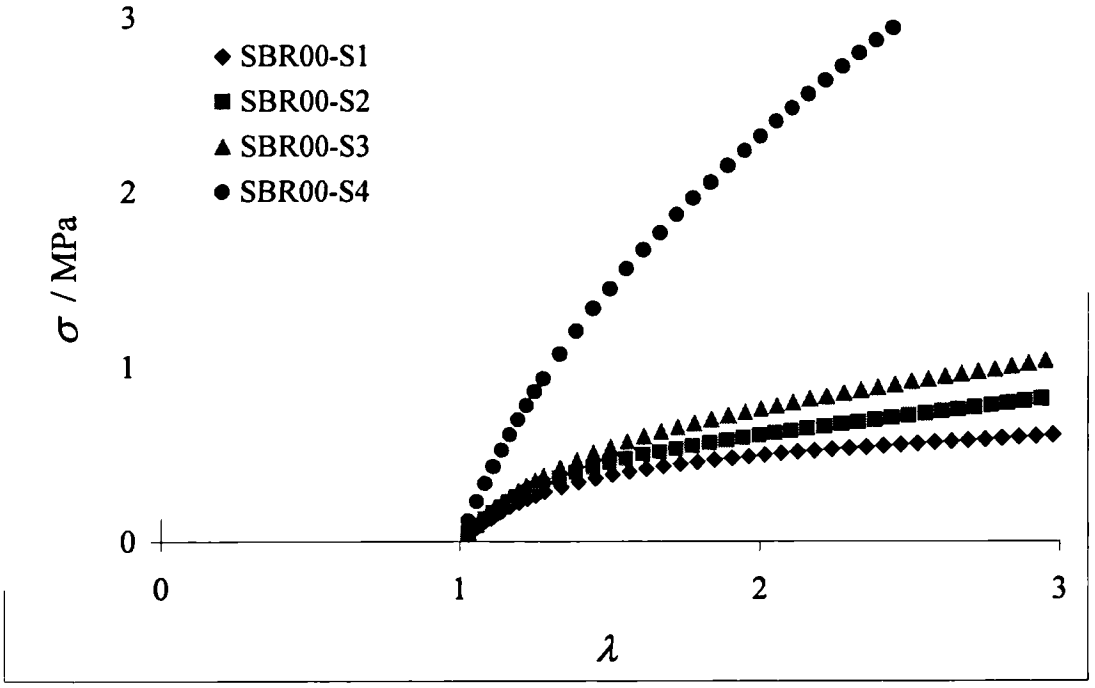

Figure 3-2(a). Tensile stress-strain curves for unfilled sulphur cured SBR of different cross-link densities (M_c) at a strain rate of $8.33x10^{-1}s^{-1}$.

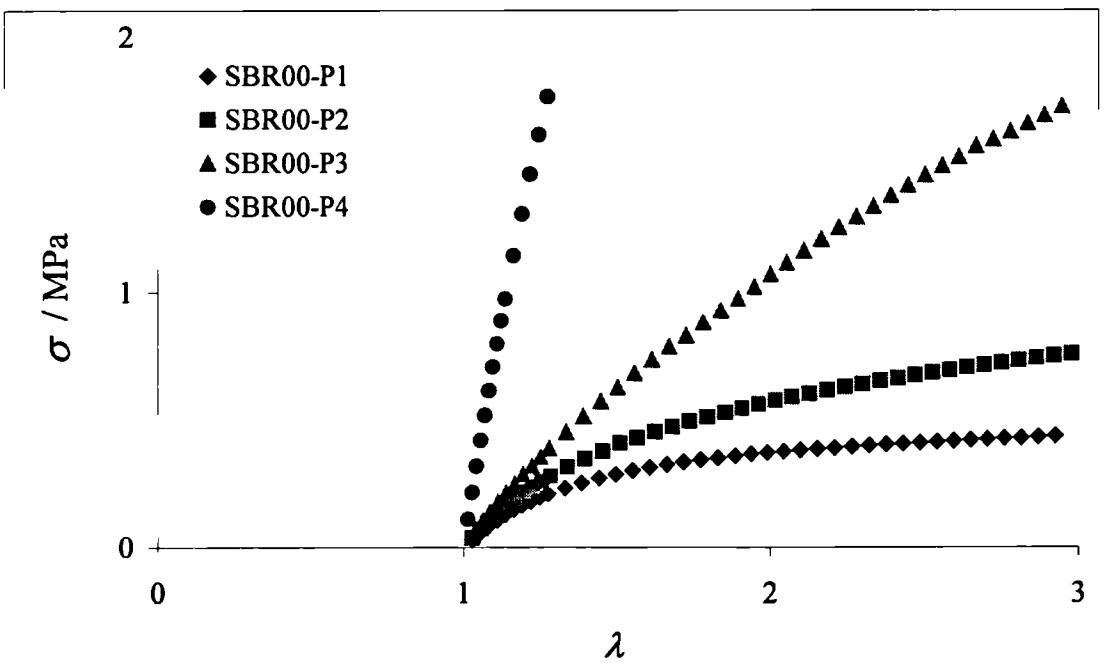

Figure 3-2(b). Tensile stress-strain curves for unfilled peroxide cured SBR of different cross-link densities (M_c) at a strain rate of $8.33x10^{-1}s^{-1}$.

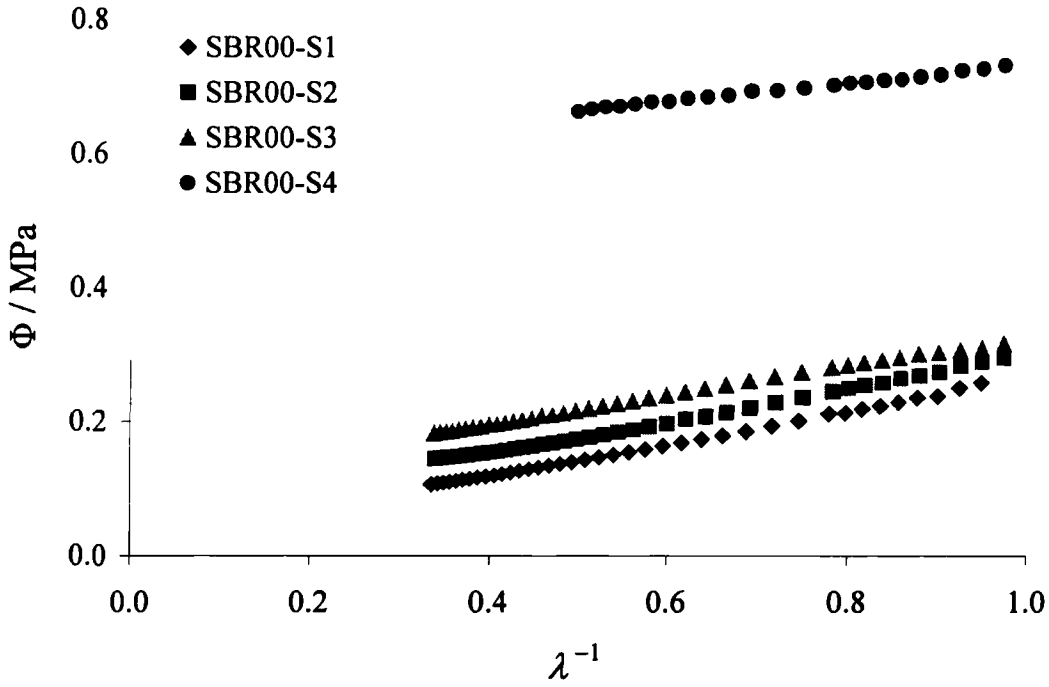

Figure 3-3(a). Mooney-Rivlin plots for unfilled SBR of different M_c cross-linked with sulphur at a strain rate $8.33x10^{-1}s^{-1}$.

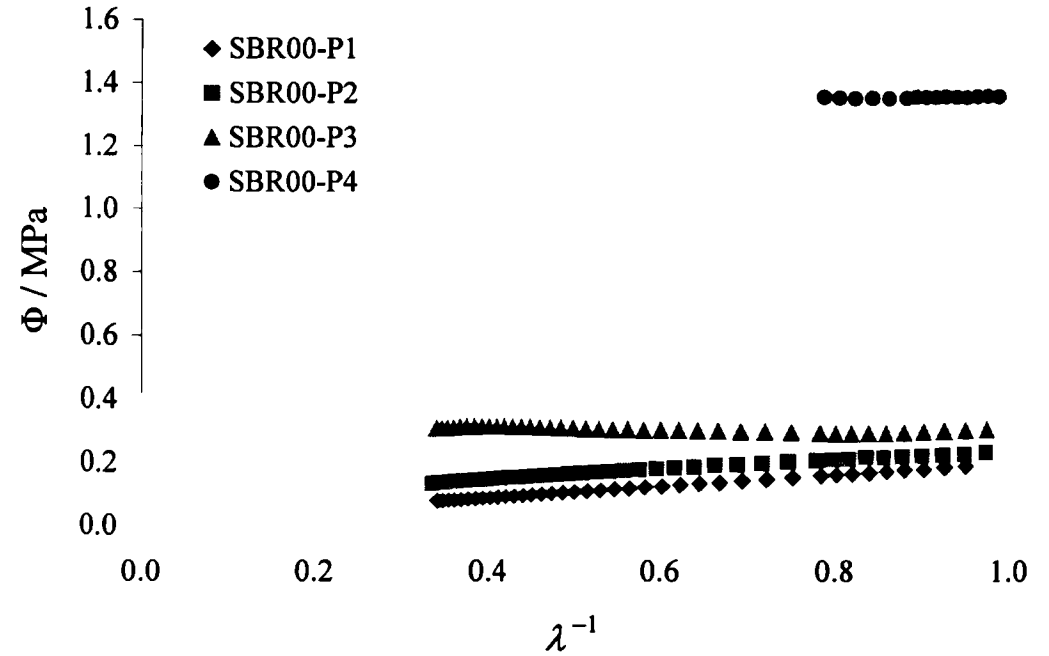

Figure 3-3(b). Mooney-Rivlin plots for unfilled SBR of different M_c, cross-linked with peroxide at a strain rate of $8.33x10^{-1}s^{-1}$.

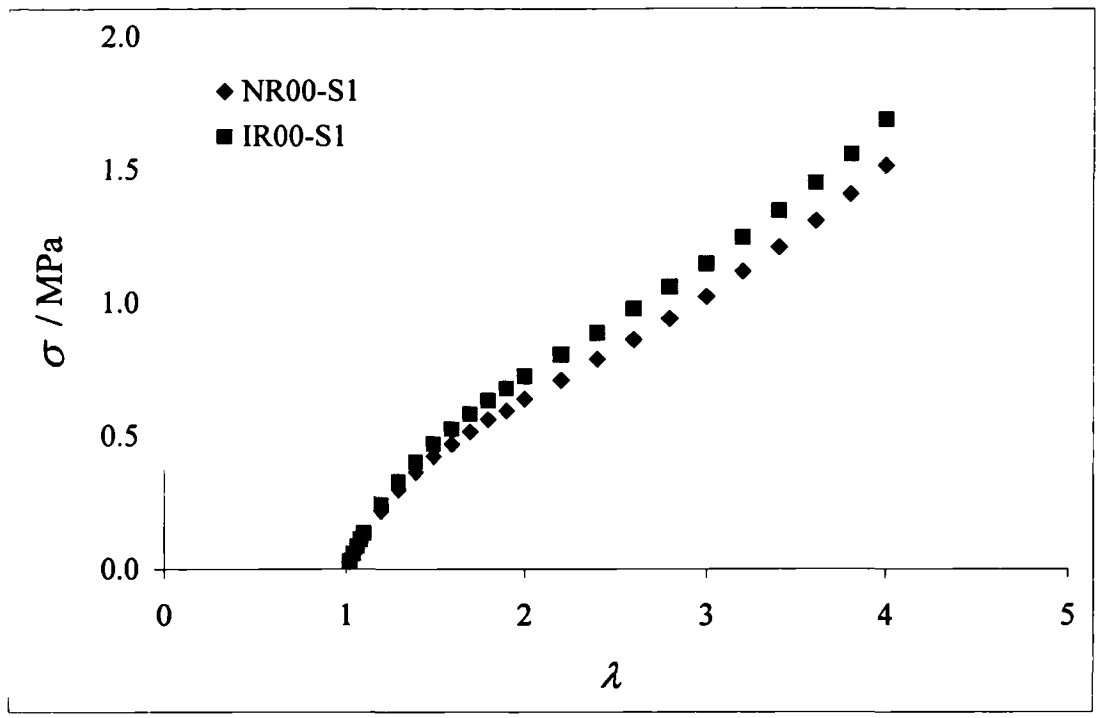

Figure 3-4. The tensile stress-strain curves for unfilled NR and IR at a strain rate of $8.33x10^{-1}s^{-1}$.

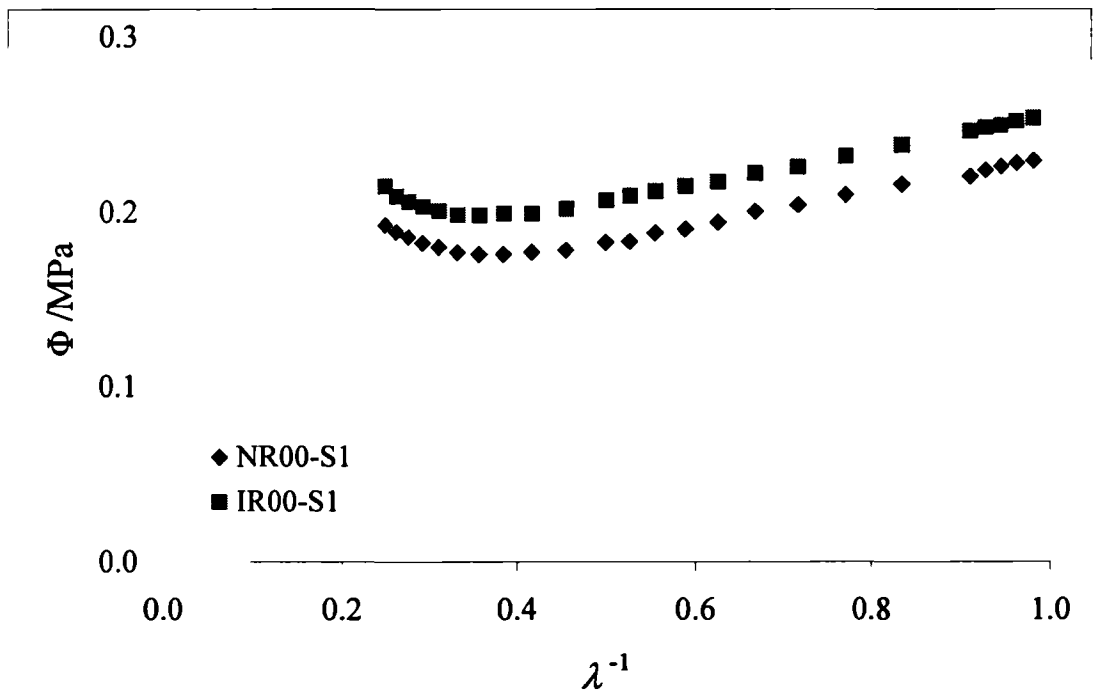

Figure 3-5. Mooney-Rivlin plots for unfilled NR and IR at a strain rate of $8.33x10^{-1}s^{-1}$.

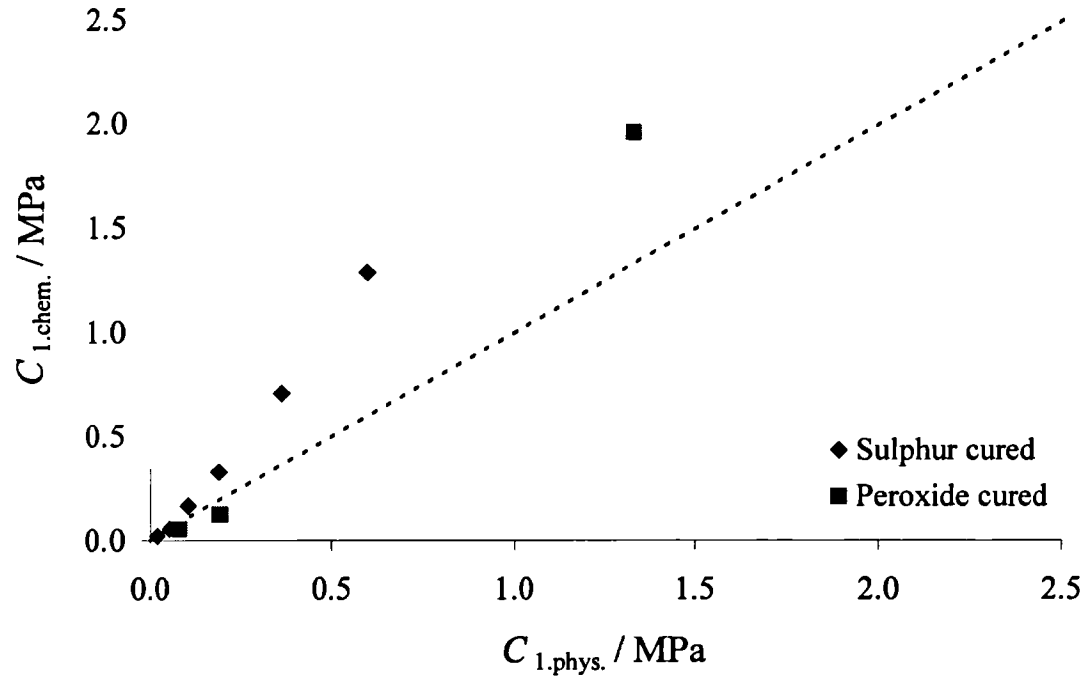

Figure 3-6. Comparison between C_1 from tensile mechanical measurement ($C_{1.phys}$) and from equilibrium swelling ($C_{1.chem}$) for differently cross-linked SBR. Dotted line represents slope 1.

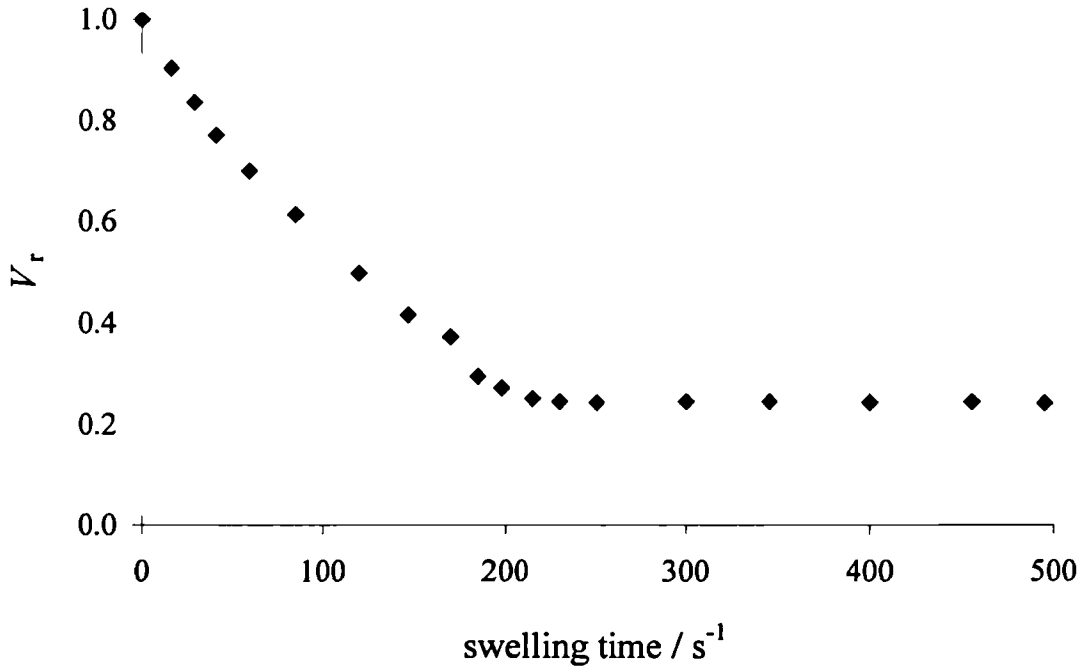

Figure 3-7. Volume fraction of rubber, V_r, as a function of time for SBR00-P1 swollen with DBA at 20°C.

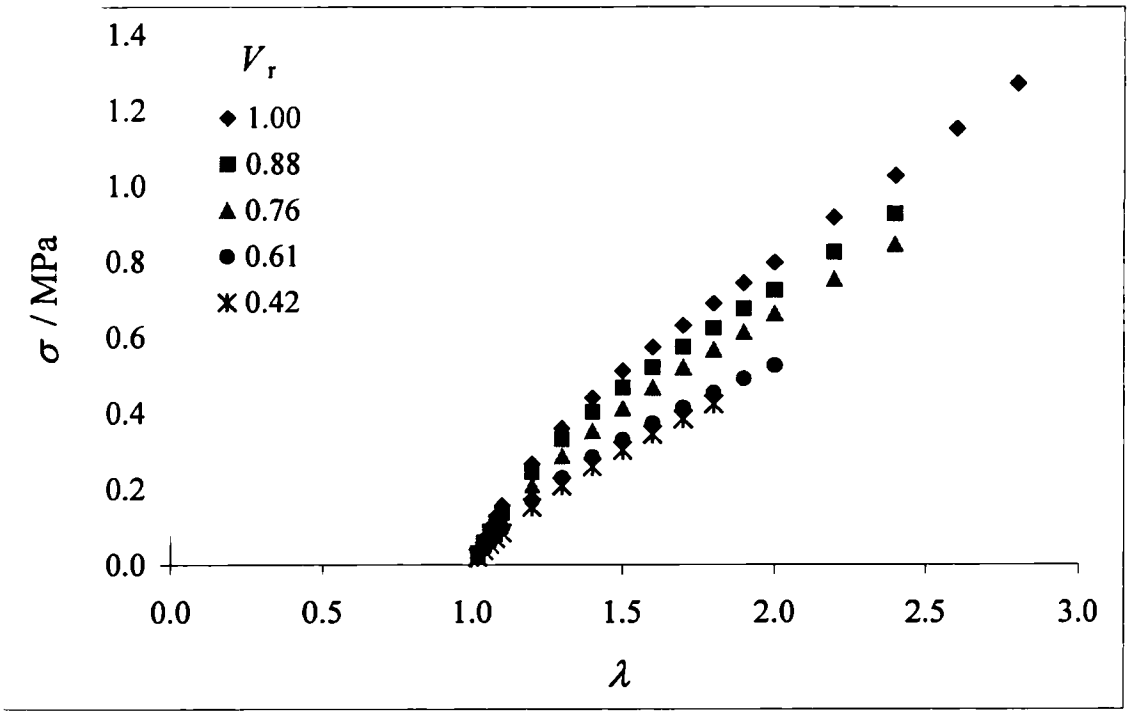

Figure 3-8. The tensile stress-strain behaviour of SBR00-S3 swollen with DBA to various volume fractions of rubber measured at a strain rate of $8.33x10^{-1}s^{-1}$.

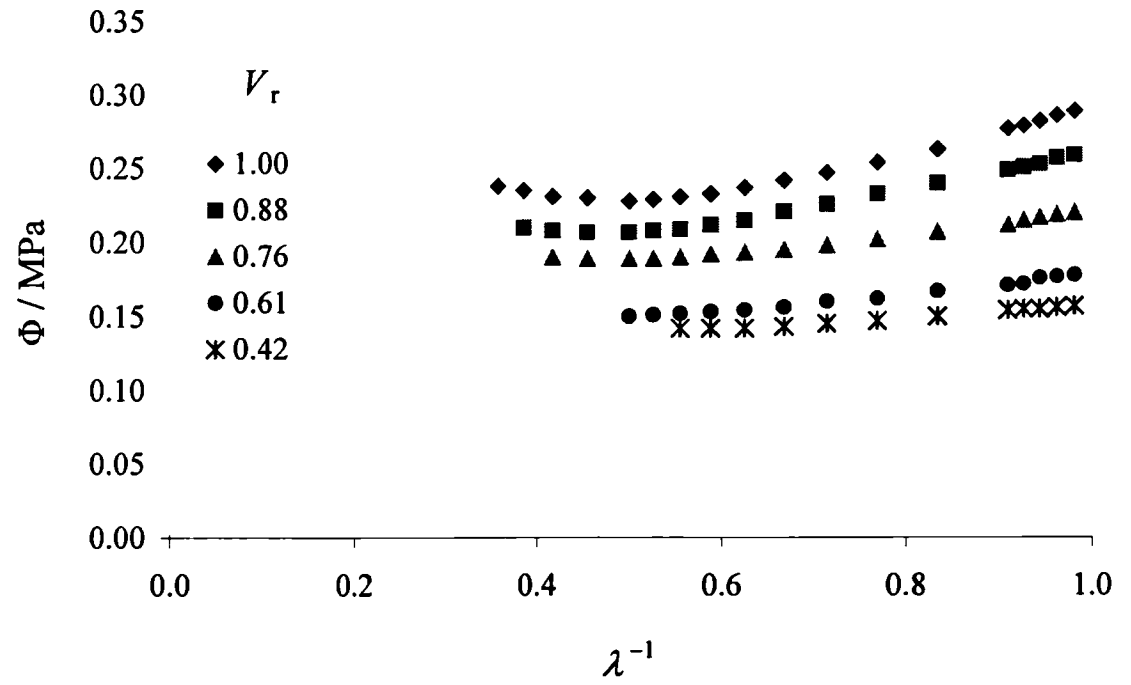

Figure 3-9. The Mooney-Rivlin plot for SBR00-S3 swollen with DBA to various volume fractions of rubber measured at a strain rate of $8.33x10^{-1}s^{-1}$.

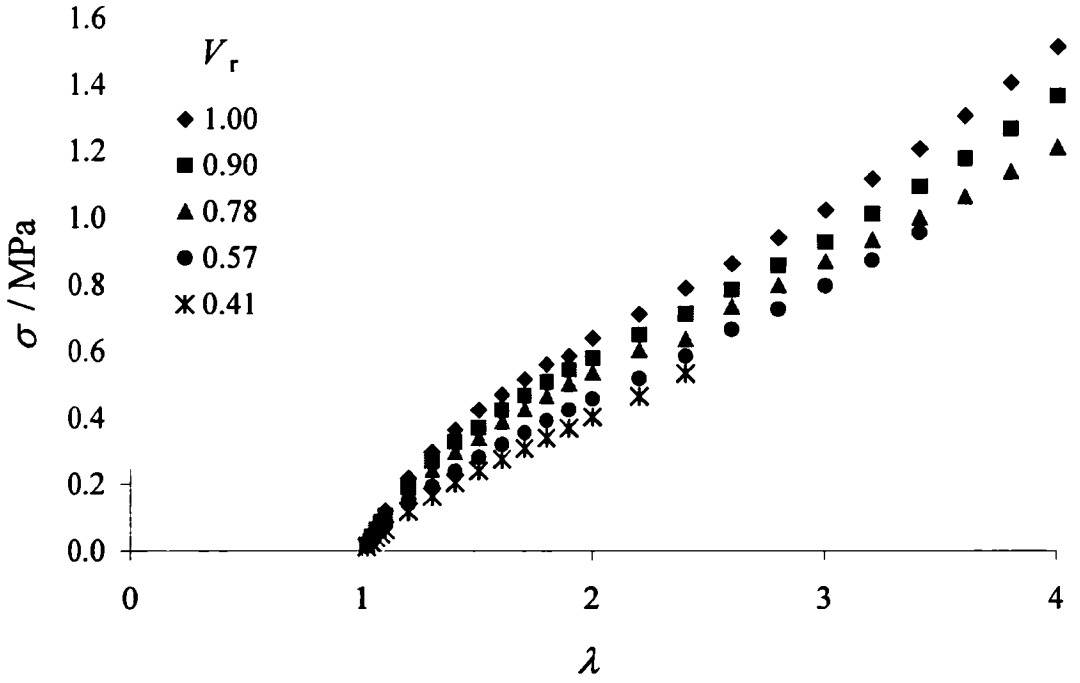

Figure 3-10. The tensile stress-strain behaviour for NR00-S1 swollen with DBA to various volume fractions of rubber measured at a strain rate of $8.33 \times 10^{-1} s^{-1}$.

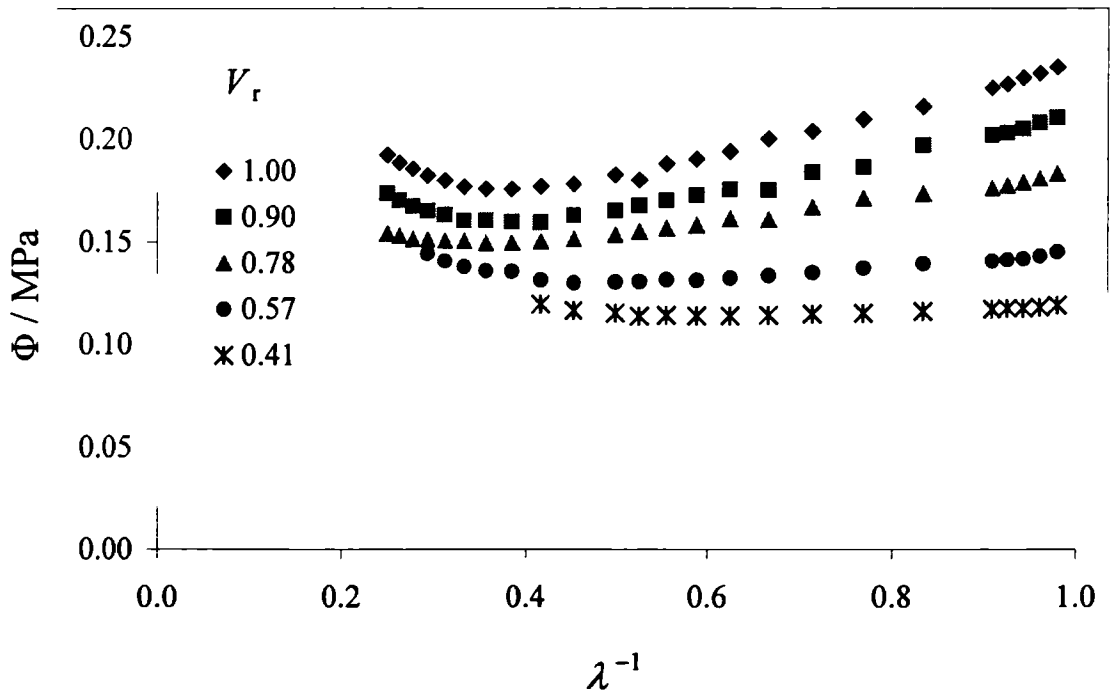

Figure 3-11. The Mooney-Rivlin plot for NR00-S1 swollen with DBA to various volume fractions of rubber measured at a strain rate of $8.33 \times 10^{-1} s^{-1}$.

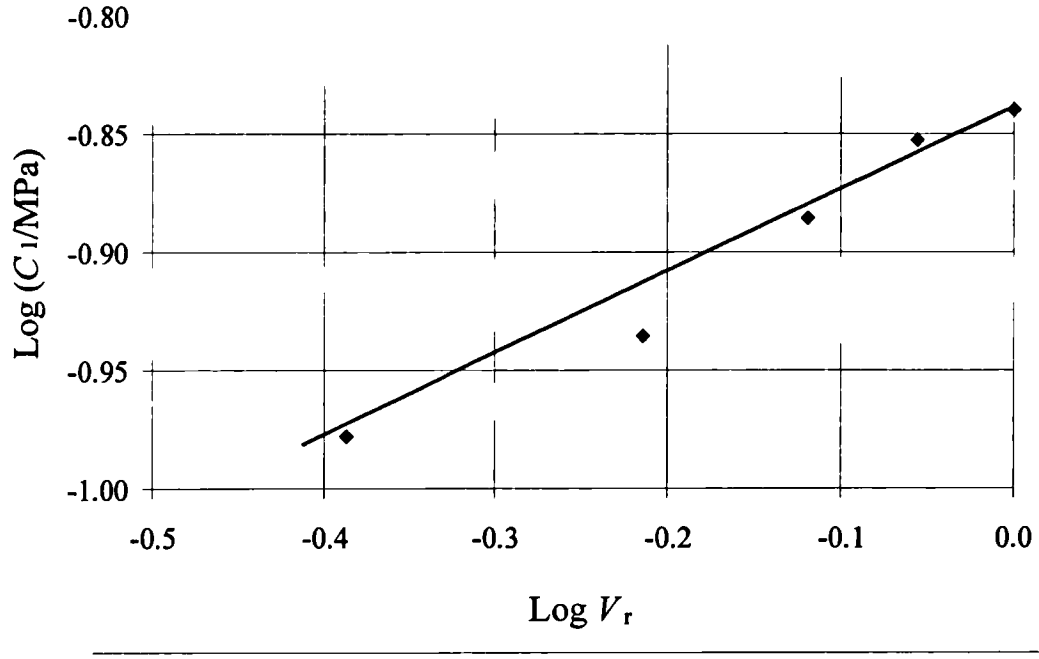

Figure 3-12. The double logarithmic plot of C_1 as a function of V_r for SBR00-S3 swollen with DBA. (the solid line is of slope 1/3).

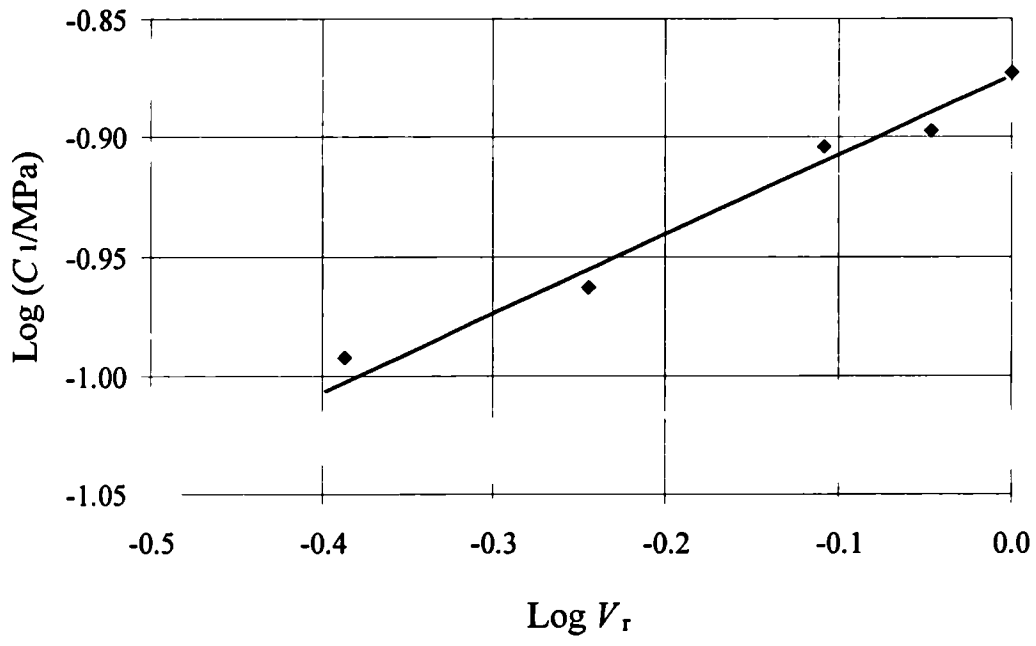

Figure 3-13. The double logarithmic plot of C_1 as a function of V_r for NR00-S1 swollen with DBA. (the solid line is of slope 1/3).

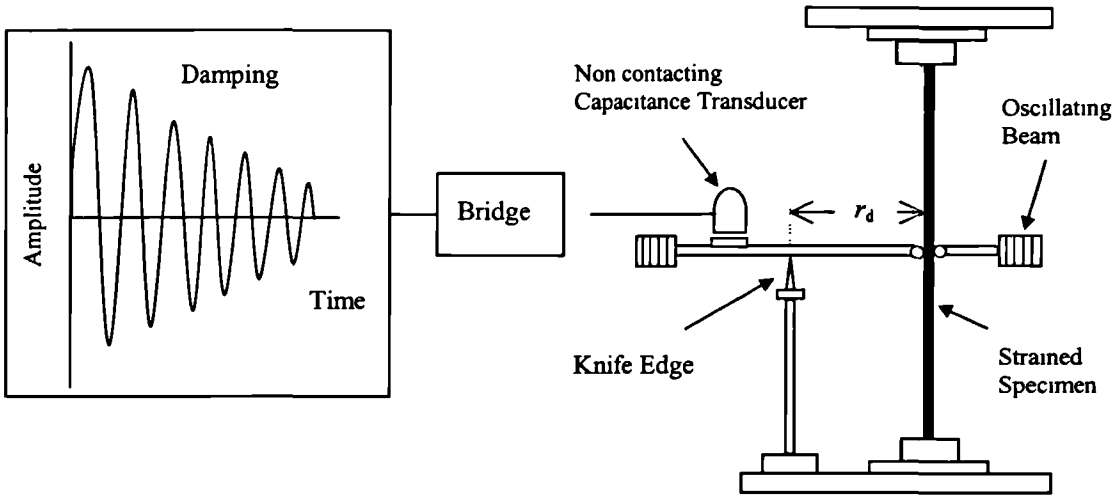

Figure 3-14. Schematic diagram of a simple oscillating beam apparatus for characterising the dynamic mechanical properties of rubber.

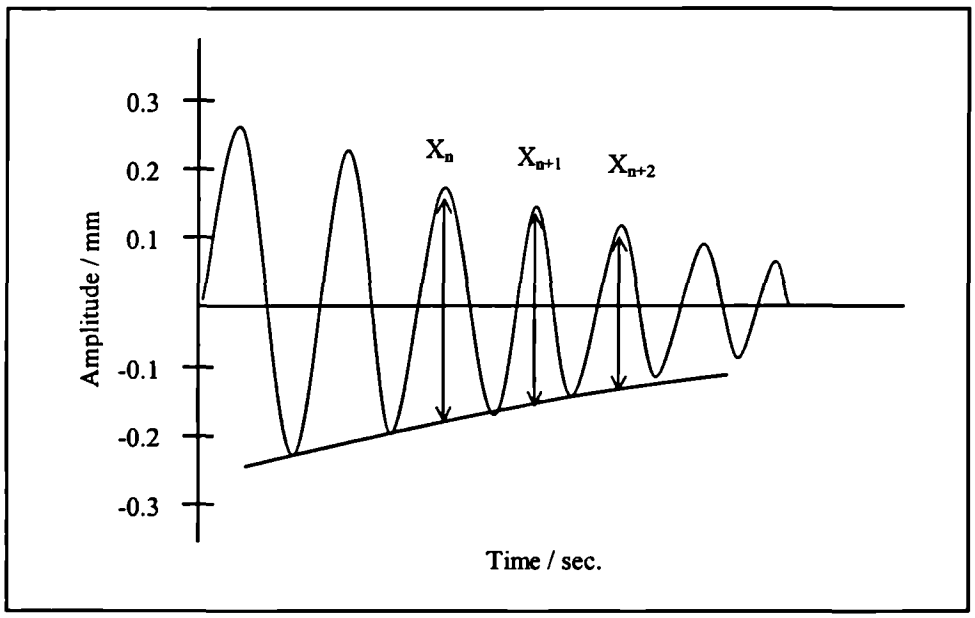

Figure 3-15. The oscillating signals from the capacitance transducer over successive cycles used for calculating the logarithmic decrement.

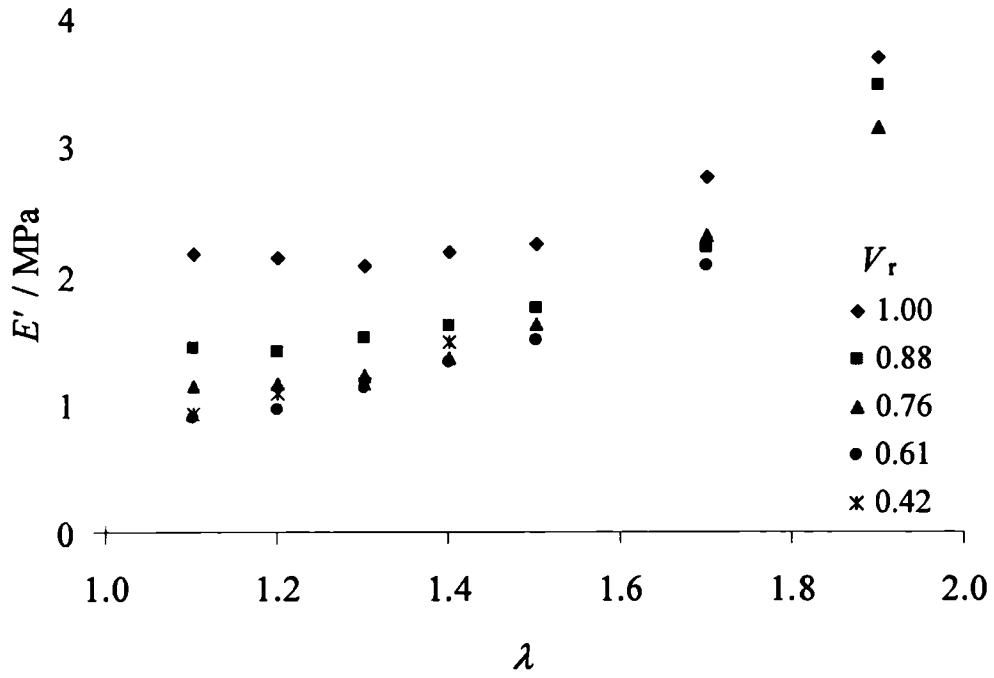

Figure 3-16. The dynamic storage modulus, E', as a function of pre-strain for SBR (SBR00-S3) unswollen and swollen with DBA.

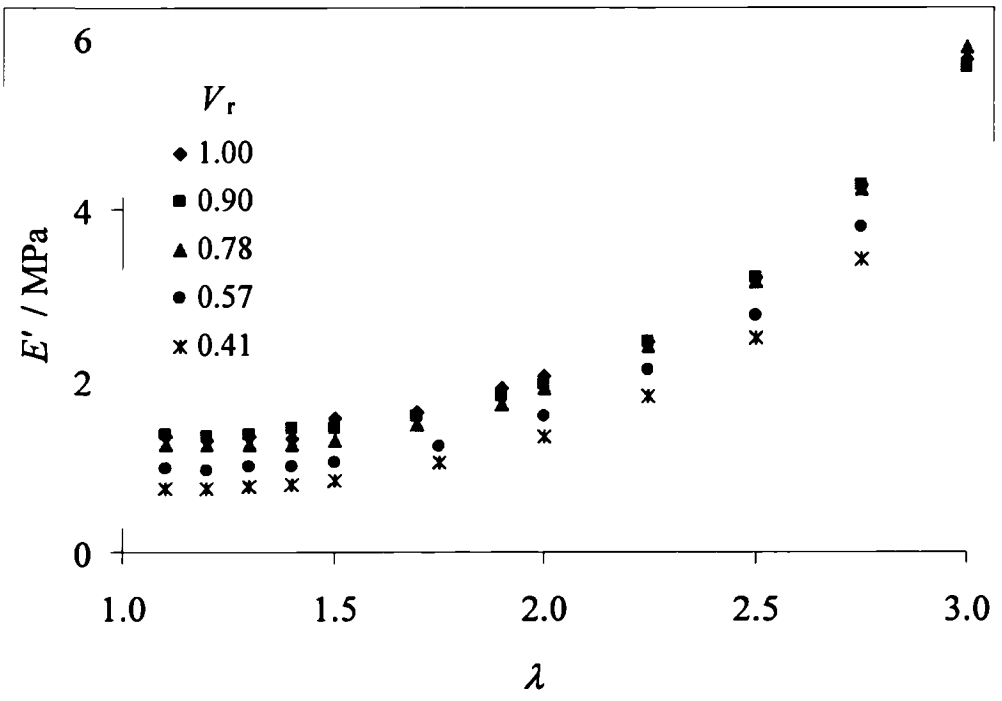

Figure 3-17. The dynamic storage modulus, E', as a function of pre-strain for NR (NR00-S1) unswollen and swollen with DBA.

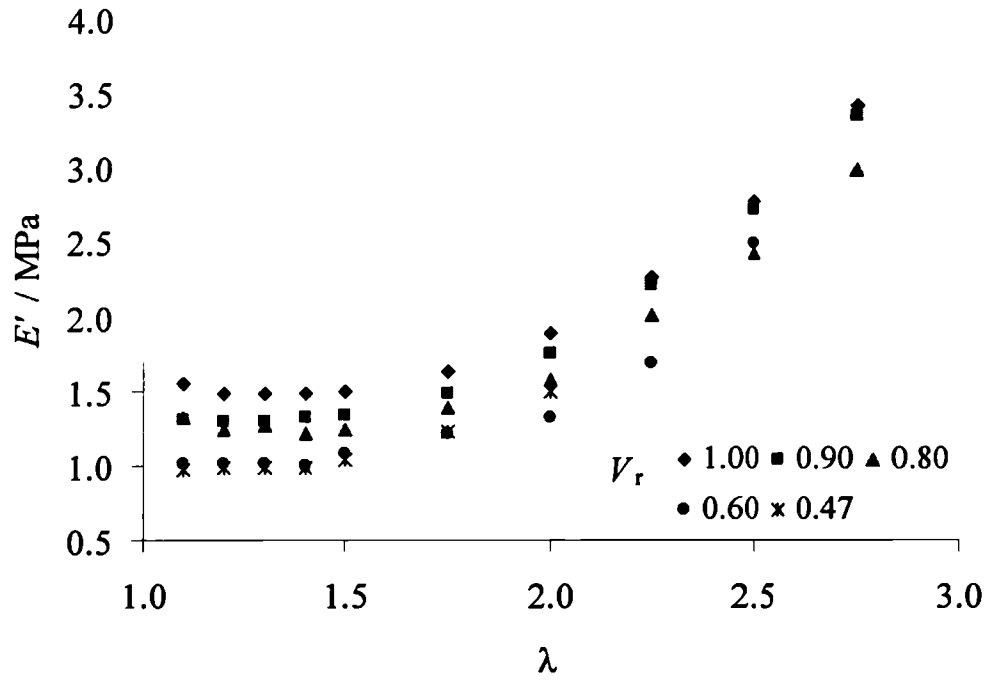

Figure 3-18. The dynamic storage modulus, E', as a function of pre-strain for IR (IR00-S1) unswollen and swollen with DBA.

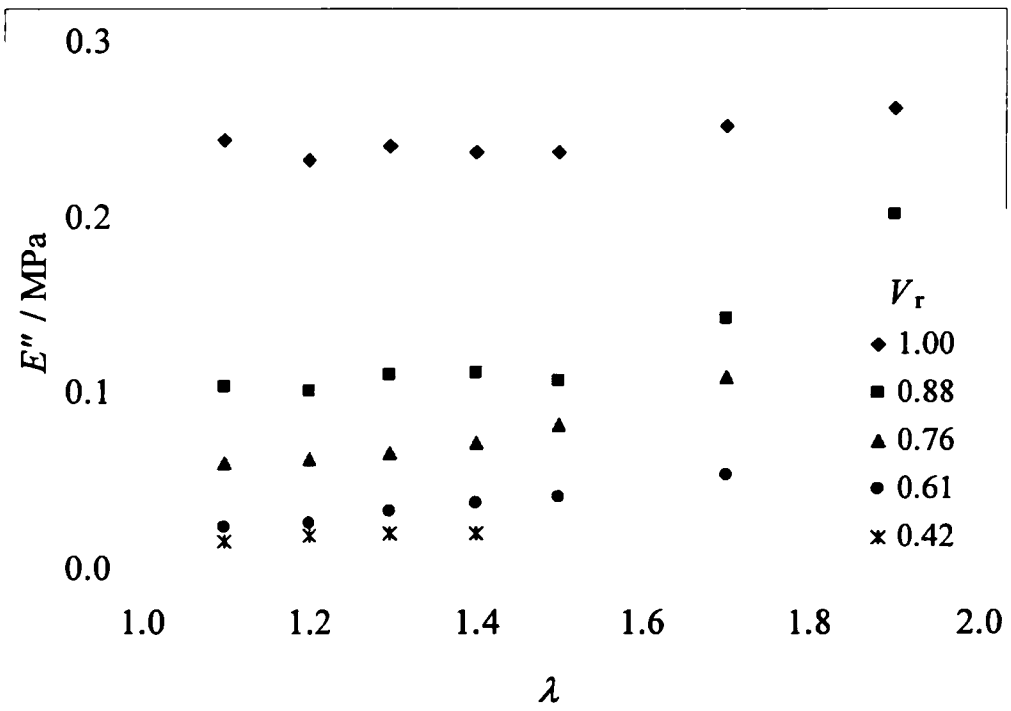

Figure 3-19. The dynamic loss modulus, E'', as a function of pre-strain for SBR (SBR00-S3) unswollen and swollen with DBA.

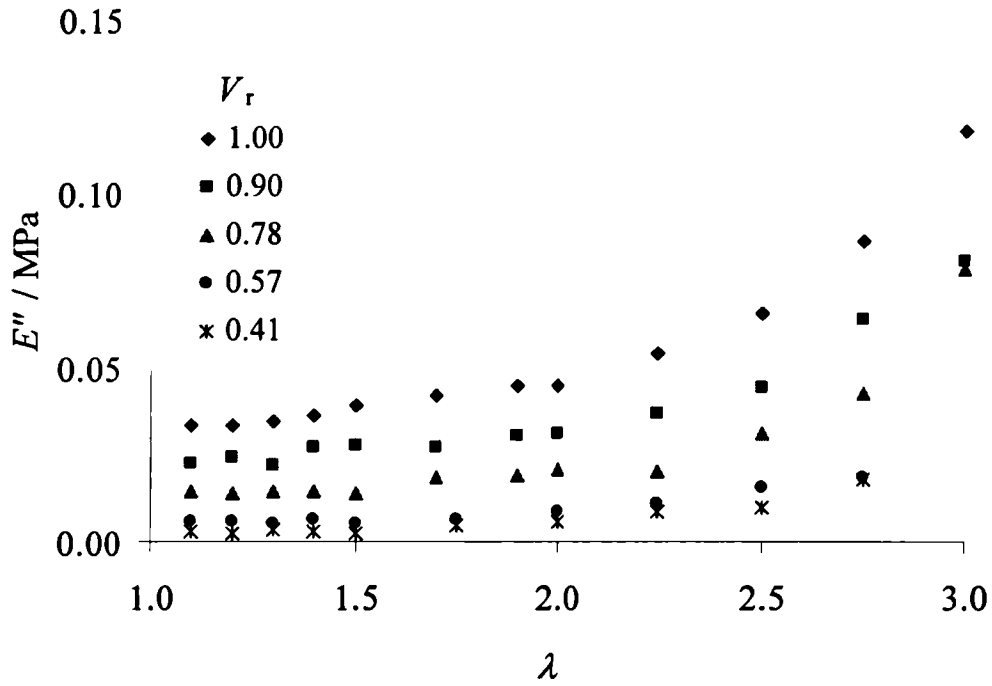

Figure 3-20. The dynamic loss modulus, E'', as a function of pre-strain for NR (NR00-S1) unswollen and swollen with DBA.

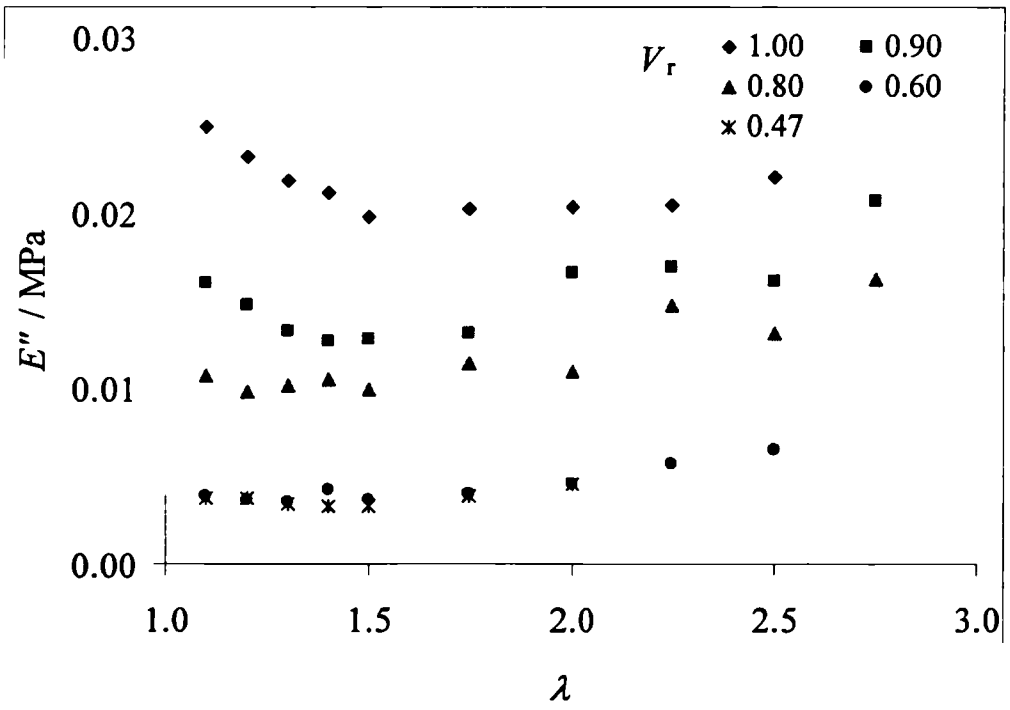

Figure 3-21. The dynamic loss modulus, E'', as a function of pre-strain for IR (IR00-S1) unswollen and swollen with DBA.

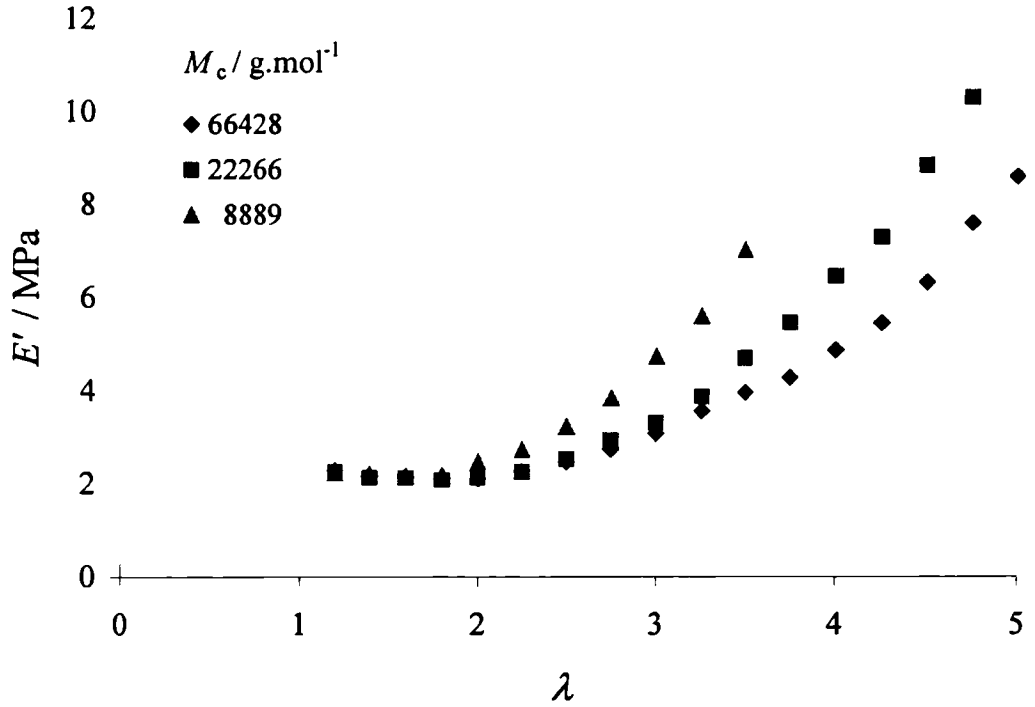

Figure 3-22. The dynamic loss modulus, E' as a function of pre-strain for unswollen SBR (SBR00-S3) of different degrees of M_c.

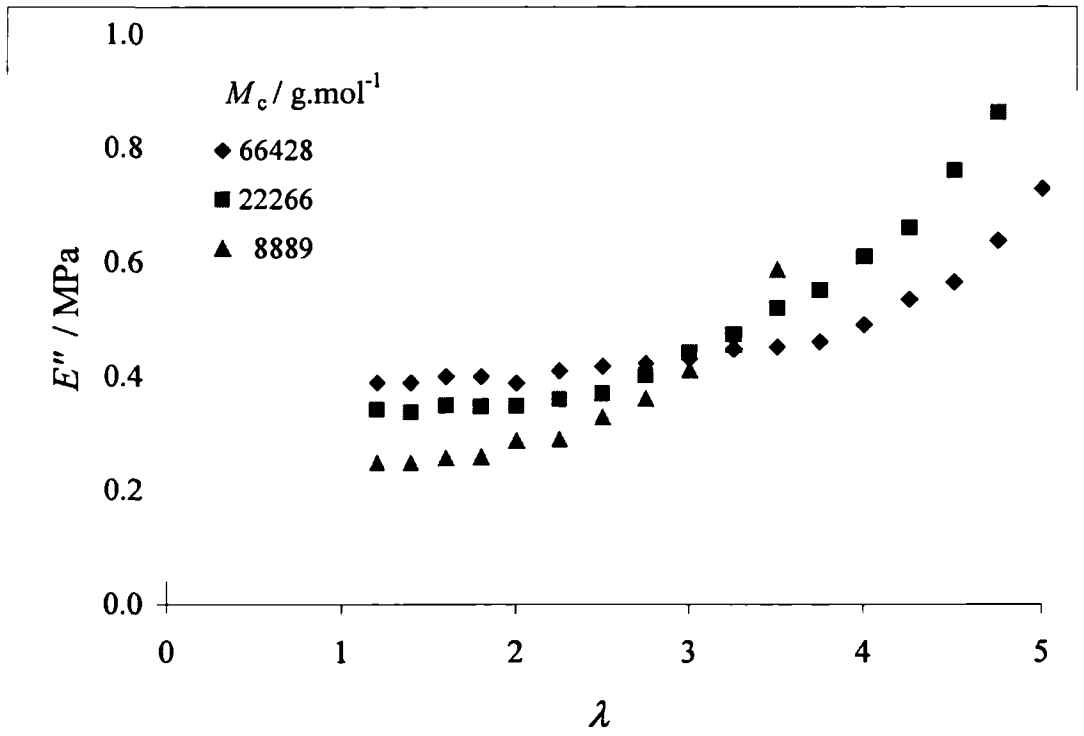

Figure 3-23. The dynamic storage modulus, E'', as a function of pre-strain for unswollen SBR (SBR00-S3) of different degree of M_c.

Chapter Four

Constant rate of grip separation crack growth behaviour (trouser tear)

4-1. Introduction

As was discussed in section 2-2, crack growth in rubber has been described in terms of the tearing energy concept[7-9]. The visco-elastic losses (energy dissipation process) at the crack tip as a crack grows play an important role in determining the strength of the rubber and hence in determining the magnitude of the tearing energy T. When these visco-elastic losses are minimised then the major work done is only that required to break chemical bonds, the rubber vulcanizate shows a minimum tearing energy, termed the threshold tearing energy, T_o[20-22]. Generally this T_o value can be determined experimentally at low crack growth rates, at high temperatures and when the rubber material is highly swollen with a low viscosity liquid using a constant rate of grip separation crack growth measurement (trouser tear test). Of these possibilities, the swelling technique is the most efficient in reducing the visco-elastic losses, but all three will be used here to obtain the maximum effect to investigate the effect of the magnitude of the visco-elastic losses on crack growth behaviour of rubbers.

As was discussed in section 2-3-4, a discrepancy exists between the tearing energy against rate relationship obtained from constant rate of grip separation crack growth measurements and that obtained by a static, constant T, crack growth measurement[8] (figure 2-23). For a non-crystallising rubber, it has been found that the crack growth behaviour can be categorised into three regions on a plot of tearing energy versus crack growth rate, with a distinct change in fracture surface roughness and a clear transition in the static, constant T, crack growth measurement. However, these transitions are not observed in constant rate of grip separation crack growth measurements.

While the principle aim of this thesis is to investigate the mechanisms of crack growth during static, constant T, crack growth tests for a non-crystallising

rubber with widely different visco-elastic properties, for comparison purposes, constant rate of grip separation crack growth (trouser tear) behaviour was investigated. Crack growth measurements were carried out over a wide range of extents of swelling (volume fraction of rubber, V_r) and this work is discussed in this chapter.

4-2. Experimental procedure

4-2-1. Constant rate of grip separation crack growth measurement

Constant rate of grip separation crack growth measurements were carried out using a simple extension (trouser type) test piece as illustrated in figure 2-2(a). These test pieces were prepared by cutting a rectangular parallel-sided test piece from a large moulded sheet. The approximate dimensions of the test pieces were 30mm wide, 60mm long and 1mm thickness.

Crack growth measurement was carried out by separating the legs of the specimen at a uniform rate by a moving crosshead operated at a constant rate by two vertical drive screws in an INSTRON testing machine. The separating crosshead speed ranged from 5 $mm.min^{-1}$ to 500 $mm.min^{-1}$, which provided a range of crack growth rates from 42 $\mu m.s^{-1}$ to 4200 $\mu m.s^{-1}$. Most of the crack growth measurements were carried out at a monitored room temperature of 20°C±3°C. In addition, tests at different temperatures were carried out inside a temperature chamber controlled to ±3°C. Before each test, the test piece was pre-heated to the required testing temperature in the chamber for 15 minutes.

For this extended trouser test specimen, the magnitude of the tearing energy, T, is given by[7-9]

$$T = \frac{2F\lambda}{h} - wW \qquad (4\text{-}1)$$

where F is the applied force, λ is the extension ratio in the legs, h is the thickness of the specimen in the unstrained state, w is the total width of the test piece and W is the elastic stored energy density in the legs of the test piece that are tested in simple extension. The applied force, F, was approximately constant during steady crack growth (figure 2-11(b)), but showed large fluctuations during stick-slip or knotty

crack growth (figure 2-11(c)&(d)). Here for the tearing energy calculation, an average value of the peak force was used in equation (4-1). The force-time curve for each test was recorded using a X-t plotter. The nominal stress in the legs of the test piece was calculated and the corresponding extension ratio, λ, was determined from the independently measured stress-strain curve for each material. The magnitude of the elastic stored energy density, W, was obtained using the following relationship[90][91].

$$W = C_1(I_1 - 3) + C_2(I_2 - 3) \tag{4-2}$$

where C_1 and C_2 are the material constants obtained from a Mooney-Rivlin plot and I_1 and I_2 are the strain invariants calculated using the following equations.

$$I_1 = \lambda_1^2 + \lambda_2^2 + \lambda_3^2 \tag{4-3}$$

$$I_2 = \lambda_1^2\lambda_2^2 + \lambda_2^2\lambda_3^2 + \lambda_3^2\lambda_1^2 \tag{4-4}$$

where λ_1, λ_2, and λ_3 are the principle extension ratios. The crack growth rate, r, at a rate of grip separation, S, was determined using the following relationship

$$r = \frac{S}{2\lambda} \tag{4-5}$$

Each test was carried out with 5 test specimens and the average values were used for every plot.

4-3. Results and discussion

4-3-1. Effect of swelling on the crack growth behaviour

It was expected that the magnitude of the tearing energy necessary to drive a crack at a given rate would decrease with an increase in the extent of swelling (decreasing the volume fraction of rubber, V_r) as the visco-elastic losses decreased. Hence, the effect of swelling was studied first. In this measurement Dibutyl Adipate (DBA) was employed as the swelling liquid.

The value of the measured tearing energy, T, as a function of V_r for different rates, r, for NR (NR00-S1) is given in figure 4-1 and T as a function of r for a range

of V_r values for NR (NR00-S1) is given in figure 4-2. As expected, a large effect of swelling was clearly observed, with decreasing V_r or r, the magnitude of T decreases as the visco-elastic losses decrease. However, even in the most highly swollen material (equilibrium swelling state), V_r=0.41, the magnitude of T was still rate dependent. Furthermore, the lowest magnitude of T measured (T=1.46 kJ.m^{-2}) was very small but was still much larger than the magnitude of theoretically calculated threshold tearing energy, T_o, at around 50 J.m^{-2}. This clearly indicated that a large amount of viscous work must still be carried out during crack growth even in a system of low V_r and r values. On figure 4-2 is shown the standard deviation error bars for each values of the tearing energy. It is noted that the percentage deviation at less than 8% was small and for all subsequent plots only the average value is plotted.

The corresponding results for IR (IR00-S1) are given in figures 4-3 and 4-4. A similar tendency to those for NR was observed and the magnitudes of T for a given rate, r, were also comparable to those for NR (NR00-S1). This agreement was expected as the polymer structure and the measured mechanical properties, such as the tensile stress-strain curve and the dynamic mechanical properties (chapter 3), were almost the same for the NR and the IR compounds.

The results for unfilled SBR (SBR00-S3) are given in figures 4-5 and 4-6. Again the magnitude of T measured decreased with decreasing V_r or r as the visco-elastic losses in the rubber decreased. The measured T values for a given crack growth rate were much smaller than those for NR and IR. Even at the lowest magnitude of V_r and at the slowest r, the measured magnitude of T for NR and IR was more than 10 times higher than that for SBR. It seems that even in this swollen condition, strain crystallisation was still being developed to an extent enough to play a significant role in the crack growth (tear) behaviour for these materials.

The T values measured at a rate of 420 μm.s^{-1} are plotted as a function of the dynamic loss modulus, E'', measured at an extension ration of λ=1.3 for NR (NR00-S1), IR (IR00-S1), and SBR (SBR00-S3) in figure 4-7. In the trouser tear test, the strain at the crack tip is much higher than the strain level of λ=1.3 and hence it might seem more appropriate to plot of the magnitude of T against the magnitude of E'' measured at a higher strain state. However, as was shown in figure 3-19, the magnitude of E'' varied little over a wide range of λ and hence the magnitude of E'' at an extension ratio of λ=1.3 could represent the order of the magnitude of E'' for these

materials at a more appropriate higher strain. It is worth noting that a linear relationship was observed for SBR, a non-crystallising rubber. This linear relationship between T and E'' has been reported previously for unfilled amorphous materials as was illustrated in figure 2-15[32]. This clearly suggested that the tearing energy was the same for all unfilled non-crystallising rubbers under the conditions of equal segmental mobility and that the rate and temperature dependence of T would arose solely from corresponding changes in segmental mobility. Hence, it seems that the magnitude of E'', the direct measure of internal viscosity of the rubber, is proportional to the magnitude of T for unfilled non-crystallising rubber. (However, this is not totally true, as the effective crack tip diameter is not considered here. As will be fully discussed in chapter 5, the crack tip diameter plays an important role in determining the magnitude of T. Hence it seems that the magnitude of the effective crack tip diameter did not vary greatly under the test conditions used to obtain the data shown in figure 4-7, resulting in the dependence of T solely on segmental mobility or visco-elastic losses.) For NR and IR, both strain crystallising rubbers, the relationship is no longer a proportional one and T increases much more rapidly with increasing E''. This difference must be associated with the crystallisation process as the strength of these materials arises from both visco-elastic losses and strain crystallisation.

4-3-2. Effect of temperature on the crack growth behaviour

As was shown in section 4-3-1, the magnitude of T was rate dependent even for the lowest V_r tested at the slowest rate. This indicated that visco-elastic losses still played a role in determining the strength of the rubber even in these extreme conditions. In an attempt to approach threshold tearing energy values the effect of temperature on the trouser tear test was examined.

The effect of temperature on the trouser tear tests for SBR (SBR00-S3; cross-linked with 1.5 phr sulphur, M_c=9889 g.mol^{-1}) unswollen and swollen with DBA to V_r=0.38 are illustrated in figures 4-8 and 4-9. A large effect of temperature was observed, with an increasing temperature of test, the magnitude of T at a given rate decreased as visco-elastic losses decreased. Furthermore, the dependence of the magnitude of T on r reduced with increasing temperature. For unswollen SBR (figure

4-8) the magnitude of T at the highest temperature was still rate dependent, suggesting that the visco-elastic losses still played a role in determining the magnitude of T and hence the tear (crack growth) behaviour for this material. For highly swollen SBR (figure 4-9), it was seen that at 40 to 80 °C the measured magnitude of T became essentially independent of rate, yielding the threshold tearing energy, T_o, of 58 J.m^{-2}. This value was in line with previously determined experimental values[21-23] for a range of materials and with theoretical predictions and hence gave confidence in the accuracy of these measurements.

The results for SBR (SBR00-S1; cross-linked with 0.5 phr sulphur, M_c=66428 g.mol^{-1}) highly swollen with DBA to V_r=0.27 are illustrated in figure 4-10. The same tendency is observed with the result of SBR00-S3 with M_c=9889 g.mol^{-1} as is shown in figure 4-9. The determined T_o value for this material was 64 J.m^{-2}. It should be noted here that the measured T_o value for lightly cross-linked SBR (SBR00-S1) of 64 J.m^{-2} was slightly larger than that for more highly cross-linked SBR (SBR00-S3) of 58 J.m^{-2}. It has been proposed that the magnitude of T_o can be scaled with the cross-link density, M_c[24] (ref. eq (2-25)), as

$$T_o \propto M_c^{\frac{1}{2}} \qquad (4\text{-}6)$$

These results agreed with this T_o theory.

4-3-3. Effect of cross-link density and the types of cross-link on the crack growth behaviour

In this research, materials with a wide range of cross-link densities, M_c, for both sulphur and peroxide cured SBR were examined as it has been suggested that different cross-link systems can result in widely different strengths, even when compared at a similar M_c[34]. The results at a rate of 420 mm.s^{-1} for unfilled SBR of wide range of M_c are illustrated in figure 4-11. Here the shear modulus, G_s, which was determined from the material constants C_1 and C_2, measured in chapter 3, was used as a measure of the cross-link concentration. Clearly the magnitude of T decreased with increasing shear modulus for both cross-link systems. Over the measured range, the magnitude of T was higher for sulphur cured SBR than that for peroxide cured SBR. This was in line with the suggestion that the poly-sulphidic

cross-links broke before the main backbone chain under the high stresses around the crack tip resulting in higher measured strengths for poly-sulphidic cross-linked systems than for C-C cross-linked systems[34].

4-4. *Summary and conclusion*

(1) The magnitude of T decreases with decreasing rate and V_r, or increasing M_c and temperature in the test as the visco-elastic losses decrease.

(2) For the strain crystallising materials, NR and IR, crystallisation can take place and this plays a significant role in determining the magnitude of T and hence tear (crack growth) behaviour, even at the slowest rate and the lowest V_r at room temperature.

(3) For the essentially non strain crystallising material, SBR, a linear relationship between T and E'' is observed, suggesting that the tearing energy is the same for unfilled non-crystallising rubbers under the condition of equal segmental mobility and that the rate and temperature dependence of T would arise solely from the corresponding changes in segmental mobility (if effective crack tip diameter for each material is almost the same).

(4) The value of threshold tearing energy, T_o, can be determined experimentally by testing at high temperature, a low tear (crack growth) rate, and when the rubber is highly swollen with a low viscosity liquid.

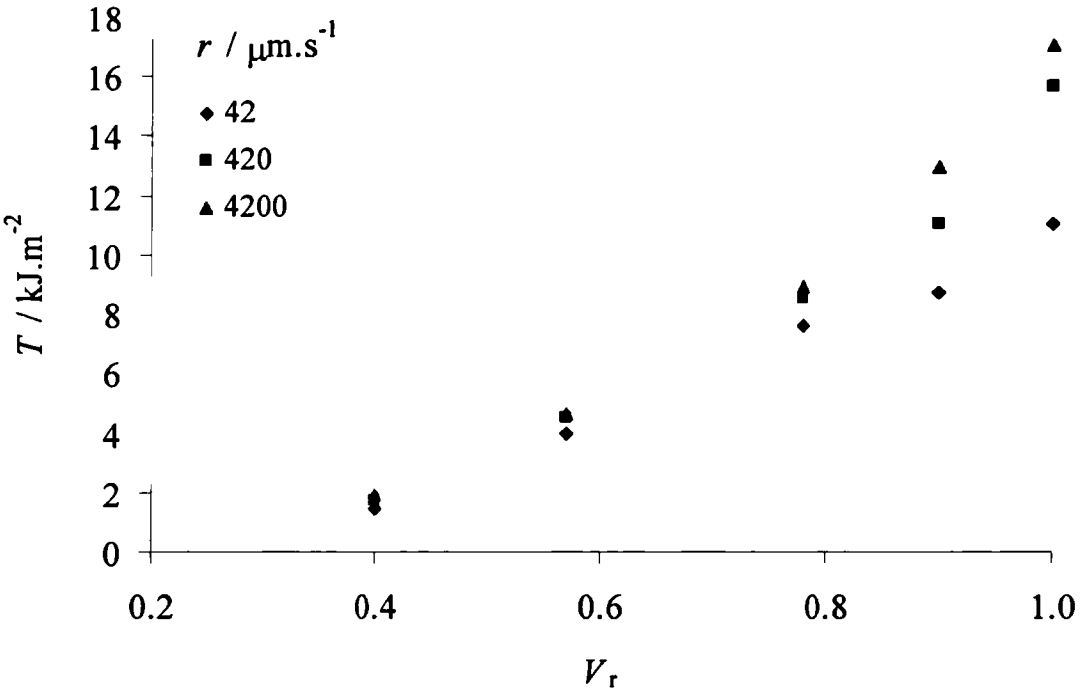

Figure 4-1. The tearing energy, T, as a function of volume fraction of rubber, V_r, for a range of rates, r, for NR (NR00-S1) swollen with DBA.

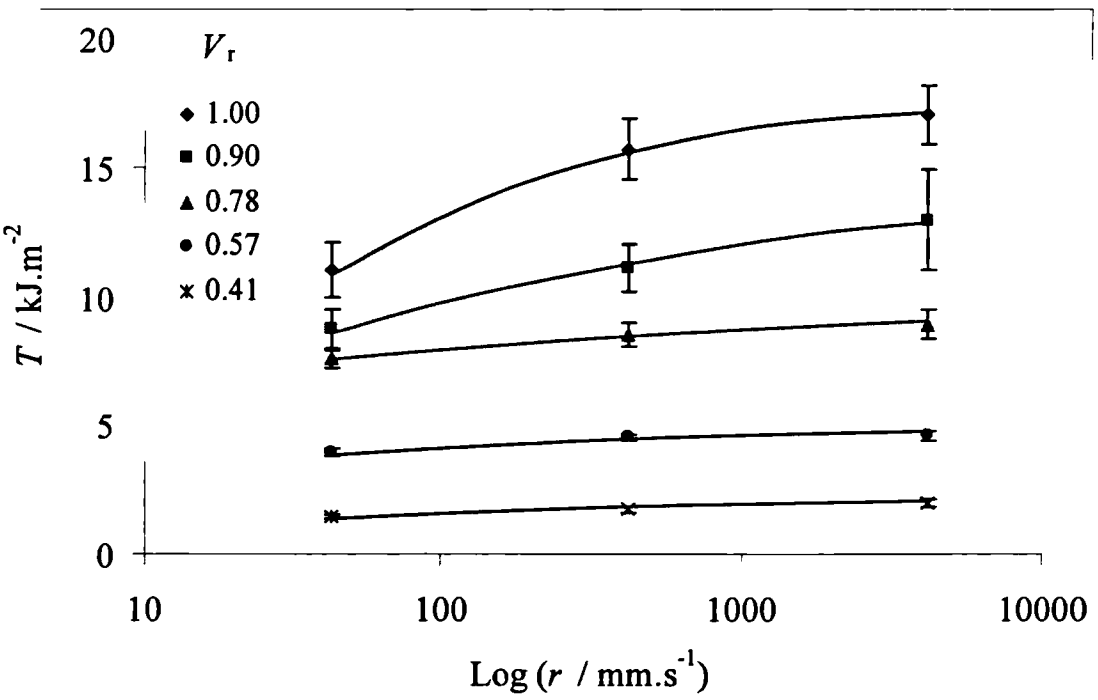

Figure 4-2. The tearing energy, T, as a function of rate, r, for a range of volume fraction of rubber, V_r, for NR (NR00-S1) swollen with DBA.

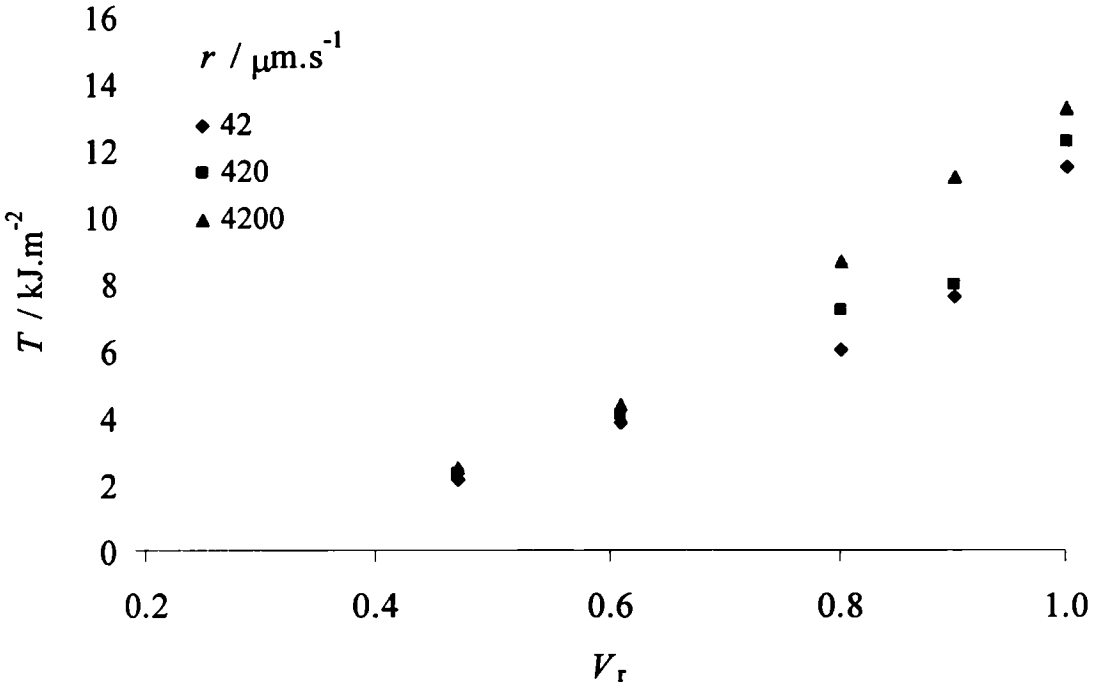

Figure 4-3. The tearing energy, T, as a function of volume fraction of rubber, V_r, for a range of rates, r, for IR (IR00-S1) swollen with DBA.

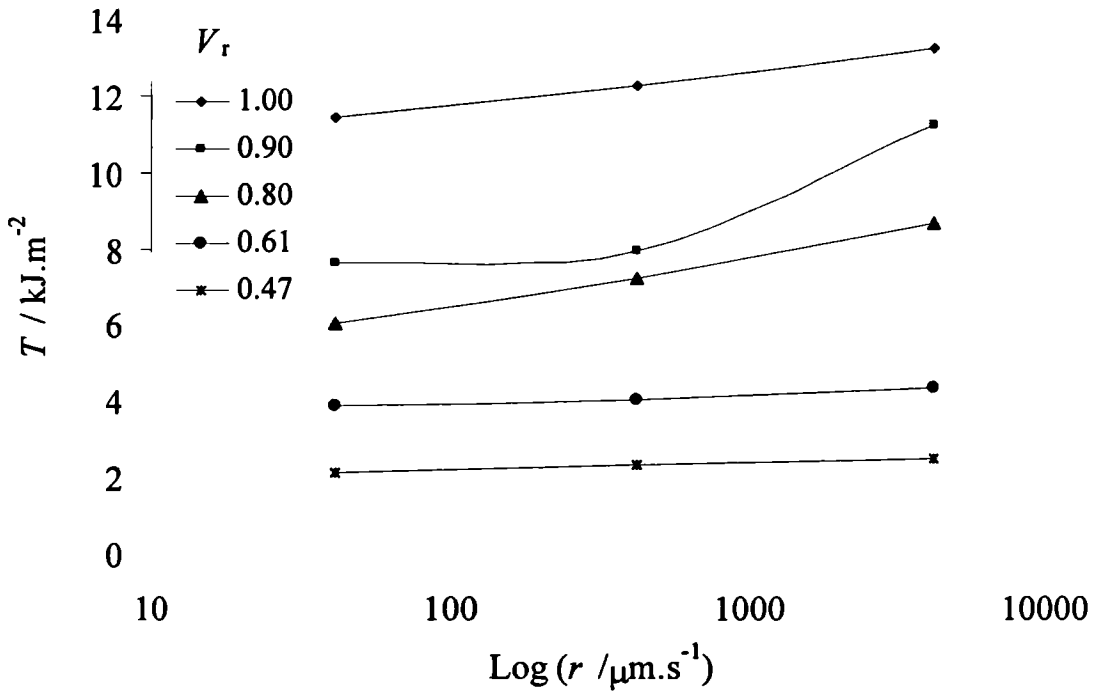

Figure 4-4. The tearing energy, T, as a function of rate, r, for a range of volume fraction of rubber, V_r, for IR (IR00-S1) swollen with DBA.

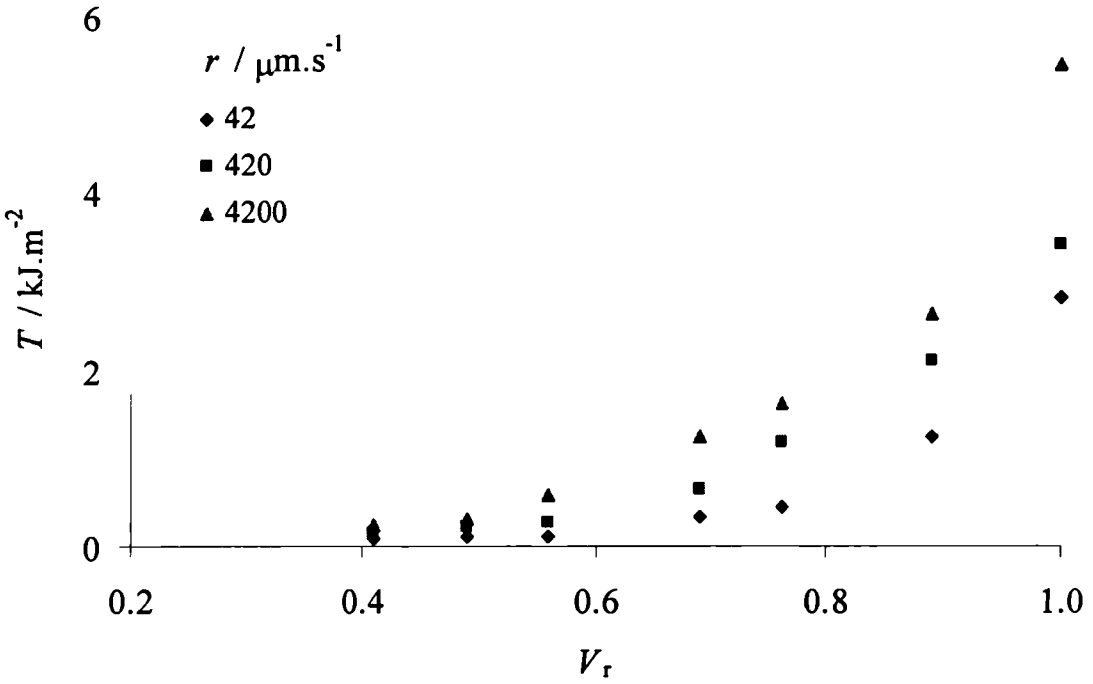

Figure 4-5. The tearing energy, T, as a function of volume fraction of rubber, V_r, for a range of rates, r, for SBR (SBR00-S3) swollen with DBA.

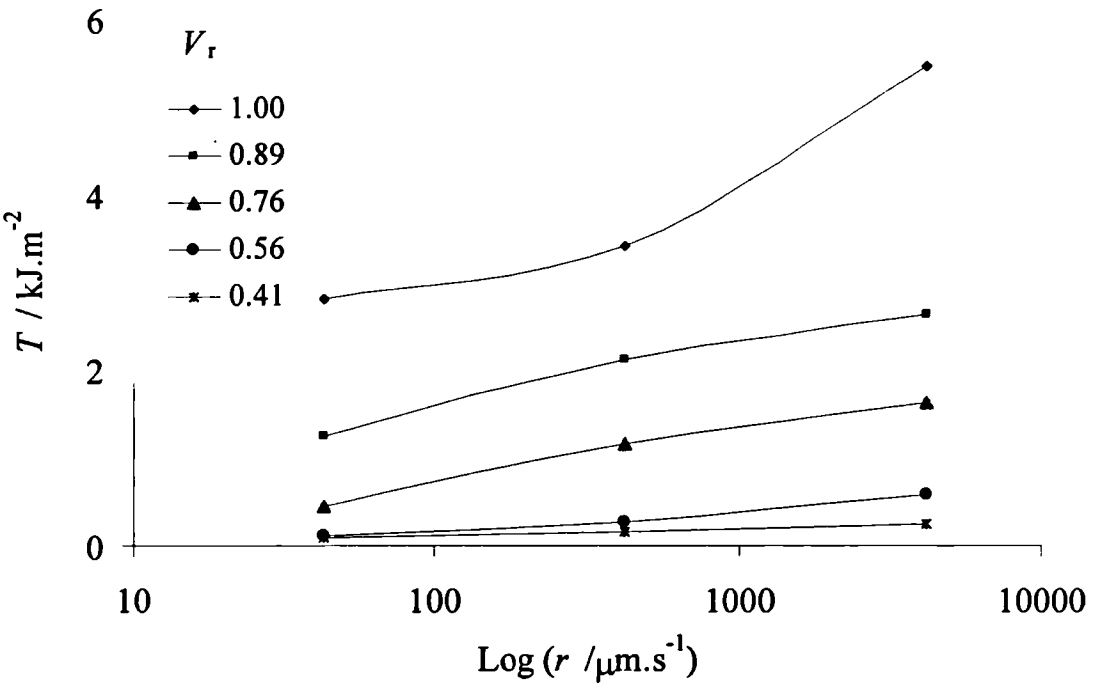

Figure 4-6. The tearing energy, T, as a function of rate, r, for a range of volume fraction of rubber, V_r, for SBR (SBR00-S3) swollen with DBA.

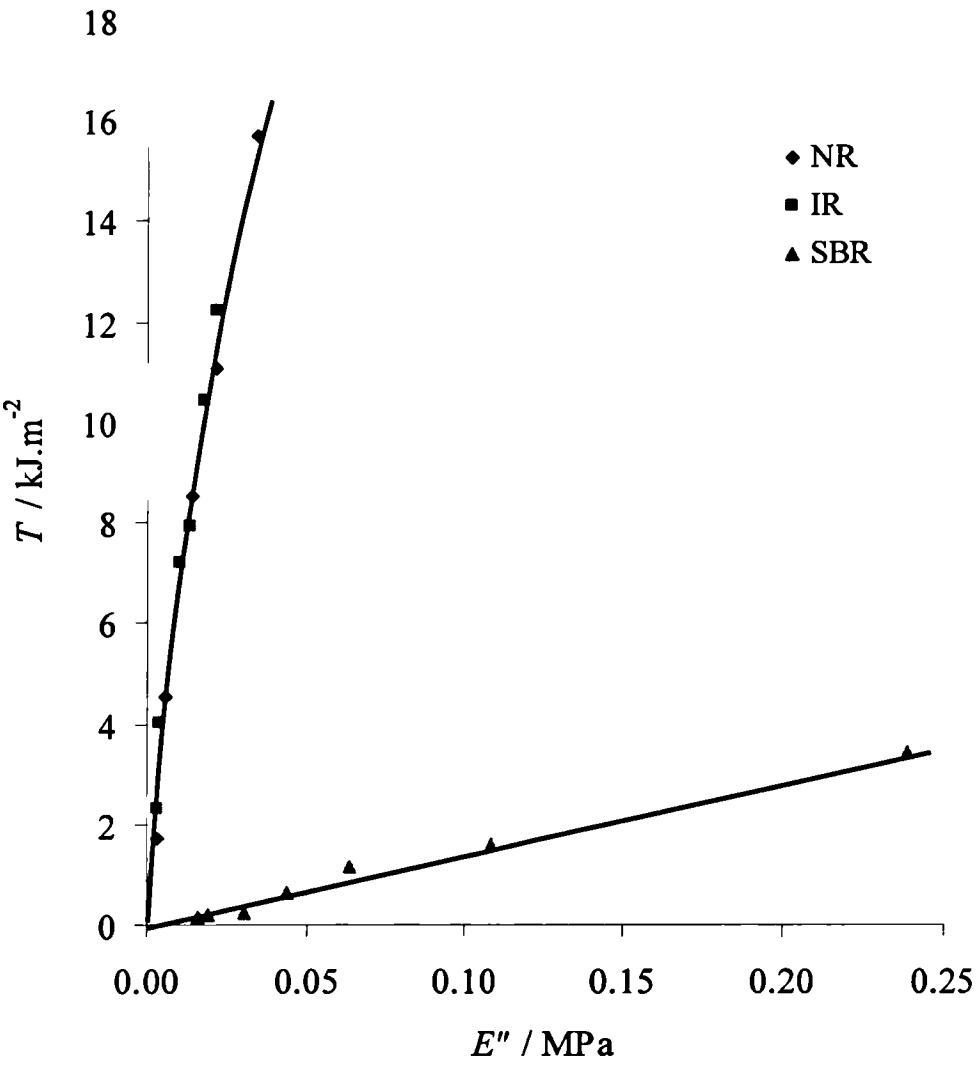

Figure 4-7. The tearing energy, T, at a rate of 420μm.s^{-1} as a function of dynamic loss modulus, E'', at an extension ratio of λ=1.3 for NR (NR00-S1), IR (IR00-S1) and SBR (SBR00-S3).

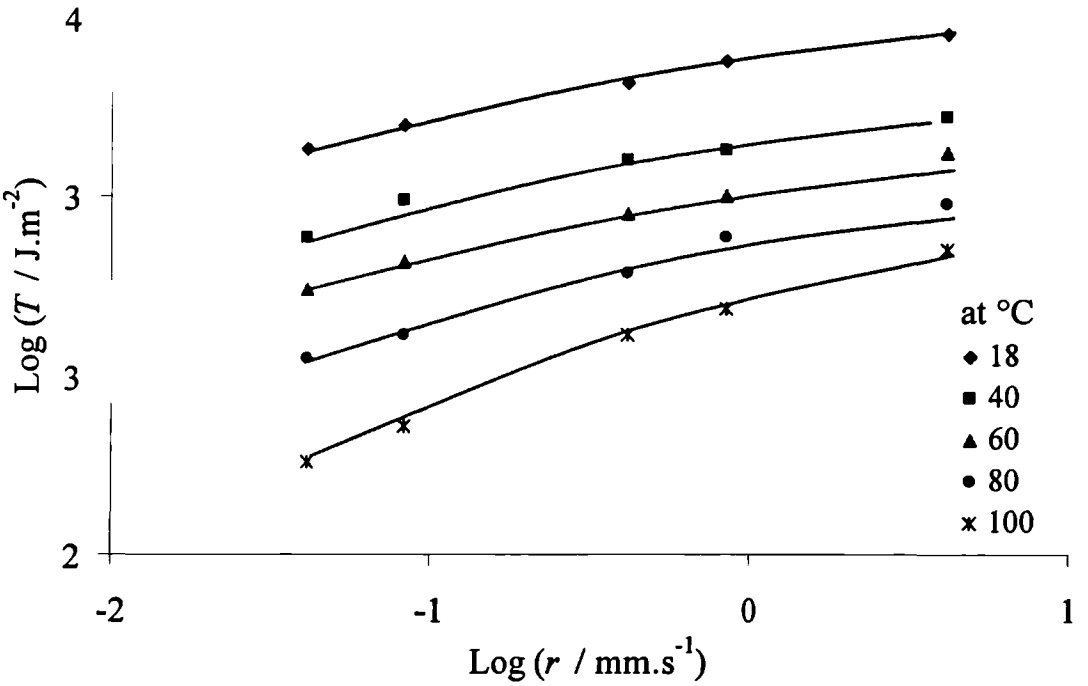

Figure 4-8. The tearing energy, T, as a function of rate, r, for a range of test temperatures for unswollen SBR (SBR00-S3) cured with 1.5phr sulphur, M_c=9889 g.mol^{-1}.

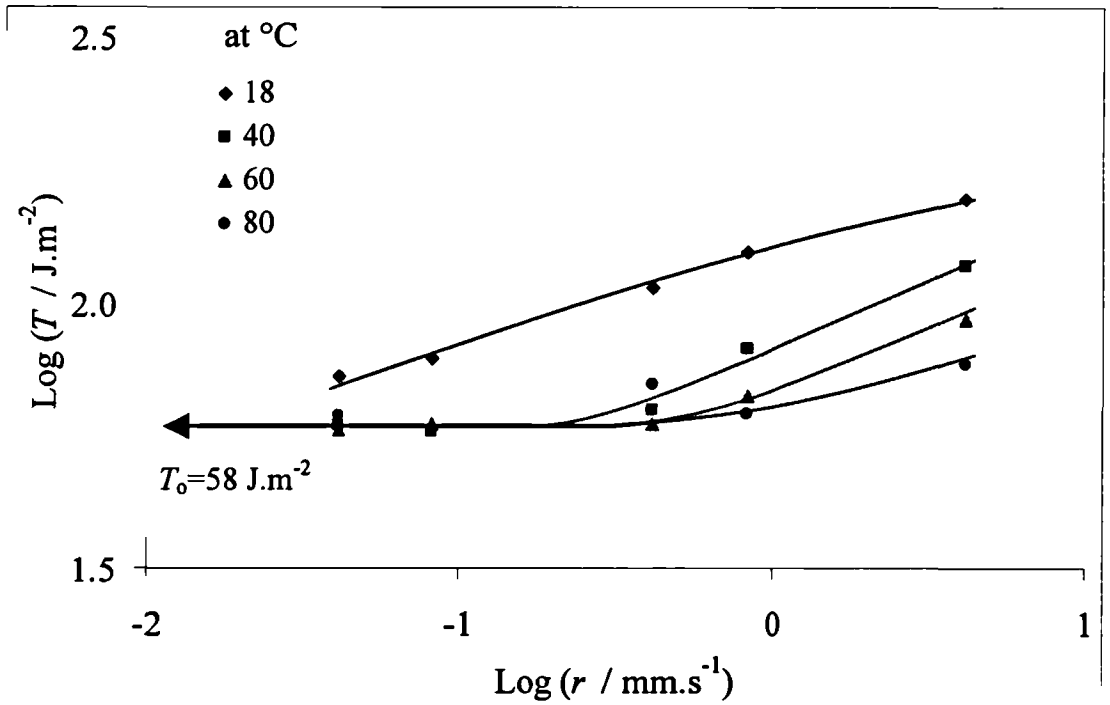

Figure 4-9. The tearing energy, T, as a function of rate, r, for a range of test temperatures for SBR (SBR00-S3), cured with 1.5phr sulphur, M_c=9889 g.mol^{-1}, and swollen with DBA to V_r=0.38.

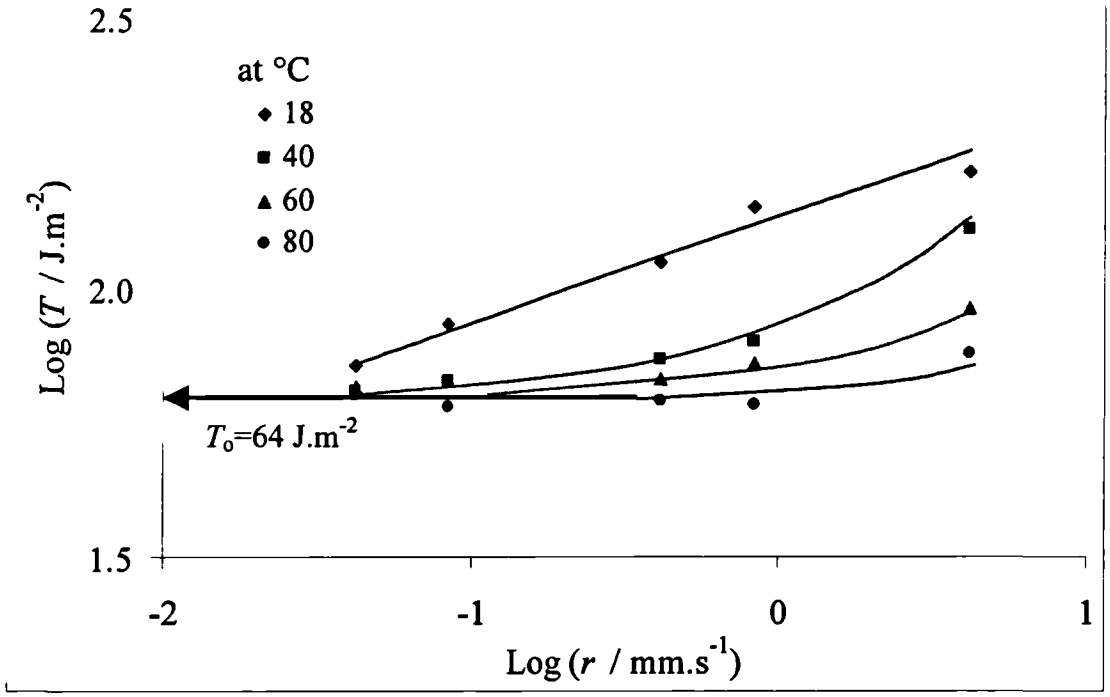

Figure 4-10. The tearing energy, T, as a function of rate, r, for a range of test temperatures for SBR (SBR00-S1), cured with 0.5phr sulphur, M_c=66428 g.mol^{-1}, and swollen with DBA to V_r=0.27.

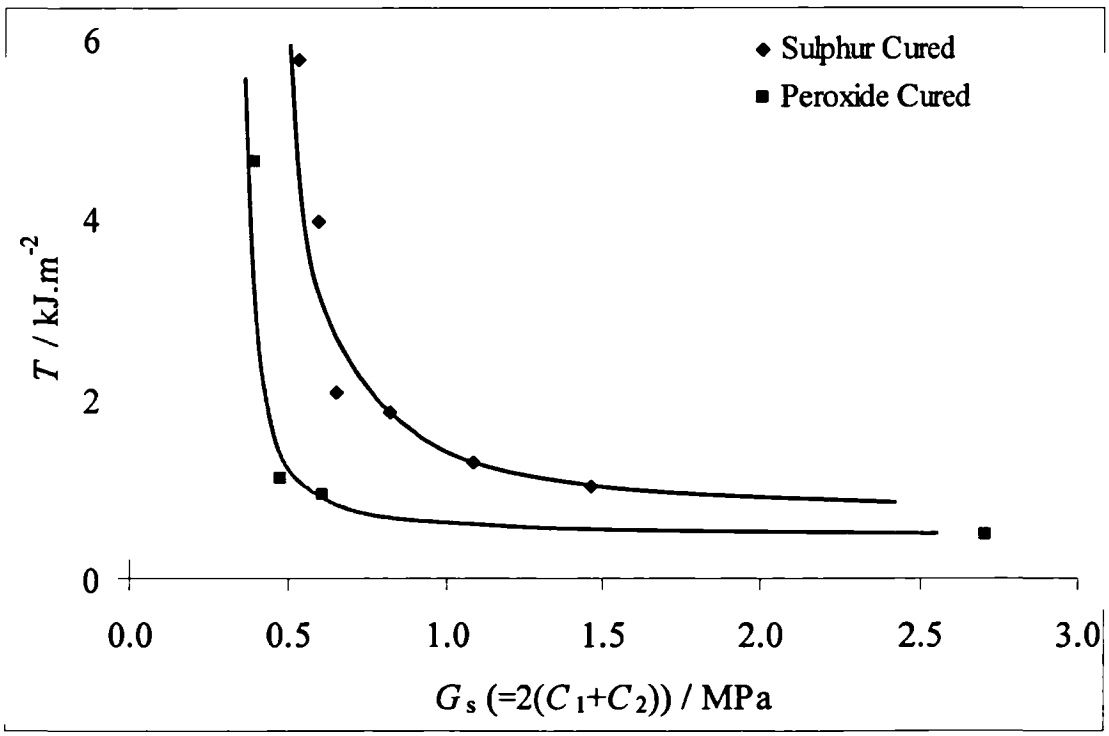

Figure 4-11. The tearing energy, T, as a function of the shear modulus, G, for a range of M_c for both sulphur and peroxide cured SBR at the rate of 420μm.s^{-1}.

Chapter Five

Static crack growth behaviour

5-1. Introduction

Crack growth in rubber has been successfully described utilizing a fracture mechanics approach based on the tearing energy concept [7-9]. The tearing energy, T, is equivalent to the total elastic energy released in a body per unit area of one of the fracture surfaces of the crack as the crack grows. The magnitude of T has been found to uniquely describe the crack growth rate, r, for a given rubber. This magnitude is also determined by the visco-elastic work done at the crack tip as a crack propagates. This work[11-17][19] can be represented by

$$T = W_{ht} k_D d \tag{5-1}$$

where W_{ht} is the strain energy per volume lost at break in the crack tip region, d is representative of an effective crack tip diameter and k_D is the scaling factor. W_{ht} is related to hysteresis and will be scaled with the dynamic loss modulus, G''. d is related to the volume of material at the crack tip in which energy is lost as the crack advances. It is hence the product of W_{ht} and d, which is characteristic of a given crack growth rate for a given rubber. For a non-crystallising rubber it is known that the magnitude of T depends basically on the crack growth rate and temperature, in a manner which follows the visco-elastic behaviour as predicted by the WLF relationship, with T increasing with increasing crack growth rate and decreasing temperature.

As was mentioned in section 2-3-4, especially for a non-crystallising rubber, a large discrepancy exists between the tearing energy versus crack growth rate relationship derived from constant force (static crack growth measurement) and from the constant extension rate (average crack growth) measurement[8]. Static crack growth measurement (constant force) is a more useful experimental technique from which to obtain fundamental and spontaneous crack growth behaviour in a rubber under a given stress field. For a non-crystallising rubber, it is found that static crack growth behaviour can be represented by three regions on a plot of tearing energy

versus crack growth rate, with clear transitions as illustrated in figure5-1. This behaviour cannot be observed in constant extension rate tests. At fast crack growth rates (region-C), the surfaces are very smooth, like a glassy fracture and cracks grow at a constant rate in a manner controlled by the visco-elastic behaviour of the rubber, being scaled by the WLF relationship. At slow crack growth rates (region-A), crack growth is fairly steady but the fracture surface is now clearly rough. In the intermediate region (region-B) crack growth takes place in a stick-slip manner with a resultant rough and smooth surface. This abrupt change in crack growth behaviour between the slow and fast crack growth rate regions is thought to be associated with a distinct change in surface roughness due to crack tip blunting. It has been suggested[30][40] that this surface roughening observed in the slow crack growth rate region results from the intersection of the major propagating crack with growing cavities as illustrated schematically in figure5-2. At fast crack growth rates, it is assumed that the elastic modulus ahead of the crack tip is increased substantially suppressing cavity growth and that the fast rate of crack growth does not allow time for cavities to grow.

Cavitation in rubber is thought to be initiated from flaws, which grow primarily due to hydrostatic stresses[35-39]. The magnitude of the hydrostatic stress, P_c, required to produce cavitation is of the order of Young's modulus as

$$P_c = \frac{5}{6}E + \frac{2\gamma}{r_o} \qquad (5\text{-}2)$$

where E is Young's modulus, γ is the surface energy and r_o is the initial radius of a flaw. However this criterion for cavitation is only strictly applicable for a hydrostatic stress (equi tri-axial stress) field. It is assumed that tri-axial stresses are generated at a crack tip but they are clearly not equal in magnitude in all directions[42]. Furthermore how cavities result in crack tip blunting is not at all clear, hence this cavitation process and the detailed mechanisms which determine static crack growth behaviour need to be fully investigated. In particular the factors, which determine the nature of the transitions in the crack growth behaviour, need to be evaluated.

Such a detailed investigation, which attempts to further our understanding of the mechanisms of the transitions in static crack growth behaviour, is described in this chapter, particularly in light of the cavitation concept. It was proposed to carry out crack growth experiments on a non-crystallising rubber, SBR, with widely

different visco-elastic properties, to be achieved by swelling with liquids, varying temperatures, altering the average molar mass between cross-links and by filling with carbon black. Hence, the main purpose of this study was to investigate the effect of the magnitude of visco-elastic losses (energy dissipation) on the transition between the slow and the fast crack growth regions and also the crack tip behaviour. Crack growth experiments were also carried out on specimens of different thicknesses, which would have different magnitudes of dilatational stresses ahead of the crack tip, with hence a different propensity to cavitate.

In addition, it is well known that a strain crystallising rubber, such as NR, shows strength anisotropy[92-94]. Catastrophic crack growth investigations clearly show that a highly pre-strained unfilled NR is significantly weaker in the direction of pre-strain than in the direction at right angles due to this strength anisotropy[92]. It is generally considered that the strength anisotropy might be responsible for the phenomenon known as knotty crack growth, where the advancing crack profile spontaneously deviates from the anticipated direction, hence causing crack tip blunting[14-17]. In those circumstances strength anisotropy is clearly associated with the developed roughness on fracture surfaces. Even though SBR is a non-crystallising rubber, it might be that a small-scale strength anisotropy developed at the high strains ahead of a crack tip may result in rough fracture surfaces. Therefore static crack growth measurements in pre-strained specimens of unfilled SBR were also carried out to investigate this possibility.

5-2. *Experimental procedure*

5-2-1. Static, constant T, crack growth measurement

The majority of static crack growth measurements carried out here utilised a "pure shear" test piece as illustrated in figure 5-3. Pure shear deformation is achieved by straining a strip of rubber in its height direction, normal to its long dimension, to an extension ratio λ_1, while maintaining the length of the long transverse dimension unchanged (λ_2=1). To achieve pure shear deformation requires the application of a tensile stress σ_1 in the height direction and a stress σ_2 in the transverse direction to maintain an extension ratio of λ_2=1. However, if the width (length) of the specimen

is more than 6 times its height[92] then the direct application of a transverse stress is not required, as the required stresses are automatically generated as a result of the restraints induced by the specimen grips. Except in the vicinity of the free edges, the state of strain in such a test piece is one of substantially uniform homogeneous pure shear. The specimens used in this study were 175mm or 240mm long, about 15 to 20mm in height and usually about 1mm thick. The specimen width was hence approximately 8 times the height. The rubber sheet specimen was ink marked with a suitable of grid of lines (figure 5-3). Crack growth rate measurement (crack length measurement) was only conducted on cracks of sufficient length to be growing in the pure shear region of the test piece as determined by FEA[92].

For this extended pure shear test specimen, the tearing energy, T, is given by

$$T = Wl_o \qquad (5\text{-}3)$$

where W is the elastic stored energy density in the pure shear region and l_o is the unstrained height[8-9]. In this work the magnitude of the elastic stored energy density, W, was calculated from stress-strain curves of pure shear specimens determined by using an INSTRON type tensile testing machine. As it is strictly the elastic energy released by crack growth, which provides the driving force, it is the energy released by the rubber on retraction that is relevant and this is affected by stress relaxation occurring while the test piece is held strained during crack growth. To reduce this effect, the stress-strain measurements to determine the magnitude of W were carried out at a very low strain rate of 8.33×10^{-2} %.s^{-1}. Especially for un unfilled SBR, the difference in the elastic stored energy density, W, between the loading and unloading curve was small at around 10%, and was considered insignificant when compared to the other uncertainties in the fracture behaviour. So for all this work the loading curve only was used for determining the magnitude of W.

Prior to crack growth testing, each test piece was deformed to a certain strain (λ_1). Unstrained and strained heights were measured at 4 different positions on the specimens between the grips using the vernier scale on a travelling microscope. Then a cut was introduced using a razor blade into one of the free specimen edges and the position of the crack tip as a function of time was recorded. To determine very fast crack growth rates, a high-speed video camera and a video recorder that was equipped with a time-lapse function was used to photograph the rubber specimens marked with a 2.0mm square grid mesh. This video camera took a maximum of 50

picture frames per second. The crack length growth per frame, at 1/50 s, was measured on the flat screen under slow playback. The positions of the crack tip in each frame were marked on the flat screen. The length between two successive markings is the crack growth per 1/50 s, hence giving the crack growth rate. This method enabled fast crack growth rates to be accurately measured up to approximately $1 m.s^{-1}$.

5-2-2. Static, constant T, crack growth measurement under pre-strain

To carry this out strip specimens were cut from flat sheets to the following dimensions: 250mm in width, 30-40mm in height, and 1-2mm in thickness. They were then clamped and stretched along the long direction in a rectangular frame with one side sliding edge as shown in figure 5-4. The strip of pre-strained rubber was then gripped along its long free edges with the pure shear grips as shown in figure 5-4. The pre-strained test piece was then extracted from the straining frame by cutting the rubber specimen at the pure shear grip ends. The pre-strain remained applied due to the constraint of the grips, except in the vicinity of the grip ends. The state of strain in such a test piece is substantially uniform homogeneous pre-strained pure shear as shown in figure 5-5 and figure 5-6. Before crack growth testing the test piece was deformed to a certain strain (λ_1') and a cut was inserted in one edge. The unstrained height (l_o') and strained height (l') were measured at 4 different positions as for non pre-strain crack growth measurement. For definition purposes, all the dimensions referred to in the pre-strained state are indicated by the prime sign.

For this pre-strained pure shear test specimen, the tearing energy, T, is given by following equation[92][95].

$$T = W_s l_o' \sqrt{\lambda_2} \qquad (5\text{-}4)$$

where W_s is the elastic stored energy density in the pre-strained specimen resulting from the extension λ_1, λ_2 is the extension ratio of the pre-strain and l_o' is the unstrained height after pre-strain. The magnitude of the elastic stored energy density under pre-strain, W_s, was calculated from stress-strain measurements of the pre-strained pure shear specimen determined using an INSTRON type tensile machine. The pre-strained specimen (figure 5-5 and 5-6) was also extended at the slow rate of

$8.33x10^{-2}$ %.s^{-1} and the stress-strain curve was recorded using an X-Y plotter. The magnitude of W_s was then calculated by integrating this stress-strain curve referring to the pre-strained specimen dimensions. Then a cut was introduced using a razor blade into one specimen edge and the position of the crack tip as a function of time was recorded, if necessary by using a high-speed video camera. In the calculation of the crack growth rate, r, for this pre-strained specimen, the original specimen dimensions (non pre-strained dimensions) were used.

5-2-3. Fracture surface profile measurement

As was referred to in the introduction and illustrated in figure 5-1, the nature of the fracture surface is related to the mechanism of crack growth. Hence a CCD laser surface profilometer was employed here to measure the fracture surface profiles of a range of fractured specimens. The instrument was used as follows: an infrared laser light was reflected from an object surface and was focused to a spot by an objective lens. When the lens/surface distance changed due to the surface topography during scanning, a feedback control circuit moved the objective lens accordingly to restore the focus. This lens movement was proportional to the surface height variations, and hence gave a measure of the surface profile. As strongly scattering or highly absorbing surfaces sometimes make the measurement impossible, a gold coating would usually be employed which increases the reflectivity of the surfaces and improves the resolution. However, in this study, surface profile measurement was carried out without using a surface coating, as there were difficulties associated with coating the swollen specimens. The light spot of 1μm in diameter was used and this could be considered as the test resolution. A typical surface area was selected and the rectangular area of 10mm long and 2mm in thickness was measured. The obtained surface profile data was then exported to the PC and was analysed using EXCEL software.

5-3. Results and discussion

5-3-1. Outline of static, constant T, crack growth behaviour

The tearing energy, T, as a function of crack growth rate, r, relationships (T/r relationship) at room temperature for various SBR compounds, cross-linked with 1.5 phr sulphur (SBR00-S3) and containing 10 and 50 phr of HAF carbon black (SBR10-S1 and SBR50-S1) or swollen with a low molar mass liquid (DBA) are illustrated in figure 5-7. Photomicrographs of the fracture surfaces resulting from cracks growing in the crack growth rate regions A, B, C or at the boundaries between the regions, as defined in figure 5-1, are given in figure 5-8. In figure 5-8, two photomicrographs are shown for each fracture condition. In each case the top micrograph is taken looking down onto the fracture surface and the crack growth direction is right to left. The bottom micrograph shows a cross-section of the fracture surface profile, indicating the surface roughness through the specimen thickness direction.

Unfilled / un-swollen SBR

As described in the section 5-1 (figure 5-1), unfilled/unswollen SBR (SBR00-S3) showed a very clear change from smooth behaviour at fast crack growth rates in region-C to rough behaviour at low crack growth rates in region-A. In the slow crack growth region (region-A) the fracture surface was very rough and cracks grew in a relatively steady manner. In the fast crack growth region (region-C) cracks grew in a very steady manner with a smooth and glassy fracture surface. In the intervening region-B, a mixed behaviour was observed showing rough/smooth surfaces. In this region stick/slip crack propagation occurred with the crack growing in slow and fast bursts. The average values of these combined crack growth rates are plotted in figure 5-7.

Swollen SBR

Dibutyl Adipate (DBA) was used as a swelling liquid as it is a very low viscosity liquid and it can swell rubber to a large extent. Hence, it is a useful liquid for investigating the effect of swelling over a wide range of degrees of swelling. With decreasing volume fraction of rubber, V_r, or increasing volume fraction of

liquid, (*i.e.* decreasing internal viscosity) the clear transition points, which were observed in the un-swollen SBR, became less clear. The crack growth behaviour of lightly swollen SBR, V_r=0.8, can still be divided into three regions showing stick/slip behaviour in the intermediate region, but the transition points were not as sharp. The highly swollen SBR, V_r=0.4, exhibited a linear *T/r* relationship, over the entire measured crack growth rate regime. The cracks propagated in a relatively steady manner over the range of rates measured without showing any stick/slip behaviour, even though the fracture surface changed from very rough to relatively smooth with increasing crack growth rate. It seemed that the extent of the rough surface region increased with decreasing volume fraction of rubber or increasing volume fraction of low molar mass liquid.

Carbon black filled SBR

The carbon black filled materials (increasing internal viscosity of rubber) showed a different crack growth behaviour from that of the unfilled SBR. Surprisingly the filled materials did not show a stick/slip region, which results in the *T/r* relationship exhibiting a drastic jump from region-A to region-C at a certain tearing energy. Furthermore, the fracture surfaces generally became much smoother with increasing carbon black content. Even in region-A, for the 50 parts carbon black filled material a relatively smooth surface was seen.

General outline of static crack growth

It would be expected that an abrupt change in crack growth behaviour, as for the carbon black filled materials, between the slow and fast crack growth rate regions would be associated with a distinct change in surface roughness but this was not observed for the highly filled carbon black material. Furthermore, for the swollen materials a change in roughness was observed with no marked change in crack growth behaviour. Therefore, it may be that the static crack growth behaviour, such as transition points and jumps (discontinuous relation observed in the carbon black filled SBR) cannot be simply related to surface roughness but are a complex interaction of various crack tip blunting processes and the visco-elastic losses at the crack tip.

The magnitude of tearing energy clearly must depend on the magnitudes of both W_{ht} and d in the relationship

$$T = W_{ht} k_D d \qquad (5\text{-}1)$$

Here, for all the rubber materials, the magnitude of the tearing energy at a given crack growth rate increased with increasing visco-elastic losses in the material at the crack tip.

The observed fracture surfaces tended to become smoother with increasing visco-elastic losses (increasing rate, increasing volume fractions of rubber and increasing carbon black content). If crack propagation is due to the intersection of the advancing major crack with growing cavities ahead the crack tip causing crack tip blunting, hence resulting in rough fracture surfaces, it may be that the ease of cavity growth is largely associated with the magnitude of the visco-elastic work done. This and other possibilities in the relationship between W_{ht} and d are investigated in the following sections.

5-3-2. Static crack growth for unfilled SBR

5-3-2-1. Stick-slip behaviour

The unfilled/unswollen SBR (SBR00-S3) showed a very clear change from smooth behaviour at fast crack growth rates in region-C to rough behaviour at slow crack growth rates in region-A (figure 5-7). In the intervening region-B, a mixed behaviour was observed. In this region cracks propagate either in a slow (stick) or in a fast (slip) manner resulting in a combination of rough and smooth surfaces. The average value of those fast and slow crack growth rates was plotted on figure 5-7 for the stick-slip region averaged over the total crack growth length of 160mm (c_{total}). Actual crack growth rates were measured over much shorter crack growth increments (c_1) utilising the high-speed video recorder and the Force-Time chart recorder for each crack extension. This enabled the process to be examined in more detail by the use of histograms of crack growth rate frequency. The form of the histograms is of an incremental plot of crack growth frequency (c_1/c_{total}) against incremental crack growth rate for SBR00-S3 as shown in figure 5-9. In the slow crack growth region-A, where cracks grew in relatively steady manner, the crack growth rate distribution

was broad but the rate could reasonably be represented by a mean or average value (figure 5-9(a)). In the fast crack growth region-C, where cracks grew in steady manner, the distribution was narrow and cracks were seen to grow at a very precise rate (figure 5-9(c)). In the stick-slip region-B the distribution was clearly bi-modal and cracks either grew at a slow or fast rate (figure 5-9(b)). These fast and slow rates are plotted together with the average rate in figure 5-10. It was clear that cracks grew in this transition region at rates associated with either the high energy/fast rate process or the low energy/slow rate process. Hence, the increments of crack growth in the stick-slip region were either associated with the relatively steady slow crack growth of region-A or with the steady fast crack growth of region-C.

This methodology of representing and measuring crack growth in the stick-slip regions was used throughout this work for all materials where it was appropriate.

5-3-2-2. Static crack growth under pre-strain

Cavitation has sometimes been employed to interpret the crack growth behaviour and roughening of fracture surfaces for not only rubber but also other materials, such as metals, ceramics and plastics. However, the cavities themselves have not been directly observed even though their presence have been inferred[31][42]. Hence, as was mentioned in section 5-1, as alternative source of the fracture surface roughness may be the development of strength anisotropy. Though SBR is a largely non-crystallising rubber, it may be possible that the small-scale strength anisotropy is developed in the high strain regions ahead of the crack tip resulting in crack tip deviation and hence producing a rough fracture surface. Therefore, this effect was investigated here utilising a pre-straining experiment.

In this investigation 25% or 50% pre-strain were applied as described in the section 5-2-2. The effect of the pre-strain on the T/r relationship for unfilled and unswollen SBR (SBR00-S3) is illustrated in figure 5-11. Here only the average value of crack growth rate is plotted for the stick-slip region. It should be noted that the magnitude of the tearing energy plotted in figure 5-11 was calculated using equation (5-3), and hence is only applicable to cracks growing in the horizontal direction. Due to the effect of the pre-strain, growing cracks tended to deviate from this horizontal direction towards a direction normal to the pre-strain direction. Furthermore, the

measured crack growth rate varied widely with crack growth direction. In the case of the lowest tearing energy, the resulting crack growth rate in the horizontal direction was very slow with its major growth direction tending very much to be in the normal direction. As the crack direction deviated, the measured crack growth rate increased. This variation of crack growth rate with crack growth direction increased with increasing pre-strain. This variation of crack growth rate is plotted in figure 5-11 as an error bar. The variation decreased with increasing the tearing energy for both the 25% and 50% pre-strained material. Clearly no significant effect of pre-strain was observed in the fast crack growth region as the cracks grew straight with no deviation from the horizontal direction. The data in figure 5-11 are re-plotted in figure 5-12 using only the horizontal crack growth rates. From this figure it was clear that no effect of pre-strain was observed on the crack growth rates measured for a given value of T. The incremental crack growth rates are plotted as a function of crack growth angle (deviation from the anticipated horizontal crack growth direction) in figure 5-13. In this figure, the aspect extension ratio ($R_a = \lambda/\lambda_{pre\text{-}strain}$) was employed to characterise the crack growth behaviour under pre-strain. The angle from the horizontal, at which the maximum crack growth rate was observed, varied from 90° to 0° with increasing magnitude of R_a. At low values of R_a, the maximum crack growth rate was obtained at large angles to the horizontal direction and the measured crack growth rate in the horizontal direction was sometimes more than two orders of magnitude slower than this maximum rate. Conversely for high R_a values, the maximum crack growth rate was always observed to be in the horizontal direction. It was interesting to note that cracks grew in all directions with almost the same rate for R_a=1, equi-biaxial extension. This clearly indicated that the angular dependence of the crack growth rate was associated with the maximum energy release direction. The maximum energy release direction would be largely perpendicular to the horizontal for low values of R_a. Therefore, it is suggested for unfilled/non-crystallising materials, such as SBR that cracks grow in the direction that release the maximum energy release. If the incremental crack growth rate for each direction were plotted with the appropriate magnitude of tearing energy corresponding to each crack growth direction, then the T/r relationship in figure 5-11 would be a single master curve.

Clearly the results showed no significant effect of pre-strain in developing small-scale strength anisotropy for unfilled SBR. It was hence thought unlikely that the surface roughness observed in the slow crack growth region for unfilled SBR be associated with crack growth deviation due to strength anisotropy.

5-3-2-3. Effect of thickness of the specimen

It was suggested in section 2-3-4 that cavitation played an important role in static crack growth behaviour[31][42]. This cavitation process is thought to be associated with fracture surface roughness and the effective crack tip diameter (crack tip blunting), hence affecting the magnitude of the tearing energy via d in equation (5-1).

It has been suggested that rubber can cavitate under hydrostatic tension and that the critical hydrostatic tension for opening up cavities is given as in equation (5-2). Variation in specimen thickness alters the magnitude of tri-axial stress field in the high strain region ahead of a crack tip; decreasing in magnitude with decreasing thickness. Hence, it is expected that the size and density of cavities would decrease with decreasing thickness resulting in smoother fracture surfaces, smaller effective tip diameters and hence lower tearing energies for a given crack growth rate. It should also be noted that the scale of the roughness developed is of the order of a few tenths of a millimetre. Hence, if the specimen thickness were of the order of the expected surface roughness, this should have a considerable effect on the resultant roughening process, hence affecting the T/r relationship. For all these reasons the effect of specimen thickness was studied.

The resultant effect of specimen thickness on the T/r relationship for the unfilled/unswollen SBR (SBR00-S3) is illustrated in figure 5-14. Only average values of crack growth rate in the stick-slip region are plotted in this figure. Incremental crack growth rates, fast, slow and average values are plotted for the thinnest specimen in figure 5-15. It was clear that the specimen thickness had no effect on the measured crack growth rates in the fast crack growth region-C. The observed fracture surfaces in this region were all smooth suggesting no (or less) occurrence of cavitation. The visco-elastic losses by only a very small amount done at the crack tip would be affected by the specimen thickness. Hence, according to

equation (5-1), a *T/r* relationship independent of specimen thickness implied that the effective crack tip diameter, *d*, was constant, as was the magnitude of the tearing energy. This assumption was clearly consistent with the experimental results in figure 5-14. Conversely a large effect of specimen thickness was observed in the slow crack growth region-A. Here the magnitude of tearing energy necessary to drive a crack at a given rate decreased with decreasing specimen thickness. This indicated that the effective crack tip diameter, *d*, reduced with decreasing specimen thickness. Decreasing the specimen thickness reduces the magnitude of tri-axial stresses ahead of the crack tip, hence reducing the growth of cavities. This would reduce the effective crack tip diameter in thinner specimens if crack growth results from the intersection of a major crack with growing cavities, hence reducing the magnitude of the tearing energy necessary to drive a crack at given rate, as observed in figure 5-14. An interesting feature was observed in figure 5-15. The thinnest specimen showed stick-slip behaviour over the region of measured crack growth rates where stable slow crack growth was observed in the 1.10mm thickness specimen. At this magnitude of tearing energy for the thinner specimen, the crack tip would tend to blunt due to the cavitation process. However, cavity production was clearly not sufficient to cause slow crack growth. Increments of fast crack growth occur until halted by intersection with a cavity, to be followed by another increment of fast growth as it escapes from the cavity. This stick/slip effect hence may result from a low density of cavities in this very thin specimen. It is assumed that if the specimen were infinitely thin then cracks would only grow in a fast crack growth manner.

5-3-2-4. Effect of temperature

As was suggested in section 2-3-2, the influence of visco-elastic losses on tearing energy has been inferred from the equivalence of changes in rate and temperature on the magnitude of the tearing energy, which have been represented by the well-known Williams-Landel-Ferry (WLF) relation[26-31]. For a non-crystallising rubber, the visco-elastic losses taking place in a material decrease with increasing temperature, hence decreasing the magnitude of the tearing energy. If crack growth in a rubber is governed merely by the magnitude of the visco-elastic losses, then the *T r* relationship at different temperatures would fall onto a single master curve by

using the WLF equation. However, it was assumed in section 5-2-3-3 that cavitation, hence crack tip blunting, plays an important role in the slow crack growth region. If this assumption were true, time-temperature superposition (WLF relation) would not work in this region. The effect of temperature on the *T*/*r* relationship was studied to investigate the validity of these ideas.

For the unfilled/unswollen SBR (SBR00-S3) the results are illustrated in figure 5-16. As expected the tearing energy necessary to drive a crack at a given rate decreased with increasing temperature as the visco-elastic losses decreased. These data were shifted using the usual form of the WLF relationship given as

$$\log a_T = \frac{-8.86(\theta - \theta_S)}{101.6 + \theta - \theta_S} \qquad (5\text{-}5)$$

where $\theta_S = \theta + 50°C$ as illustrated in figure 5-17. The data tended to superimpose particularly in the fast crack growth region (region-C), where the cracks exhibited smooth surfaces. Data in the stick-slip region also seemed to fall onto a master curve. Conversely the data in the slow crack growth region (region-A) did not converge. The fact that the results from different temperatures tended to superpose in the fast crack growth region was not surprising as the large visco-elastic losses at these crack growth rates were likely to dominate the crack growth process. It has been suggested that cavitation would be less developed in this region resulting in smooth fracture surfaces. Hence, the crack growth behaviour in this region would be governed simply by the visco-elastic losses. The superposition in the stick-slip region was more surprising as it was expected that another factor such as the variation in crack tip behaviour would play an important role. Clearly the WLF relationship did not work well in the slow crack growth region-A, where rough fracture surfaces were developed, suggesting that here the effective crack tip diameter, *d*, also varied with temperature. In fact, fracture surfaces at a given rate became rougher with increasing temperature. This may be due to the temperature dependence of the cavity formation process. With increasing temperature the extent of cavitation increased as the elastic modulus decreased and hence *d* increased resulting in rougher fracture surfaces. However, the magnitude of the tearing energy is dependent on both W_{ht} and *d*. With increasing temperature W_{ht} decreased but *d* increased. The resultant magnitude of the tearing energy necessary to drive a crack at a given rate decreased with increasing temperature (figure 5-16). This indicated that while crack tip blunting via cavitation

plays an important role in crack growth behaviour in the slow crack growth region-A, the main factor determining the tearing energy was still W_{ht}.

5-3-2-5. Effect of average molar mass between cross-link (M_c)

As described in the previous section 5-3-2-4, visco-elastic losses play a significant role in the crack growth behaviour of rubber. With increasing visco-elastic losses in the material, the magnitude of the tearing energy necessary to drive a crack increases and it is the major factor which determines the tearing energy, particularly in the fast crack growth region where smooth fracture surfaces are developed. The average molar mass between cross-links, M_c, is one of the major factors, which determines the visco-elastic behaviour of rubbers. Therefore, the effect of average molar mass between cross-links on the *T/r* relationship was investigated here.

The effect of average molar mass between cross-links, M_c, on the *T/r* relationship for unfilled/unswollen SBR cross-linked with sulphur is shown in figure 5-18. At fast crack growth rates all the materials exhibited very smooth fracture surfaces. Rough surfaces were observed at slow crack growth rates. In addition, in the slow crack growth region-A, the extent of roughness increased with decreasing M_c. All materials exhibited stick-slip behaviour in the intermediate crack growth region-B, resulting in mixed rough/smooth fracture surfaces. Each individual incremental crack growth rate was measured for all materials using the high-speed video recorder, but all three resultant values, slow, fast and average, are plotted only for the lowest M_c material. Again it was clear that the transition region-B consists of increments of crack growth by either the fast or slow crack growth process. In each region the magnitude of *T* necessary to drive a crack at a given rate decreased with decreasing M_c as the visco-elastic losses decreased. However, a much larger effect of M_c was observed in the slow crack growth region-A than in the fast crack growth region-C. The lowest M_c material showed no region-A of crack growth by the slow crack growth process, even at the lowest tearing energy. The magnitude of this lowest tearing energy was very close to the threshold tearing energy, T_o, for this material. This indicated that with decreasing M_c the crack growth behaviour tended to be governed by the fast crack growth process as in region-C.

The effect of M_c on the *T/r* relationship for unfilled/unswollen SBR cross-linked with Dicumyl peroxide is illustrated in figure 5-19. All three incremental values of the crack growth rate in the stick-slip region are now plotted. Again, the magnitude of the tearing energy decreased with decreasing M_c as visco-elastic losses decreased. This effect of M_c was much greater in the slow crack growth region-A than in the fast crack growth region-C. For the peroxide cured materials, the extent of the stick-slip region decreased with decreasing M_c. The most tightly cross-linked material (with the lowest M_c) showed only a fast crack growth region with smooth glassy fracture surfaces at all the measured crack growth rates. A significant effect of M_c on the *T/r* relationship was evidenced by the disappearance of the rough/slow crack growth region. This region seemed to be associated with cavitation ahead of the crack tip, hence affecting the crack tip diameter, *d*. The magnitude of the elastic modulus increased with decreasing M_c, hence the magnitude of the critical tri-axial stresses necessary to open cavities would increase resulting in cavity growth suppression. If no cavities were present the crack tip diameter would become relatively sharp, hence the magnitude of *T* would be determined largely by the visco-elastic losses in the crack tip region. The reduction in magnitude of *T* with the decrease in M_c in the fast crack growth region will scale with the reduction in the visco-elastic losses, W_{ht}, only, as *d* is assumed not to vary. A larger reduction in *T* with the decrease in M_c was observed in the slow crack growth region. This may be due to the cavitation process, determining the effective crack tip diameter. The decrease in M_c will reduce both the visco-elastic losses in the crack tip region, W_{ht}, and the effective crack tip diameter, *d*, resulting in a larger reduction of *T* in this region-A.

The magnitude of the tearing energy necessary to drive a crack at a rate of 1.0 $m.s^{-1}$ in the fast crack growth region is plotted as a function of M_c in figure 5-20, for both the sulphur and the peroxide cured material. A line of slope 1/2 is drawn on the figure corresponding to

$$T \propto M_c^{\frac{1}{2}} \qquad (5\text{-}6)$$

This kind of power relation had been found for a non-crystallising rubber when *T* was measured in a cutting experiment, where essentially the crack tip diameter was independent of crack growth rate[7]. The magnitude of *T* increases due to the increase

in the energy loss W_{ht} alone. However it has been found that the magnitude of the tearing energy necessary to drive a crack at a given rate is greater in systems with sulphidic cross-links than in systems with short C-C cross-links resulting from peroxide curing[16-17][33-34]. In the present case, however, the magnitude of the tearing energy depended to a first approximation only on the molar mass between cross-links in this fast crack growth region. Hence, it would appear that the major effect of M_c on the magnitude of T was via W_{ht} with d changing little in this region where cavitation did not occur.

The contribution of the poly-sulphidic cross-link chains to the visco-elastic losses in this region must be small although it may not be negligible as is shown if you were to compare the relative slopes for the peroxide and sulphur cured materials in figure 5-20.

5-3-2-6. Effect of swelling

As was shown in the previous section, at least for the peroxide cured materials, decreasing M_c resulted in a tendency (figure 5-19) for fast crack growth, with smooth fracture surfaces being observed at all tearing energies. As one effect of decreasing M_c is to decrease the visco-elastic losses, it might be expected that increasing the extent of swelling would have a similar effect. However, for swollen sulphur cured materials (figure 5-7), while the behaviour of the material swollen to V_r=0.8 followed the general pattern of slip/stick behaviour and of a rough to smooth transition with increasing rate, the highly swollen material, V_r=0.4, showed mostly rough surfaces with no transition points. This suggested that the crack growth behaviour tends to be governed mostly by the slow crack growth process in high liquid content materials resulting in rough fracture surfaces. As decreasing the average molar mass between cross-links and increasing the volume fraction of swelling liquid both reduce the visco-elastic losses in the material, it is an interesting question as to why the observed effects on the T r relationship were so very different. Hence, in an attempt to understand the crack growth behaviour of swollen materials more detailed experiments were carried out.

The results for the most lightly cross-linked SBR cured with Dicumyl Peroxide (SBR00-P1) are shown in figure 5-21. The three incremental crack growth

rates are plotted in the stick-slip region. The magnitude of tearing energy for a given crack growth rate decreased with increasing volume fraction of swelling liquid as visco-elastic losses decreased. The effect of swelling was much larger on the slow crack growth region than on the fast crack growth region. The reduction in tearing energy necessary to drive a crack at a given rate in the fast crack growth region seemed to correspond merely to the associated reduction in the visco-elastic losses. Unswollen and lightly swollen (V_r=0.75 and 0.50) materials exhibited the stick-slip behaviour but the extent of the stick-slip region decreased with increasing swelling. As was also observed in figure 5-7, the highly swollen materials (V_r=0.24) showed no transition points at measured rates even though the fracture surface changed from rough to relatively smooth with increasing rate. The slope of the *T/r* plot for the highly swollen material was around 1/4, which was comparable with that observed for all materials in the slow crack growth region. This clearly indicated that the crack growth behaviour of highly swollen materials was governed by the slow crack growth process. Increasing the extent of swelling hence resulted in a tendency for the slow crack growth process to dominate, producing rough fracture surfaces. It may be that in highly swollen materials, as cavitation occurs so easily ahead of the crack tip that cracks grow by the slow crack growth process at all magnitudes of tearing energy. This supposes that the normal mechanisms of cavity suppression at high crack growth rates do not apply. This may be because the rate effect will not increase the elastic modulus (tri-axial stress field) ahead of the crack tip enough to suppress cavity nucleation and cavities grow so rapidly in these highly swollen materials that they are always able to grow to a finite size before being overtaken by the major crack.

The *T/r* relationships for the most highly swollen material for two different specimen thicknesses for SBR00-S3 are shown in figure 5-22. Each incremental crack growth rate in the stick-slip region is plotted in this figure. As was observed in section 5-3-2-3 (figure 5-15), the magnitude of the tearing energy necessary to drive a crack at a given rate decreased with decreasing specimen thickness. With reducing specimen thickness, the crack growth behaviour tended to be governed by the fast crack growth process. Here the specimen thickness of 1.50mm exhibits no transition points and no stick-slip behaviour, showing mostly rough fracture surfaces at all measured crack growth rates. Furthermore, the observed slope was approximately 1/4, which indicated that the crack growth behaviour was governed by the slow crack

growth process over all measured crack growth rates, where crack tip blunting, caused by the cavitation process, would be significant. However, the thinner specimen exhibited stick-slip behaviour over a wide range of rates. The magnitude of the measured lowest tearing energy was very close to the magnitude of threshold tearing energy, T_o, hence it was clear that the thinner specimen did not show any independent slow crack growth process behaviour even in this highly swollen state. Clearly while the swelling reduced the elastic modulus making cavity nucleation easier, decreasing the specimen thickness reduced the magnitude of the generated tri-axial stresses making cavitation more difficult. The result for the thinnest samples was that cracks grew mostly in the fast crack growth mode with little (or no) crack tip blunting.

5-3-2-7. State of the strain at the tip

As was discussed in section 5-3-2-3, a large effect of specimen thickness on crack growth behaviour has been observed for an unfilled SBR particularly in the slow crack growth region-A. This thickness effect may be associated with the cavitation process and hence the effective crack tip diameter, *d*. With decreasing specimen thickness, cavitation and hence crack tip blunting, may be suppressed as the tri-axial stresses in the high strain region ahead the crack tip were reduced in magnitude. Therefore, the state of strain at the crack tip was clearly of interest in relation to cavitation and the effective crack tip diameter, *d*. It is known that the specimen thickness at the crack tip is often appreciably greater than would be expected if the material were in simple extension at the breaking elongation, λ_b[42]. Thus the rubber at the tip seems to be stressed perpendicular to the plane of the sheet. However, the breaking elongation, λ_b, is not likely to be significantly affected by these stresses since the breaking elongation in equi-biaxial tension is much the same as in simple uni-axial extension[40]. The stresses through the thickness presumably arise due to the fact that the effective crack tip diameter is substantially smaller than the specimen thickness. As mentioned previously, the magnitude of the tearing energy is related to the visco-elastic losses in the crack tip region, W_{ht}, and the effective crack tip diameter, *d*, as

$$T = W_{ht} k_D d \qquad \text{giving} \qquad d = \frac{T}{W_{ht} k_D} \tag{5-1}$$

From dimensional considerations, it can be deduced that the strained specimen thickness, h, at the crack tip can be related to d and the unstrained thickness h_o, given as,

$$\frac{h}{h_o} = \lambda_3 = f\left(\frac{d}{h_o}, \lambda_b\right) \tag{5-8}$$

where f represents an unknown function and λ_b is the breaking elongation. Thus with equation (5-1) we have

$$\lambda_3 = f\left(\frac{T}{h_o}, \lambda_b\right) \tag{5-9}$$

Visual observations of the crack tip strain (λ_3) through the thickness direction for an unfilled SBR for different specimen thicknesses at various crack growth rates in the slow crack growth region-A were carried out. These were measured utilising a travelling microscope on pure-shear test specimens at various tearing energies. The results obtained with an unfilled SBR (SBR00-S3) for various initial specimen thicknesses are shown in figure 5-23. In this figure the results for the various specimen thicknesses did not fall onto a single master relationship in accordance with equation (5-9). The magnitude of strain through the specimen thickness at the crack tip, λ_3, at a given T/h_o decreased with increasing specimen thickness, h_o. This clearly implied that the crack tip diameter, d, was strongly related to the specimen thickness, increasing with increasing specimen thickness as the magnitude of tri-axial stress increased. This result and its interpretation showed a good correspondence with the effect of thickness of the specimen on the T/r relationship as shown in figure 5-14 and 5-15. A large effect of specimen thickness was observed on the crack growth behaviour for an unfilled SBR in the slow crack growth region and in the stick-slip region. The magnitude of tearing energy at a given rate decreased with decreasing specimen thickness. This occurred as decreasing the specimen thickness reduced the magnitude of the tri-axial stresses in the crack tip region, hence the cavitation process was suppressed, resulting in a sharpening of the crack tip, reducing the diameter, d. These results obtained from the tip strain measurements

strongly supported the importance of the cavitation process on the crack tip diameter and in determining the crack growth behaviour of rubbers.

5-3-2-8. Criteria for cavitation

As was discussed throughout this chapter, cavitation could play an important role in determining crack growth behaviour. Some factors, which are assumed to be associated with the cavitation process, have been investigated, such as average molar mass between cross-links, swelling, specimen thickness and temperature. It is clear that the criteria for opening up cavities will be associated with the tri-axial stress field ahead of a crack tip, but determining quantitative criteria at the crack tip for cavitation is very difficult as the stress field ahead of the tip is complicated. However a qualitative rationale may be developed along the following lines.

It is known that under tri-axial stresses, such as exist near a crack tip in plane strain conditions, cavities are initiated in rubbery materials. A simple model to describe the growth of a spherical microvoid subjected to a hydrostatic pressure in a rubbery material, gives the following relationship[35-38].

$$\frac{P}{E} = \frac{(5 - 4\lambda^{-1} - \lambda^{-4})}{6} \tag{5-10}$$

$$\lambda = \frac{r}{r_o} \tag{5-11}$$

where P is the inflating pressure, E is Young's modulus, r_o is the initial radius of the initial flaw, and r is the radius of an inflated cavity. This model indicates that the cavities will expand infinitely at a critical pressure of $5E/6$. This value is taken as the critical pressure for cavity formation, P_c, given as

$$P_c = \frac{5E}{6} \tag{5-12}$$

Later, it was suggested that when the volume under the dilatational stress, $P=(\sigma_{XX}+\sigma_{YY}+\sigma_{ZZ})/3$, is small, the critical pressure for crack initiation is much larger than the predicted value given in equation 5-12. This was considered to be due to the

extra effect of surface energy and a modified criterion given as the following equation[39] was produced.

$$P_c = \frac{5E}{6} + \frac{2\gamma}{r_o} \qquad (5\text{-}2)$$

where γ is the surface energy. This implies that the surface energy is dominant when the size of cavity is relatively small. Here it should be noted that these models were derived from the assumption of elastic instability.

According to the equation (5-2), the magnitude of the tri-axial stress required to produce cavitation can be remarkably small, of the order of Young's modulus, which is approximately ~2MPa. However it is clear that an extended rubber sheet specimen of pure shear test piece dimensions does not show cavities, hence does not break, under large deformation where the stress in the rubber is much greater than critical stress calculated from the equation (5-2). This is because that the criterion for cavitation in equation (5-2) is strictly applicable only for a uniform (equi) tri-axial stress field. Ahead of a crack in a deformed rubber sheet specimen, the stress field is also of non-uniform tri-axial stresses. The principle stresses ahead of such a crack tip as a function of distance from the crack tip, L_X, for a pure shear specimen extended in a Y direction with a stress of σ_Y are schematically illustrated as figure 5-24[96]. Here the principle stresses are the stresses in the centre of the specimen thickness. σ_{YY} has a maximum value at the crack tip. σ_{YY} decreases gradually with increasing the distance from the tip, L_X, and finally saturate at the stress of σ_Y. σ_{XX} is zero at the tip. σ_{XX} increases with L_X, shows a peak at a distance L_X' and then saturates at a certain stress (approximately 1/2 of σ_Y). This distance L_X' between crack tip and peak maximum is thought to be of the order of the crack tip diameter. σ_{ZZ} has a maximum value at the crack tip. This gradually decreases with increasing L_X and finally reaches zero. Therefore, at certain distances from the crack tip, of the order of the crack tip diameter, tri-axial stresses are generated. Hence, it can be expected that the cavitation would be developed under this tri-axial stress field. Critical values of the tri-axial stress for opening up cavities, P_c', could be represented as

$$P_c =< f(\sigma_{XX}, \sigma_{YY}, \sigma_{ZZ}) \qquad (5\text{-}13)$$

where, $\sigma_{XX} > 0$, $\sigma_{YY} > 0$, $\sigma_{ZZ} > 0$ and f represents an unknown function. The magnitude of P_c' would also depend on the magnitude of the local elastic modulus.

In all the results of static, constant T, crack growth behaviour in the slow crack growth region, the extent of surface roughness decreased with increasing crack growth rate. The increase in crack growth rate will increase the modulus ahead of the crack tip due to visco-elastic effects. This will in turn increase the critical tri-axial stress necessary for cavitation. It is presumed that the rate increase will not increase the generated tri-axial stresses proportionally. Hence the propensity to cavitate will tend to decrease with increasing crack growth rate. As was observed in the effect of specimen thickness (figures 5-14, 5-15), the magnitude of the tearing energy necessary to drive a crack at given rate increases with increasing specimen thickness in the rough surface region. The principal stress through the specimen thickness direction, σ_{ZZ}, at the tip increases with increasing specimen thickness as evidenced by the measured crack tip strain (figure 5-23). Therefore, it is expected that the extent of cavitation would increase with increasing specimen thickness resulting in crack tip blunting. Hence the magnitude of the tearing energy to drive a crack at a given rate increases via the increase in the crack tip diameter, d. As was observed in the figures 5-14, 5-15, 5-21 and 5-22, the extent of roughness increased with increasing temperature and extent of swelling. It may be that the magnitude of P_c', necessary for cavitation, decreased with increasing temperature and extent of swelling resulting in rough fracture surfaces.

From the results shown in figures 5-18 and 5-19, it was seen that the extent of roughness at a given crack growth rate in the slow crack growth region decreased with increasing M_c. The observed fracture surfaces for the high M_c material were much smoother than for the low M_c materials. With increasing M_c, the elastic modulus and hence the critical tri-axial stresses required for the cavitation, P_c', would be decreased. Therefore, it appears that high M_c materials are more likely to cavitate resulting in rougher fracture surfaces. However, the experimental results contradict this conclusion. One possible explanation for this conclusion may arise if you consider that cavitation may become so easy that all the flaws in front of the crack tip may expand, irrespective of their initial size. Hence, the need to deviate from the crack plane is reduced as the crack propagates. Thus resulting in a smoother fracture surface.

5-3-2-9. Proposed mechanism of static, constant T, crack growth for unfilled SBR

As was discussed through out this chapter, the cavitation process, hence the effective crack tip diameter, d, may play an important role in static crack growth behaviour especially in the slow crack growth region. Under certain tri-axial stresses, above the critical tri-axial stress, P_c', ahead of the crack tip, rubber could cavitate. It has been suggested that for most situations the advancing major crack intersects with these growing cavities developing crack tip blunting (increasing the crack tip diameter, d) resulting in rough fracture surfaces. However, this cavitation process seems not to occur (or is less significant) in the fast crack growth region. Due to the rate effect, the elastic modulus and hence the critical necessary tri-axial stress ahead of the crack tip, P_c', increases with increasing crack growth rate. Therefore, it seems that the cavitation process would be suppressed at a certain crack growth rate, r_c, where the tri-axial stresses ahead of the crack tip would be lower in magnitude than the critical tri-axial stress necessary to open cavities at this rate, P_c'. A large difference in crack tip diameter would developed at this r_c or P_c'. Below r_c or above P_c' cavitation would take place causing an increase in crack tip diameter. Conversely above r_c or below P_c' cavitation would not occur and hence cracks would grow with a sharp crack tip diameter. As rubber is an inhomogeneous material, the magnitude of r_c or P_c' would be extended to a range. This could explain the observed stick-slip behaviour in the intermediate range between the slow crack growth region and the fast crack growth region.

As was discussed throughout this chapter, the tearing energy can be represented as

$$T = W_{ht} k_D d \qquad (5\text{-}1)$$

here, W_{ht} is related to the hysteresis and can be scaled with the dynamic loss modulus, G'' as

$$W_{ht} \propto G'' \qquad (5\text{-}14)$$

Hence tearing energy can also associated with G'' as

$$T \propto G'' k_D d \qquad (5\text{-}15)$$

Some of the typical data for G'' as a function of frequency, ω, in a double logarithm plot for unfilled SBR is illustrated in figure 5-25[97]. It is worth noting that the G''/ω

relationship shows an upturn at a certain frequency/rate and the observed slopes are approximately 1/4 in the low ω region and 1/2 in the high ω region. If the equation (5-15) works well and the magnitude of d is relatively constant over the range of ω, then the T/r relationship would show a similar curve to figure 5-25 as illustrated in figure 5-26. It is interesting to note that the experimentally observed slopes in the T/r relationship for all the SBR materials were approximately 1/4 in the slow crack growth region and 1/2 in the fast crack growth rate region. These values show good agreement with the slopes in G''/ω relationship (figure 5-25). However as was discussed throughout this chapter, most of the materials and specimens show two transition points as illustrated in figure 5-1 and do not show the single relationship as illustrated in the figure 5-26. This is because the variation in the magnitude of d is not included in figure 5-26. The magnitude of d would be larger in the slow crack growth region when compared to that in the fast crack growth region. This would imply that the magnitude of T in the slow crack growth region would be scaled up correspondingly via equation (5-15) due to the increase in d as illustrated in figure 5-27. With this concept the experimentally obtained T/r relationship can be generated.

5-3-3. Static, constant T, crack growth for carbon black filled SBR

As was reported in section 5-3-1, carbon black filled SBR exhibited a different behaviour from that observed for unfilled SBR. Stick-slip behaviour was not observed, which resulted in a discontinuity in the *T/r* relationship with a distinct jump from the slow crack growth region-A to the fast crack growth region-C occurring at a certain tearing energy. The extent of fracture surface roughness decreased with increasing carbon black content. However, it should be noted that the 50phr carbon black filled SBR (SBR50-S1) exhibited a smooth fracture surface even in region-A (figure 5-8). It was suggested in section 5-3-2 that the cavitation process played an important role in static crack growth behaviour and in surface roughness development for unfilled SBR. The major general questions to be posed here are to what extent does cavitation occur in carbon black filled materials and in particular; why does the carbon black filled material show a discontinuity in the *T/r* relationship? Why does the highly filled SBR exhibit a smooth fracture surface even in region-A? Does the cavitation process play a role in static crack growth behaviour in filled SBR? Clearly it seems that the static crack growth mechanisms for the carbon black filled SBR will be different from the mechanisms for unfilled SBR. It was to answer some of these questions that further investigations were carried out on the static crack growth behaviour of carbon black filled SBR. The results of which are discussed in this section.

5-3-3-1. Effect of thickness of the specimen

As was reported in section 5-3-2, a large effect of specimen thickness was observed in the slow crack growth region-A for unfilled SBR with no effect occurring in the fast crack growth region-C. This was thought to be associated with the cavitation process, which could cause crack tip blunting in region-A. This cavitation would be developed under the tri-axial stress field ahead of a crack tip and hence is suppressed with decreasing specimen thickness as the tri-axial stresses are reduced. If the mechanism of crack growth in carbon black filled SBR is similar to that for unfilled SBR, or if this cavitation process also plays an important role, a large effect of specimen thickness on static crack growth behaviour would be

observed. Hence the effect of specimen thickness on the *T/r* relationship was investigated here.

The results for 50phr carbon black filled SBR cross-linked with 3.0phr sulphur (SBR50-S2) are illustrated in figure 5-28. Here the thickness of the specimen was varied from 2.10mm to 0.50mm. Clearly no significant effect of specimen thickness was observed in either the fast or the slow crack growth regions. For all specimen thicknesses discontinuities were observed in the *T/r* relationship but the observed fracture surfaces were all relatively smooth in both the fast and the slow crack growth regions. No effect of specimen thickness in the fast crack growth region was expected, as the cavitation process was not expected to occur, or would be less significant, resulting in cracks growing with a sharp tip diameter. However, the fact that no effect of specimen thickness was observed in the slow crack growth region was surprising. Hence, further measurements to determine the thickness effect were carried out using thinner specimens of a 50phr carbon black filled SBR cross-linked with 1.5phr sulphur (SBR50-S1), the results of which are illustrated in figure 5-29. Again clearly no significant effect of specimen thickness was observed in either the slow or the fast crack growth regions. These results implied that the cavitation process did not occur in highly carbon black filled SBR. In fact, the observed fracture surfaces in region-A were all relatively smooth for all specimen thicknesses. Furthermore, the lack of cavitation was not that surprising, as the large elastic modulus and hence the large critical tri-axial stresses at a crack tip necessary to open cavities, P_c', may be high enough to suppress cavity formation for a highly filled SBR. This effect could increase with increasing extent of carbon black loading, causing an increased difficulty to cavitate. However, it should be noted here that the highly filled SBR also showed a distinct change in the *T/r* relationship between region-A and region-C following the general pattern as illustrated in figure 5-1. This discontinuity and change in slope of the *T/r* relationship results in much larger values of *T* being necessary to drive a crack at a given rate in region-A, than would be the case if the *T/r* data from region-C were just extrapolated to lower *T* values. It may be that a distinct change in effective crack tip diameter takes place between the two regions even though cavitation does not occur, hence increasing the magnitude of *T*. If this is the case, another factor must exist for highly filled SBR, which increases the effective crack tip diameter, *d*, in the slow crack growth region-A.

What causes this increase in the crack tip diameter? Why does this effect disappear suddenly at a certain crack growth rate or tearing energy? Some clues to answer these questions can be seen in the fracture surface profiles. Optical micrographs of through thickness cross-sections of fracture surfaces for the *T/r* results of different specimen thicknesses, given in figure 5-28, are shown in figure 5-30. The cross-sections of fracture surface profiles are further illustrated with the three dimensional fracture surface profiles, which show the surface feature more clearly, for a thickness of 2.1mm taken from specimens for which the *T/r* data is given in figure 5-29, as illustrated in figure 5-31. For the fast crack growth region-C, cracks grew on a relatively flat plane. This is reasonable because essentially cracks will grow chasing the maximum energy release direction, which will be generated on a flat plane, normal to the principal specimen extension. Of course rubber is an inhomogeneous material especially when filled with carbon black and hence sometimes the crack growth will deviate from this flat plane. It is worth noting that the cross-sections of the fracture surfaces from region-A showed a groovy shape, which seemed to effectively increase the crack tip deviation. Furthermore, this groovy shape was not observed in the unfilled SBR. This may indicate that the local maximum energy release direction varied through the specimen. The pure shear test geometry yields a near plane strain state, which generates maximum through the thickness stresses in the centre of the thickness. Therefore, the observed groovy shape may suggest that the local crack growth direction through the thickness tended to deviate from a flat plane with increasing stress. Furthermore, this deviation phenomenon may be rate dependent as this groovy shape was not observed in the fast crack growth region-C and the transition between region-A and region-C occurred dramatically at a specific tearing energy or crack growth rate. From these features it can be implied that the effect of strength anisotropy may be present. As was presented in chapter 2, carbon black reinforcement can cause the occurrence of sufficient strength anisotropy at a crack tip to result in the deviation of the crack tip. This phenomenon, also called knotty-tearing, is believed to be promoted by the presence of carbon black or strain-induced crystallisation. This reinforcing effect is restricted to a limited range of crack growth rates and temperatures and is virtually absent outside this range. This region where reinforcement occurs depends on the types and amounts of fillers and rubbers employed. This possible factor, which

introduces crack tip deviation, into the crack growth behaviour will be discussed in a later section.

5-3-3-2. Effect of temperature

The addition of carbon black clearly causes a large increase in strength as the visco-elastic losses necessary for crack growth increase with increasing carbon black content. It also introduces a discontinuity in the *T/r* relationship, as crack growth rates over a range of nearly four orders of magnitude are not observed. This suggests that changes in the crack tip profile may be developed in the slow crack growth region-A due to some effect such as cavitation processes or strength anisotropy. It is thought that both visco-elastic losses and strength anisotropy are influenced by the temperature, hence the effect of temperature on the *T/r* relationship was investigated here.

Static crack growth rate measurements were carried out over a range of temperatures for the 10phr carbon black filled SBR (SBR10-S1) and the results are illustrated in shown in figure 5-32. The magnitude of the tearing energy necessary to drive a crack clearly decreased with increasing temperature as the visco-elastic losses necessary decreased. The discontinuity in the *T/r* relationship, observed at room temperature, was not observed at the elevated temperatures. Furthermore, the extent of roughness in the slow crack growth region-A increased with increasing temperature. Stick-slip behaviour was observed at intermediate values of *T*, resulting in the appearance of rough/smooth fracture surfaces at elevated temperatures. An attempt was made to superimpose these data utilising the WLF equation as illustrated in figure 5-33. The superimposition worked reasonably well in the fast crack growth rate region where smooth fracture surfaces were observed at all temperatures. This clearly indicated that the nature of the crack tip changed little with changing temperature and crack growth rate in this region and that the temperature dependence of the tearing energy necessary to drive a crack at a given rate arose purely from a decrease in visco-elastic losses as the temperature increased. However, the data in the slow crack growth region and the stick-slip region did not fall onto the master curve. This implied that in these regions variations in the effective crack tip diameter

might be due to crack tip deviations due to strength anisotropy becoming more important.

At high crack growth rates the role of carbon black is to markedly increase the visco-elastic losses, resulting in significant increases in the values of W_{ht} in equation (5-1). Conversely at low crack growth rates it will also change the crack tip profile, which plays an important role in crack growth behaviour. What is not clear is why a discontinuity in crack growth behaviour was observed for these materials at 20°C but was not observed at elevated temperatures.

The effect of temperature on the *T/r* relationship for the 50phr carbon black filled SBR (SBR50-S1) is illustrated in figure 5-34. As expected the magnitude of the tearing energy necessary to drive a crack decreased with increasing temperature as the necessary visco-elastic losses decreased. However, the discontinuity in crack growth rates was now clearly observed at both temperatures. In addition the fracture surfaces in the slow crack growth region were smooth but also showed a groovy shape on the cross-sections of the fracture surface profiles at both temperatures. This implied that a distinct change in crack tip deviation behaviour took place between the two crack growth regions even at the elevated temperature. However, the cavitation process has already been ruled out as a possible factor as the observed fracture surfaces are relatively smooth even in the slow crack growth region-A. It may be that the magnitude of the elastic modulus and hence the magnitude of the critical tri-axial stress, P_c', may be high enough to suppress cavitation even at the elevated temperatures for this highly carbon black filled SBR.

The fact that the discontinuity in the *T/r* relationship for these materials at room temperature disappears with increasing temperature for the 10phr filled SBR but not for the 50phr filled SBR may suggest that the origin of the discontinuity is associated with the fraction of carbon black present in the material and that it has a rate and temperature dependence. In section 5-3-3-1, it was noted that strength anisotropy depend on the extent of the carbon black content and was also rate dependent. It is possible that at high crack growth rates, strength anisotropy will not be developed ahead of the advancing crack tip, hence cracks tip deviation did not occur. Cracks hence grow with a relatively sharp tip diameter in a flat plane and the resulting tearing energy being governed merely by the magnitude of the visco-elastic losses, W_{ht}. However, below certain crack growth rates or magnitudes of tearing energy, strength anisotropy may have time to develop ahead of the crack tip, causing

considerable crack tip deviation. It may be possible that if the extent of this strength anisotropy effect was not high for the low carbon black filled material, then increasing the temperature may reduce the anisotropy enough to inhibit the discontinuity resulting in observed stick-slip behaviour. A more detailed discussion of the possible role of strength anisotropy will be given in later section.

5-3-3-3. Effect of average molar mass between cross-link (M_c)

Even though a strength anisotropy effect on static crack growth behaviour was dismissed for unfilled SBR (section 5-3-2-2), it was suggested above that strength anisotropy may play an important role in determining the form of the *T/r* relationship for carbon black filled SBR. This would result in a drastic change in the crack tip deviations between crack growth in region-A and in region-C and hence causing the observed discontinuous relationship. However, it is assumed that visco-elastic losses ahead of the crack tip, W_{ht}, are still the main contributor in determining the magnitude of the tearing energy. Hence a large effect of M_c on the *T/r* relationship would be expected for carbon black filled SBR, but how strength anisotropy and hence changes in crack tip deviation, would be affected by M_c was unclear. It was to address these issues that the effect of M_c on the *T/r* relationship for carbon black filled SBR was investigated.

The results for 10 and 50phr carbon black filled SBR, cross-linked with sulphur, are illustrated in figures 5-35, 5-36 respectively. Generally the same tendency was observed with decreasing M_c, for these materials as for unfilled SBR. The magnitude of the tearing energy necessary to drive a crack at a given rate decreased with decreasing M_c as the visco-elastic losses, W_{ht}, decreased. The largest effect of M_c appeared to be on the slow crack growth region rather than on the fast crack growth region. As reported previously, carbon black filled materials (SBR10-S1 and SBR50-S1) exhibited discontinuities in the *T/r* relationship. This discontinuous behaviour tended to disappear with decreasing M_c for the 10phr carbon black filled SBR. The highly cross-linked SBR showed stick-slip behaviour and the extent of this stick-slip region decreased with decreasing M_c. However, a large contrast to this behaviour was observed for the 50phr carbon black filled SBR. The discontinuity in the *T/r* relationship was observed in all the materials, for any M_c, but

the extent of this discontinuous region decreased with decreasing the magnitude of M_c. Exactly the same tendencies were reported in section 5-3-3-2, for the effect of temperature on the *T/r* relationships for both carbon black filled SBR materials. It seems that increasing the temperature or decreasing the values of M_c have an equivalent effect on the discontinuity in the *T/r* relationship observed in carbon black filled SBR materials. It is possible that if the magnitude of the strength anisotropy effect was not high (low carbon black filled material), decreasing M_c may reduce the anisotropy developed enough to limit crack tip deviation effects resulting in stick-slip behaviour. If the material were filled with a large amount of carbon black, though the magnitude of the strength anisotropy would decrease with decreasing M_c, it could still show a discontinuous relationship at low values of M_c as the magnitude of the strength anisotropy would still be high enough to develop crack tip deviations. Optical micrographs of cross-sections of fracture surfaces taken from the specimens whose *T/r* relationships are given in figure 5-36 are illustrated in figure 5-37. As was discussed in section 5-3-3-1, a groovy cross-section fracture surface profile was again observed in the slow crack growth region-A and a flat plane cross-section fracture surface profile was again observed in the fast crack growth region-C. This may support the occurrence of strength anisotropy in the slow crack growth region resulting in the distinct change in crack tip deviation between region-A and region-C.

5-3-3-4. State of strain at the tip for carbon black filled SBR

As was discussed in sections 5-3-2-3 and 5-3-2-7, a large effect of specimen thickness on crack growth behaviour has been observed for an unfilled SBR particularly in the slow crack growth region. This thickness effect was thought to be associated with the cavitation process, which increased the effective crack tip diameter. With decreasing specimen thickness, cavitation, hence the effective crack tip diameter, was suppressed as tri-axial stresses ahead of the crack tip were decreased. This was confirmed with the visual observation of the crack tip strain through the thickness as illustrated in figure 5-23. In this figure, the results for various specimen thicknesses did not fall onto single master curve, which implied that the crack tip diameter was strongly related to the specimen thickness. It was

proposed that decreasing the specimen thickness decreased the crack tip diameter as the cavitation process was suppressed.

Conversely, no effect of specimen thickness on the crack growth behaviour was observed for the 50phr carbon black filled SBR as shown in figures 5-28, 5-29. This suggested that crack tip effects due to cavitation which would be related to the specimen thickness were absent for this carbon black filled material. If this assumption were true, the magnitude of the crack tip strain, λ_3, at a given T/h_o for various specimen thicknesses would fall onto a single master curve in accordance with equation (5-9). Therefore, visual observation of the crack tip strain through the specimen thickness for 50phr carbon black filled SBR specimens of various thicknesses was carried out.

This crack tip strain through the thickness direction (λ_3) at various crack growth rates in the slow crack growth region-A was measured utilising a travelling microscope in pure-shear test specimens at various applied tearing energies and the results obtained are shown in figure 5-38. In this figure the results for various specimen thickness fell onto a single curve in accordance with equation (5-9). This single relationship implied that the magnitude of tri-axial stresses developed ahead of the crack tip was independent of the specimen thickness. Hence, leading to no thickness effect on crack growth due to cavitation as observed.

5-4. Summary and conclusions

(1) The relationship between the tearing energy, T, necessary to drive a crack and the consequent crack growth rate, r, is found to be of the form illustrated in figure 5-1 where the T/r relationship can be divided into three regions.

(2) In region-C, where fast steady crack growth occurs producing smooth surfaces, it is proposed that the increase in the magnitude of T necessary to drive a crack at fast rates arises from an increase in the magnitude of the visco-elastic work that has to be done in the crack tip region with increasing rate rather than from an increase in the crack tip diameter. This is evidenced by the fact that the data in this region scale with the WLF relationship for both unfilled (figure 5-17) and carbon black filled materials (figure 5-33).

(3) In region-C, the magnitude of T necessary to drive a crack at a given r decreases with increasing extent of swelling, decreasing average molar mass between cross-links, M_c, and increasing temperature as the visco-elastic losses at the crack tip decrease.

(4) In the slow crack growth region-A, although the visco-elastic losses at the crack tip is still the main contributor to the magnitude of T, the crack tip profile behaviour plays an important role in determining the magnitude of T and hence the static crack growth behaviour. However, mechanisms responsible for this behaviour may be different for unfilled and carbon black filled materials.

(4-1) *Unfilled materials*

In this region, rough surfaces are observed and it has been postulated that the origin of the roughness may be cavitation ahead of the crack tip due to tri-axial stresses. The extending crack would intersect with growing cavities causing an increase in crack tip diameter and hence in the magnitude of T. This hypothesis is supported by the observed specimen thickness effects. For the unswollen materials in region-A, the magnitude of T necessary to drive a crack at a give rate decreases with decreasing specimen thickness in a manner that would be expected from the decrease in magnitude of the tri-axial stresses and hence the propensity to cavitate. Even for the highly swollen materials, reducing the thickness results in a decrease in the magnitude of T and a change from rough to stick-slip behaviour.

(4-2) *Carbon black filled materials*

In carbon black filled materials, the fracture surfaces do not appear very rough, even at low crack growth rates and there appears to be no direct effect of specimen thickness on the magnitude of T. However, there is a clear transition in the T/r relationship with a significant discontinuity. Furthermore, it is not possible to superpose the temperature/rate data using the WLF relationship suggesting that in the slow crack growth rate region there is a significant crack tip effect. It may be that cavitation does not occur to any significant extent as the elastic modulus and hence the critical tri-axial stresses necessary to open cavities, P_c', would increase significantly with increasing carbon black content enough to suppress cavity growth. However, a non-plainer, groovy cross-section fracture surface profile has been observed in this region but not in the fast crack growth region for carbon black filled materials. This may be due to a local deviation of the crack growth direction due to the development of strength anisotropy ahead of the crack tip. This will lead to the magnitude of the applied T necessary to drive a crack at a given rate being increased, as it will grow, in a direction other to that of maximum release of elastic stored energy. The extent of development of this strength anisotropy will depend on; crack growth rate, temperature, M_c, and carbon black content. At fast crack growth rates (region-C), no time is available to develop strength anisotropy and cracks will grow mostly in the horizontal plane in the direction of maximum elastic stored energy release. A crack growing at the highest T value in region-B in a direction along way from the horizontal will require a large excess in T to drive it. If the crack deviates to a horizontal direction this large excess energy will cause a large increase in crack growth rate, which will continue, as strength anisotropy will have insufficient time to develop. This will result in the discontinuity in the T/r relationship. The magnitude of the discontinuity will depend on the extent to which strength anisotropy is developed in region-A. The greater the extent the greater the magnitude of the discontinuity. If the extent is not large, the excess energy necessary to drive a crack will be small and stick-slip behaviour will occur.

(5) The extent and nature of the stick-slip transition region is clearly affected by the materials variables. It becomes a discontinuity for carbon black filled materials, but tends to reduce in extent with extent of swelling, with decreasing average molar mass between cross-links and with increasing temperature.

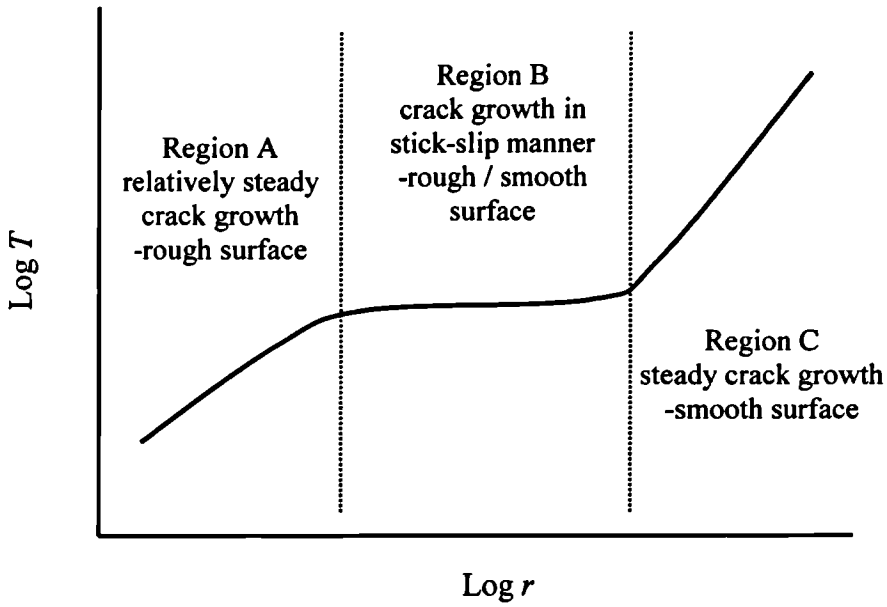

Figure 5-1. Schematic figure illustrating the relationship between tearing energy, T, crack growth rate, r, (T/r relationship) for a non-strain crystallising rubber.

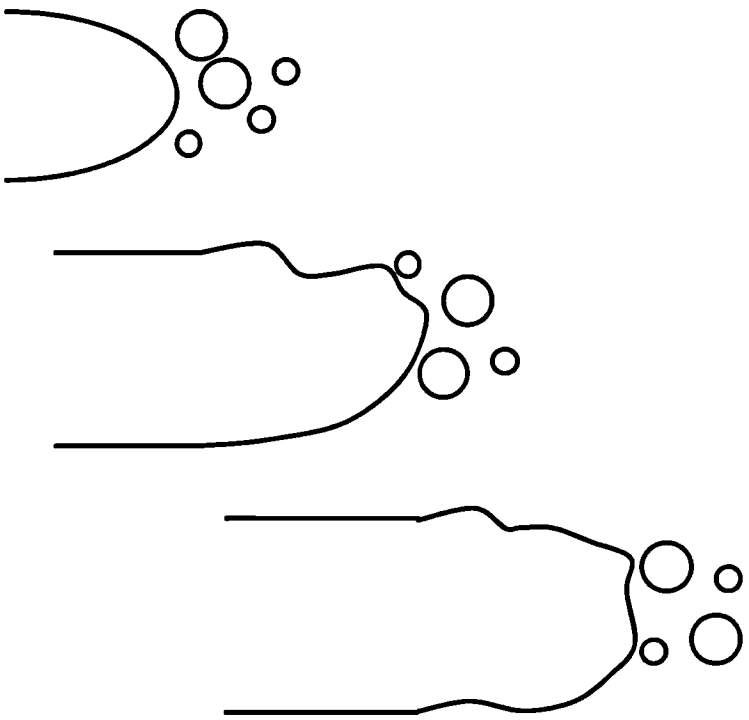

Figure 5-2. Schematic figure illustrating fracture surface roughening by intersection of the propagating major crack with growing cavities ahead of the crack tip.

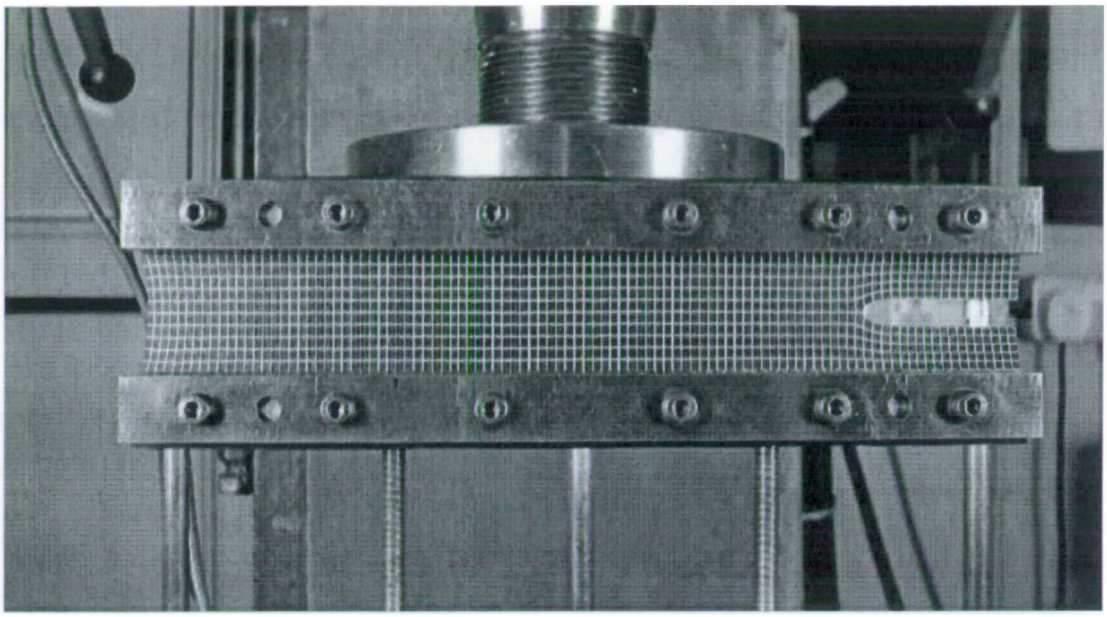

Figure 5-3. "Pure shear" test specimen used in investigating static, constant T, crack growth measurement.

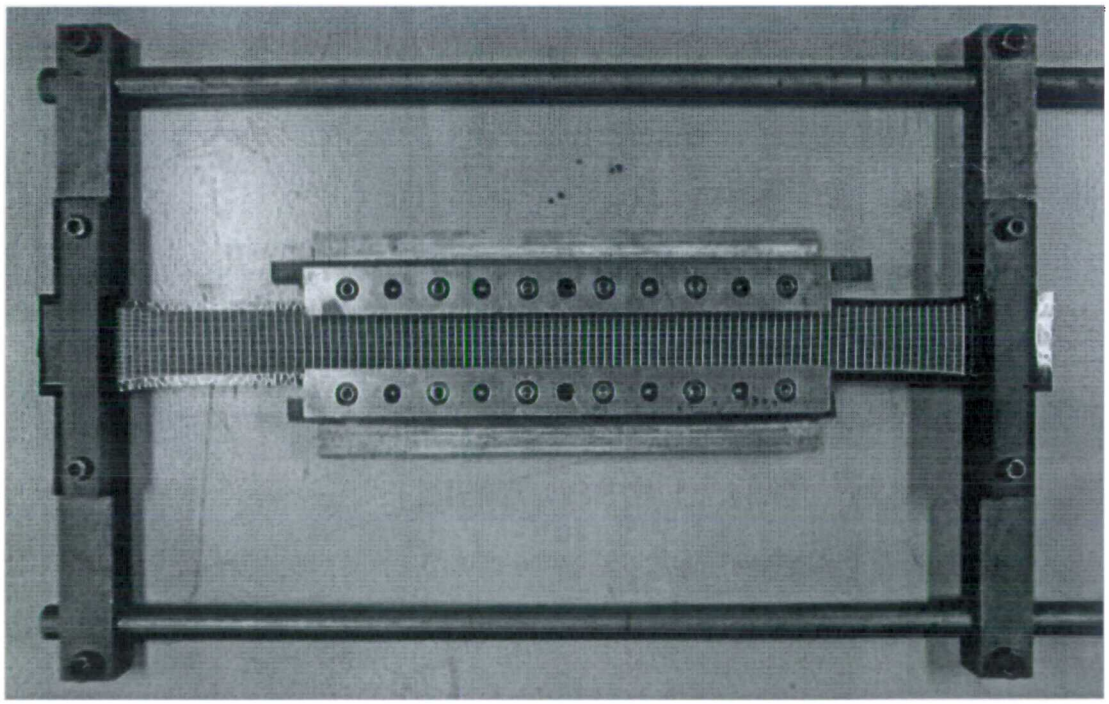

Figure 5-4. Rectangular frame with one side sliding edge used to pre-strain a pure shear test specimen.

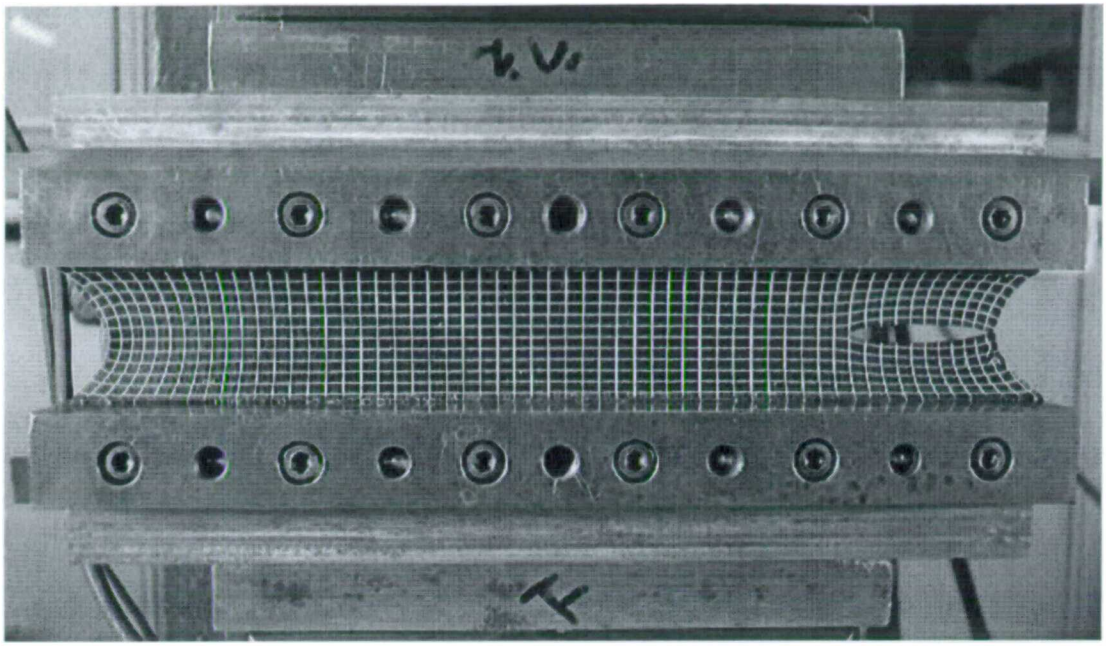

Figure 5-5. Pre-strained pure shear test specimen in which the region of homogeneous pre-strained pure shear deformation can be estimated as the region where the vertical grid lines remain vertical.

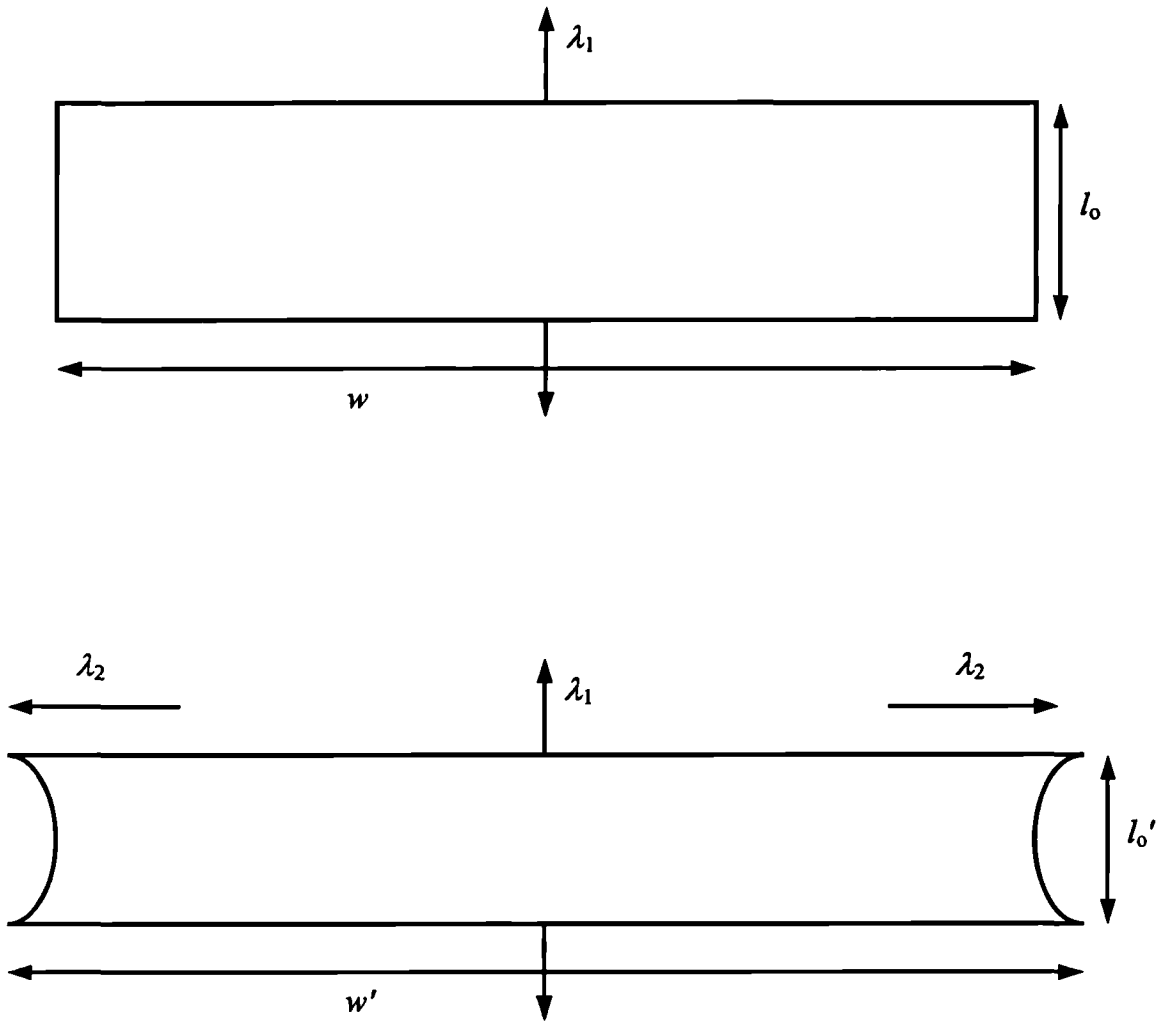

Figure 5-6. Schematic diagram illustrating specimen dimensions before and after pre-strain.

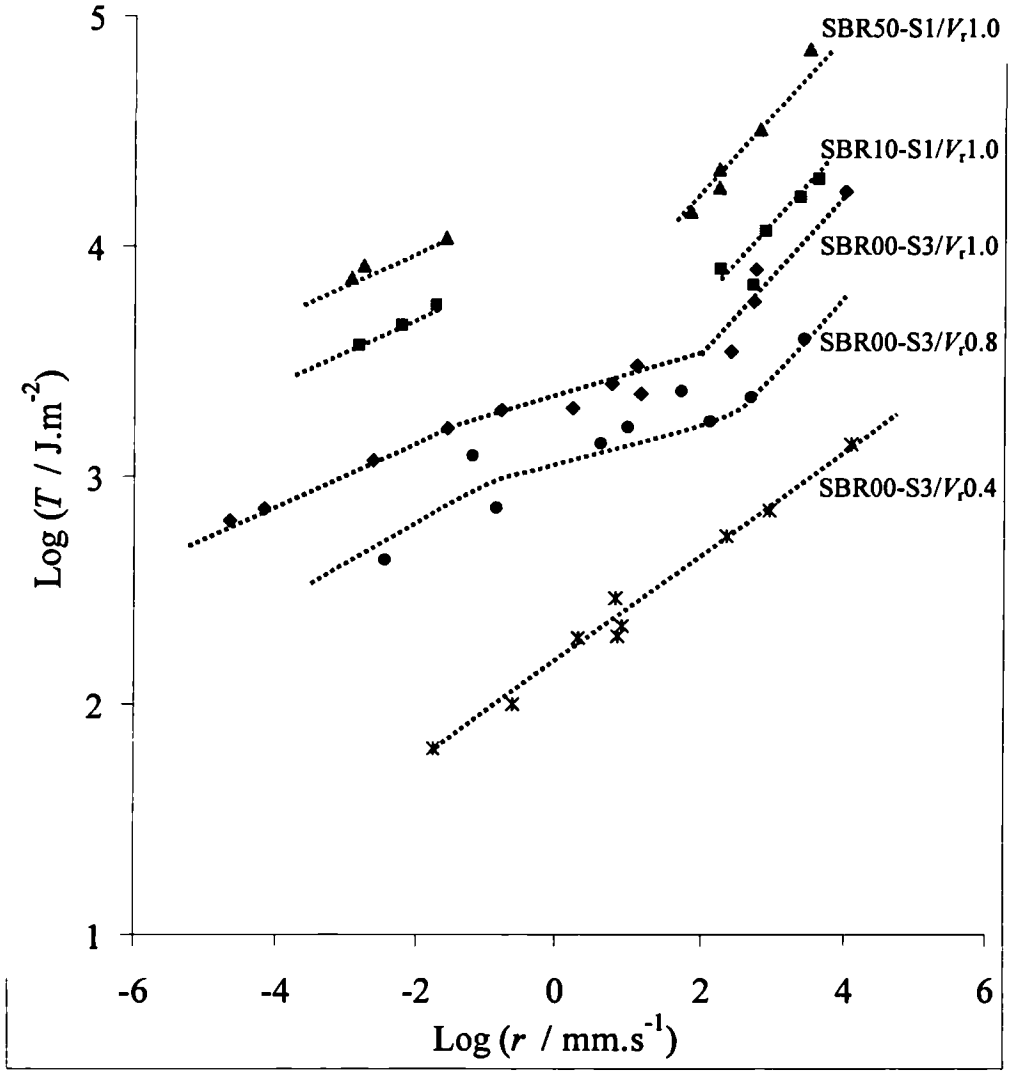

Figure 5-7. The tearing energy, T, as a function of crack growth rate, r, for a series of HAF carbon black filled SBR (SBR10-S1, SBR50-S1) or unfilled SBR (SBR00-S3) swollen with DBA to various degrees of volume fraction of rubber, V_r.

Figure 5-8. Optical micrographs of the fracture surfaces of the specimens used to generate figure 5-3. The top micrograph was taken looking down onto the fracture surface. The direction of the crack growth is right to left. The bottom micrograph shows cross-section of fracture surface profile.

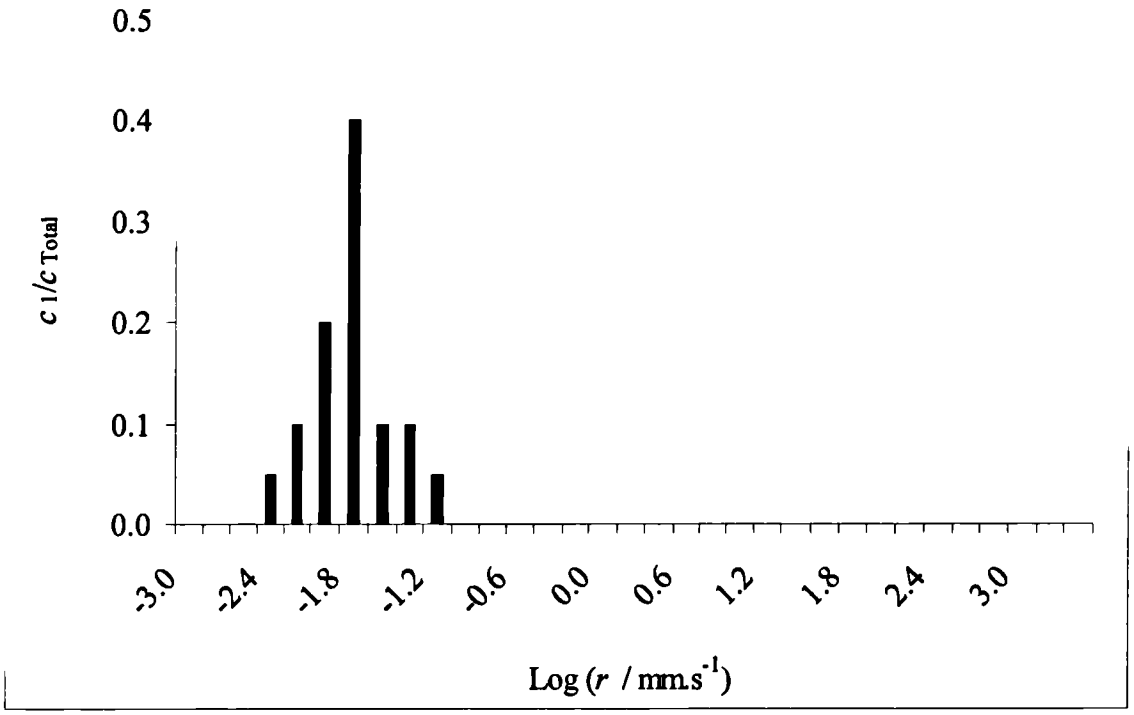

Figure 5-9(a). The frequency distribution of crack growth rates for SBR (SBR00-S3) in the relatively steady crack growth region (region-A).

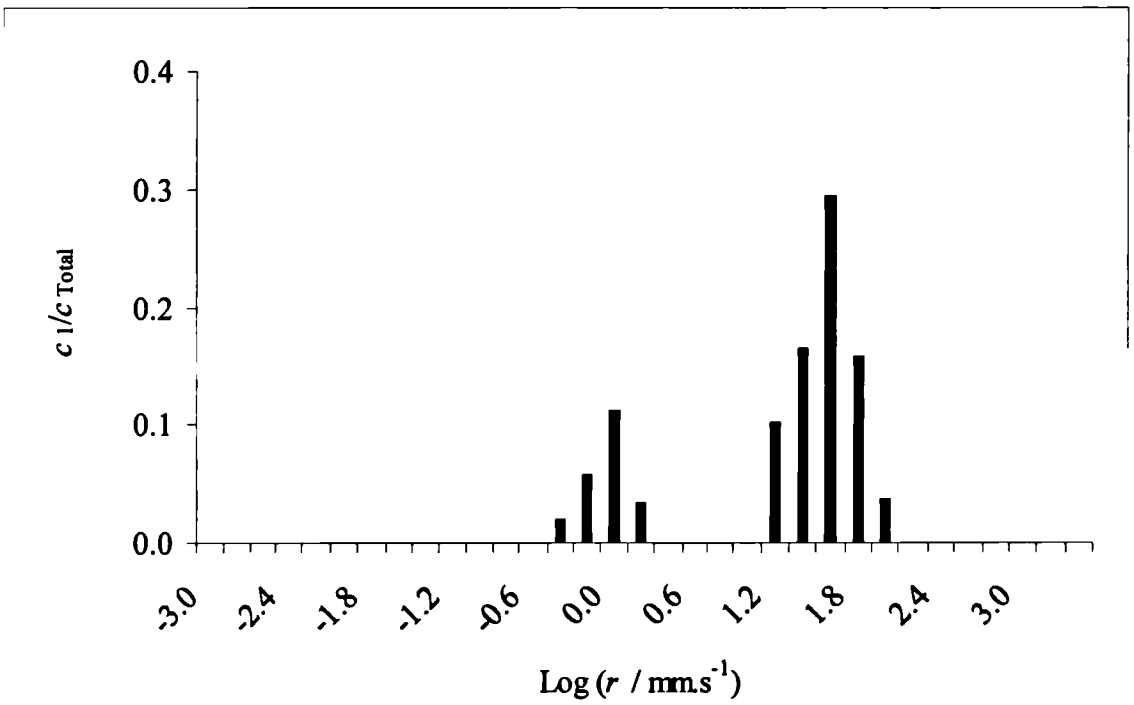

Figure 5-9(b). The frequency distribution of crack growth rates for SBR (SBR00-S3) in the stick-slip region (region-B).

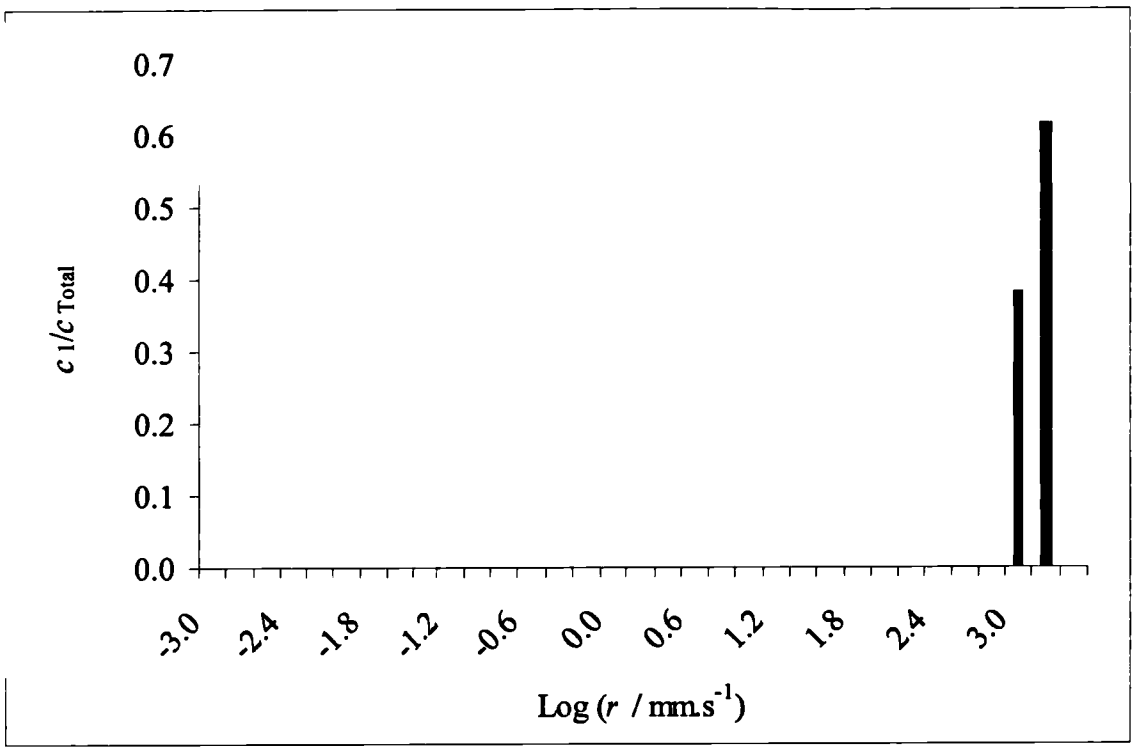

Figure 5-9(c). The frequency distribution of crack growth rates for SBR (SBR00-S3) in the steady crack growth region (region-C).

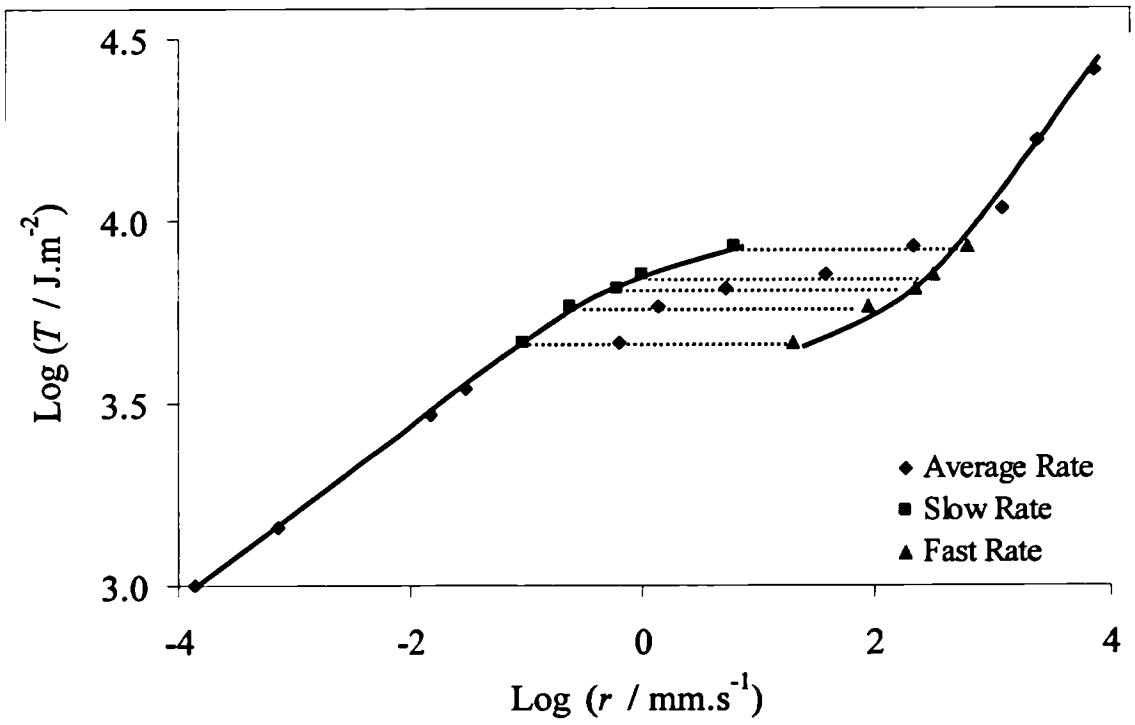

Figure 5-10. The tearing energy, T, as a function of crack growth rate, r, for SBR (SBR00-S2) showing the fast, slow and average rates in the stick-slip region.

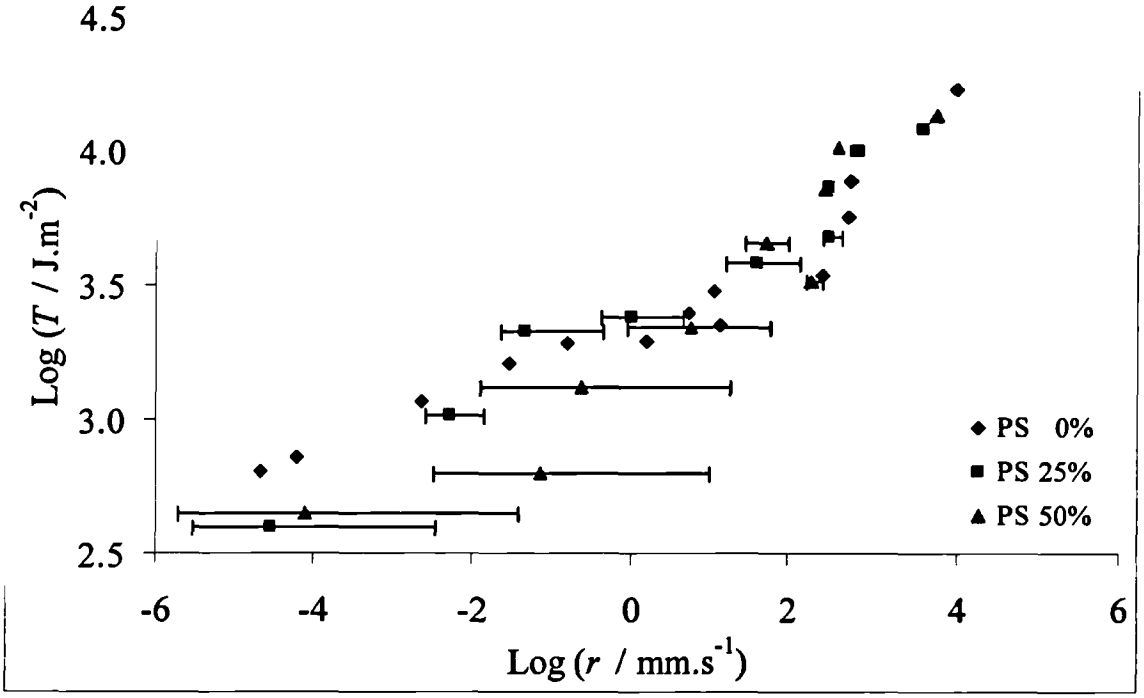

Figure 5-11. The effect of pre-strain on the *T/r* relationship for SBR (SBR00-S3).

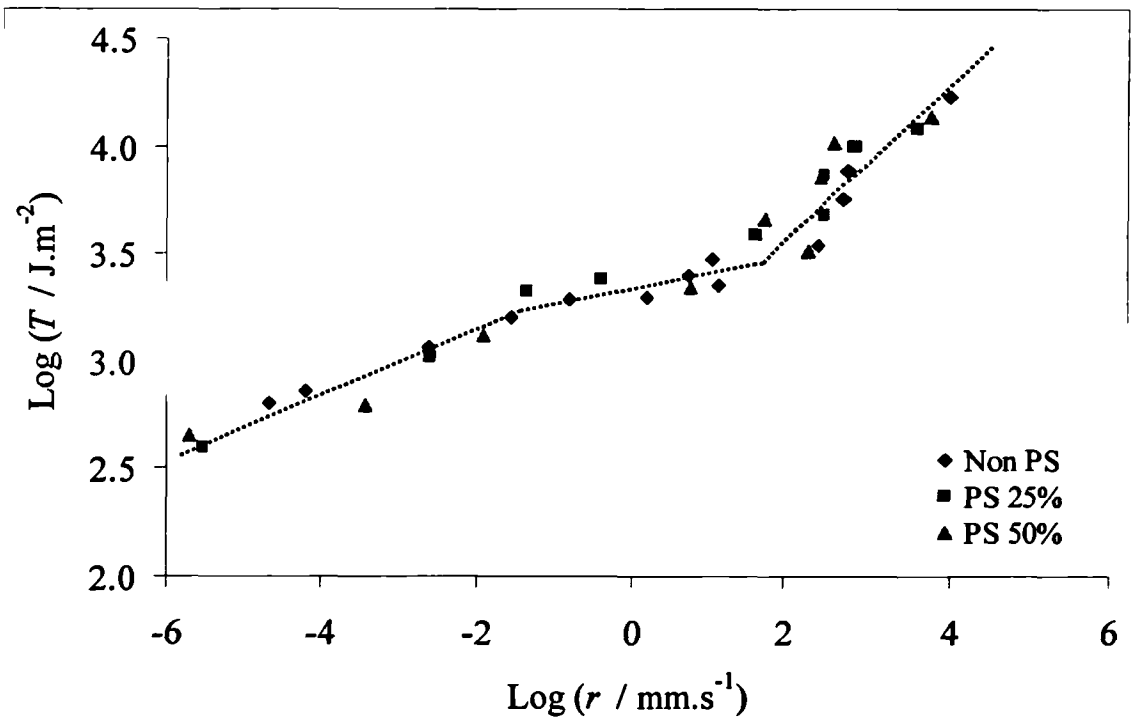

Figure 5-12. The data in figure 5-11 are re-plotted using only the horizontal crack growth rates.

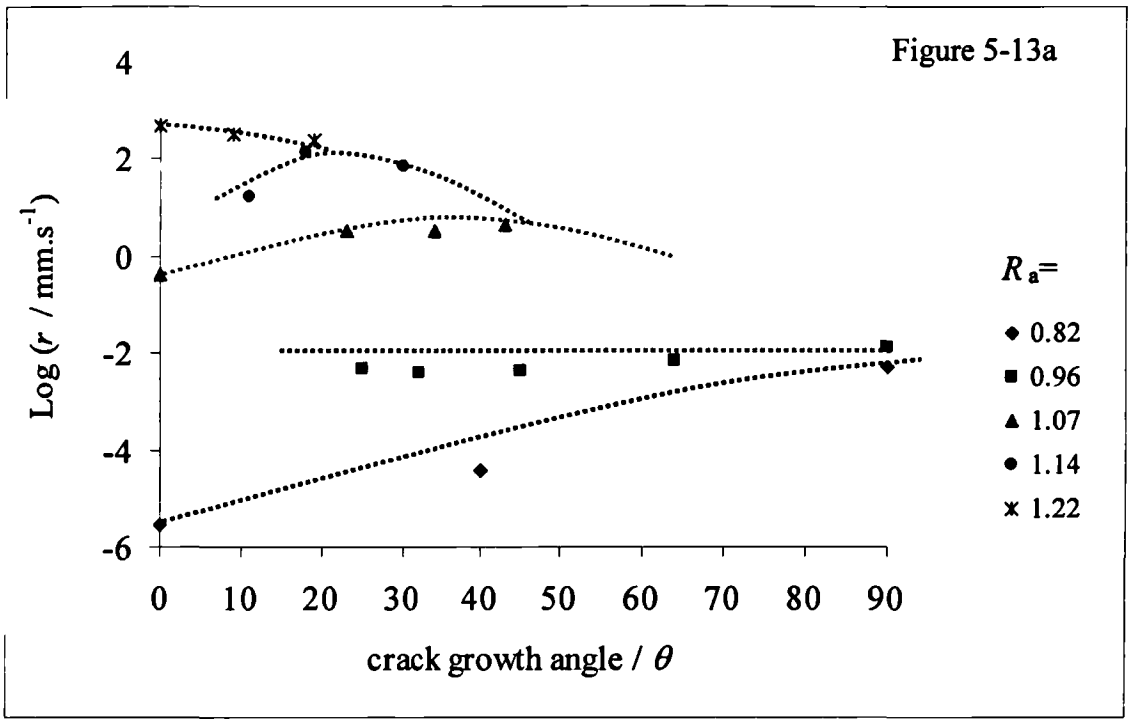

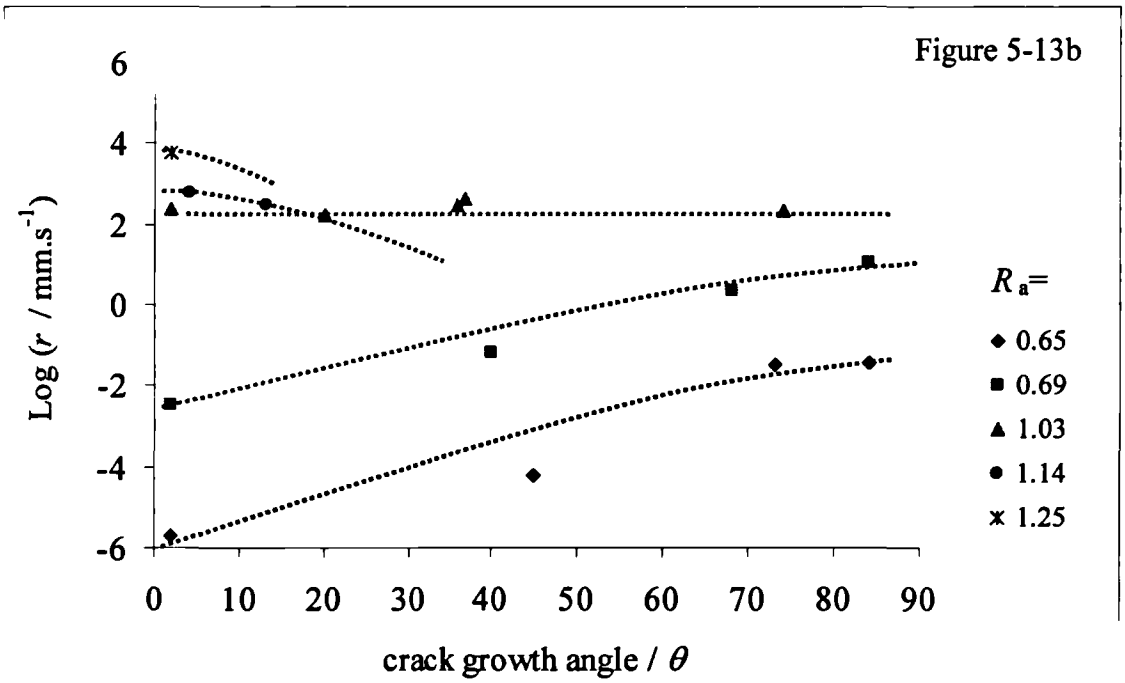

Figure 5-13. Crack growth rate as a function of crack growth angle (from the horizontal direction) for SBR (SBR00-S3) for different R_a values. (a)pre-strain 25% and (b)pre-strain 50%.

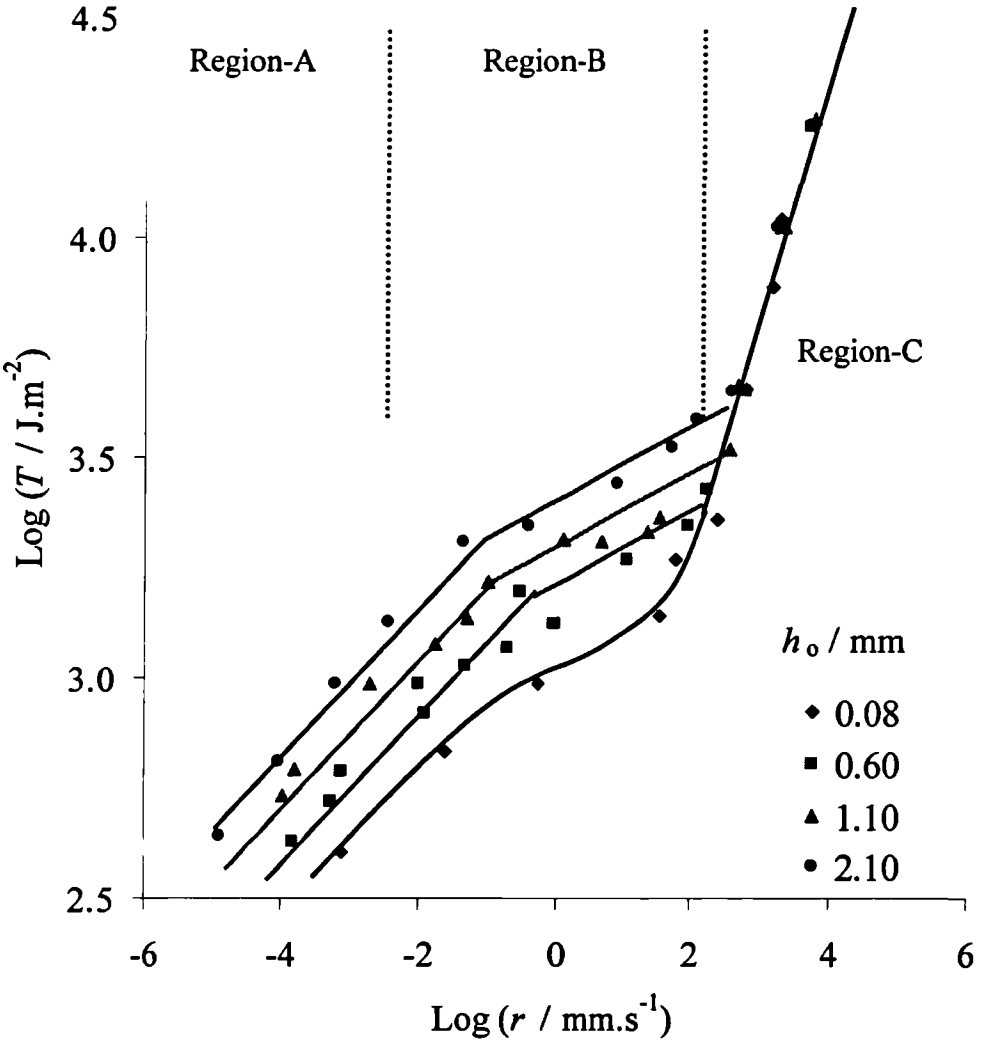

Figure 5-14. The effect of specimen thickness on the *T/r* relationship for SBR (SBR00-S3).

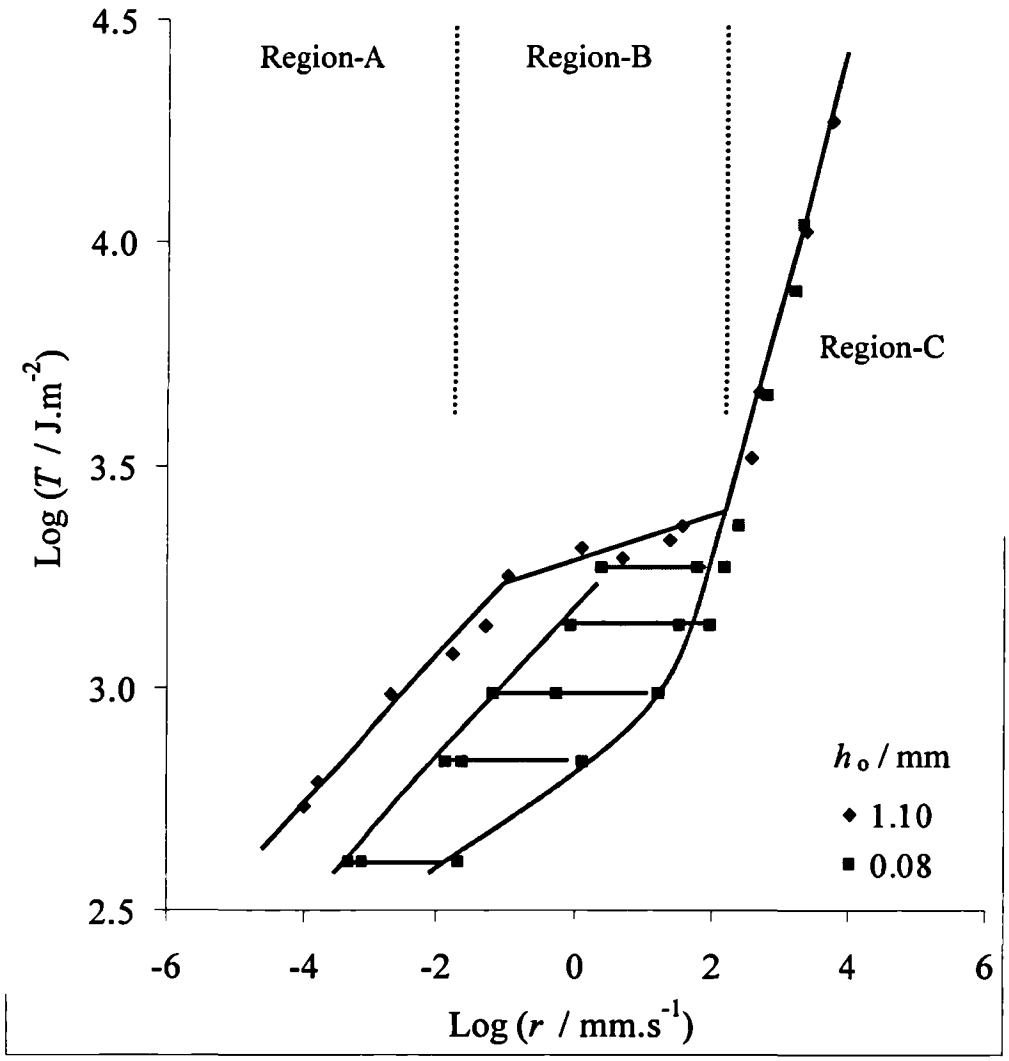

Figure 5-15. The effect of specimen thickness on the *T/r* relationship for SBR (SBR00-S3).

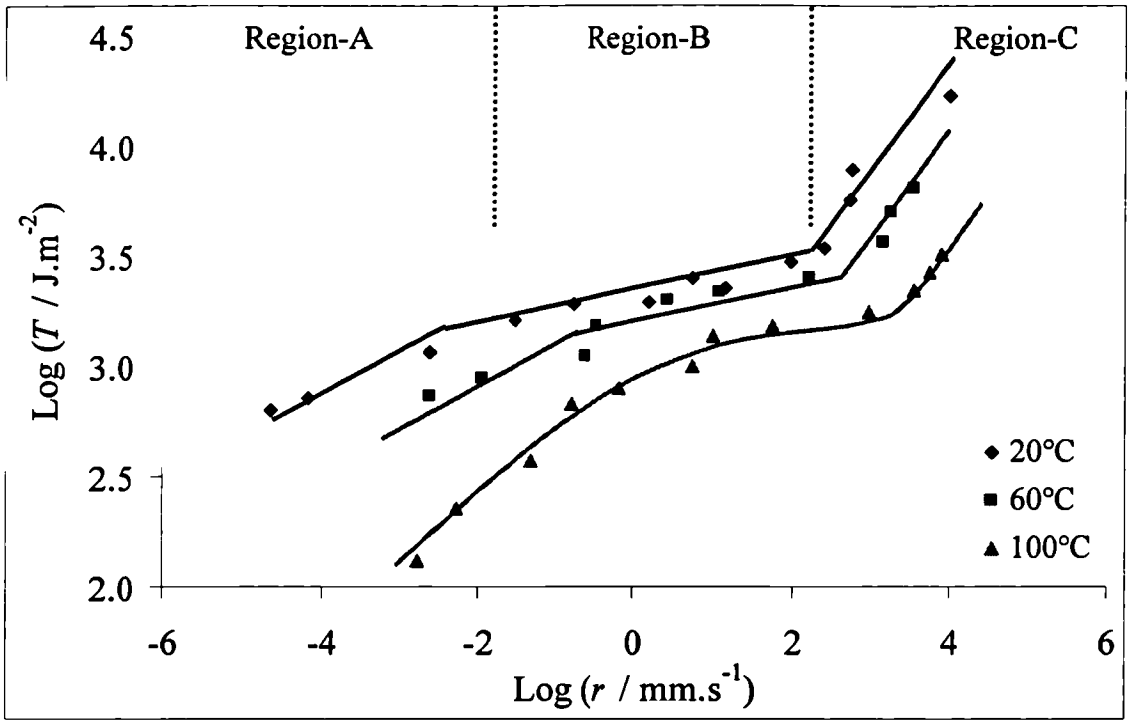

Figure 5-16. The effect of temperature on the *T/r* relationship for SBR (SBR00-S3).

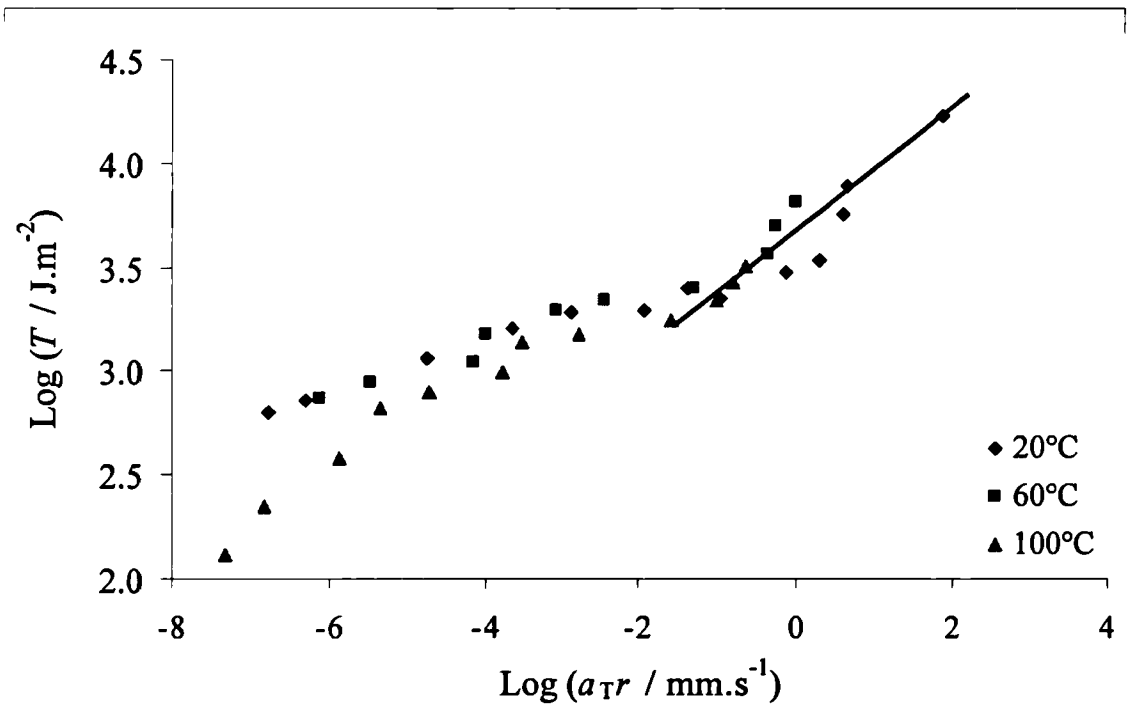

Figure 5-17. Attempted superposition of the date given in figure 5-16 using the WLF shift factor a_T.

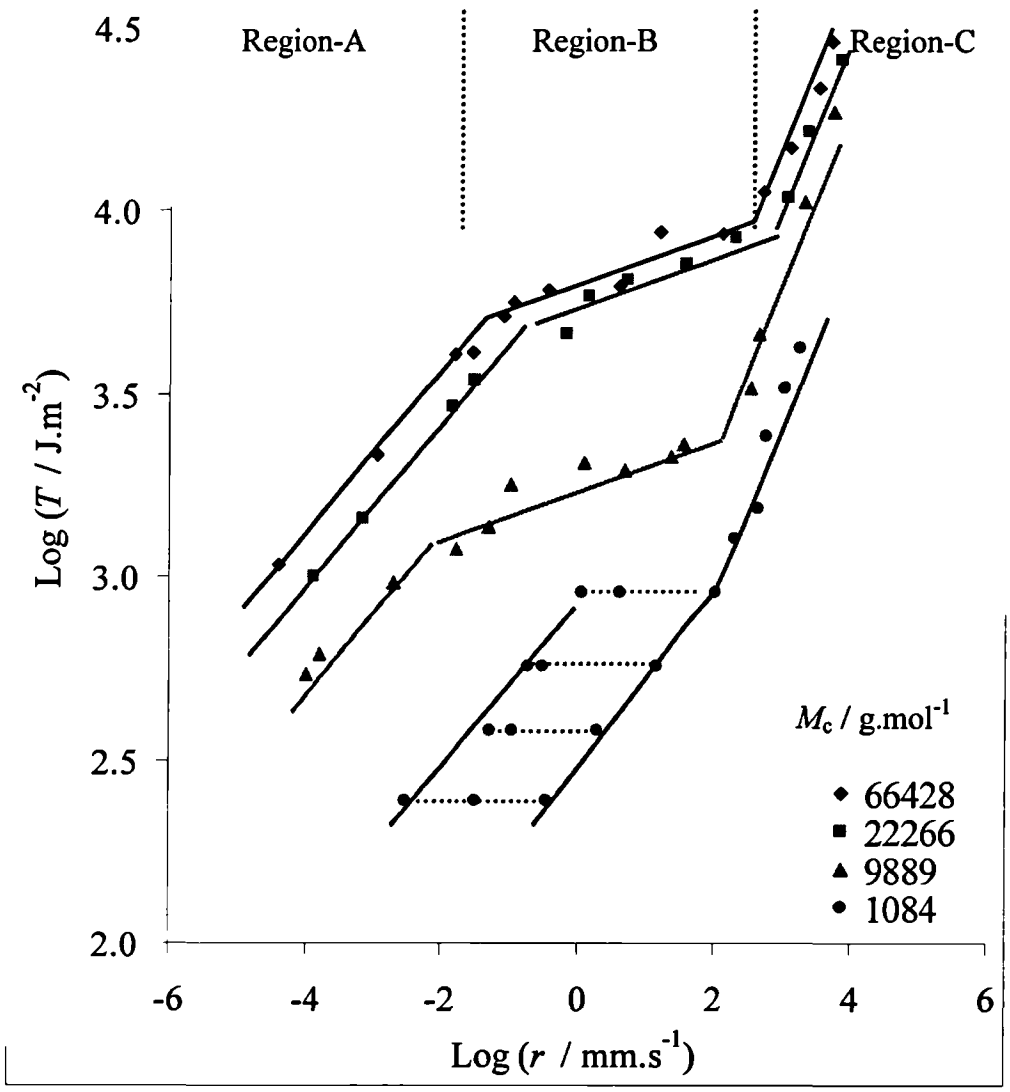

Figure 5-18. The effect of average molar mass between cross-links, M_c, on the *T/r* relationship for SBR cross-linked with sulphur.

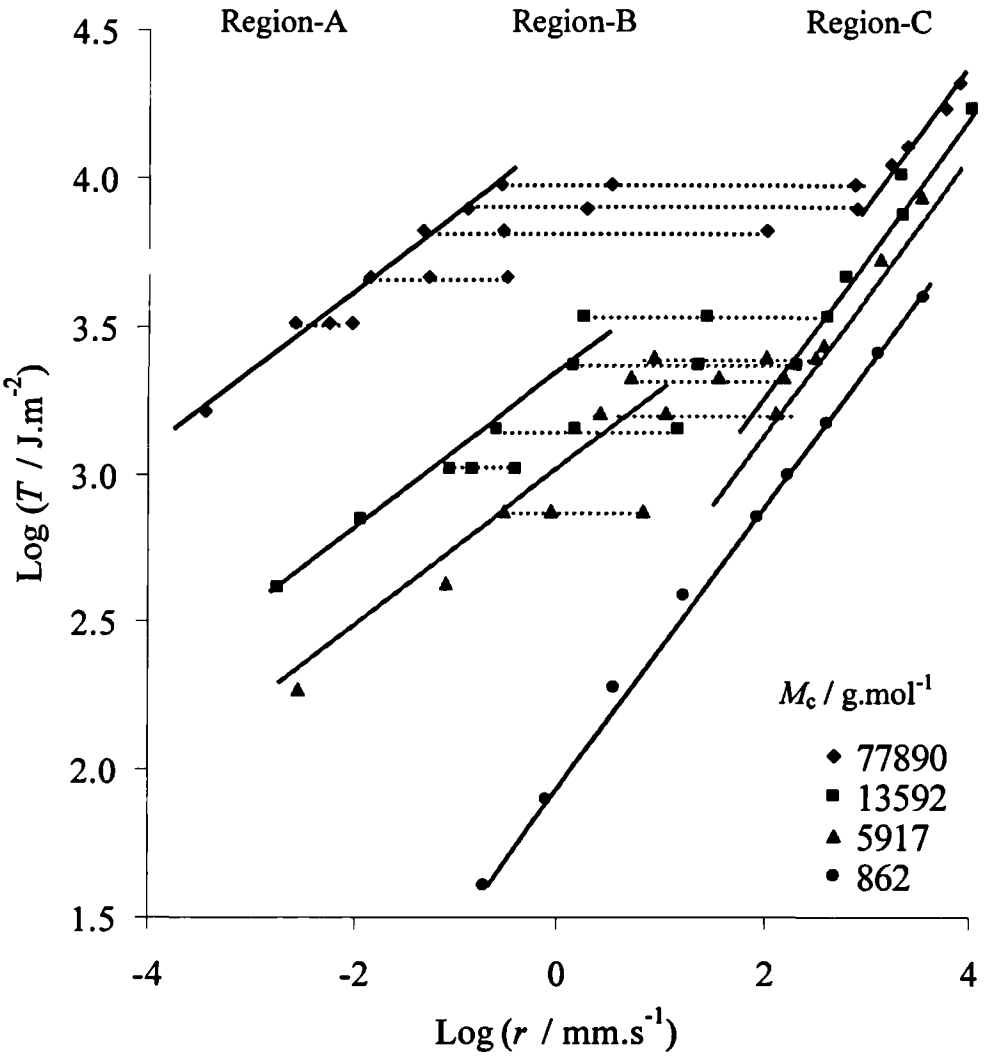

Figure 5-19. The effect of average molar mass between cross-links, M_c, on the T/r relationship for SBR cross-linked with Dicumyl Peroxide.

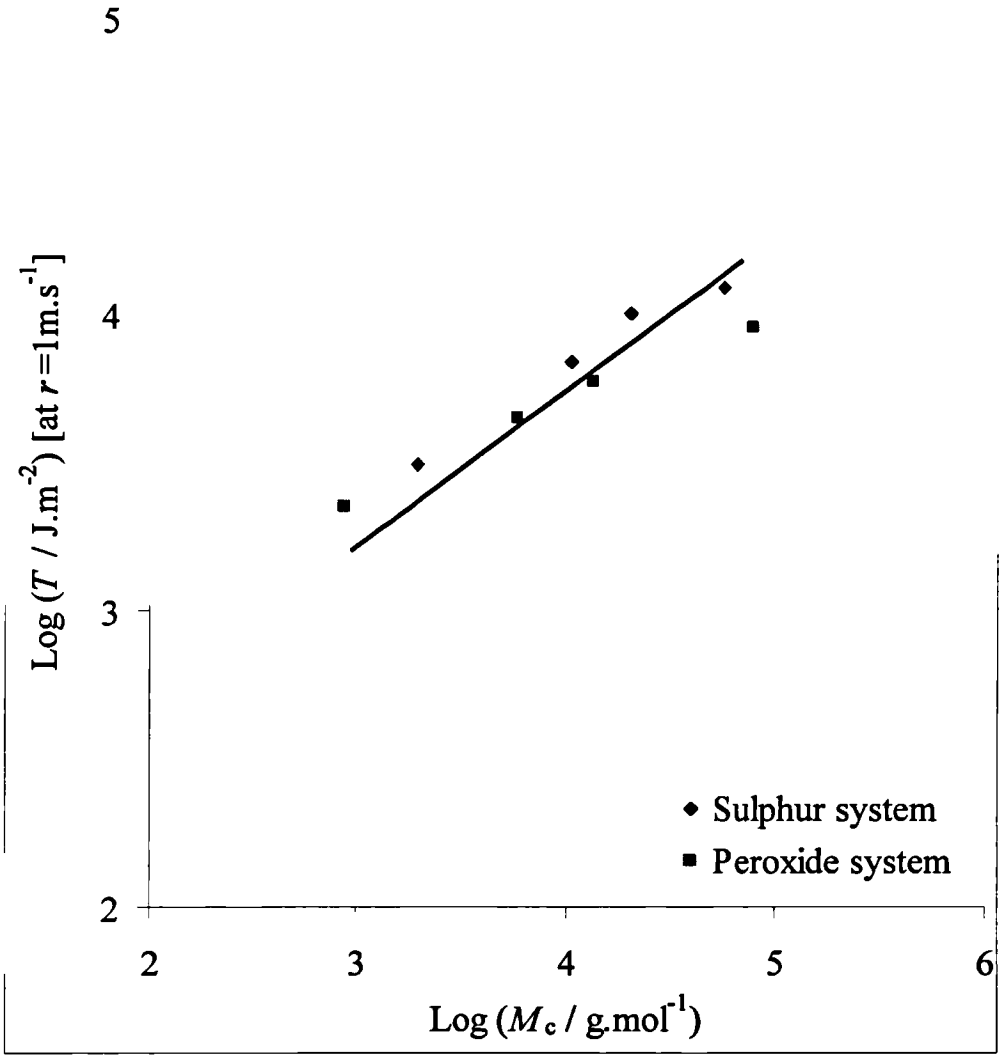

Figure 5-20. The variation of the tearing energy, T, with the average molar mass between cross-links, M_c, for SBR cross-linked with sulphur and peroxide during fast crack growth in region-C at a rate of 1.0 m.s^{-1}. A line of slope ½ is shown to correspond with the prediction in equation (5-6).

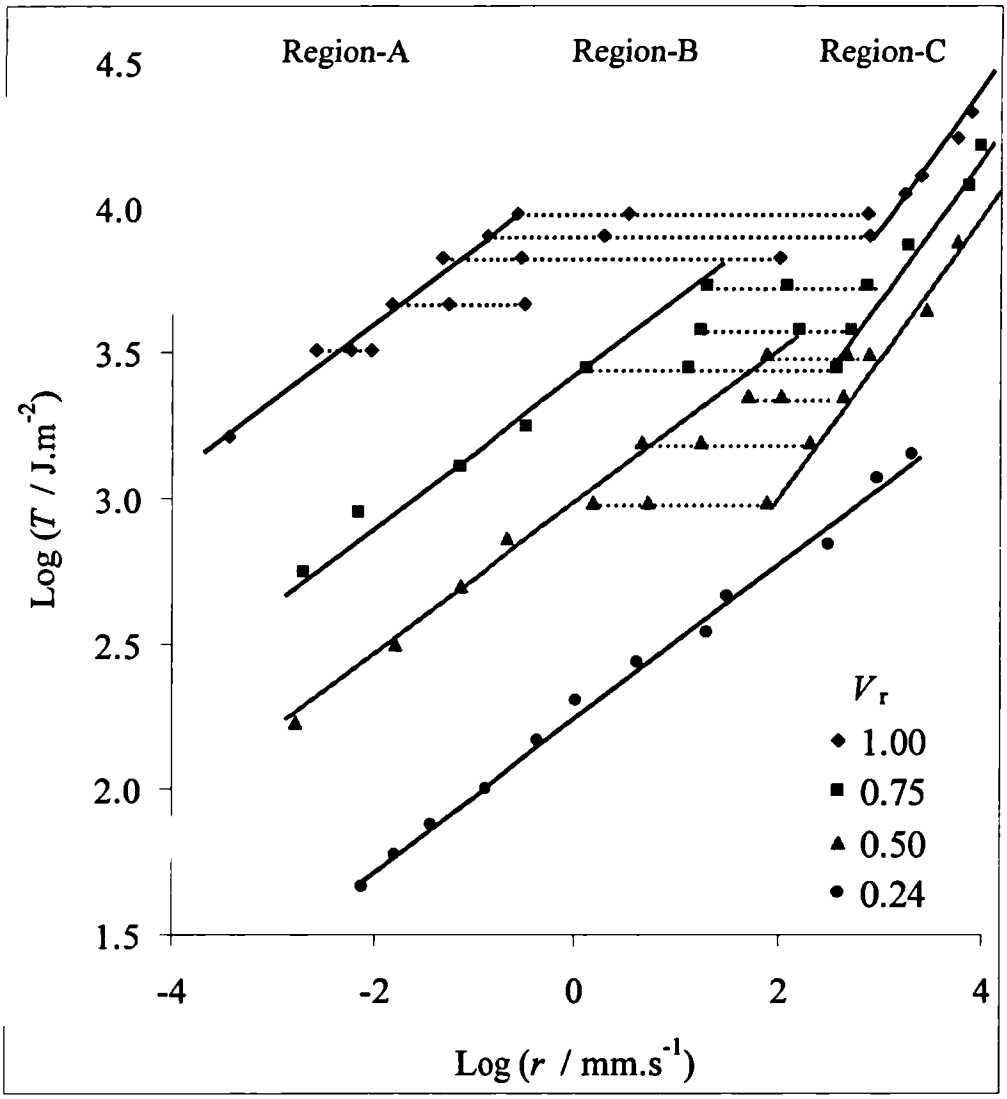

Figure 5-21. The effect of swelling with DBA on the *T/r* relationship for the SBR00-P1 most lightly cross-linked SBR with Dicumyl Peroxide.

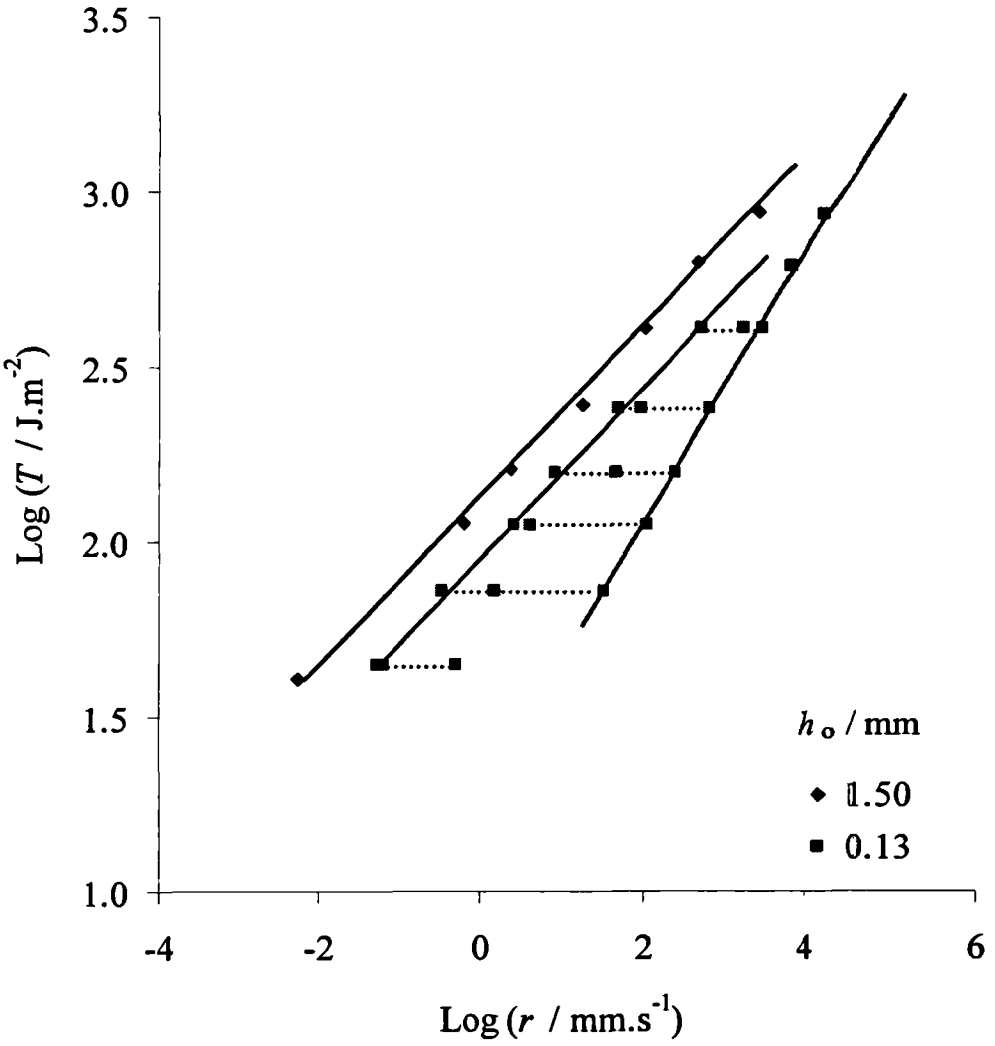

Figure 5-22. The effect of swelling on the *T/r* relationship for SBR (SBR00-S3) of different specimen thicknesses swollen with DBA to V_r=0.38.

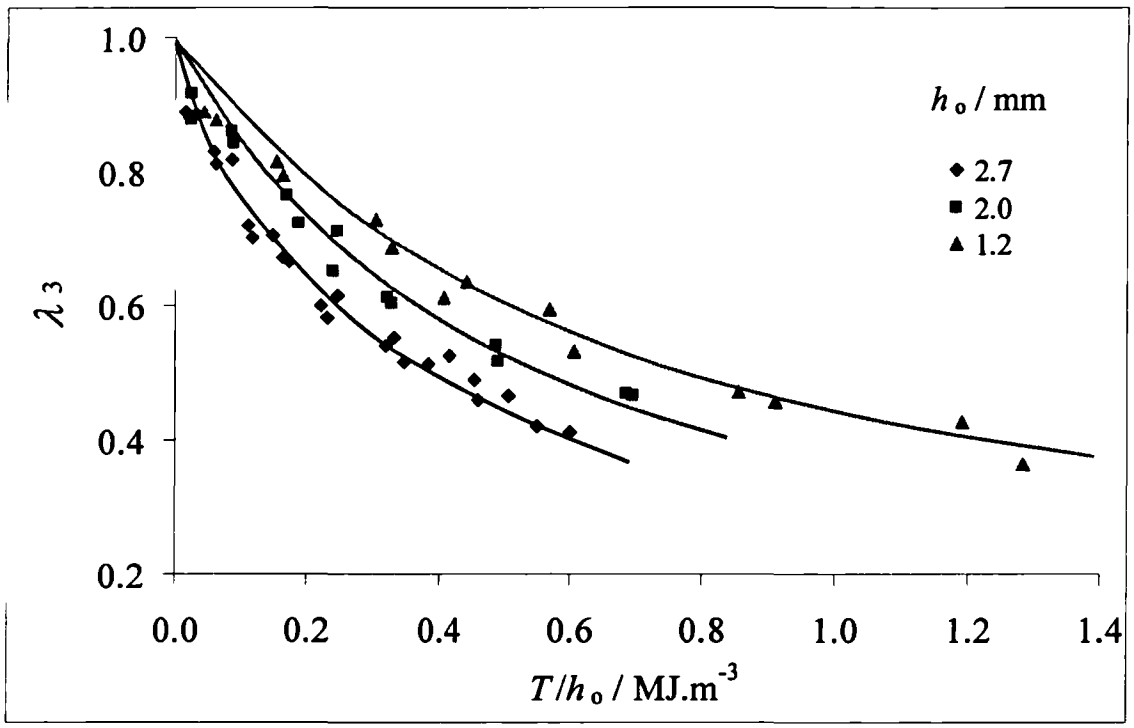

Figure 5-23. Strain at the crack tip in the thickness direction λ_3 as a function of tearing energy T to unstrained thickness h_0 for SBR (SBR00-S3).

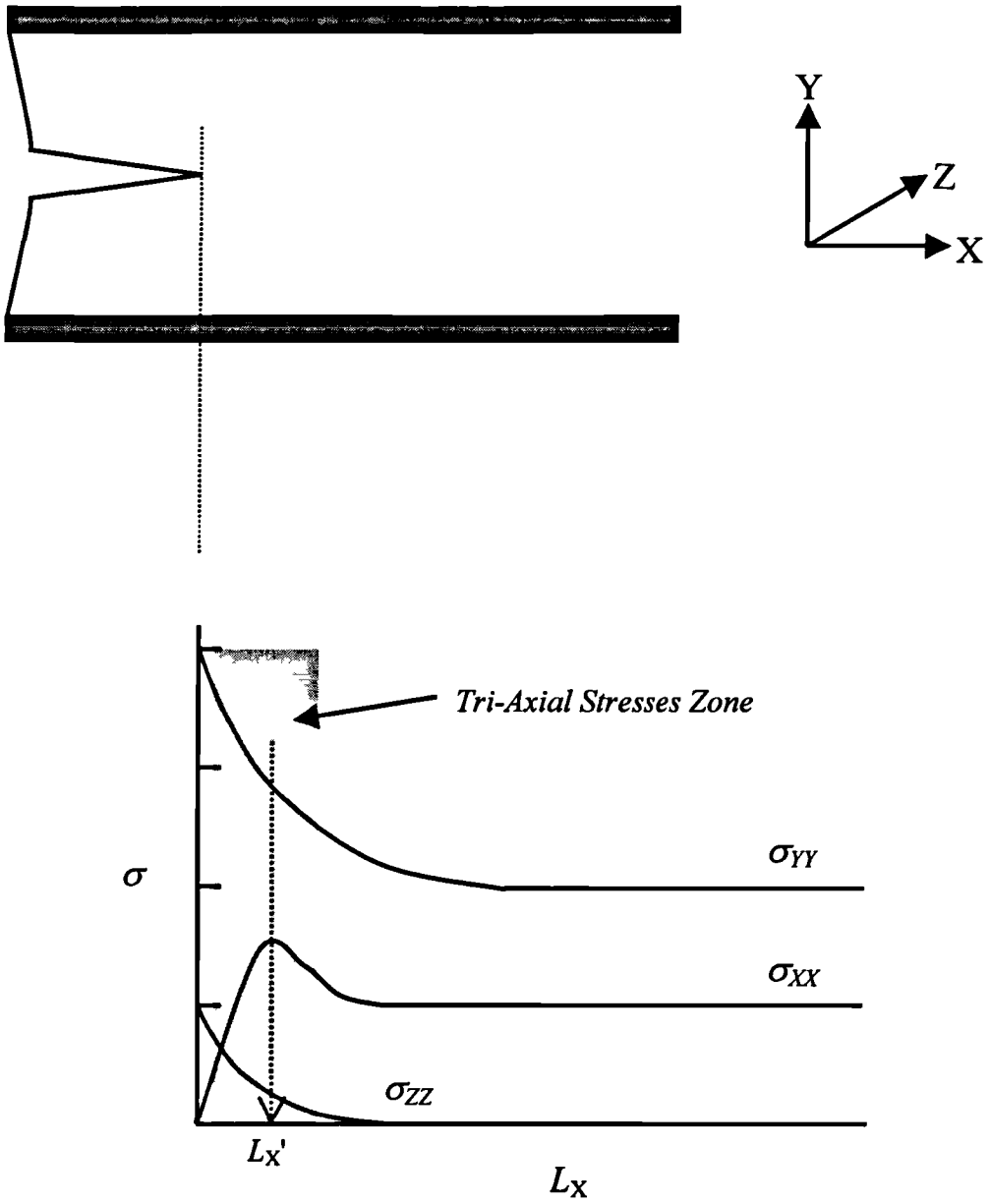

Figure 5-24. Schematic figure illustrating the tri-axial stress field ahead of a crack tip[96].

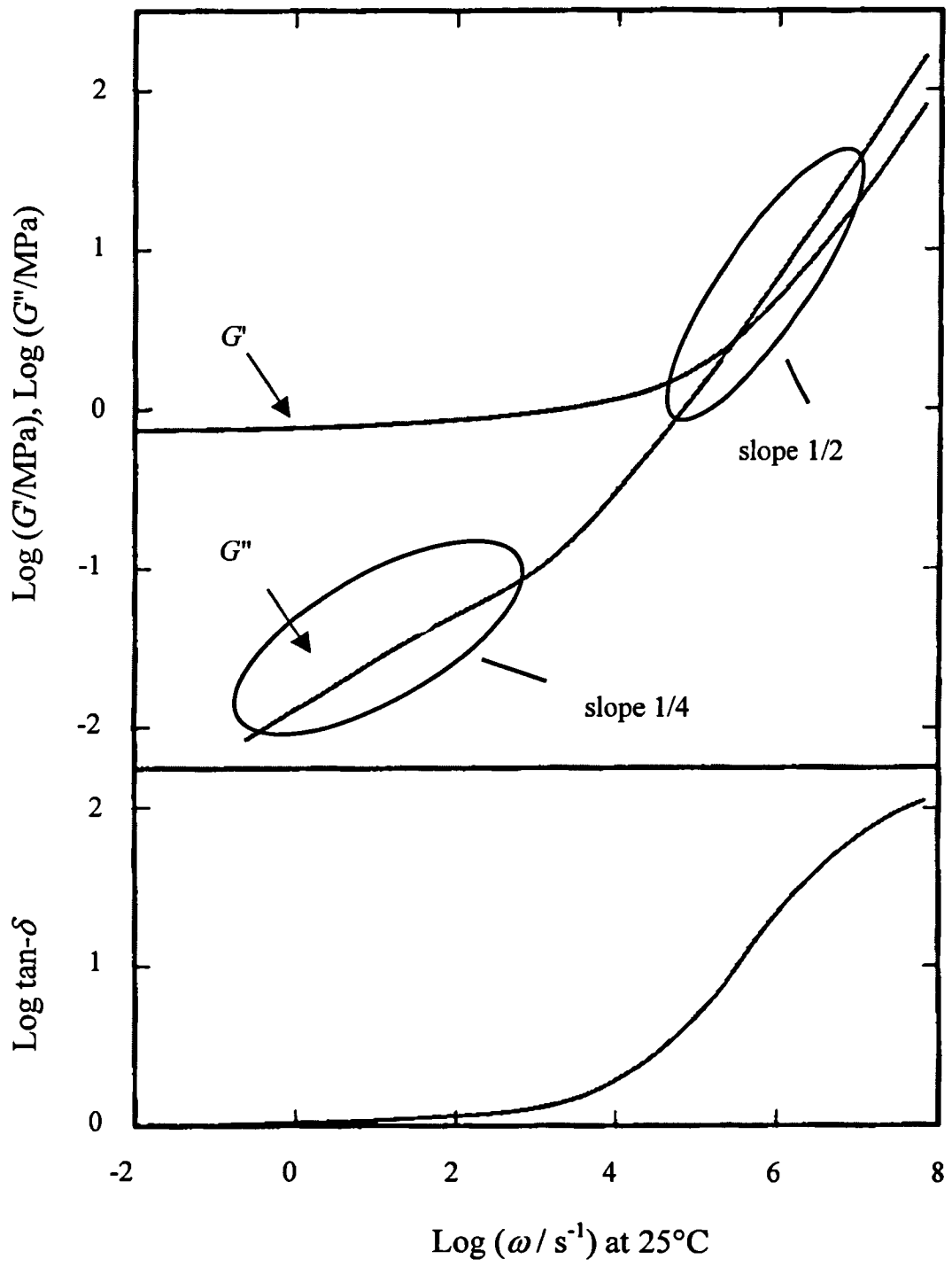

Figure 5-25. Diagrammatic representation of the effect of frequency, ω, on the dynamic mechanical properties of unfilled SBR[97].

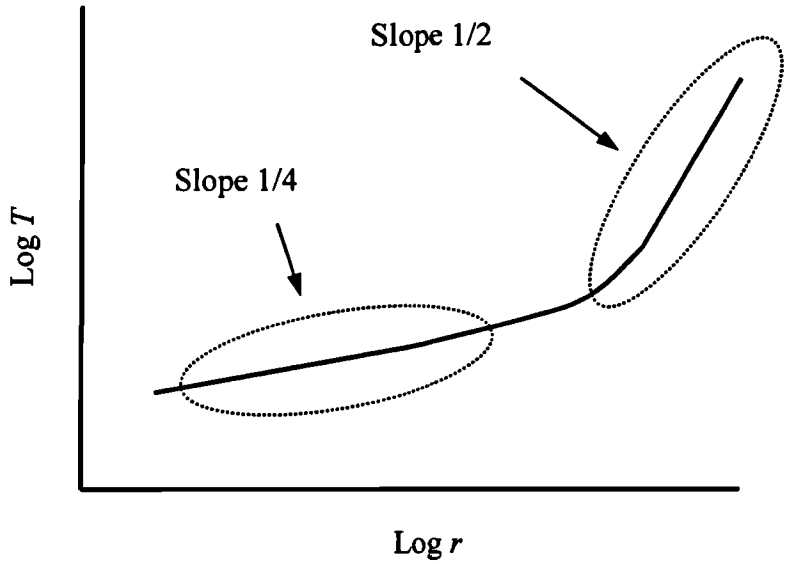

Figure 5-26. Schematic diagram illustrating the *T/r* relationship when the crack tip diameter, *d*, is assumed to be the sharpest possible at all rates.

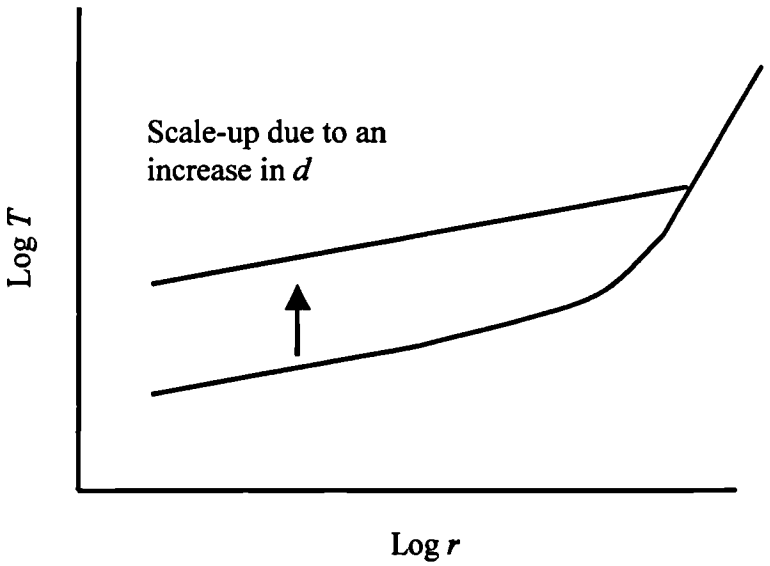

Figure 5-27. Schematic diagram illustrating the effect of an increase in crack tip diameter on the form of the *T/r* relationship.

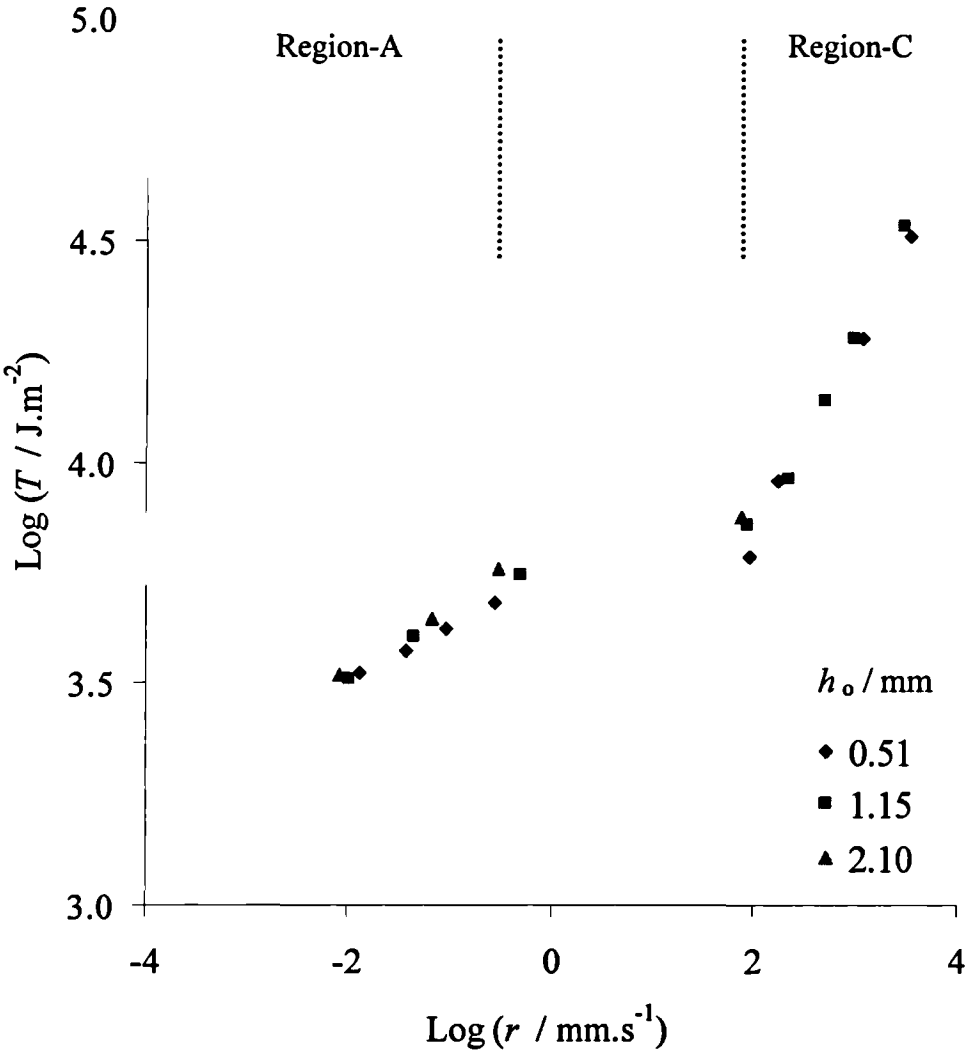

Figure 5-28. The effect of specimen thickness on the *T/r* relationship for a 50phr carbon black filled SBR cross-linked with 3.0phr sulphur (SBR50-S2).

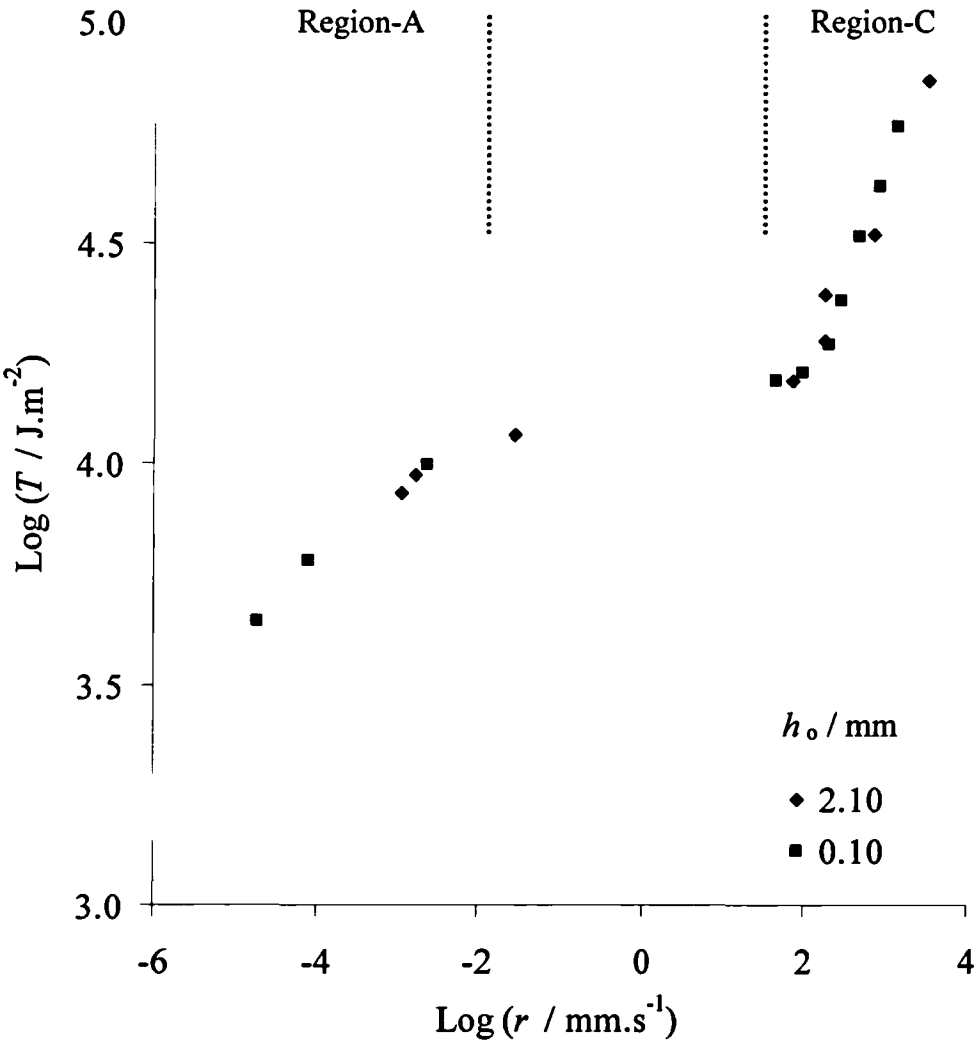

Figure 5-29. The effect of specimen thickness on the *T/r* relationship for a 50phr carbon black filled SBR cross-linked with 1.50phr sulphur (SBR50-S1).

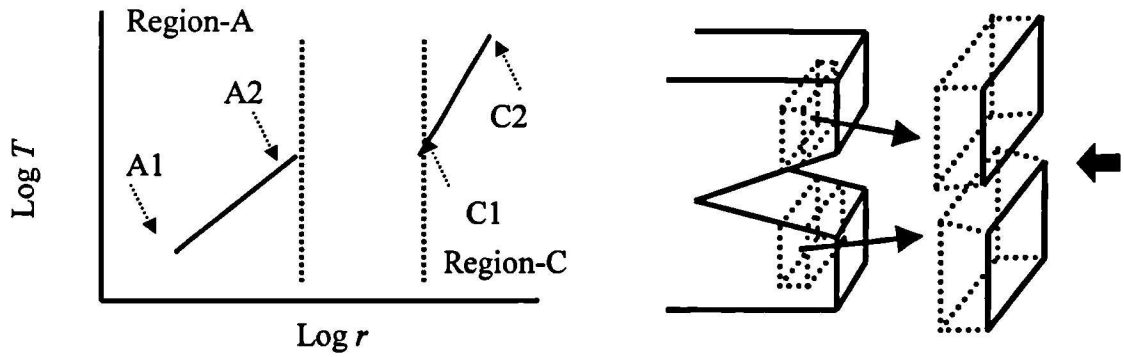

	h_o=0.51mm (x 20)	h_o =1.15mm (x 5)	h_o =2.10mm (x 5)
Region-A A1	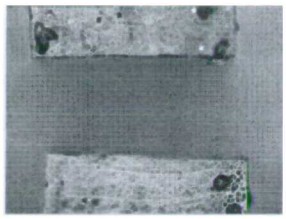		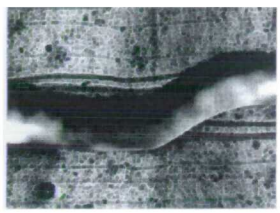
Region-A A2	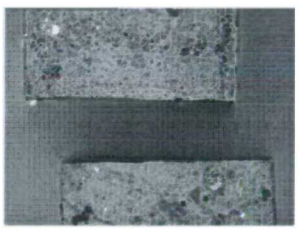	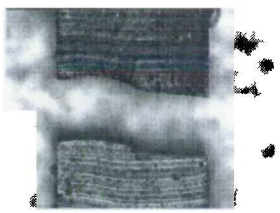	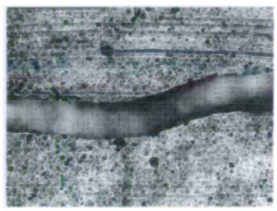
Region-C C1	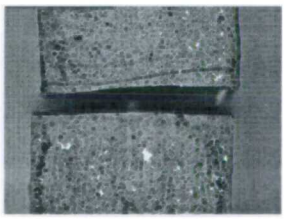	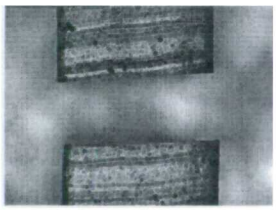	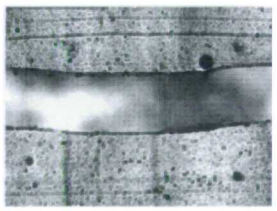
Region-C C2	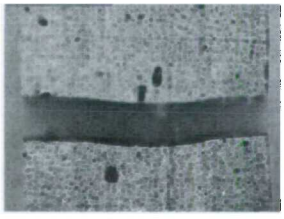	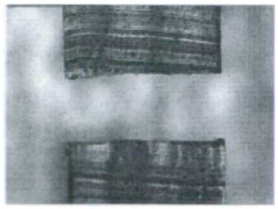	

Figure 5-30. Optical micrographs of cross-sections of fracture surface profiles for different specimen thicknesses taken from figure 5-28.

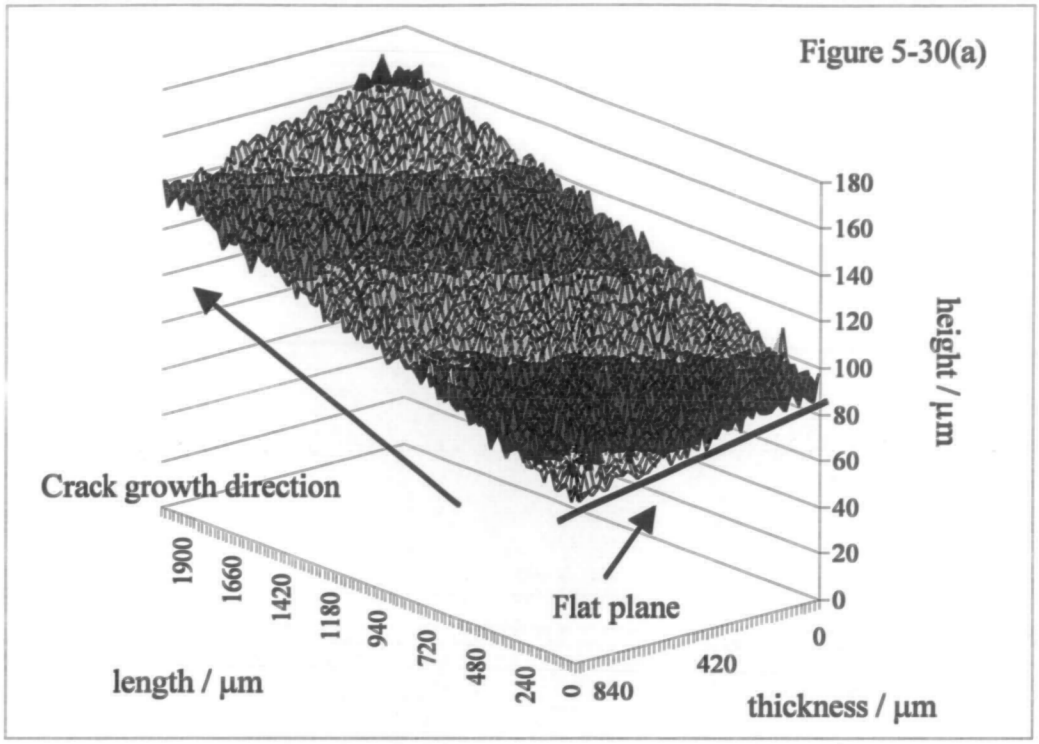

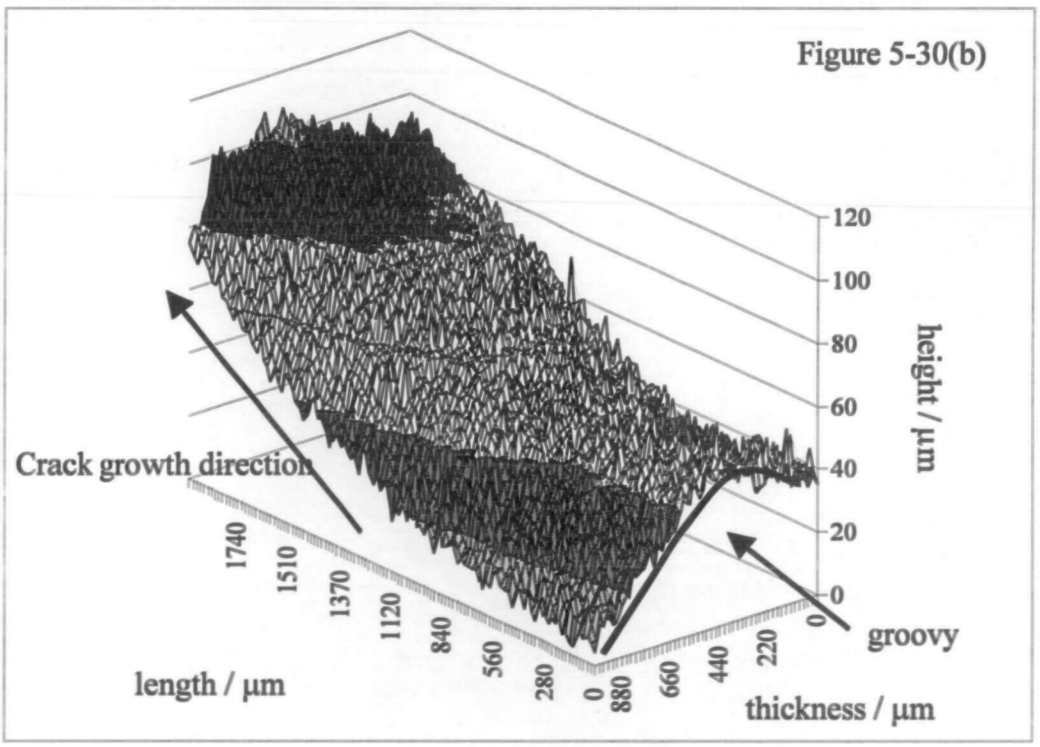

Figure 5-31. The three dimensional fracture surface profile for a 50phr carbon black filled SBR (SBR50-S1). (a) surface profile taken from the fast crack growth region-C, (b) surface profile taken from the slow crack growth region-A.

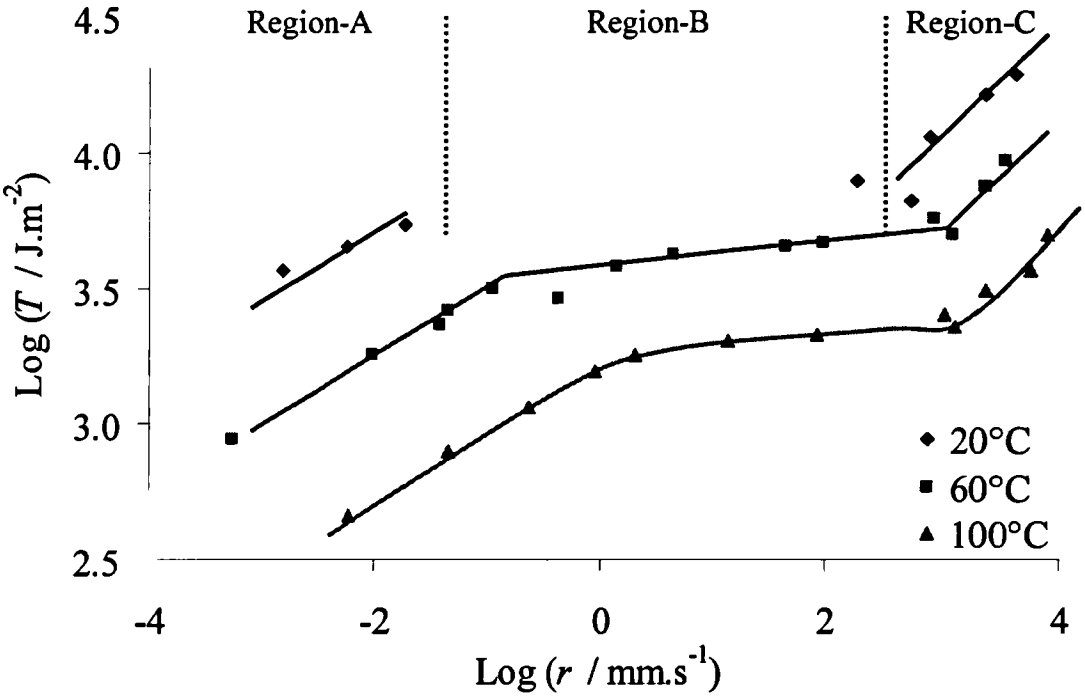

Figure 5-32. The effect of temperature on the *T/r* relationship for a 10phr carbon black filled SBR (SBR10-S1).

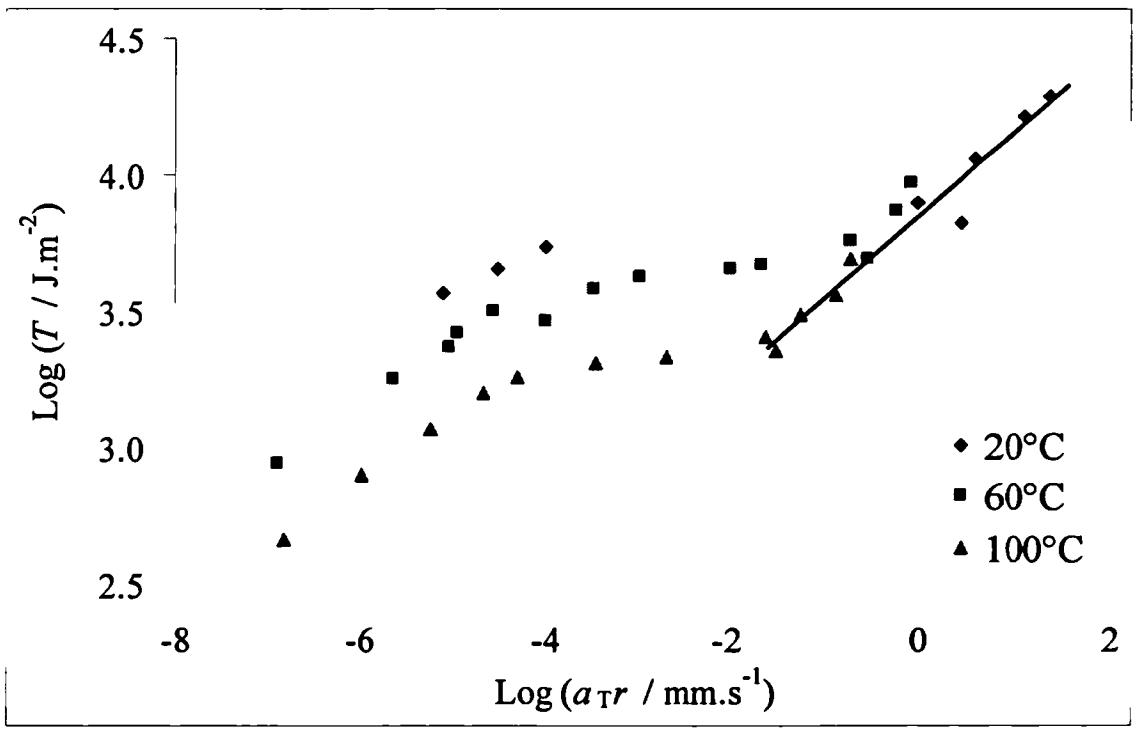

Figure 5-33. Attempted superposition of the data given in figure 5-32 using the WLF shift factor a_T.

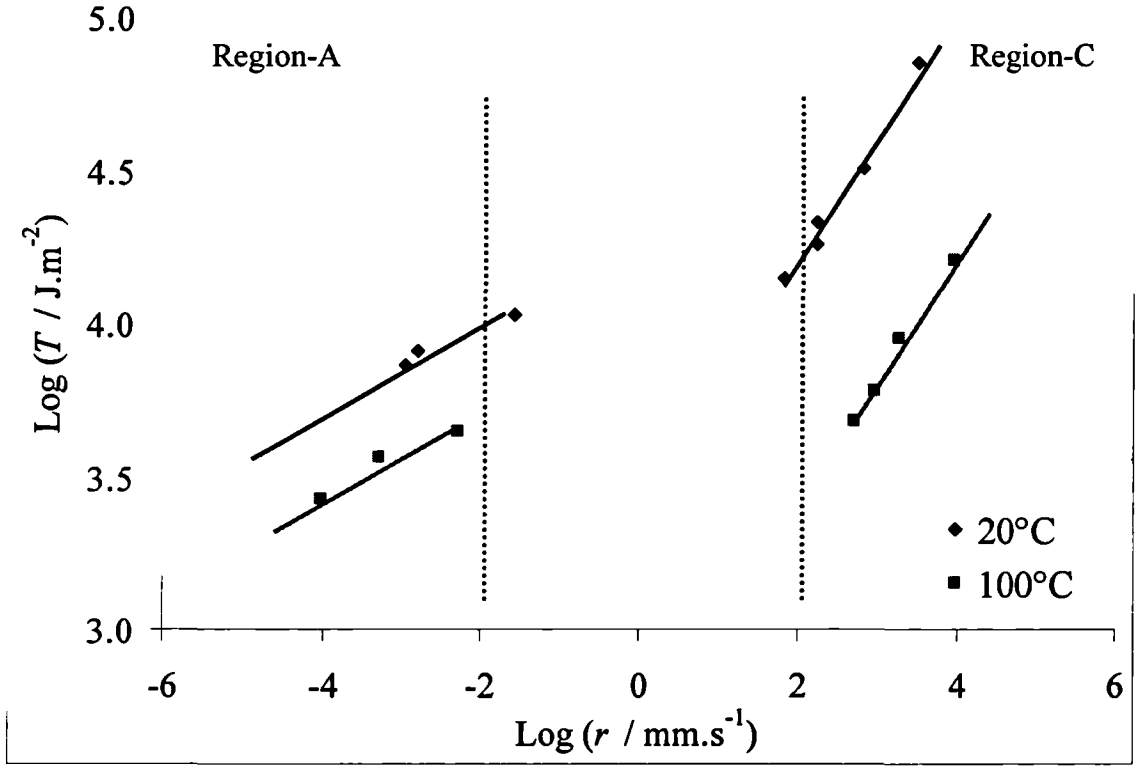

Figure 5-34. The effect of temperature on the *T/r* relationship for a 50phr carbon black filled SBR (SBR50-S1).

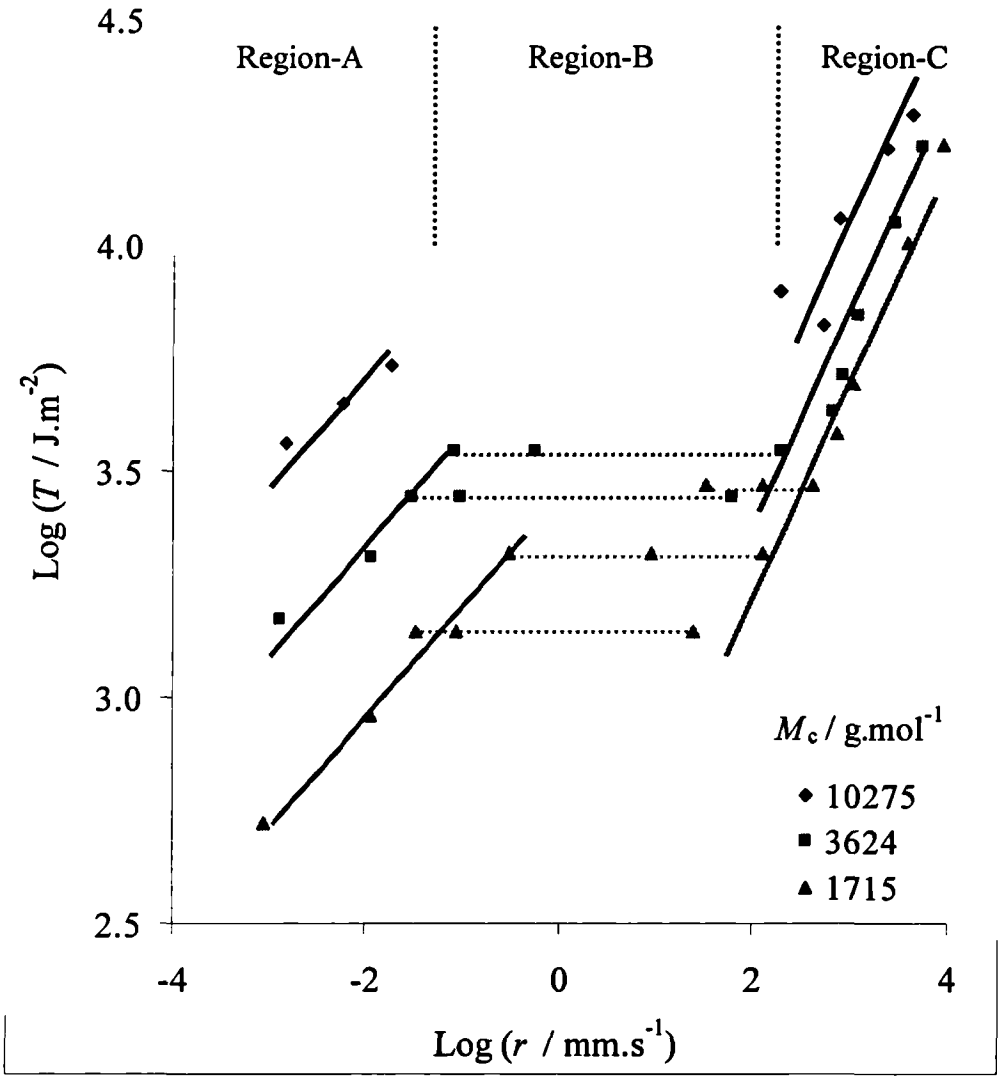

Figure 5-35. The effect of the average molar mass between cross-links, M_c, on the *T/r* relationship for a 10 phr carbon black filled SBR cross-linked with sulphur.

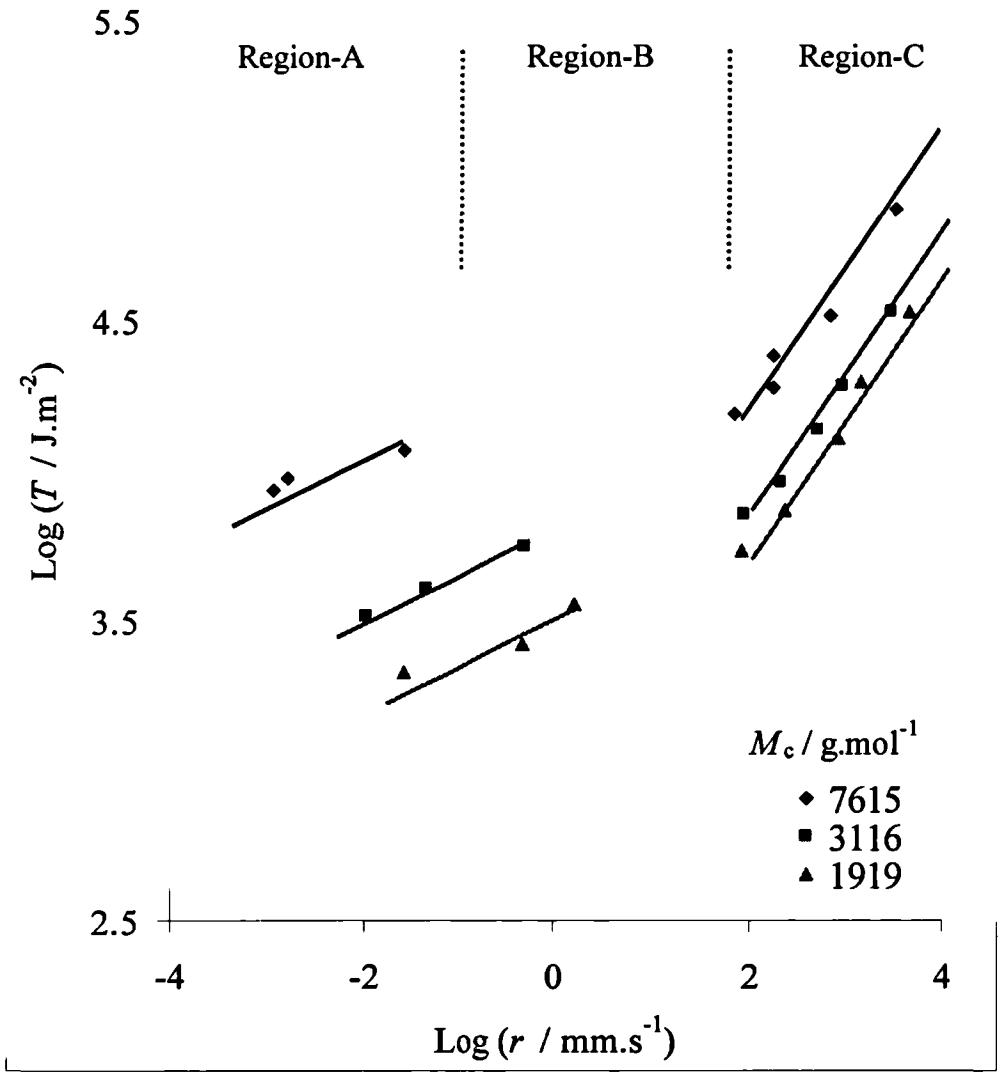

Figure 5-36. The effect of the average molar mass between cross-links, M_c, on the *T/r* relationship for a 50phr carbon black filled SBR cross-linked with sulphur.

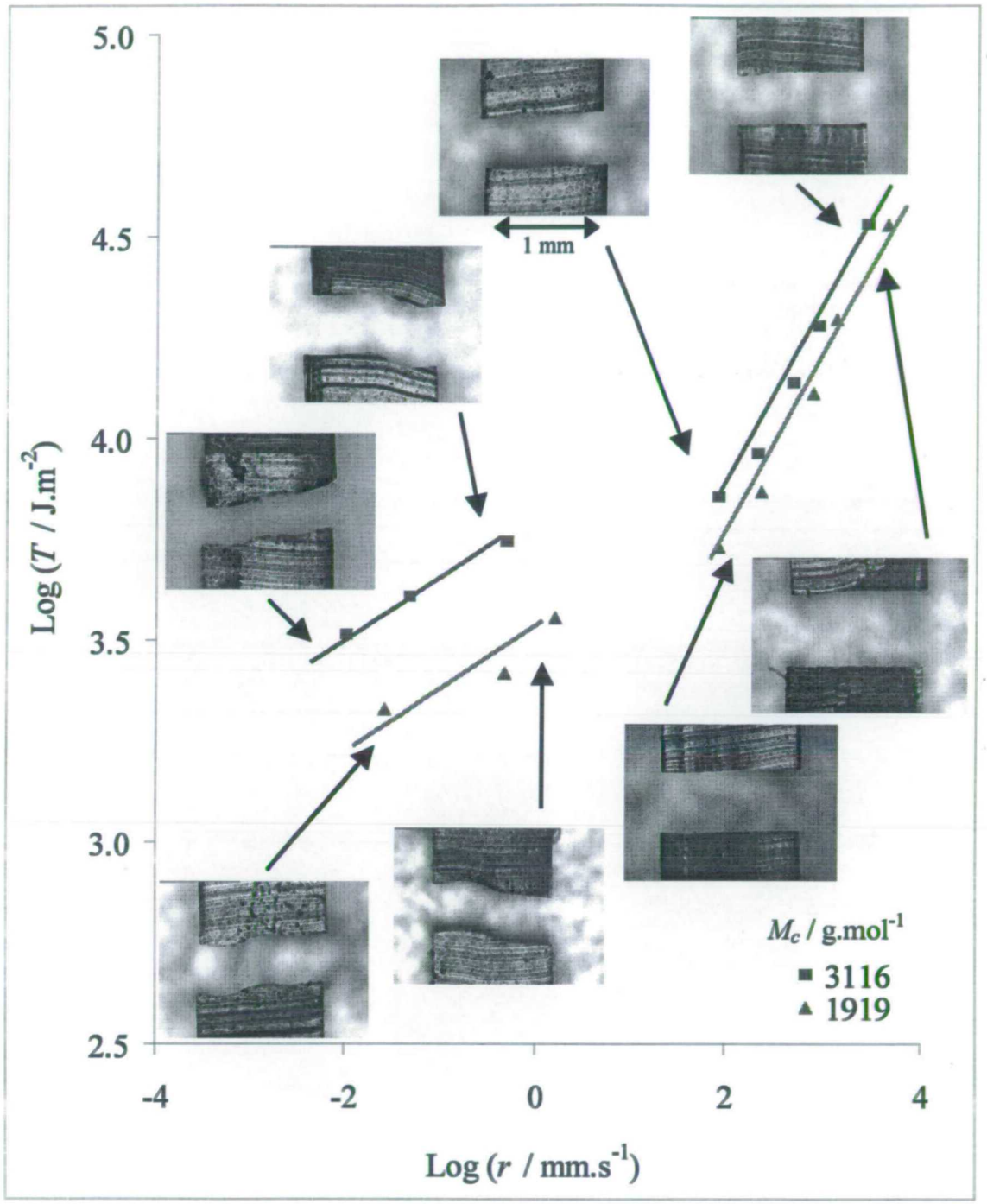

Figure 5-37. Optical micrographs of cross-sections of the fracture surfaces for a 50phr carbon black filled SBR (SBR50-S2 and SBR50-S3) at various points on the *T/r* relationship.

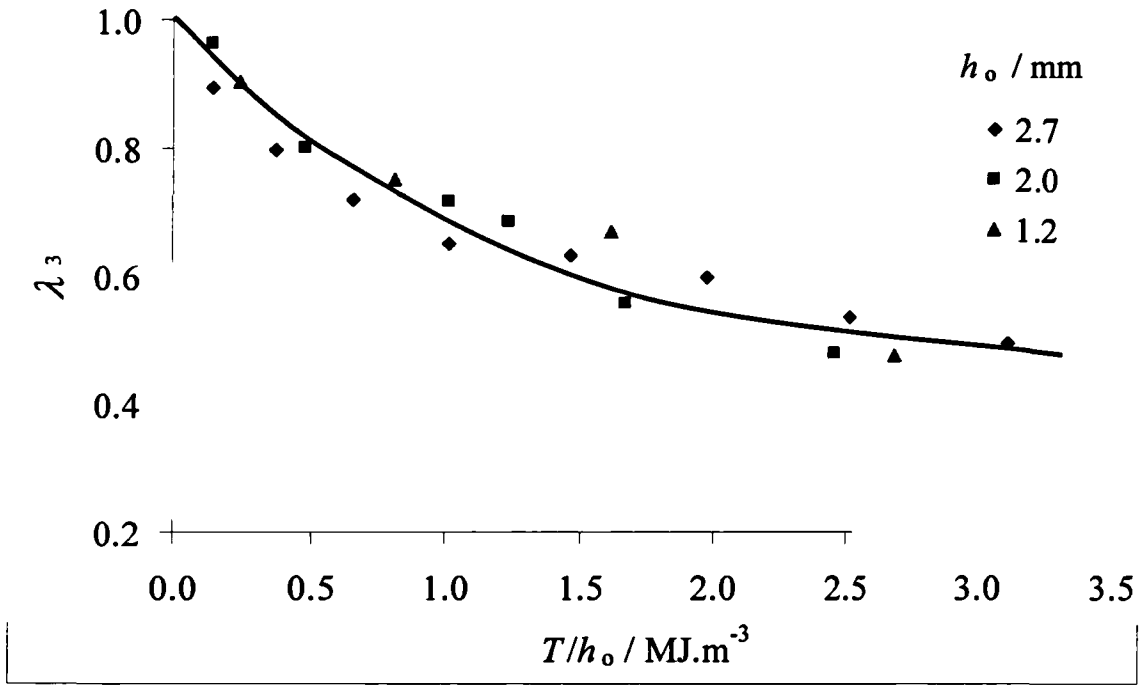

Figure 5-38. The strain at the crack tip in the thickness direction, λ_3, as a function of tearing energy T for various unstrained thicknesses h_o for a 50 phr carbon black filled SBR (SBR50-S2).

Chapter Six

Cyclic crack growth behaviour

6-1. Introduction

As was discussed for the static crack growth behaviour in chapter 5, cyclic crack growth behaviour can also be described in terms of the tearing energy concept[51-53]. It is well established that the relationship between the crack growth increment per cycle, dc/dn, and the tearing energy, T, is characteristic for a given rubber, and that this relationship is independent of the test piece geometry. In this representation of the cyclic crack growth data, it is generally assumed that the cracks grow at the maximum tearing energy during a cycle. Furthermore, dc/dn is thought not to be much influenced by the way in which this maximum tearing energy is reached even for a relatively viscous material. However these assumptions have not been fully examined. As was reviewed in chapter 2, dc/dn over a wide range can be represented as being related to T by $dc/dn = B(T/T_u)^{\beta}$ (equation 2-32), where B and β are material's constants and T_u=1.0J.m^{-2} and is included to make T/T_u dimensionless. For most rubber vulcanizates, the value of the exponent β lies between 2 and 6, depending strongly on the type of rubber and to a lesser extent on other factors such as the cross-link density and the type of the cross-link. It tends to have a lower value if the rubber exhibits a higher mechanical hysteresis, since cyclic crack growth is mainly governed by energy dissipative processes arising from internal molecular motion and/or from strain-crystallisation.

As was described in the previous chapter, the magnitude of the tearing energy necessary to drive a crack was significantly influenced by the visco-elastic losses in the rubber. If the rubber were highly swollen, with a low viscosity liquid, the magnitude of the crack growth rate dc/dt (=r) at a given tearing energy increased as the visco-elastic losses decreased. It was hence expected that swelling a rubber would significantly influence cyclic crack growth behaviour. However, very limited research has been carried out in this area[64] and therefore an experimental investigation was carried out here in an attempt to clarify the effect.

The crack growth increment during each cycle, d*c*/d*n*, is considered to result from the sum of two different components; the time dependent component, $(dc/dn)_{-time}$, and the cyclic component, $(dc/dn)_{-cycle}$[52-53] as

$$\frac{dc}{dn} = \left(\frac{dc}{dn}\right)_{-time} + \left(\frac{dc}{dn}\right)_{-cycle} \qquad (6\text{-}1)$$

The first depends only on the length of time of a cycle (the reciprocal of the frequency for a given cycle shape/form) and on the magnitude of the tearing energy at each time during the cycle. The second is genuine cyclic growth with a given increment of crack growth occurring in a given cycle independent of the length of time of the cycle. The extent of this crack growth increment depends on the details of the loading and unloading process[53]. For a non-crystallising rubber, significant effects of cyclic frequency on d*c*/d*n* have been found, reflecting the time dependent element of crack growth[49]. With increasing frequency, d*c*/d*n* at a given tearing energy decreases as the length of time of a cycle decreases. However, the detailed magnitudes of the contributions of these two components to d*c*/d*n* have not been determined. The $(dc/dn)_{-time}$ component can be predicted by utilising the results of the static crack growth measurements given in chapter 5. Hence, when d*c*/d*n* is determined as a function of frequency, in the present chapter, then by subtracting $(dc/dn)_{-time}$ the magnitude of $(dc/dn)_{-cycle}$ can be determined.

As was discussed in the previous chapter, strength anisotropy, which is induced by carbon black loading, had a significant effect on static crack growth behaviour in carbon black filled SBR and is likely to play an important role in cyclic crack growth behaviour. Cyclic crack growth measurement under pre-strain would be an ideal technique for studying the effect of strength anisotropy as it can reduce this effect significantly.

Therefore, experiments on cyclic crack growth of unfilled, unswollen and swollen SBR, and non pre-strained and pre-strained carbon black filled SBR specimens were carried out in an attempt to elucidate the mechanisms responsible for time and cyclic dependent crack growth.

In addition, some attempt was made to determine the magnitude of the high strain energy loss / mechanical hysteresis in the carbon black filled material as a function of strain rate as this may be significant in determining the magnitude of the tearing energy necessary to drive a crack at a given cyclic rate.

6-2. Experimental procedure

6-2-1. Cyclic crack growth measurement

The pure shear specimen test geometry was employed to obtain cyclic crack growth data. This specimen geometry is advantageous because the tearing energy, T, at a given specimen extension is independent of crack length and can be calculated simply as

$$T = Wl_o \tag{6-2}$$

where W is the elastic stored energy density in the central pure shear region of the specimen and l_o is the unstrained height of the specimen. The specimens were either 175 mm or 240 mm long, about 15 to 20 mm in height and usually of 1mm thickness. An initial horizontal crack of 40 mm in length was introduced on the central axis of the specimen, at one edge, using a razor blade. This produced a crack tip sufficiently far enough from the specimen edge to avoid the complications associated with edge effects.

Cyclic crack growth experiments were carried out at room temperature by imposing a sinusoidal waveform on the crosshead in the direction of specimen extension using a servo-hydraulic testing machine. Cyclic frequencies, of a constant waveform, from 0.01Hz to 5.0Hz were imposed to determine the effect of frequency on cyclic crack growth behaviour.

The pure shear test piece was strained to a maximum strain of between 2 to 35 % and was relaxed to zero strain during each cycle. This is known as a fixed-displacement fully relaxing test. To determine the tearing energy using equation 6-2, the magnitude of the elastic strain energy density, W, had to be determined for each of the extended conditions. The magnitude of W can be obtained from a force-deflection curve at a given temperature, strain amplitude and frequency, by integration of the curve and by dividing by the volume of the specimen. The force-deflection curve was plotted with an X-Y plotter and the integration was carried out manually utilising the trapezium method. The force-deflection behaviour and hence the magnitude of W, changed with changing frequency as rubber is a visco-elastic material. Therefore, the force-deflection curve should be determined at the same frequency as that of the cyclic crack growth measurement to determine the appropriate value of tearing energy. However, it was difficult to determine the

appropriate force-deflection curve at frequencies above 2.0Hz as the response time of the test system was too slow. Hence, for the present study the force-deflection behaviour at a frequency of 1.0Hz was employed for tearing energy calculations for all measurements at frequencies above 1.0Hz. The magnitude of the tearing energy determined in this way would be slightly smaller than the real value, but the effective error will be negligibly small when plotted on a double logarithm plot of T/T_u versus dc/dn. Stress softening also occurs during cyclic deformation and hence the force-deflection curve will change as the specimen is increasingly cycled. Therefore, to minimize this effect the force-deflection curve used to determine the tearing energy was plotted after the first one hundred cycles at each strain amplitude.

The initial rapid dc/dn, which occurs over the initial increase in crack length of 0.05 to 0.5mm due to the initially extremely sharp crack resulting from the razor blade incision, was neglected in measuring the crack growth per cycle. The crack length was measured with the aid of a high-speed video camera and video recorder. The crack growth per cycle, dc/dn, was then plotted as a function of tearing energy on a double logarithm plot.

6-2-2. Cyclic crack growth measurement under pre-strain

The procedures for preparing specimens for cyclic crack growth measurement under pre-strain were the same as those described in section 5-2-2. Rubber strips were cut from flat sheets to the following dimensions, 250mm in width, 30-40 mm in height, and 1-2 mm in thickness. They were then clamped and stretched in the long direction with a sliding rectangular frame (figure 5-4). The strip of pre-strained rubber was then gripped along its free long edges with the pure shear grips. The pre-strained test piece was then extracted from the frame by cutting at the pure shear grip ends. The pre-strain remained applied due to the constraint of the grips, except in the vicinity of the edges. The state of strain in such a test piece is substantially uniform homogeneous pre-strained pure shear. An initial horizontal cut of 40 mm length was then introduced on the central axis at one edge of the test piece using a razor blade. The tip was hence far enough from the edge to avoid edge effects.

For this pre-strained pure shear test specimen, the tearing energy, T, is given by following equation[92][95].

$$T = W_s l_o' \sqrt{\lambda_2} \tag{6-3}$$

where W_s is the elastic stored energy density in the pre-strained specimen resulting from the extension λ_1, λ_2 is the extension ratio of the pre-strain and l_o' is the unstrained height after pre-strain. The magnitude of the elastic stored energy density under pre-strain, W_s, was calculated from force-deflection curve plotted with a X-Y plotter by integration of the curve and by dividing by the volume of the specimen. The specimen dimensions after pre-strain were used to calculate the extension ratio and the volume of the specimen. The force-deflection curve was measured after the first one hundred cycles at each strain amplitude to allow for any cyclic stress softening effects. This force-deflection curve was measured at the appropriate frequency up to an imposed frequency of 1.0Hz. For an imposed frequency of a over 1.0Hz, T was calculated using the 1.0Hz force-deflection curve to avoid difficulties resulting from the slow electrical response time of the system.

The crack growth per cycle was measured over a wide range of frequency with the aid of a high-speed video camera and video recorder. The crack length was determined with respect to the non pre-strained ($\lambda_1=\lambda_2=1$) specimen dimensions. The initial rapid crack growth per cycle due to the initial sharp crack introduced by the razor blade was neglected in the crack growth measurement. The crack growth per cycle, dc/dn, was then plotted as a function of tearing energy on a double logarithm plot.

6-2-3. *Calculation of the contribution of the time dependent component during cyclic crack growth*

The experimentally measured crack growth per cycle, dc/dn, can be regarded as the sum of two different components; the time dependent component, $(\mathrm{d}c/\mathrm{d}n)_{\text{-time}}$, and the cyclic component, $(\mathrm{d}c/\mathrm{d}n)_{\text{-cycle}}$, as

$$\frac{\mathrm{d}c}{\mathrm{d}n} = \left(\frac{\mathrm{d}c}{\mathrm{d}n}\right)_{\text{-time}} + \left(\frac{\mathrm{d}c}{\mathrm{d}n}\right)_{\text{-cycle}} \tag{6-1}$$

This implies that $(\mathrm{d}c/\mathrm{d}n)_{\text{-time}}$ and $(\mathrm{d}c/\mathrm{d}n)_{\text{-cycle}}$ are independent processes that take place in parallel and make independent contributions to $(\mathrm{d}c/\mathrm{d}n)_{\text{-total}}$. This may not be strictly true but the concept is a useful one, as the current work will illustrate. The

time dependent element of crack growth per cycle, $(dc/dn)_{-time}$, can be determined mathematically by utilising the static, constant T, crack growth measurement using the following procedure. From the plot of the force-time relationship during cyclic loading [figure 6-1a], the tearing energy versus time relationship [figure 6-1b] is calculated

$$T = f(t) \tag{6-4}$$

From the static crack growth measurements (chapter 5), we have the crack growth rate, dc/dt, as a function of tearing energy given as

$$\frac{dc}{dt} = B_S\left(\frac{T}{T_u}\right)^{\beta_S} \tag{6-5}$$

where B_S and β_S are the static crack growth constants and T_u=1.0 J.m^{-2} and is included to make T/T_u dimensionless. Substituting equation (6-4) into (6-5) we have

$$\frac{dc}{dt} = B_S(f(t))^{\beta_S} \tag{6-6}$$

Therefore the increment of crack growth per cycle, Δc, and hence $(dc/dn)_{-time}$, will be given by integrating equation (6-6) as

$$\Delta c = \int_0^{t_1} B_S(f(t))^{\beta_S}\, dt = \left(\frac{dc}{dn}\right)_{-time} \tag{6-7}$$

where t_1 is the time period of one cycle [figure 6-1c], equivalent to the reciprocal of the frequency, for the appropriate frequency. Finally, we can deduce the residual element of cyclic crack growth, $(dc/dn)_{-cycle}$, using equation (6-1).

6-2-4. Mechanical hysteresis measurement under cyclic deformation

The magnitude of the mechanical hysteresis was measured utilising the pure shear test piece and an INSTRON type tensile testing machine. Both loading and unloading stress-strain curves were determined using an X-Y plotter and extension rates of 0.416, 4.16 and 41.6%.s^{-1}. The magnitude of the elastic stored energy density, W_{-load}, was calculated by integrating the obtained loading stress-strain curve. The magnitude of the elastic stored energy density with respect to the unloading

curve, $W_{-unload}$, was calculated by similarly integrating the obtained unloading stress-strain curve. The hysteresis energy density, $W_{-hysteresis}$, was determined from the obtained W_{-load} and $W_{-unload}$ as

$$W_{-hysteresis} = W_{-load} - W_{-unload} \tag{6-8}$$

For these measurements, all the stress-strain curves utilised were recorded after 20 cycles at each testing condition as the first few cycle exhibit a large Mullin's cyclic stress softening effect.

6-3. *Results and discussion*

6-3-1. *The effect of the nature of the rubber on cyclic crack growth behaviour*

While the main aim of this chapter was to study cyclic crack growth in SBR, for comparison purposes, the effect of the nature of the rubber on dc/dn was determined for unfilled NR (NR00-S1), SBR (SBR00-S3) and IR (IR00-S1) at a single frequency of 5.0Hz. The results are presented as a double logarithmic plot of dc/dn as a function of the maximum tearing energy during a cycle, T/T_u, as shown in figure 6-2. The crack growth behaviour in region III (see figure 2-33) can be written generally as

$$\log\left(\frac{dc}{dn}\right) = \beta \log\left(\frac{T}{T_u}\right) + \log B \tag{6-9}$$

where β is the slope, log B is the intercept on the Y-axis and both are referred to as material crack growth constants. The magnitudes of β and log B for these materials are shown in table 6-1. The experimentally obtained values for β and B for NR and IR were slightly different, but considering the possible experimental scatter[52], the crack growth behaviour for NR and IR can be considered roughly the same. This result was expected as IR is a synthetic rubber equivalent to NR with almost the same structure, 94 to 98% of cis-1.4 poly-isoprene. Furthermore, as the observed physical properties, such as the stress-strain behaviour and the dynamic mechanical properties measured in Chapter 3 were approximately the same, similar cyclic crack growth behaviour would be expected. SBR showed a higher crack growth per cycle

compared to NR and IR over a wide range of tearing energy. Even though the internal viscosity of SBR would be larger than for NR and IR, hence more energy would dissipated at the crack tip, it showed rapid cyclic crack growth sometimes nearly two orders of magnitude faster at higher tearing energies. This is considered to relate to the strengthening due to the significant effect of strain crystallisation in NR and IR.

The observed fracture surfaces for all these materials at all applied tearing energies were rough. Although the observed surface roughness seems to decrease slightly with increasing applied maximum tearing energy during a cycle and/or increasing crack growth per cycle, no significant change in the extent of surface roughness was observed.

6-3-2. The effect of swelling on cyclic crack growth behaviour

As was discussed in chapter 5, the magnitude of the tearing energy is largely associated with the visco-elastic losses at the crack tip as a crack propagates. Swelling rubber with a low molar mass liquid reduces the visco-elastic losses[21][22][64][87], hence a large effect of swelling on cyclic crack growth behaviour can be expected as was observed for the static crack growth behaviour in chapter 5. This behaviour was investigated for unfilled NR (NR00-S1) and SBR (SBR00-S3) at a cyclic frequency of 5.0Hz. Dibutyl Adipate (DBA) was employed as the swelling liquid as it swells rubber to a large extent. The results are illustrated in figures 6-3 and 6-4 and the values of the crack growth constants, B and β, from region III, are given in table 6-2. With decreasing volume fraction of rubber (with increasing extent of swelling) dc/dn, at a given value of T, increased as the visco-elastic losses decreased. This implied that the visco-elastic losses were one of the major factors in determining cyclic crack growth behaviour as observed for the static crack growth measurement. The magnitude of the slope β did not change significantly with decreasing V_r for unfilled NR, but increased slightly with decreasing V_r for unfilled SBR. The swelling effect was much greater for unfilled SBR than for unfilled NR. In the case of unfilled NR, dc/dn, at a given tearing energy, increased approximately one order of magnitude with increasing extent of swelling up to the equilibrium state (V_r=0.41). However, in the case of the unfilled SBR, dc/dn at a given tearing energy

increased by more than four orders of magnitude under the same circumstances. This difference must depend on the extent to which d*c*/d*n* is governed by the visco-elastic losses at the crack tip. This effect would be expected to be greater for SBR, while in the case of NR strain crystallisation at the crack tip would be expected to play a significant role probably even for the highly swollen material.

For both NR and SBR, the extent of fracture surface roughness at a given crack growth per cycle seemed to increase slightly with increasing extent of swelling. This tendency agreed well with the tendency observed in the static, constant *T*, crack growth measurement as the visco-elastic losses, and hence the effective elastic modulus, decreased resulting in the cavitation process occurring more easily, especially for the unfilled SBR.

6-3-3. Contribution of the two different components to the overall cyclic crack growth behaviour

6-3-3-1. Unfilled SBR (SBR00-S3)

The static, constant *T*, crack growth rate data, d*c*/d*t*, as a function of tearing energy, *T*, for unfilled/unswollen SBR (SBR00-S3) as determined in chapter 5 is re-plotted in figure 6-5. As was discussed in the previous chapter, the d*c*/d*t* vs. *T* relationship can be divided into three regions, slow, fast and the stick-slip region. In the stick-slip region, cracks grow by both the slow and the fast crack growth processes. The crack growth rates plotted in the stick-slip region consisted of the averages of these observed increments of slow and fast crack growth. The calculated static crack growth constants, B_S and β_S, for the slow and the fast crack growth regions are tabulated in table 6-3. The time dependent component of crack growth per cycle, $(dc/dn)_{time}$, for each frequency was calculated using these values from the slow crack growth region and equation (6-7).

The cyclic crack growth results are illustrated in figure 6-6 and the values of the crack growth constants, *B* and β, for each frequency are given in table 6-4. Clearly a significant frequency effect was observed. $(dc/dn)_{total}$ increased with decreasing frequency for large values of the tearing energy. At very low values of tearing energy there was no frequency effect. As a result of this frequency effect, the

obtained slope, the magnitude of β, increased with decreasing frequency. At higher values of $(dc/dn)_{-total}$, the extent of the observed fracture surface roughness seemed to increase slightly with decreasing applied cyclic frequency as the tearing energy necessary to drive a crack at given $(dc/dn)_{-total}$ decreased corresponding with the result obtained in chapter 5. However, this variation in surface was very small in this crack growth region. Utilising the static crack growth constants from the slow crack growth region, $(dc/dn)_{-time}$ values are also plotted as dashed lines in figure 6-6. It was clear that the values of $(dc/dn)_{-total}$ asymptote to the value of $(dc/dn)_{-time}$ at high values of T and low cyclic frequencies. Utilising the data in figure 6-6 the crack growth per cycle as a function of the inverse of frequency ($1/f$) at different tearing energies was calculated as illustrated in figure 6-7 for both $(dc/dn)_{-total}$ and $(dc/dn)_{-time}$. As the waveform was independent of cyclic frequency, then on such a plot, if cyclic crack growth were dominated by the time dependent component $(dc/dn)_{-time}$, then $(dc/dn)_{-total}$ would be proportional to $1/f$. At the largest tearing energy (log $(T/J.m^{-2})=3.3$) and the fastest crack growth per cycle, the experimentally determined values of $(dc/dn)_{-total}$ did agree very well with the calculated values of $(dc/dn)_{-time}$. Clearly, under these circumstances cyclic crack growth was dominated by the time dependent component. At the lowest tearing energy (log $(T/J.m^{-2})=2.2$) and at the slowest crack growth per cycle, at most frequencies, the experimentally determined values of $(dc/dn)_{-total}$ were frequency independent and they were always greater than the calculated values of $(dc/dn)_{-time}$. Clearly, under these circumstances crack growth was dominated by the cyclic component. At intermediate regions of tearing energy, frequency, and crack growth per cycle, both components contributed to the overall cyclic crack growth behaviour.

The cyclic crack growth component, $(dc/dn)_{-cycle}$, can be calculated using equation (6-1). These calculated values of $(dc/dn)_{-cycle}$ and $(dc/dn)_{-time}$ as a function of maximum tearing energy during a cycle are illustrated in figure 6-8 for a cyclic frequency of 5.0Hz. Clearly under these circumstances $(dc/dn)_{-cycle}$ was much greater than $(dc/dn)_{-time}$. This supports the contention that cyclic component dominates the cyclic crack growth at the lower values of T and crack growth per cycle.

To demonstrate that the effect of the magnitude of the tearing energy and of the cyclic crack growth per cycle was significant in determining the relative contributions of time and cyclic dependent components to the overall cyclic crack

growth per cycle, the data in figure 6-6 was extended to higher tearing energies at a frequency of 5.0Hz. Under these circumstances it would be expected that cyclic crack growth would become dominated by the time dependent component. The situation was however likely to be complicated as at higher values of T, as illustrated in figure 6-5, the static crack growth mechanism changes from that of the slow to that of the fast region via a stick-slip region. Nevertheless measurements were made and added to those already presented in figure 6-6, as figure 6-9. A clear transition from slow to fast crack growth was observed, via a stick-slip region, in which cracks grew by either the fast or slow process. In the stick-slip region, the measured fast, slow and average values of crack growth per cycle are plotted. As was observed for the static, constant T, crack growth measurement, a drastic change in surface roughness was observed between the slow and fast crack growth regions for these cyclic measurements. A rough surface was observed in the slow crack growth region and a relatively smooth surface was observed in the fast crack growth region. Also plotted on figure 6-9 are two dotted lines, representing the calculated $(dc/dn)_{\text{-time}}$ data determined using the B_s and β_s values from the slow and fast static crack growth regions as illustrated in figure 6-5. Clearly at the highest tearing energies the agreement between the fast cyclic crack growth $(dc/dn)_{\text{-total}}$ and the $(dc/dn)_{\text{-time}}$ values calculated from the static fast crack growth rate data was excellent. This agreement was further illustrated by the agreement between the calculated and measured incremental crack growth rates, dc/dt, at various points during a cycle as illustrated in figure 6-10. Furthermore, at these high tearing energies, the agreement between the slow crack growth component of $(dc/dn)_{\text{-total}}$ with the values calculated from the static slow crack growth data, $(dc/dn)_{\text{-time}}$, was not unreasonable. This supports the contention that at high tearing energies and fast crack growth per cycle, cyclic crack growth is dominated by the time dependent component, whether cracks grow by the slow or fast process. Clearly changes in the crack tip profile, maybe as a result of cavitation, have not significantly affected this behaviour.

What is not clear, however, is why cyclic crack growth in unfilled SBR is dominated by the time dependent component at high values of T and at fast crack growth per cycle and is dominated by the cyclic component at low values of T and at slow crack growth per cycle. Clearly at low values of T increments of crack growth result from continuously loading and unloading the specimens. This crack growth

would not be observed in static tests, as the specimens are not unloaded. The question is then what happens on unloading to allow additional crack growth on reloading? Although SBR does not crystallise, it may be that an element of strain crystallisation of the butadiene component occurs in the very high strain region at the crack tip, even if this element is two dimensional and more akin to minute liquid crystals rather than to an ordered 3-D molecular array. This would form on specimen extension tending to halt or reduce crack growth to the value expected from the time dependent component. These quasi crystals would melt on unloading providing an opportunity for additional crack growth, each cycle, in the time interval before the quasi crystals reformed. At large tearing energies, at fast crack growth per cycle, no time would be available to form the quasi crystals ahead of the crack tip and hence no additional crack growth would be obtained on reloading. Hence, at these tearing energies cyclic crack growth would be dominated by the time dependent component.

6-3-3-2. Unfilled SBR (SBR00-S3) swollen by DBA

In the previous section, it was clear that cyclic crack growth was dominated by the time dependent component at high T values and/or low frequencies and dominated by the cyclic component at low T values and/or high frequencies. These effects were possibly associated with the large strain hysteresis/energy loss at the crack tip due to quasi crystallisation and/or due to normal viscous molecular behaviour in SBR. Swelling SBR with a low molar mass liquid is likely to affect both processes and hence to alter the regime of T and frequency in which cyclic crack growth is dominated by $(dc/dn)_{\text{-time}}$ or $(dc/dn)_{\text{-cycle}}$.

It was for this reason that the effect of frequency on an unfilled SBR (SBR00-S3) swollen with DBA to V_r=0.38 was studied. The results are illustrated in figure 6-11 for the frequency range 0.01 to 5.00Hz. Also plotted on the figure, as dotted lines, are the calculated values of $(dc/dn)_{\text{-time}}$. These values were obtained by utilising the static crack growth data, determined from static crack growth measurement as presented in chapter 5 and re-illustrated here in figure 6-12. The static crack growth constants obtained from this figure are given in table 6-5. These values were used in equation (6-7) to obtain the $(dc/dn)_{\text{-time}}$ values plotted in figure 6-11. The $(dc/dn)_{\text{-total}}$ data in figure 6-11 was seen to have moved to a regime of much lower T but faster

crack growth per cycle when compared to the data for the unswollen material in figure 6-6. Clearly the tearing energy necessary to drive a crack at a given dc/dn has been greatly reduced presumably as a result of energy losses at the crack tip having been reduced. There was excellent agreement between $(dc/dn)_{\text{-time}}$ and $(dc/dn)_{\text{-total}}$ suggesting that time dependent crack growth dominated the cyclic crack growth over the whole of this regime of T, frequency, and dc/dn. This was further illustrated by re-plotting the data as log dc/dn versus log f^{-1} in figure 6-13 where dc/dn was seen to clearly be proportional to f^{-1} as would be expected for time dependent crack growth.

The incremental crack growth rate, dc/dt, at the maximum tearing energy of 343J.m^{-2} and at a cyclic frequency of 5.0Hz was measured utilising the high-speed video camera and video recorder and the results are illustrated in figure 6-14. The dc/dt values calculated using the static crack growth constants are also superimposed on the figure. The excellent agreement between the two showed that cyclic crack growth was dominated by the time dependent component even at the highest frequency.

In this highly swollen material time dependent crack growth was very much faster, for a given value of T, than in the unswollen material. In fact, even in the regime where the cyclic crack growth component was dominant in the unswollen material, time dependent crack growth produced a much larger dc/dn in the swollen material. Swelling drastically reduces the molecular viscous losses at the crack tip and hence reduces the T values necessary to drive a crack at a given dc/dn. This regime of relatively fast crack growth existed in the swollen material, down to the value of threshold tearing energy T_o. In this regime of very low viscous losses, cyclic crack growth is solely time dependent with no cyclic component. A cyclic component due to quasi crystallisation will not occur as crystallisation in this highly swollen material would not be energetically favourable due the large work of un-mixing required to exclude the swelling liquid from the crystals.

6-3-3-3. Carbon black 50 phr filled SBR (SBR50-S1)

It was demonstrated in section 6-3-3-1 and 6-3-3-2 that cyclic crack growth was dominated by the time dependent component $(dc/dn)_{\text{-time}}$ in swollen SBR and in unswollen SBR at high values of T and at fast crack growth per cycle. This lead to a

significant effect of cyclic frequency on the total crack growth per cycle $(dc/dn)_{-total}$. It has been suggested that such a frequency effect is likely to be much less significant in carbon black filled SBR[45]. Furthermore the static crack growth data for 50phr carbon black filled SBR (SBR50-S1) (re-plotted in figure 6-15) showed a discontinuity in the dc/dt vs. T relationship, at log $(T/J.m^{-2})=4.0$, yielding two sets of crack growth constants (table 6-6) for the two crack growth regions. It was suggested that the development of strength anisotropy ahead of the crack tip dominated crack growth in the slow crack growth region-A but that this effect was absent during fast crack growth in region-C. To study these effects during cyclic crack growth, a range of frequencies was utilised.

The resulting data is shown in figure 6-16 as a plot of the total crack growth per cycle, $(dc/dn)_{-total}$, versus tearing energy. The data tends to be scattered but up to a tearing energy of log $(T/J.m^{-2})=4.0$ no significant effect of frequency was observed. This was in marked contrast to the data for unfilled SBR, which is superimposed on figure 6-16 showing a large frequency effect. Although smooth fracture surfaces were observed for the static, constant T, crack growth measurement, even in the slow crack growth region, the observed fracture surfaces produced by cyclic crack growth were now rough even in the slow crack growth region. This insensitivity to cyclic frequency is further illustrated by the plot of log $(dc/dn)_{-total}$ versus log f^{-1} in figure 6-17. Also superimposed on figure 6-16 are the frequency dependent values of $(dc/dn)_{-time}$ calculated using the crack growth constants from the slow crack growth region of figure 6-15. These values of $(dc/dn)_{-time}$ were clearly much less than $(dc/dn)_{-total}$, in this region and will lead to large dominant values of $(dc/dn)_{-cycle}$ as shown in figure 6-18 for the 5.0Hz data. The addition of carbon black increased the energy loss/hysteresis at the crack tip and lead to the development of strength anisotropy. It was these effects, which caused the decrease in the static crack growth rate and which in turn caused the large decrease in the calculated values of $(dc/dn)_{-time}$. However, in this slow crack growth region the cyclic component $(dc/dn)_{-cycle}$ clearly dominated cyclic crack growth. This component of crack growth resulted from unloading/reloading the specimens and was independent of time. It may be that the strength anisotropy, which develops ahead of the crack tip is, at least in part, reversible. Hence, it reduces on unloading and allows an increment of crack growth to occur upon reloading before it has fully redeveloped. This would result in time and frequency independent crack growth occurring as observed.

At tearing energies around the discontinuity in the dc/dt versus T static crack growth data, there was a similar change in the cyclic dc/dn versus T data. This is illustrated in figure 6-19 on which are now superimposed the $(dc/dn)_{\text{-time}}$ values calculated using the fast crack growth rate constants from region-C in figure 6-15. There was a suggestion of a frequency effect in this region. However at 5.0Hz, the calculated $(dc/dn)_{\text{-time}}$ was always less than $(dc/dn)_{\text{-total}}$. Furthermore, as illustrated in figure 6-20, at the highest tearing energy, T=20.4 kJ.m^{-2}, the incremental dc/dt values measured using a high-speed video camera and video recorder, were always greater than the values calculated using the static crack growth constants (figure 6-15). The equivalent figure for the unfilled SBR showed very similar rates at the highest tearing energy (figure 6-10). Hence, while for unfilled SBR, cyclic crack growth was dominated by the time dependent component $(dc/dn)_{\text{-time}}$ at the highest energies and crack growth per cycle, this was not the case for filled SBR. In fact the slope of the log dc/dn versus log T plot (figure 6-19) for a frequency of 5.0Hz was very similar in both regions suggesting that the change between regions was a discontinuous change in crack tip profile, with the sharper faster growing crack being associated with region-C. In fact, while a rough surface was observed in the slow crack growth region, a relatively smooth fracture surface was observed in the fast crack growth region. This change in surface roughness clearly supported the above contention.

It is suggested here that the frequency independent cyclic crack growth behaviour observed in figure 6-16 for carbon black filled SBR at the low tearing energies is associated with the extent of development of strength anisotropy each cycle. As it was shown in chapter 5 that pre-strain had a significant effect on the development of orientation/strength anisotropy it was decide here to study cyclic crack growth in 50phr carbon black filled SBR under 100% pre-strain (λ_2=2). The results are given in figure 6-21 together with a line representing the results for the non pre-strained material. Clearly pre-strain increased $(dc/dn)_{\text{-total}}$ for a given tearing energy, particularly at the lowest tearing energies. This presumably resulted from a reduction in the development of strength anisotropy and resulting crack tip deviation, the relative magnitude of which would be greatest at the lowest applied tearing energy. In addition, however, there was clearly now a significant frequency effect, which was absent in the non pre-strained material. The measured $(dc/dn)_{\text{-total}}$, at the different frequencies, are compared in figure 6-21 with the $(dc/dn)_{\text{-time}}$ values

calculated using the measured static crack growth constants for the pre-strained material of log (B_s/m.s^{-1})=-29.94 and β_s=6.520. The $(dc/dn)_{-total}$ values were clearly much faster suggesting that simple time dependent crack growth was not responsible for the frequency effect observed in figure 6-20. Further support was given to this suggestion by the fact that the dependencies of $(dc/dn)_{-total}$ and $(dc/dn)_{-time}$ on T were clearly very different. It may be that the frequency effect observed for the pre-strained material is associated with the effect of time/strain rate on the extent of development and/or disassembly of strength anisotropy during a cycle. Put simplistically it may be that at slow crack growth per cycle more strength anisotropy is lost during unloading resulting in a large crack growth increment per cycle upon reloading, before strength anisotropy redevelops. In non pre-strained samples strength anisotropy may develop so rapidly that this effect is not observed.

During crack growth in filled or unfilled SBR it is the high strain energy loss/hysteresis in the crack tip region which determines the magnitude of the tearing energy necessary to drive a crack. The total energy loss is the product of the energy loss per volume times the volume of highly strained material at the crack tip. However, any time/strain rate dependence of crack growth is likely to result from the strain rate dependence of high strain energy loss/hysteresis. In order to investigate this, cyclic stress strain curves were measured at these different strain rates for filled and unfilled SBR. From these the energy loss/hysteresis energy densities (W_h) were calculated from the areas within the loops and the total elastic stored energy densities (W_{-load}) from the area under the stress strain curves. These results are plotted in figures 6-22(a) and 6-22(b) for the filled and unfilled SBR as a function of increasing stored energy density or increasing cyclic stress. At the highest stresses (corresponding to the highest strains) the energy loss increased with increasing strain rate for the unfilled material. This effect would lead to a time dependent component of cyclic crack growth with the crack growth rate increasing for a given tearing energy, with decreasing frequency. For the filled material, at the highest stress or strain, the energy loss was much less sensitive to the strain rate. The slope of the lines was such that it was likely that at strains near break the energy loss would be strain rate independent. This would lead to a frequency independent cyclic crack growth per cycle as was observed.

6-4. Summary and conclusions

(1) It has been possible to determine the magnitudes of the two different components, time dependent and cyclic crack growth components, which govern cyclic crack growth behaviour, in SBR, by utilising the crack growth constants from static crack growth measurement and by the measurement of the effect of frequency on cyclic crack growth behaviour.

(2) For unfilled SBR, at the highest tearing energies for the fastest crack growth per cycle, total cyclic crack growth is dominated by the time dependent component. At low tearing energies for slow crack growth rates, total cyclic crack growth is dominated by the cyclic component and is frequency independent. It may be that the cyclic component is associated with quasi strain crystallisation of the butadiene component of SBR.

(3) For highly swollen SBR cyclic crack growth is totally dominated by the time dependent component and the total cyclic crack growth per cycle is proportional to the reciprocal of the cyclic frequency. It is presumed that quasi strain crystallisation is not energetically favoured in this highly swollen system.

(4) The crack growth per cycle is independent of cyclic frequency for the 50phr carbon black filled SBR. Crack growth is dominated by the cyclic component. This probably results from the cyclic formation/disassembly of strength anisotropy at the crack tip.

(5) For the carbon black filled SBR pre-strained 100% a cyclic effect is observed, with the total cyclic crack growth increasing with decreasing cyclic frequency. This apparent time dependent component probably results from the effect of time/strain rate on the extent of development and/or disassembly of strength anisotropy at the crack tip during a cycle.

Table 6-1. The magnitudes of measured β and log B for unfilled materials.

	NR00-S1	SBR00-S3	IR00-S1
β	2.25	3.48	1.61
Log (B / m)	-14.44	-16.60	-12.56

Table 6-2. The magnitudes of measured β and log B for different volume fractions of rubber for NR00-S1 and SBR00-S3.

	V_r	Log (B / m)	β
NR00-S1	1.00	-14.44	2.28
	0.72	-13.55	2.15
	0.41	-13.04	2.17
SBR00-S3	1.00	-14.80	2.93
	0.75	-15.06	4.04
	0.42	-13.22	4.22

Table 6-3. The measured static crack growth constants β_S and log B_S for each region for SBR (SBR00-S3).

region	Log (B_S / m.s^{-1})	β_S
slow	-18.13	5.23
fast	-8.30	2.14

Table 6-4. The magnitudes of β and log B measured at different frequencies for SBR (SBR00-S3).

Frequency	Log (B / m)	β
5.00 Hz	-15.45	3.15
1.00 Hz	-16.17	3.49
0.20 Hz	-17.43	4.05
0.03 Hz	-19.43	4.94
0.01 Hz	-20.94	5.65

Table 6-5. The measured static crack growth constants β_S and log B_S for each region for SBR (SBR00-S3) swollen to V_r=0.38.

region	Log (B_S / m.s^{-1})	β_S
slow	-1.19	4.20

Table 6-6. The measured static crack growth constants β_S and log B_S for each region for 50phr carbon black filled SBR (SBR50-S1).

region	Log (B_S / m.s^{-1})	β_S
slow	-33.15	6.94
fast	-10.90	2.34

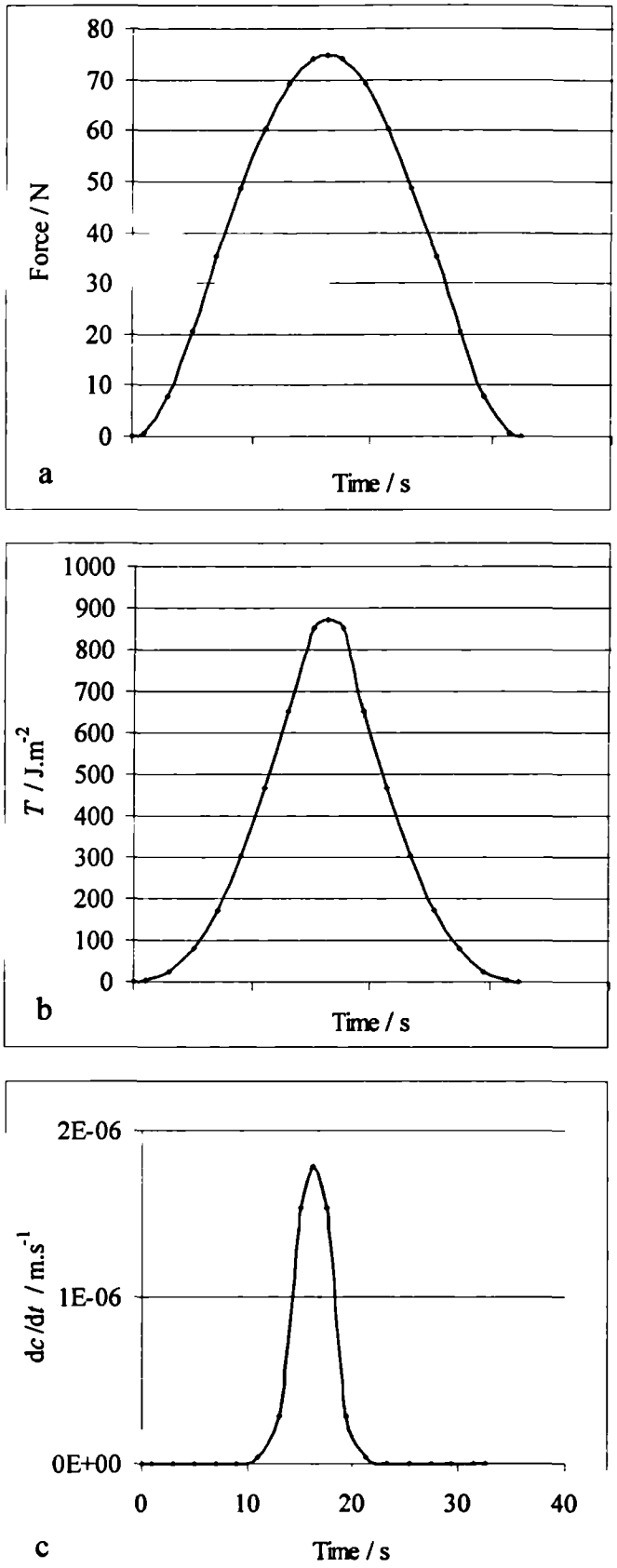

Figure 6-1. Schematic diagrams for the mathematical calculation to determine the element of time dependent crack growth per cycle, $(dc\ dn)_{\text{-time}}$.

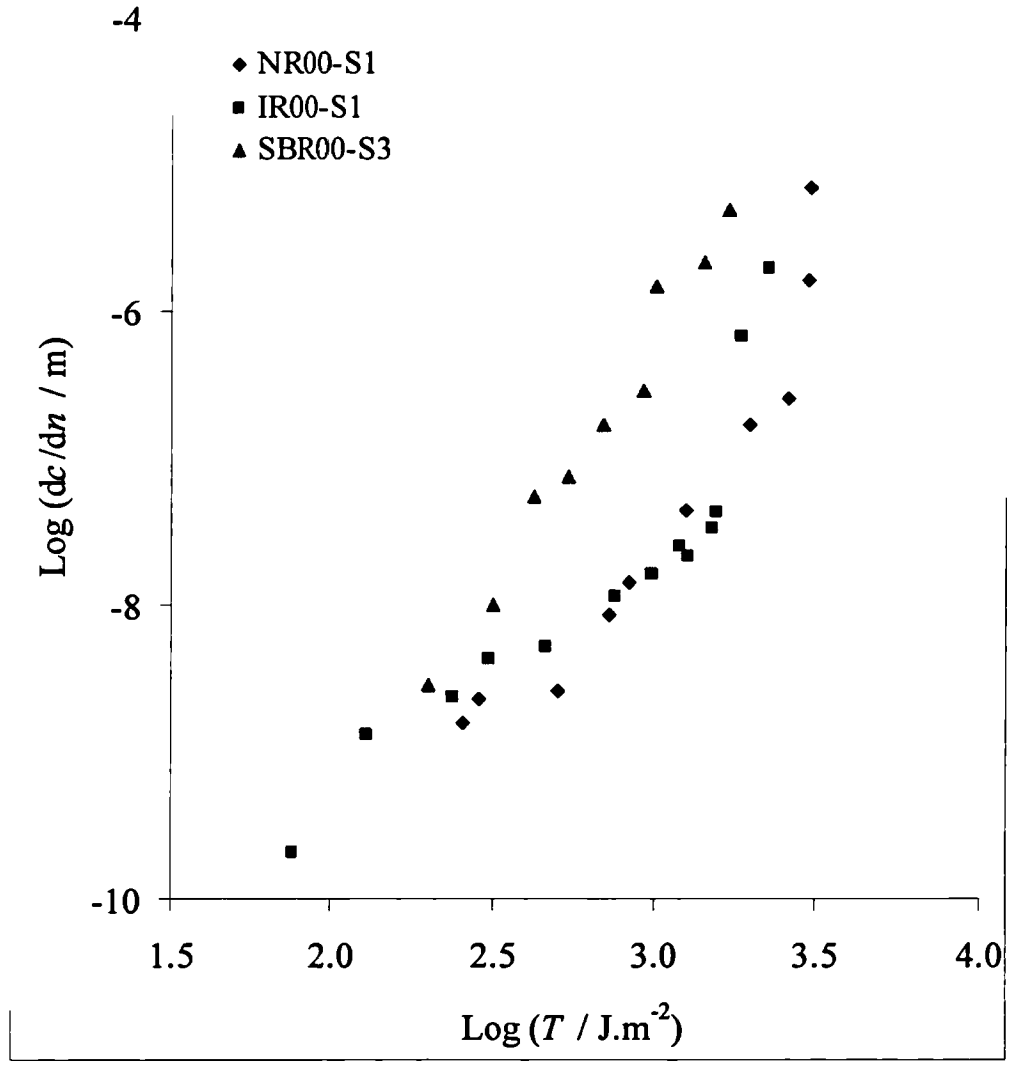

Figure 6-2. Crack growth per cycle, d*c*/d*n*, as a function of maximum tearing energy during a cycle, *T*, for unfilled materials.

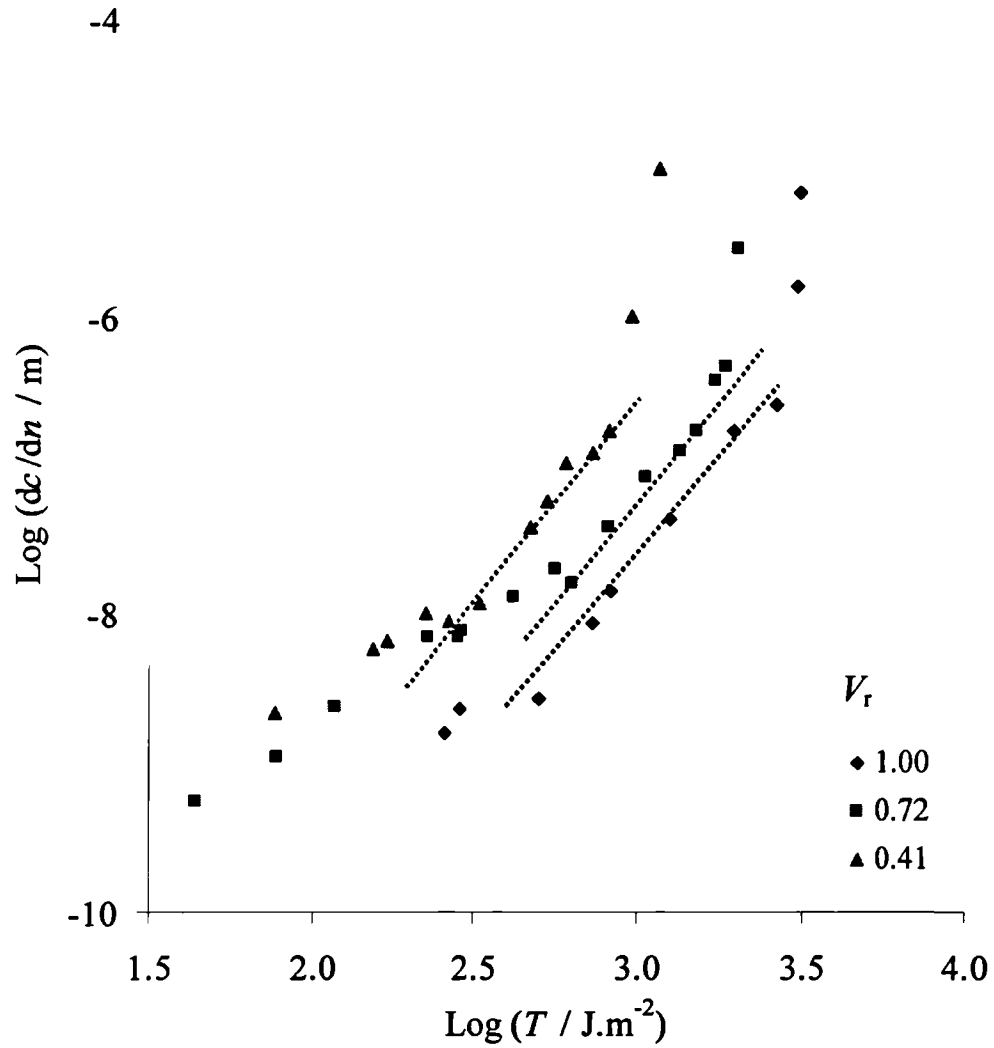

Figure 6-3 Effect of swelling on crack growth per cycle, d*c* d*n*, as a function of maximum tearing energy during a cycle, *T*, for NR (NR00-S1).

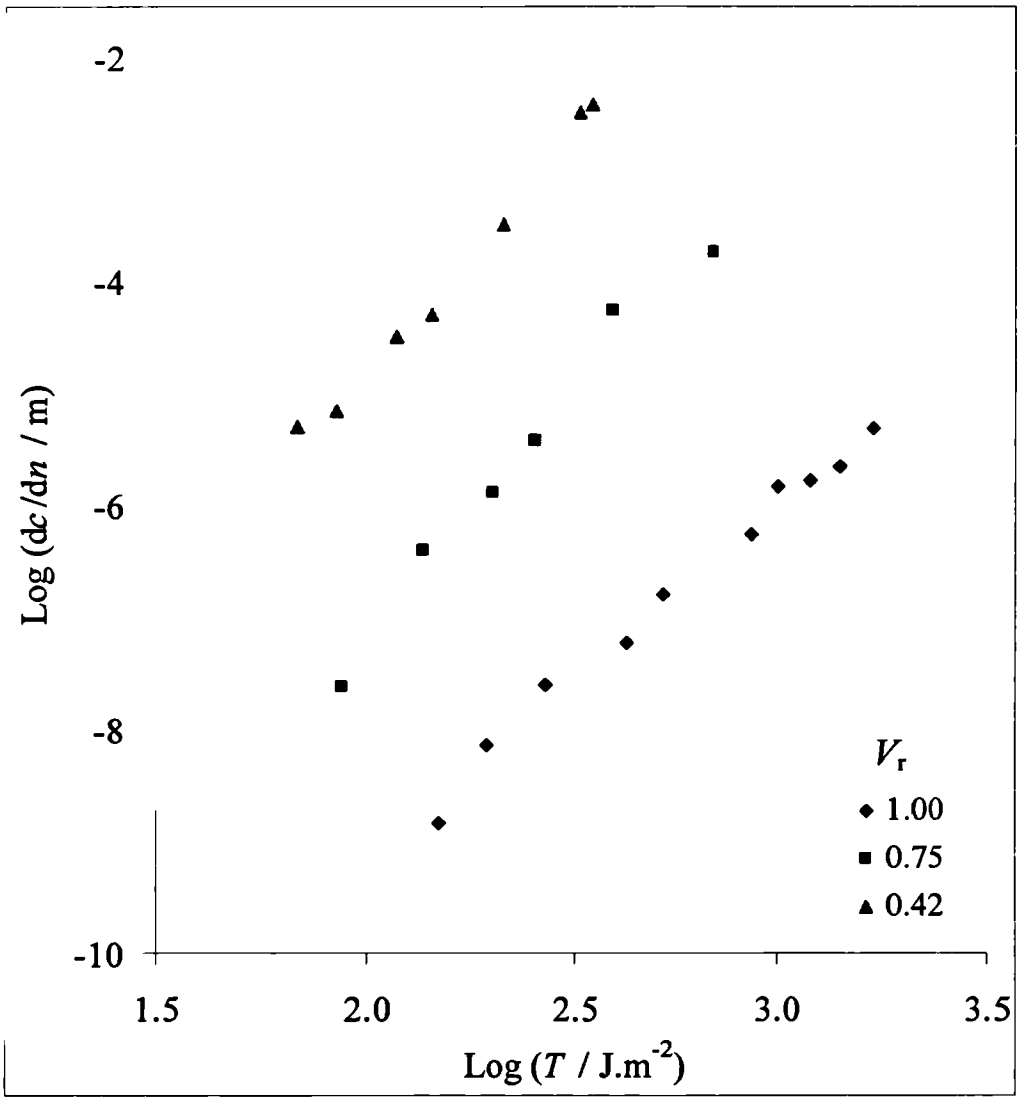

Figure 6-4. Effect of swelling on crack growth per cycle, d*c*/d*n*, as a function of maximum tearing energy during a cycle, *T*, for SBR (SBR00-S3).

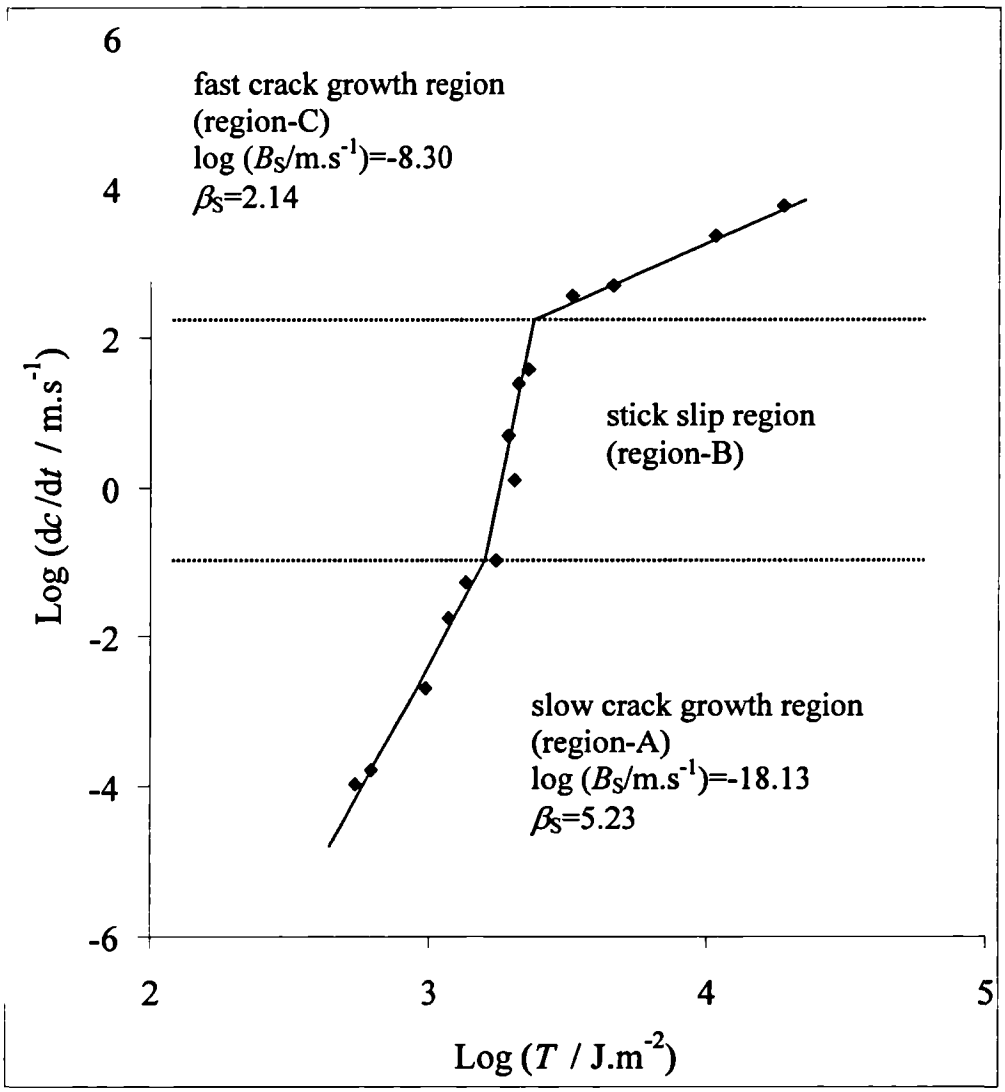

Figure 6-5. The static crack growth rate, dc/dt, as a function of tearing energy, T for SBR (SBR00-S3).

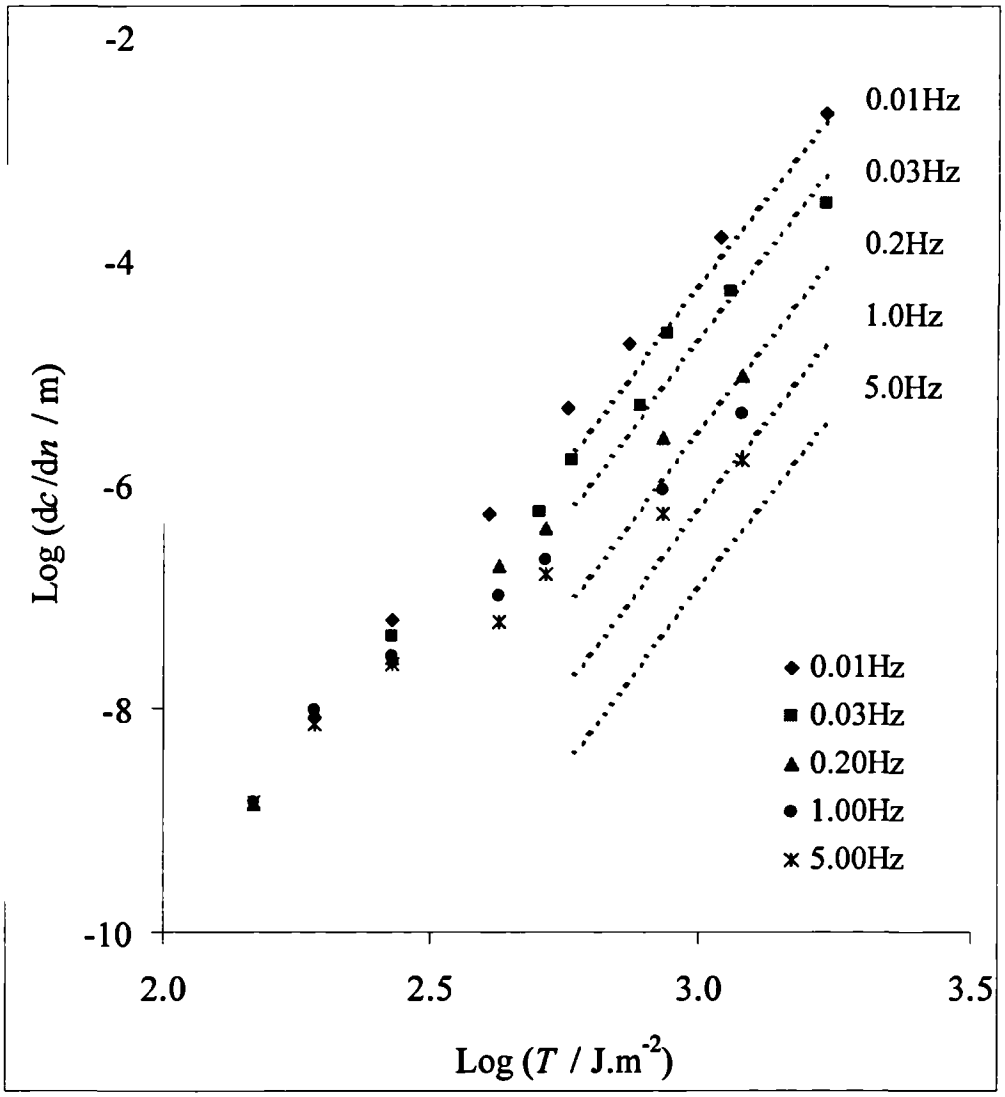

Figure 6-6. The effect of frequency on the total cyclic crack growth per cycle, $(dc/dn)_{-total}$, as a function of maximum tearing energy during a cycle, T, for SBR (SBR00-S3). The calculated values of $(dc/dn)_{-time}$ obtained using equation (6-7) for each frequency are superimposed as dashed lines.

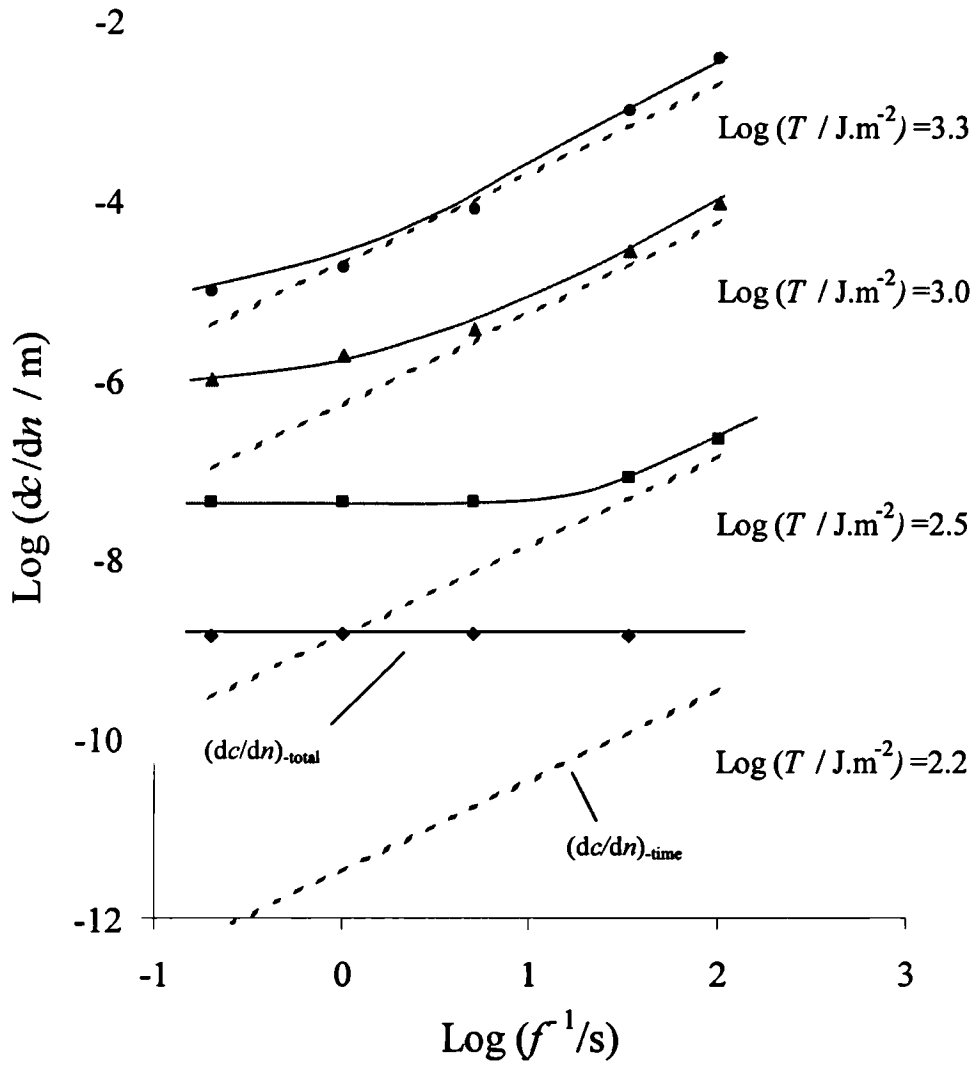

Figure 6-7. The total crack growth per cycle, $(dc/dn)_{-total}$, as a function of the inverse of the frequency at different tearing energies for SBR (SBR00-S3). The calculated values of $(dc/dn)_{-time}$ obtained using equation (6-7) are superimposed as dashed lines.

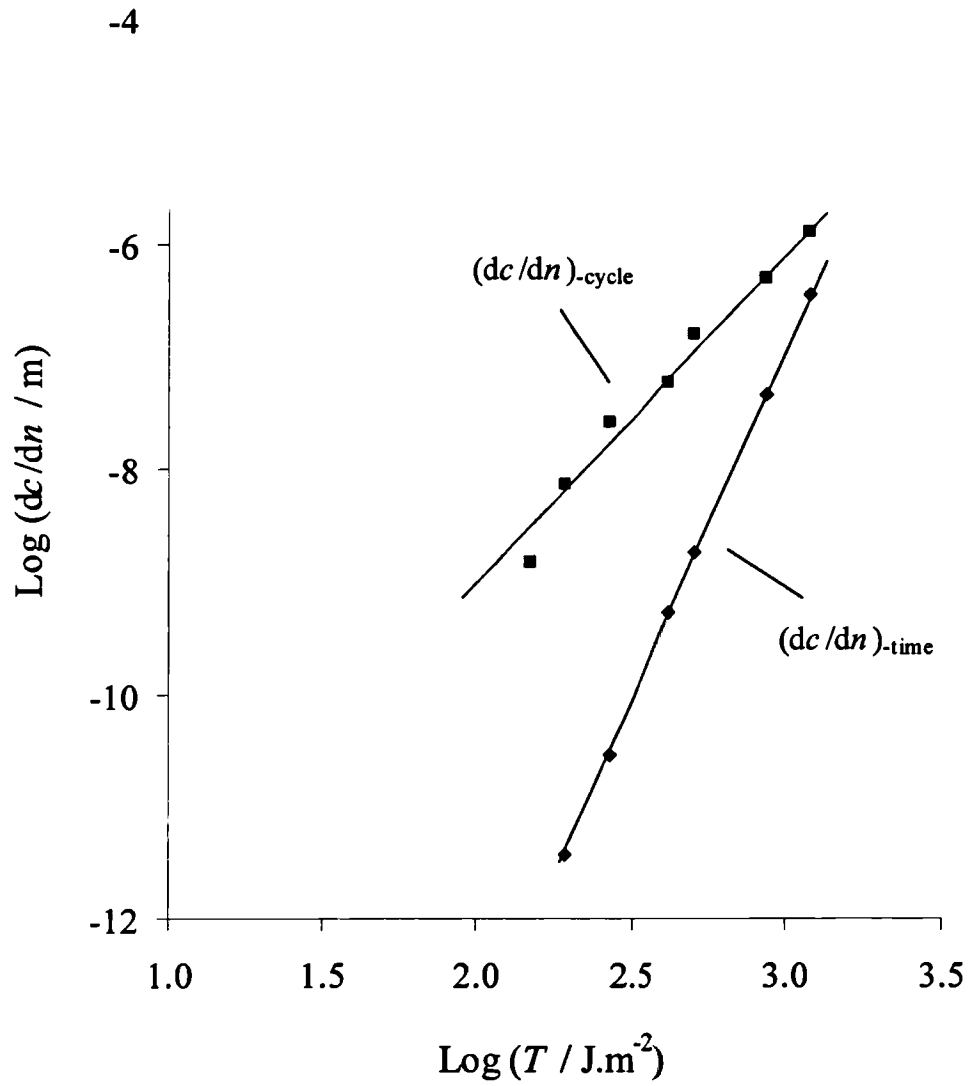

Figure 6-8. The crack growth per cycle for both $(dc/dn)_{\text{-cycle}}$ and $(dc/dn)_{\text{-time}}$ as a function of the maximum tearing energy during a cycle, T, on a double logarithm scale for SBR (SBR00-S3) at a frequency of 5.0Hz.

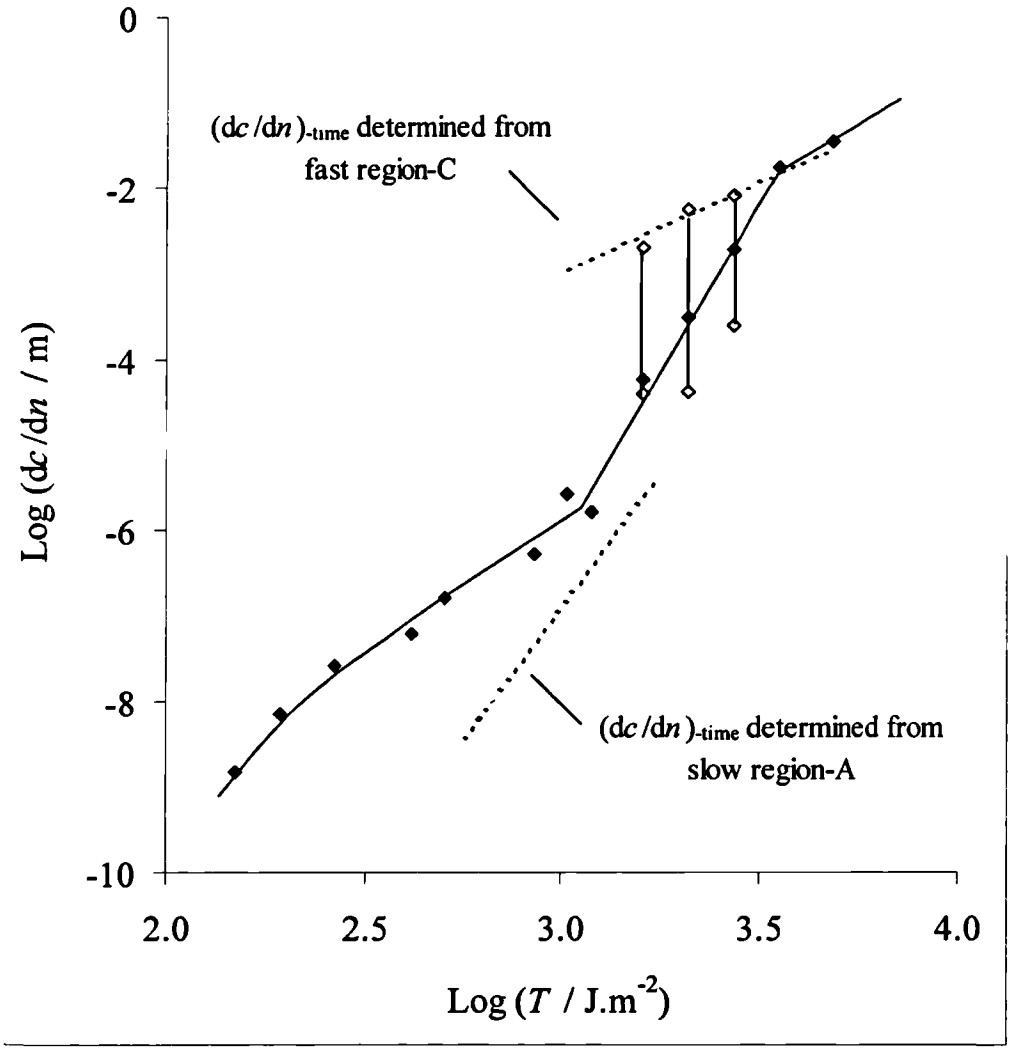

Figure 6-9. The total crack growth per cycle $(dc/dn)_{-total}$ as a function of maximum tearing energy during a cycle, T, on a double logarithm scale for SBR (SBR00-S3) over the wide range of T at a frequency of 5.0Hz. The superimposed dashed lines represent calculated values of $(dc\ dn)_{-time}$ calculated using the static crack growth constants from the slow or the fast crack growth regions.

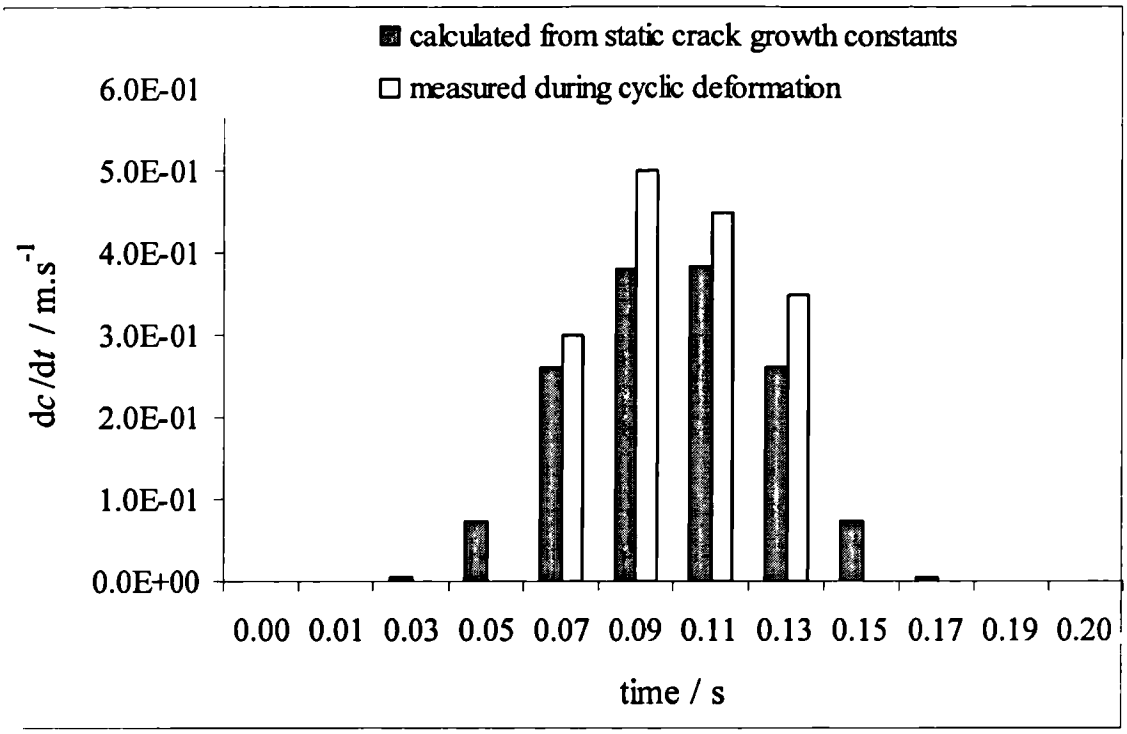

Figure 6-10. The incremental crack growth rate, d*c*/d*t*, at various points during a cycle in the fast crack growth region at the maximum tearing energy of 4.75kJ.m^{-2} and a frequency of 5.0Hz for SBR (SBR00-S3).

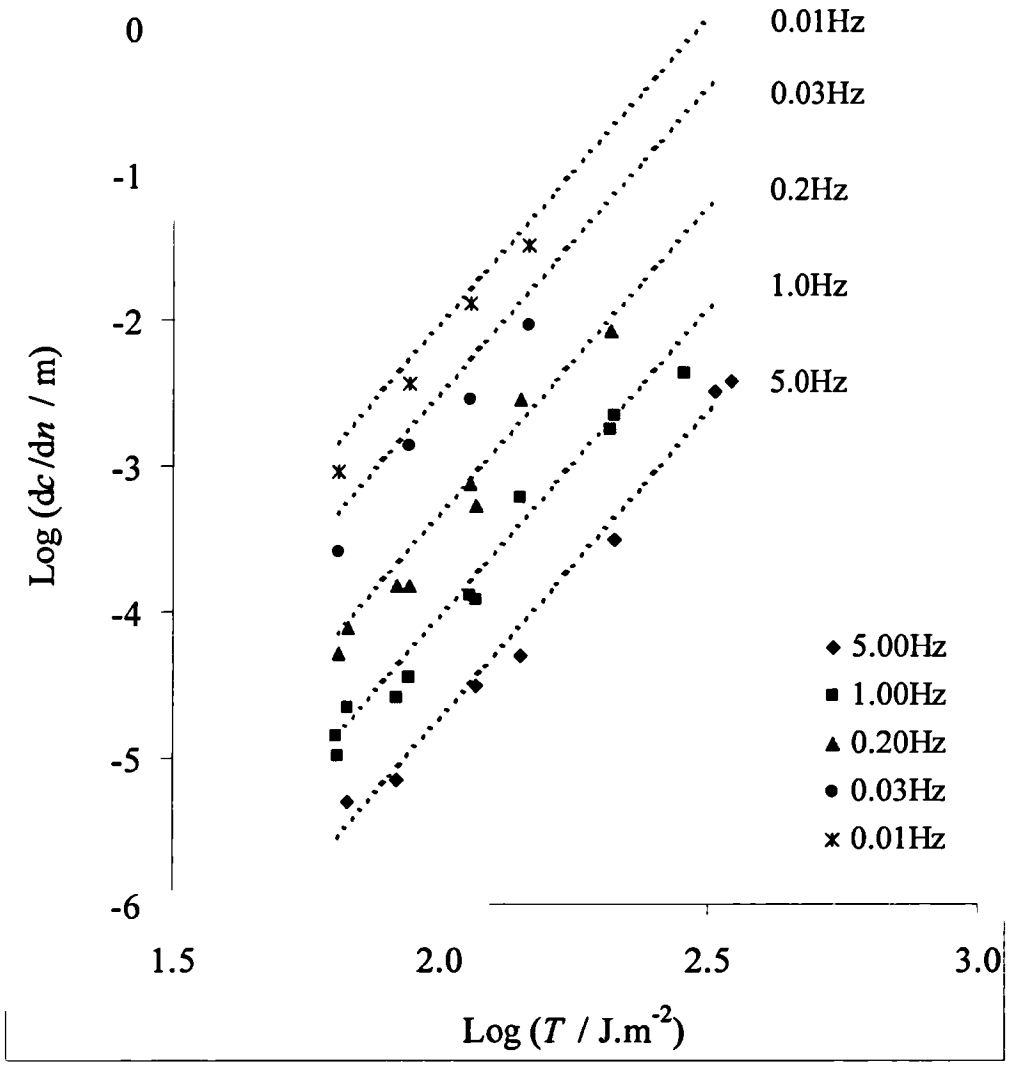

Figure 6-11. The effect of frequency on the total cyclic crack growth per cycle, $(dc/dn)_{total}$, as a function of the maximum tearing energy during a cycle, T, for SBR (SBR00-S3) swollen with DBA to V_r=0.38. The calculated values of $(dc/dn)_{time}$ obtained using equation (6-7) for each frequency are superimposed as dashed lines.

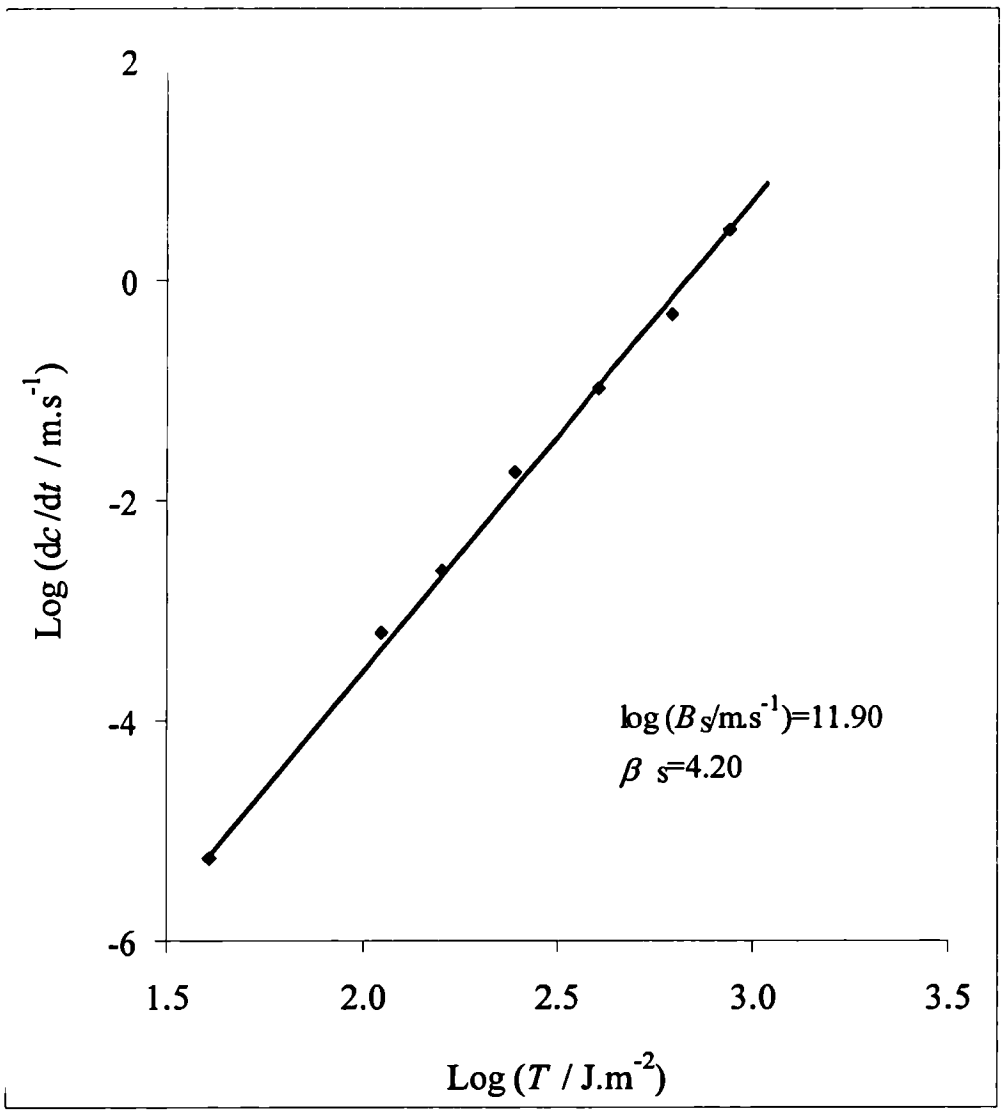

Figure 6-12. The static, constant T, crack growth rate, dc/dt, as a function of tearing energy for SBR swollen with DBA to V_r=0.38 (SBR00-S3).

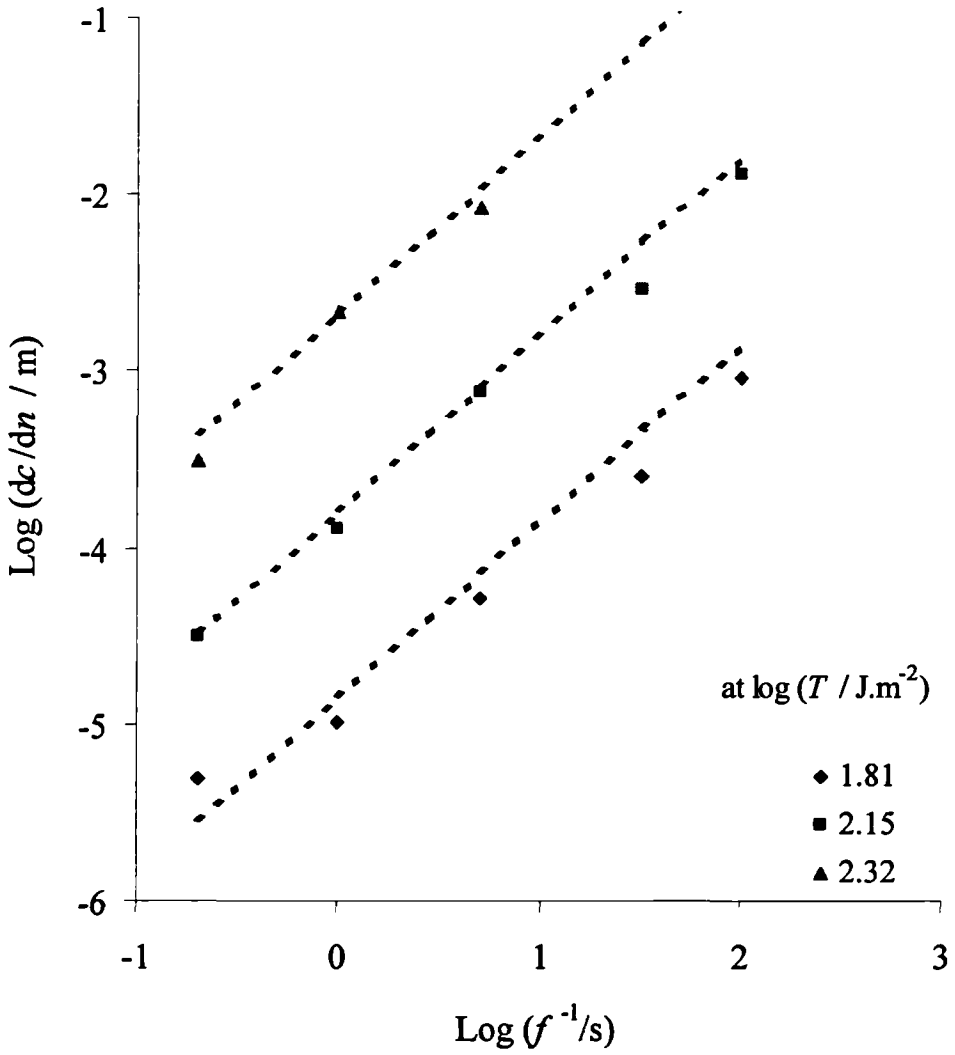

Figure 6-13. The crack growth per cycle, dc/dn, as a function of inverse of frequency at different tearing energies for both $(dc/dn)_{total}$ and $(dc/dn)_{time}$ for SBR (SBR00-S3) swollen with DBA to V_r=0.38. Calculated values of $(dc/dn)_{time}$ using equation (6-7) are superimposed as dashed lines.

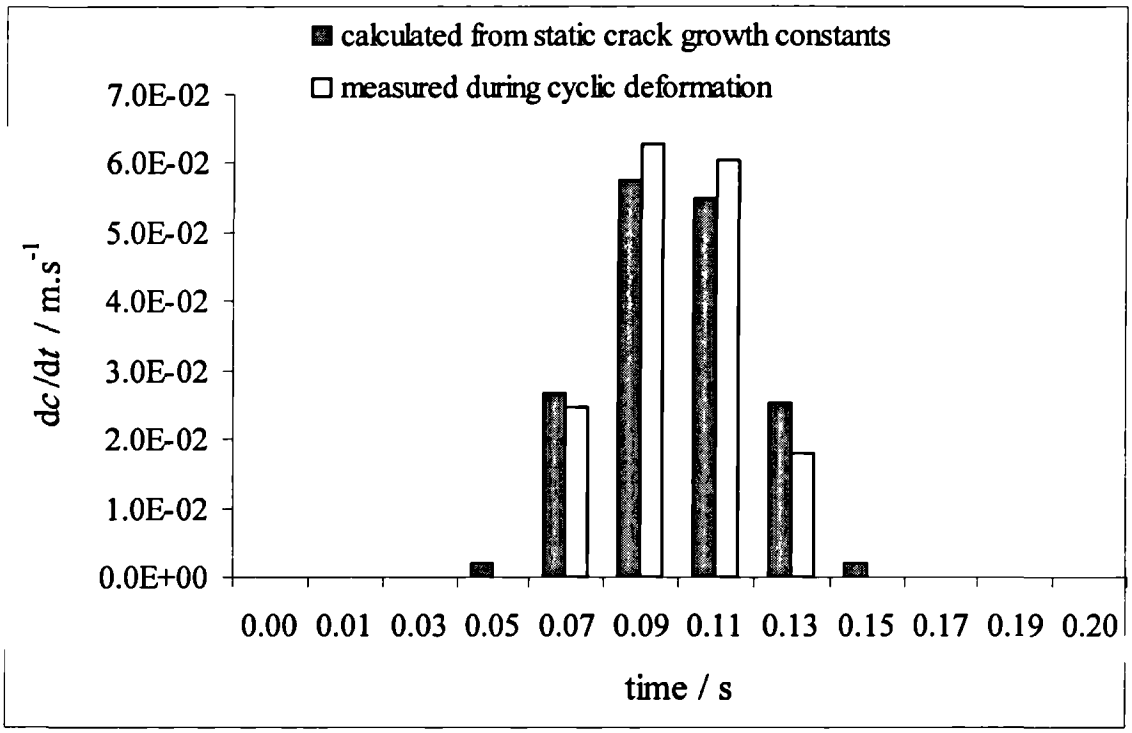

Figure 6-14. The incremental crack growth rate, dc/dt, at various points during a cycle in the fast crack growth region at a maximum tearing energy of 343 J.m^{-2} and a frequency of 5.0Hz for SBR (SBR00-S3) swollen with DBA to V_r=0.38.

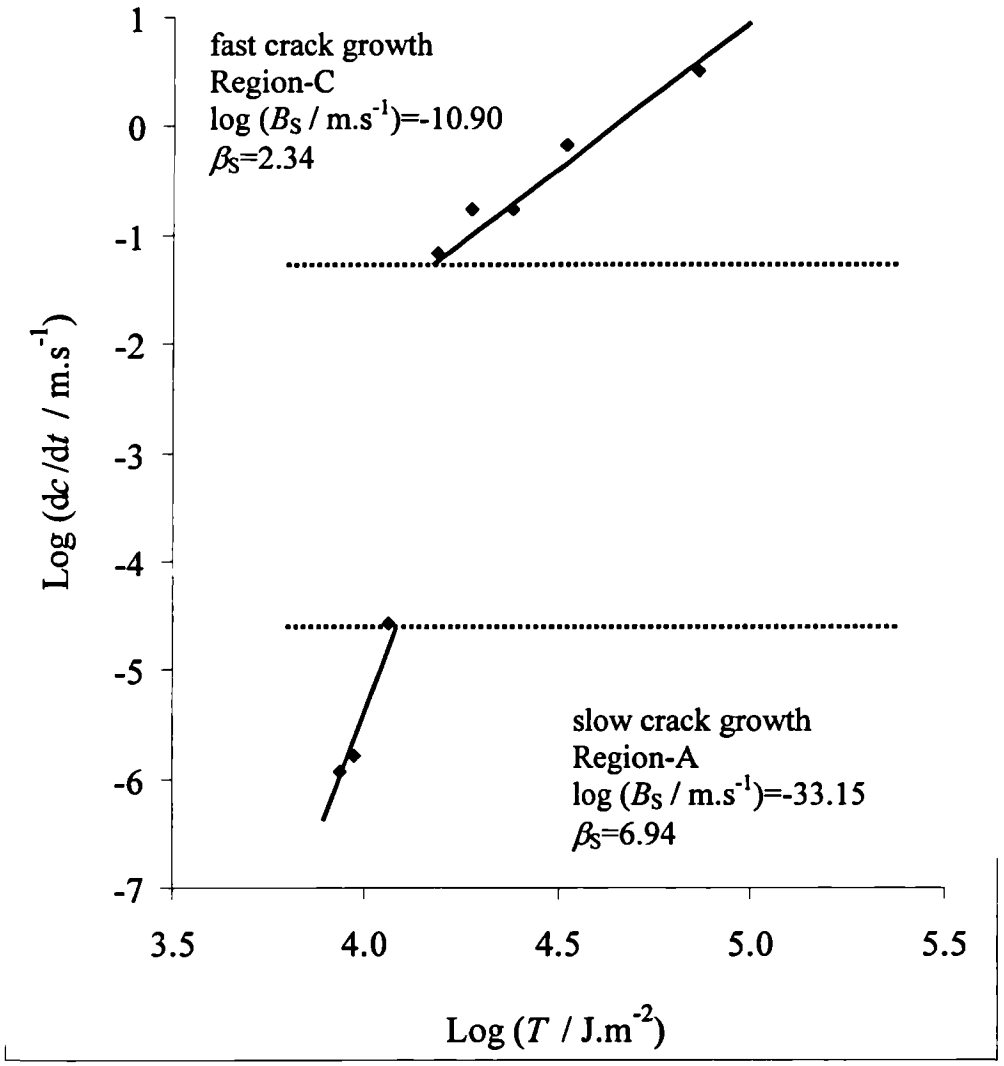

Figure 6-15. The static crack growth rate, dc/dt, as a function of tearing energy for a 50phr carbon black filled SBR (SBR50-S1).

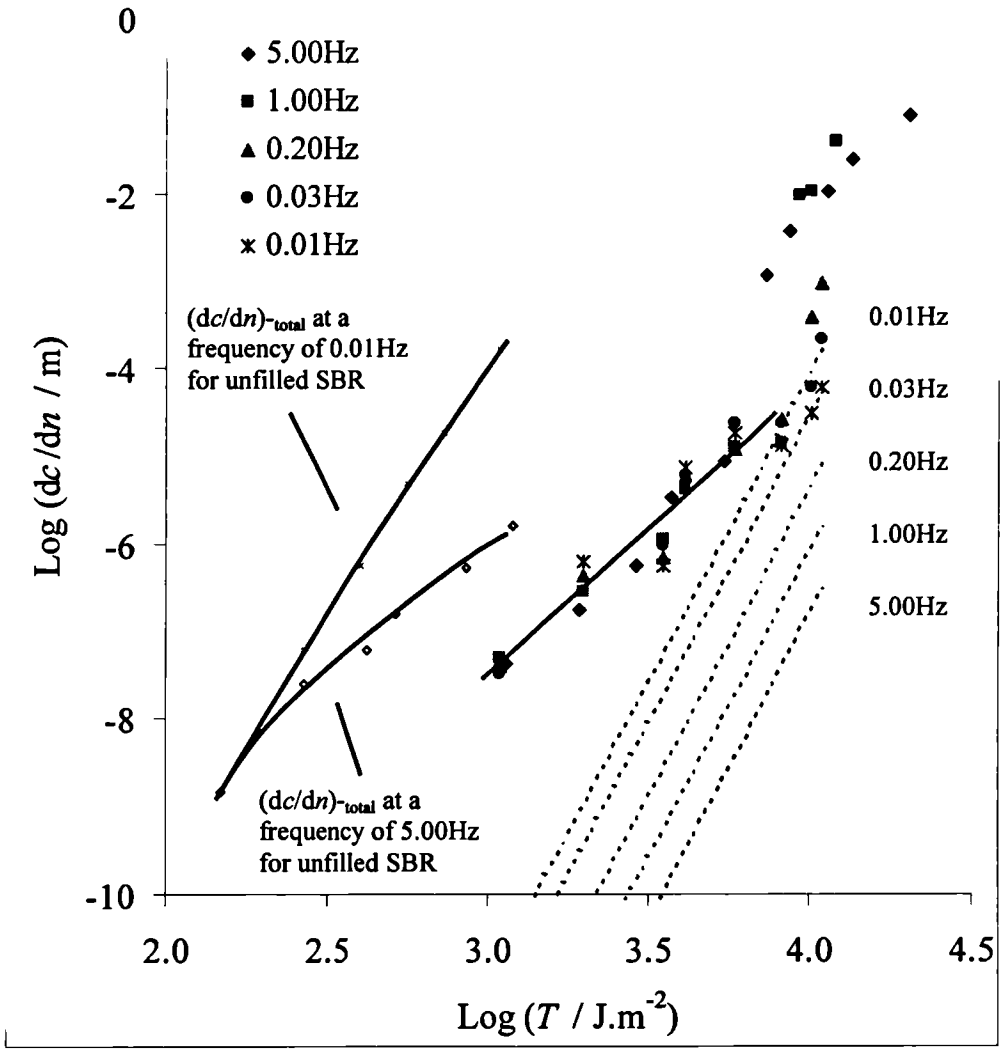

Figure 6-16. The effect of frequency on crack growth per cycle as a function of maximum tearing energy during a cycle, T, for both $(dc/dn)_{total}$ and $(dc/dn)_{time}$ for 50phr carbon black filled SBR (SBR50-S1).

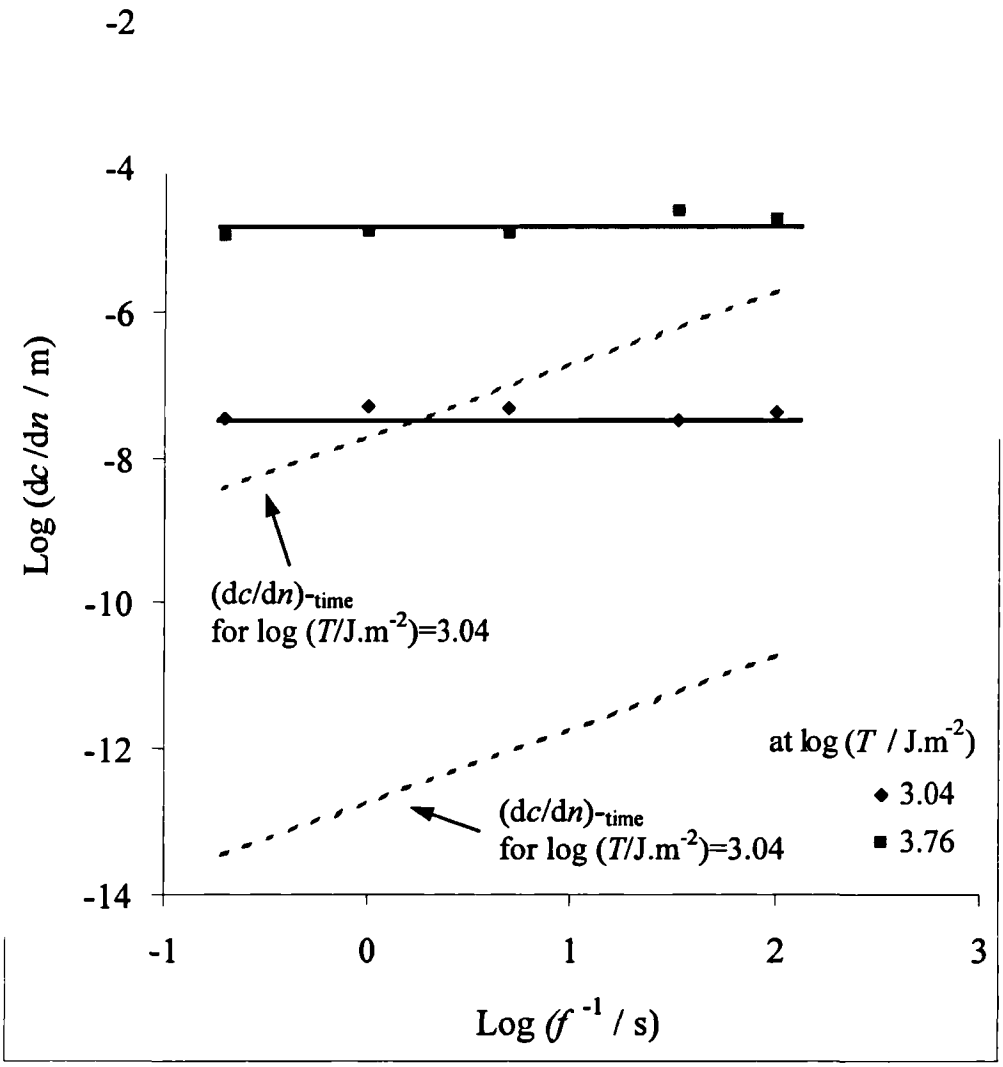

Figure 6-17. The crack growth per cycle as a function of the inverse of frequency at different tearing energies for both $(dc/dn)_{-total}$ and $(dc/dn)_{-time}$ for 50phr carbon black filled SBR (SBR50-S1).

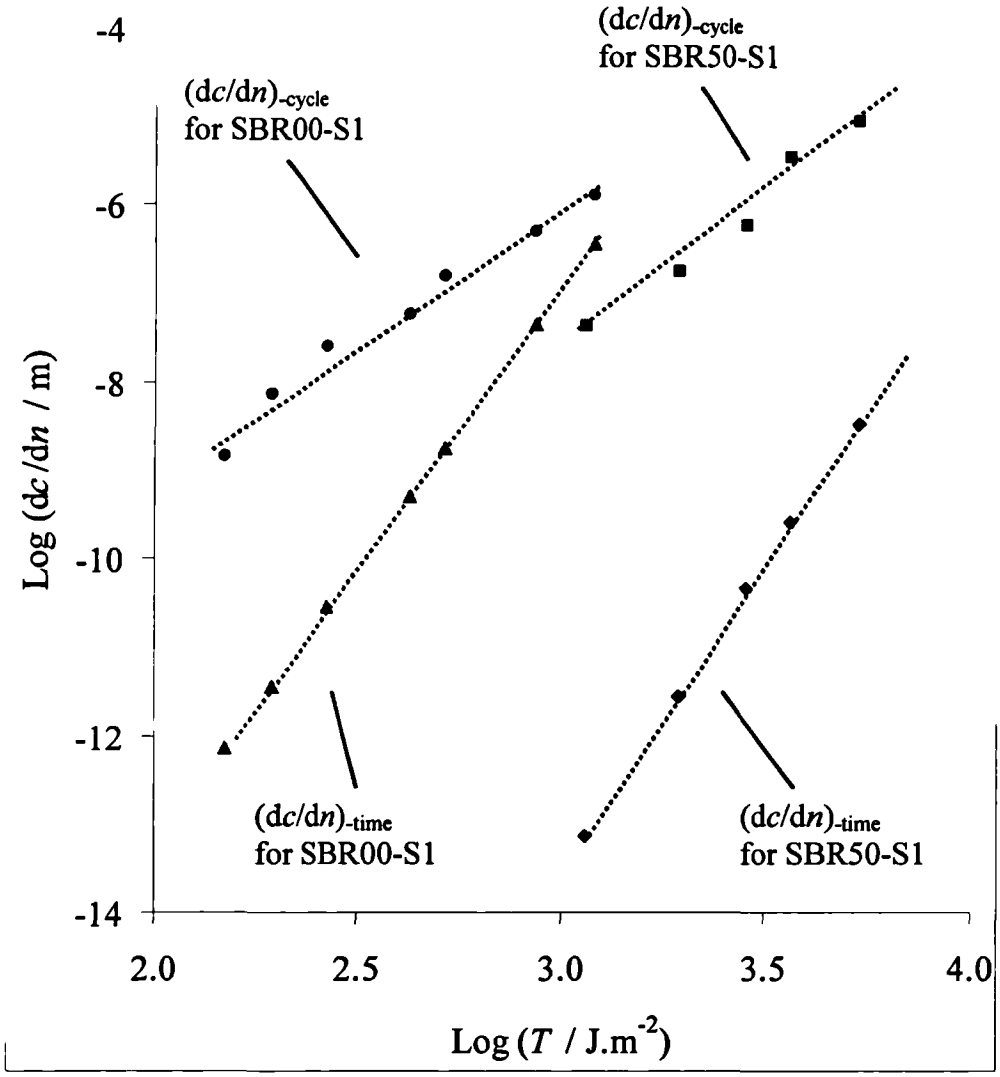

Figure 6-18. The crack growth per cycle for both $(dc/dn)_{-time}$ and $(dc/dn)_{-cycle}$ as a function of tearing energy on a double logarithm scale for unfilled SBR (SBR00-S3) and a 50phr carbon black filled SBR (SBR50-S1) at a frequency of 5.0Hz.

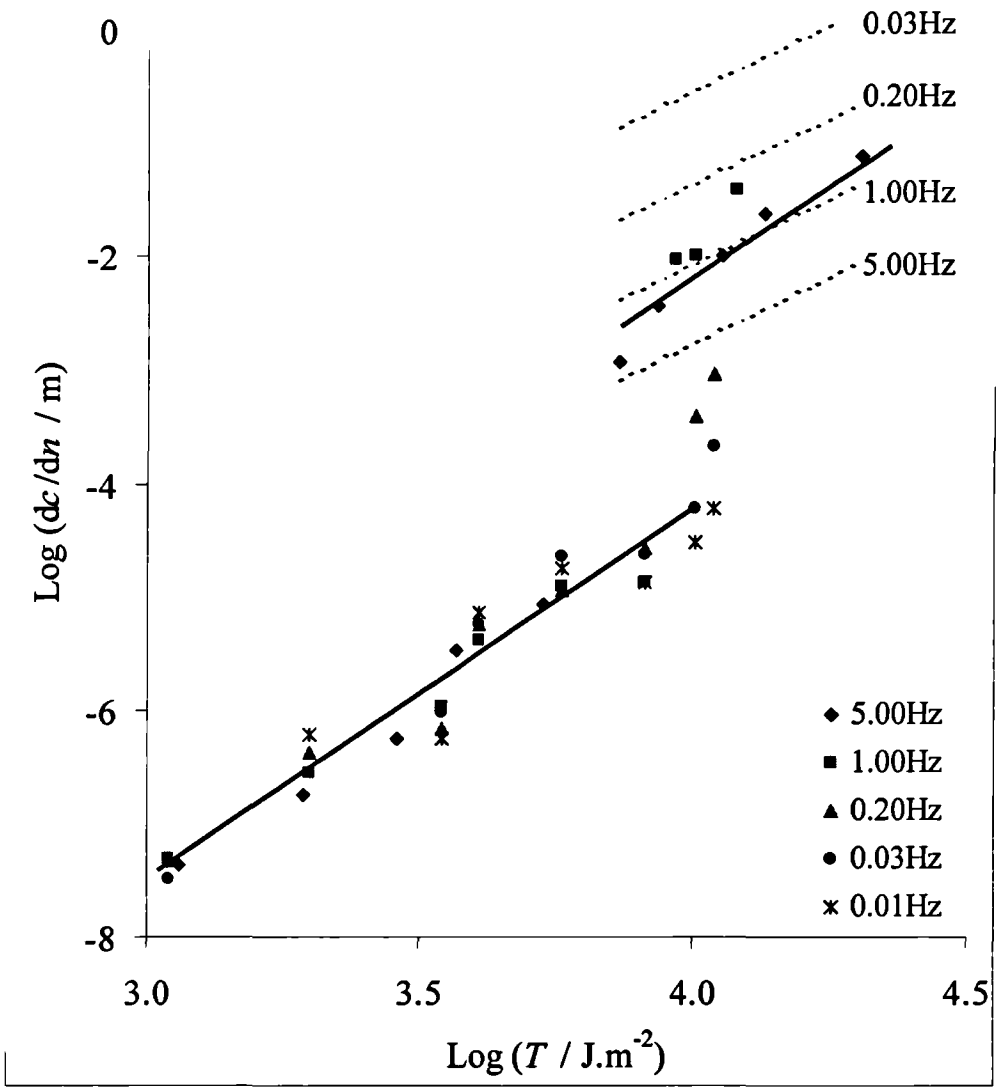

Figure 6-19. The effect of frequency on crack growth per cycle as a function of maximum tearing energy during a cycle, T, for $(dc/dn)_{\text{-total}}$ and for $(dc\ dn)_{\text{-time}}$ (shown as dashed lines) calculated from the static crack growth constants from the fast crack growth region-C for 50phr carbon black filled SBR (SBR50-S1).

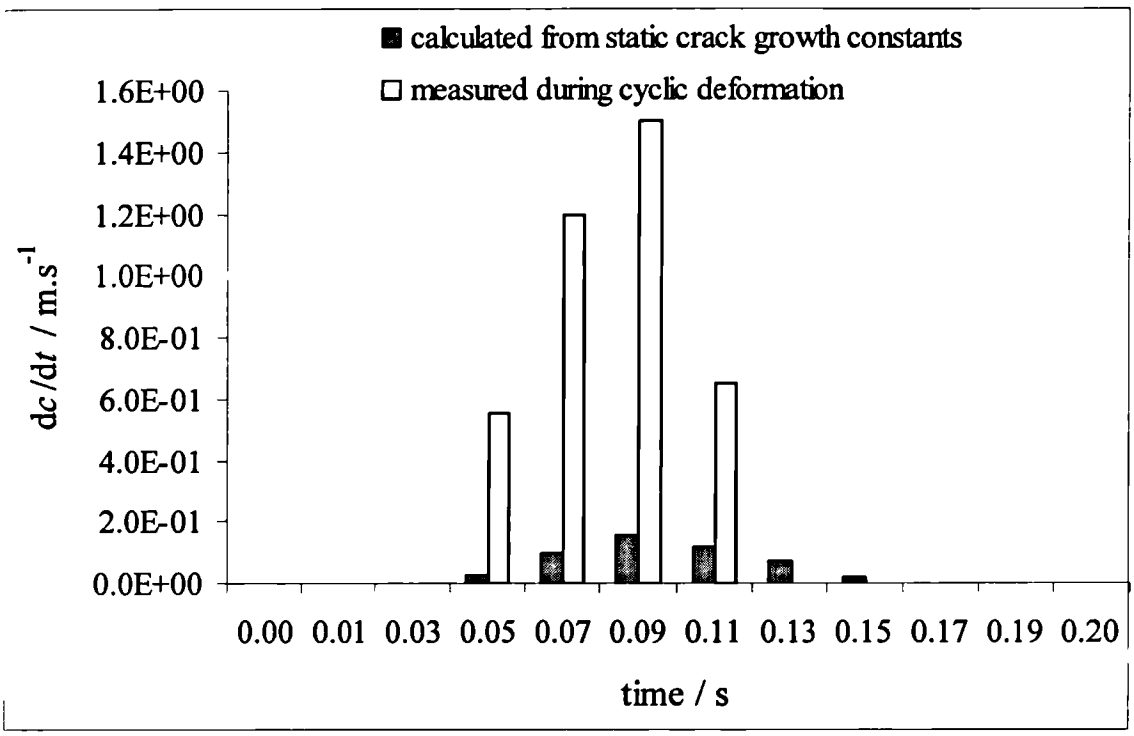

Figure 6-20. The incremental crack growth rates, d*c*/d*t*, at a maximum tearing energy of 20375 J.m^{-2} and at a frequency of 5.0Hz during cyclic deformation for 50phr carbon black filled SBR (SBR50-S1).

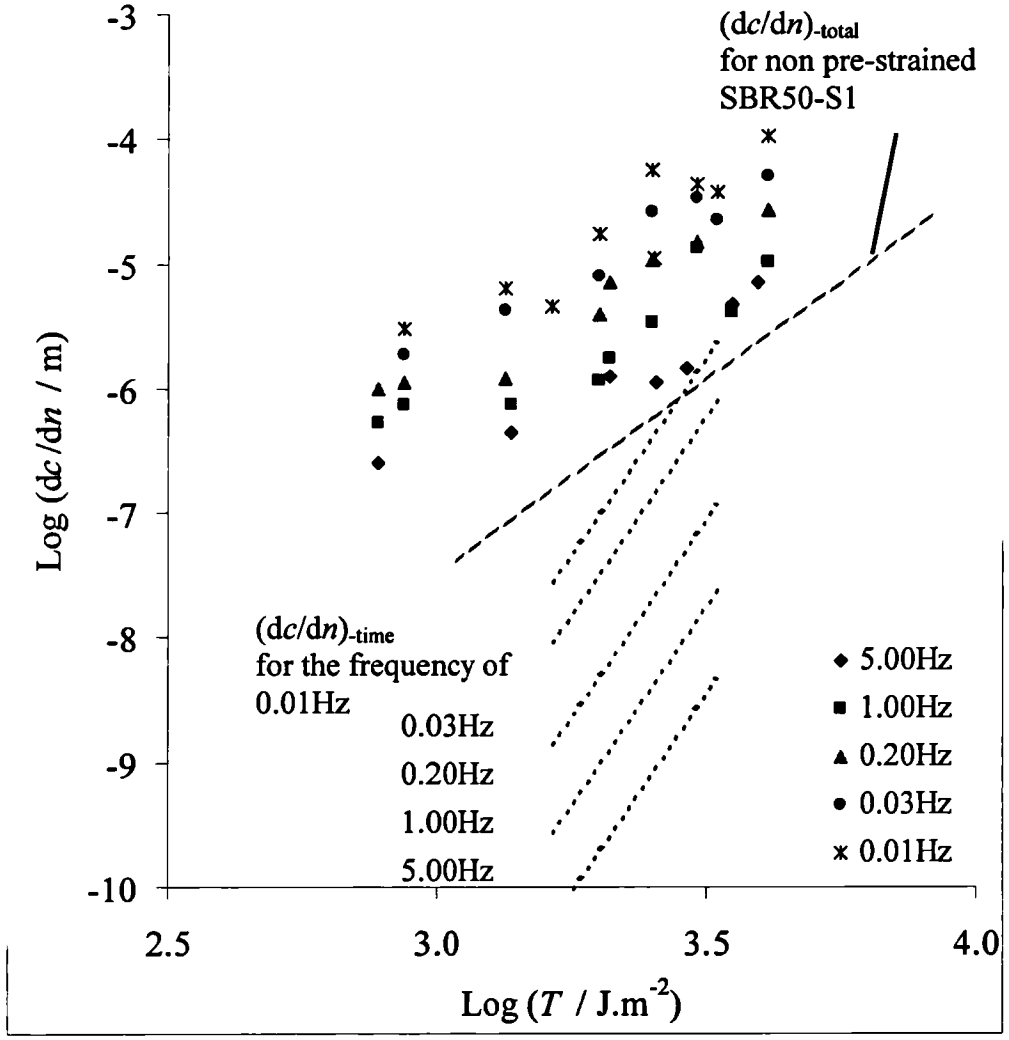

Figure 6-21. The effect of frequency on the crack growth per cycle as a function of maximum tearing energy during a cycle, T, for both experimentally determined $(dc\ dn)_{\text{-total}}$ and for theoretically calculated $(dc/dn)_{\text{-time}}$ obtained from the static crack growth constants for 50phr carbon black filled SBR (SBR50-S1) under 100% pre-strain.

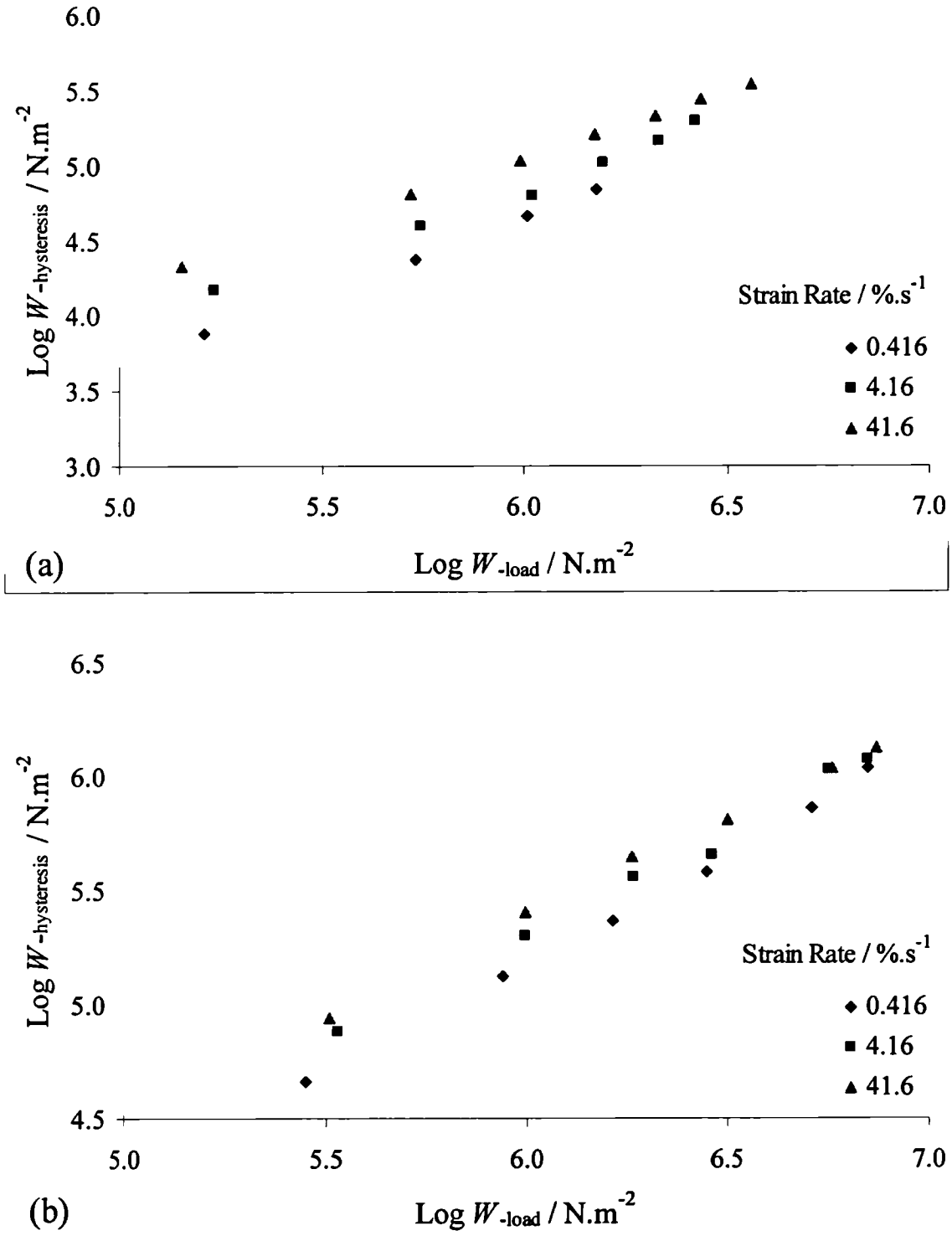

Figure 6-22. The hysteresis energy density, $W_{\text{-hysteresis}}$, as a function of elastic stored energy density, $W_{\text{-load}}$, at different strain rates during cyclic deformation for (a) unfilled and (b) 50phr carbon black filled SBR.

Chapter Seven

Tensile strength of swollen rubber

7-1. Introduction

This thesis has been concerned with crack growth in mostly SBR based rubbers from artificially introduced cracks under a number of loading systems. In chapter 4 constant rate of grip separation crack growth (trouser tearing) was studied using simple extension (trouser) specimens, in chapter 5 static, constant T, crack growth was studied in pure shear specimens and in chapter 6 cyclic crack growth behaviour was investigated. In all cases, crack growth could be described in terms of a characteristic tearing energy necessary to drive a crack at a given rate. Crack growth in tensile specimens whether from natural flaws or artificial cracks can be described by an extension of these concepts[7][8]. In rubbers, which strain crystallise, such tensile crack growth behaviour has been shown to depend on whether the bulk of a specimen or merely the crack tip has crystallised prior to crack growth[72][75][76].

If crystallisation does not take place within the bulk of the specimen then failure occurs in a manner determined by the tearing behaviour. For such a tensile test piece this is represented by[7][8]

$$T = 2kWc \tag{7-1}$$

where T is the tearing energy, c is the crack length, k is a constant which is a slightly varying function of the extension ratio, λ, which is given approximately as[10]

$$k = \frac{\pi}{\sqrt{\lambda}} \tag{7-2}$$

and W is the elastic stored energy density in the bulk of the specimen.

At tensile break, whether from an natural flaw or an artificial crack, this expression becomes

$$W_b = \frac{T_c}{2kc} \tag{7-3}$$

where W_b is the elastic stored energy density at break and the critical tearing energy, T_c, can be determined from high strain rate trouser tear tests. The tensile strength σ_b can be calculated from the magnitude of W_b and can be compared with measured values.

However, if the bulk of the specimen crystallises then cracks grow in a manner similar to the cyclic crack growth behaviour until a crack of sufficient length is achieved for catastrophic failure to occur by tearing[75]. This growth can be allowed for by writing equation (7-1) as

$$T = 2kW(c_o + \Delta c) \tag{7-4}$$

where c_o is the initial crack length, natural flaw sizes or artificial, Δc, is the increase in crack length occurring during loading of the tensile specimen to an elastic stored energy density, W. This amount of crack growth Δc is given by the cyclic crack growth relationship as

$$\Delta c = BT^{\beta} \tag{7-5}$$

where β is typically approximately 2 for a strain crystallising rubber[98][99] at high T values and hence for those materials equation (7-5) can be written as

$$T^2 = \frac{\Delta c}{B} \tag{7-6}$$

Elimination of T between equations (7-4) and (7-6) gives

$$\frac{\Delta c}{c_o} = x - 1 - \left(x^2 - 2x\right)^{\frac{1}{2}} \tag{7-7}$$

$$\text{where } x = \frac{1}{8k^2W^2c_oB} \tag{7-8}$$

As the strain in the test piece increases, W increases and hence x decreases. When $x<2$ solutions for $\Delta c/c_o$ becomes imaginary and the crack will grow indefinitely in length and catastrophic failure occurs. Thus the elastic stored energy density at break, W_b, now becomes

$$W_b = \frac{1}{4kc_o^{\frac{1}{2}}B^2} \tag{7-9}$$

utilising equation (7-4) and (7-6)

$$\Delta c = 4k^2 B(c_o + \Delta c)^2 W^2 \qquad (7\text{-}10)$$

and hence the value of B could be determined from the slope of a plot of Δc versus $(c_o+\Delta c)^2W^2$. Δc should be determined by loading specimens to given W values; ideally one cycle measurements or for a sufficiently small number of cycles to obtain accurate Δc values. If long term (10^3-10^6 cycle) cyclic fatigue data, which can be represented by,

$$\Delta c = \frac{dc}{dn} = BT^2, \qquad (7\text{-}11)$$

is used complications may arise as the crack tip may be sufficiently different to cause a significant change in the value of B. Once a value of B has been obtained, from whatever source, values of W_b and hence σ_b for given crack lengths can be calculated using equation (7-9) and can be compared to measured values. Such calculations have been carried out for NR and good agreement between calculated and measured values of σ_b has been shown for appropriate crack lengths[75][76].

The purpose of the present work was to extend this study to SBR materials but more importantly was also to utilise the above analysis to study tensile failure in swollen NR and SBR materials. As has been demonstrated in chapters 4, 5, and 6 swelling is a powerful tool with which to investigate crack growth phenomena as it influences both the visco-elastic losses and strain crystallisation and hence strongly influences the tear behaviour.

7-2. *Experimental procedure*

7-2-1. Tensile strength measurement and measurement of Δc as a function of W

Tensile strip specimens, with and without artificial cracks, 10mm wide, 50mm long and approximately 1mm in thickness, were used for these measurements. Tensile measurements were carried out at an average cross head speed of 50 $mm.min^{-1}$, giving a strain rate of $8.33x10^{-1}s^{-1}$ at an ambient temperature of 20°C ±2°C. The stress and strain, including the breaking stress and breaking strain, were

recorded using an X-Y plotter. All tests were carried out on 5 tensile specimens in each condition. The average Δc values for a given W were determined on specimens subjected to 5 to 6 loading cycles utilising an optical microscope. The magnitude of Δc per cycle was found to be approximately constant. The formulations of the mixes and the curing conditions of the rubber materials used in this study are listed in tables 3-1 and 3-2.

7-2-2. Artificial crack

A sharp razor blade was used to insert an artificial edge crack normal to the test piece edge. This crack length was varied from 0.2mm to 4.0mm. The edge of the razor blade was lubricated with a soap solution to ensure the sharpness of the crack tip. The cut length was precisely measured using an optical microscope.

7-2-3. Swelling the rubber specimens

Dibutyl Adipate (DBA) was used as the swelling liquid and specimens for testing were swollen in a glass dish to any achievable swelling ratio (volume fraction of rubber, V_r). The samples were then left in air for the time necessary to achieve homogeneous samples of the required volume fraction of rubber. The final volume fraction of rubber in the samples was determined from the rubber mass before and after swelling.

7-3. Results and discussion

7-3-1. Effect of swelling on tensile strength

The measured tensile strength as a function of volume fraction of rubber, V_r, for NR (NR00-S1) swollen with DBA for specimens without artificial notches is shown in figure 7-1. The measured tensile strength in the range V_r=0.95 to 0.70 showed a large scatter, often covering a decade in value. Furthermore the scatter tended to be bi-modal. This bi-modal scattering can be observed more obviously by

means of the plot of tensile strength distribution over a wide range of volume fraction of rubber shown in figure 7-2. With decreasing volume fraction of rubber, from V_r=1.00, the peak strength value shifted downward. However, in the range of volume fraction of rubber 0.95 to 0.70 a secondary peak of lower strength magnitude appeared. At lower volume fractions of rubber the measured tensile strength became uni-modal. In the intermediate range of volume fraction of rubber it would seem that any given test piece yielded strength values either on the high or the low curve rather than at intermediate values (figure 7-1). This abrupt fall in average tensile strength was very similar to observations in earlier work[72][75][76], which had studied the effect of temperature and the effect of initial flaw size on tensile strength. In this work the abrupt fall in tensile strength had been observed at a critical temperature or a critical initial flaw size. The abrupt fall in tensile strength implied that there may be different mechanisms operating; one being predominant at a high volume fraction of rubber and another predominant at a low volume fraction of rubber. A discussion of this is given in section 7-3-2.

The tensile strength as a function of volume fraction of rubber for SBR (SBR00-S3) swollen by DBA is shown in figure 7-3. Compared with the result for NR (figure 7-1), the SBR data showed a much reduced scatter over the whole range of volume fraction of rubber. The average values for each volume fraction of rubber fell onto a single curve.

7-3-2. Effect of initial crack size on the tensile strength

An abrupt drop in tensile strength as a function of volume fraction of rubber, V_r, for unfilled NR was observed in figure 7-1. This abrupt fall in strength was also observed in the effect of initial crack size on the tensile strength of unfilled NR[75]. It can be suggested that the tensile strength decreased steadily with increasing initial crack size up to a fairly well defined critical crack length where upon an abrupt fall in tensile strength was observed. The strength in the low strength region, where the initial crack length was greater than 2mm, was believed to be governed essentially by the tear strength properties of the rubber. However, if the initial crack size was less than 2mm, the body of the test piece was believed to reach a sufficiently high strain to become strain crystallised before the tear strength was reached. In this case the

tear process was suppressed and ultimate failure occurred by crack growth until a crack of sufficient length was achieved for catastrophic failure.

It was this work that prompted the present studies on the effect of initial crack size on tensile strength for swollen rubbers with a wide range of volume fraction of rubber. A plot of the tensile strength, σ_b, as a function of initial crack size for NR (NR00-S1) over a wide range of volume fractions of rubber, V_r, is shown in figure 7-4(a). In the range of V_r=1.00 to 0.81 the observed tensile strength decreased steadily with increasing the initial crack size up to a certain critical crack size as expected. Above the critical crack size, an abrupt fall in strength was observed. Conversely, for highly swollen NR (figure 7-4(b)) (V_r less than 0.75) the magnitude of the tensile strength gradually decreased with increasing initial crack size and no abrupt drop was observed. The critical crack size decreased with increasing extent of swelling (decreasing volume fraction of rubber). The magnitude of the measured critical crack size as a function of volume fraction of rubber is shown in figure 7-5. There was considerable uncertainty in the measurement of this critical crack size but the curve indicated that the critical crack size was effectively zero for highly swollen NR and here the tensile strength was likely to be associated with tearing. The tensile strength as a function of initial crack size for SBR (SBR00-S3) is shown in figure 7-6. The pattern was seen to be very similar to that for the highly swollen NR. The measured tensile strength decreased steadily with increasing initial crack size. No abrupt fall in tensile strength was observed. This also indicated that the critical crack size was effectively zero for unfilled SBR.

The measured Δc values are shown plotted as a function of $(c_o+\Delta c)^2W^2$ for NR (NR00-S1) in figure 7-7. Over most of the $\Delta c/W$ range a straight line can be drawn through the data of slope $4k^2B$ with B=1.88x10^{-13} N^{-2}m^3 (table 7-1). This value should be compared to the value obtained from the cyclic crack growth data ($dc/dn \cong 10^3$-10^6 cycles) of B=2.46x10^{-14} N^{-2}m^3 (table 7-1) which presumably results from a slightly blunter crack tip. The inset graph shows a regime of very small Δc, corresponding to low values of W in which cracks grow more rapidly than would be indicated by the major straight line. This effect has been observed previously[75] and maybe associated with an increment (Δc) of crack growth which occurs before the development of strain crystallisation at the crack tip.

Both equation (7-3) and (7-9) were used to calculate W_b and σ_b values for the materials. In equation (7-3) the values of T_c obtained from trouser test pieces torn at a rate of 420 $\mu m.s^{-1}$ as reported in chapter 4, and given in table 7-2, were used. The results of these calculations are shown for the unswollen NR, together with the measured σ_b data in figure 7-8. The B values from both the tensile strip and cyclic crack growth with pure shear specimens were used to calculate σ_b. At a large initial crack length the data was clearly predicted well by equation (7-3) and the values of σ_b obtained were those necessary to tear catastrophically specimens containing cracks of a given length. For specimens with a shorter initial crack length, the magnitude of the tearing energy was such that strain crystallisation took place in the bulk of the specimen before cracks could grow. Hence, cracks grow on loading by the process represented by equation (7-9) until they were of sufficient length for the specimens to fail catastrophically. If the B value obtained from the tensile data (figure 7-7) was used in equation (7-9) then the predicted curve fitted the measured σ_b versus c_o data very well. If the B value from the long time cyclic crack growth data was used, equation (7-9) tended to predict strengths, which were higher than the measured values. This was probably because this B value is associated with the growth of cracks with a blunter crack tip. Equation (7-3) was seen to predict the results well, over the whole range of crack length, for the highly swollen NR as illustrated in figure 7-9. Clearly cracks of any length resulted in failure by tearing before the bulk of the specimen crystallised. This was probably due to a combination of two factors. The very low tearing energies due to a reduction in the viscous losses at the crack tip, resulted in lower W values being necessary for failure. These values were now below the magnitude required to cause crystallisation. The other factor being that the breaking strain crystallisation will become progressively more difficult as the extent of swelling is increased. The cyclic crack growth data obtained with pure shear specimens was used to predict σ_b values for two of the swollen NR materials (V_r=0.78 and 0.42) as illustrated in figures 7-10 and 7–11. The predicted values were clearly much too high. This was presumably due to the fact that in this long term cyclic crack growth crystallisation still played a major role in crack tip blunting.

Equation (7-3) was used to calculate the σ_b versus c_o data for SBR and is shown superimposed on the measured data in figure 7-6. Clearly there was good

agreement over the whole range of c_o values. As would be anticipated for SBR, the failure process was always governed by the catastrophic tear behaviour.

Hence for both NR and SBR the tensile strengths can be predicted using the same concepts of tearing energy and crack growth as apply generally for tearing and crack growth behaviour in a variety of loading regimes.

7-4. Summary and conclusions

(1) An abrupt drop in tensile strength as a function of V_r or of initial crack sizes was observed for NR.

(2) For NR, the strength in the low strength region, where the initial crack length is greater than 2mm, is governed essentially by the tear strength properties. Conversely, when the initial crack size is less than 2mm, the body of the test piece reaches a sufficiently high strain to crystallise before the tear strength is reached. In this case the tear process is suppressed and ultimate failure occurs by a crack growth process until a crack of sufficient length is achieved for catastrophic failure.

(3) For unfilled either unswollen or swollen SBR or highly swollen NR, the abrupt drop in tensile strength does not occur and the strength is governed by tear strength properties.

(4) The tensile strength for both NR and SBR can be predicted by utilising the tearing energy concept and crack growth measurements in a variety of loading regimes.

Table 7-1. Experimentally obtained crack growth constant (B) for predicting the tensile strength for NR (NR00-S1).

	Crack growth constant, B / $N^{-2}.m^3$
Tensile strip specimen (5 cycles)	1.88×10^{-13}
Cyclic crack growth with pure shear test specimen (10^3 cycles)	2.46×10^{-14}

Table 7-2. Experimentally measured T_c values for NR and SBR materials unswollen and swollen with DBA to various extents measured in a trouser tear test at a rate of 420 $mm.s^{-1}$ (in chapter 4).

	V_r	T_c / $kJ.m^{-2}$
NR	1.00	15.68
	0.82	8.52
	0.65	4.53
	0.43	1.71
SBR	1.00	3.41
	0.78	1.16
	0.42	0.16

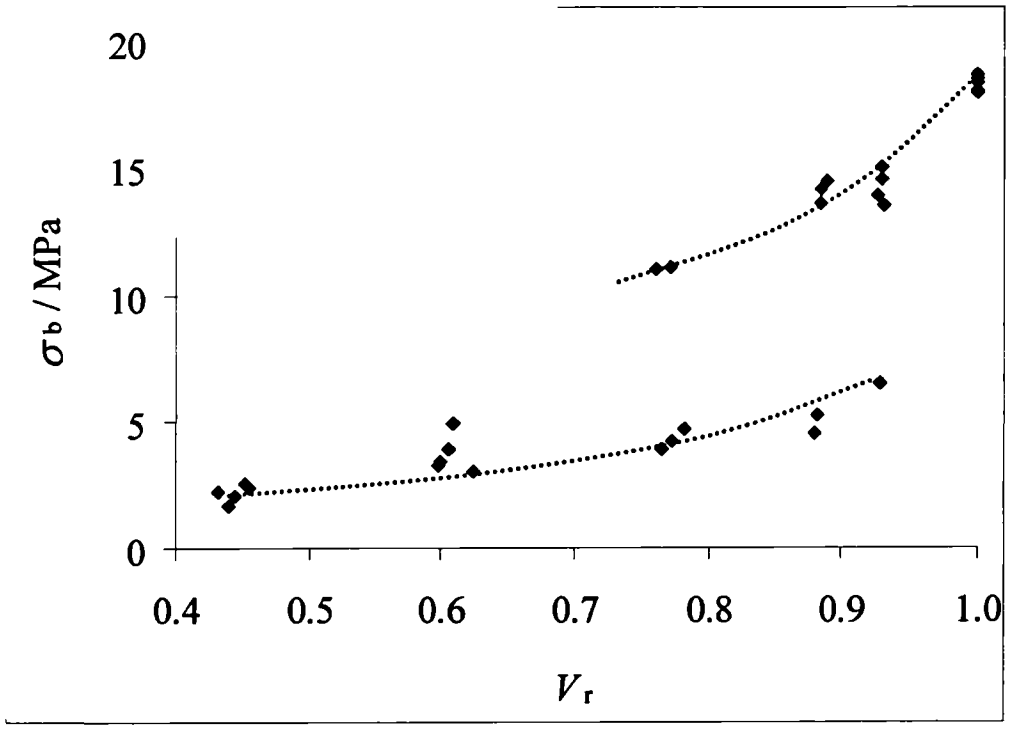

Figure 7-1. The tensile strength, σ_b, as a function of volume fraction of rubber, V_r, for NR (NR00-S1) swollen with DBA for specimens without artificial crack.

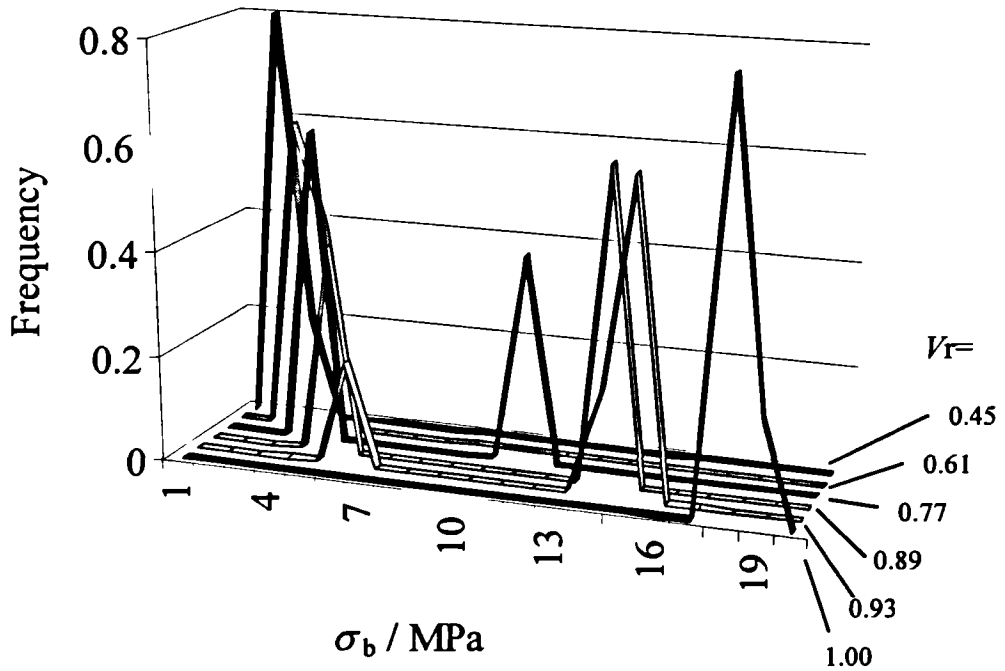

Figure 7-2. The tensile strength distributions for various volume fractions of rubber for NR (NR00-S1) swollen with DBA for specimens without artificial crack.

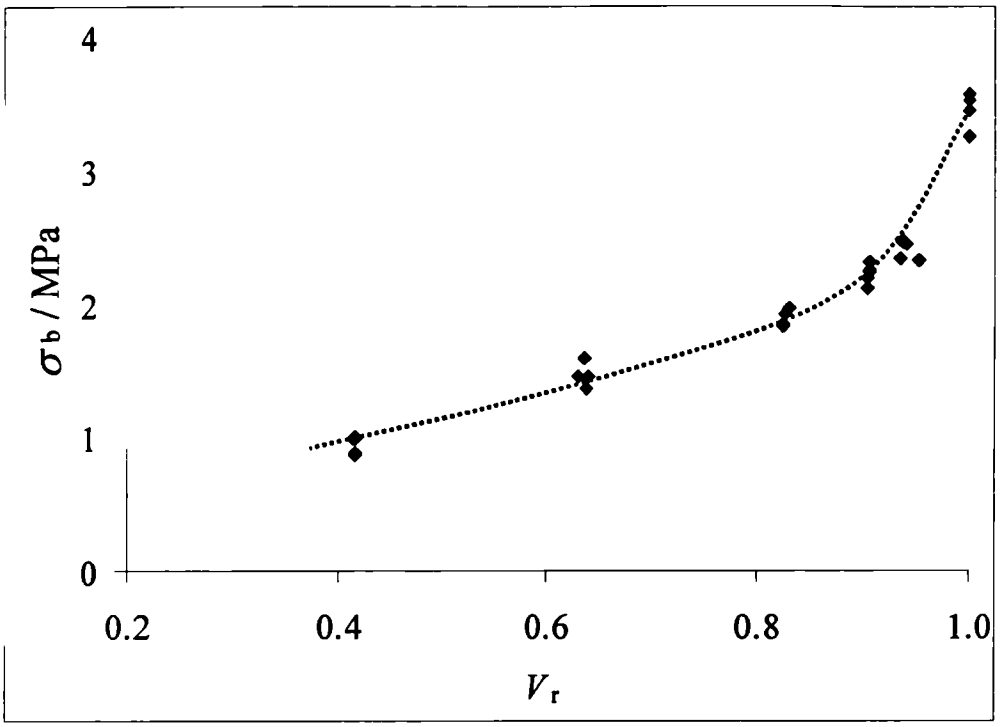

Figure 7-3. The tensile strength, σ_b, as a function of volume fraction of rubber, V_r, for SBR (SBR00-S3) swollen with DBA for specimens without artificial crack.

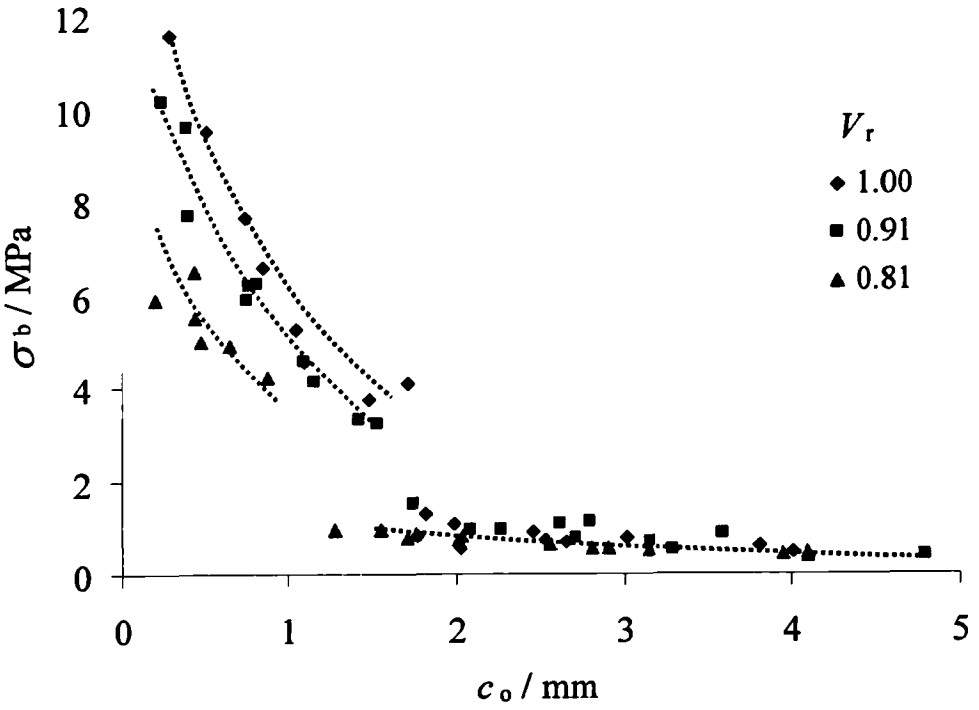

Figure 7-4(a). The tensile strength, σ_b, as a function of initial crack size for NR (NR00-S1) over a wide range of volume fraction of rubber, V_r.

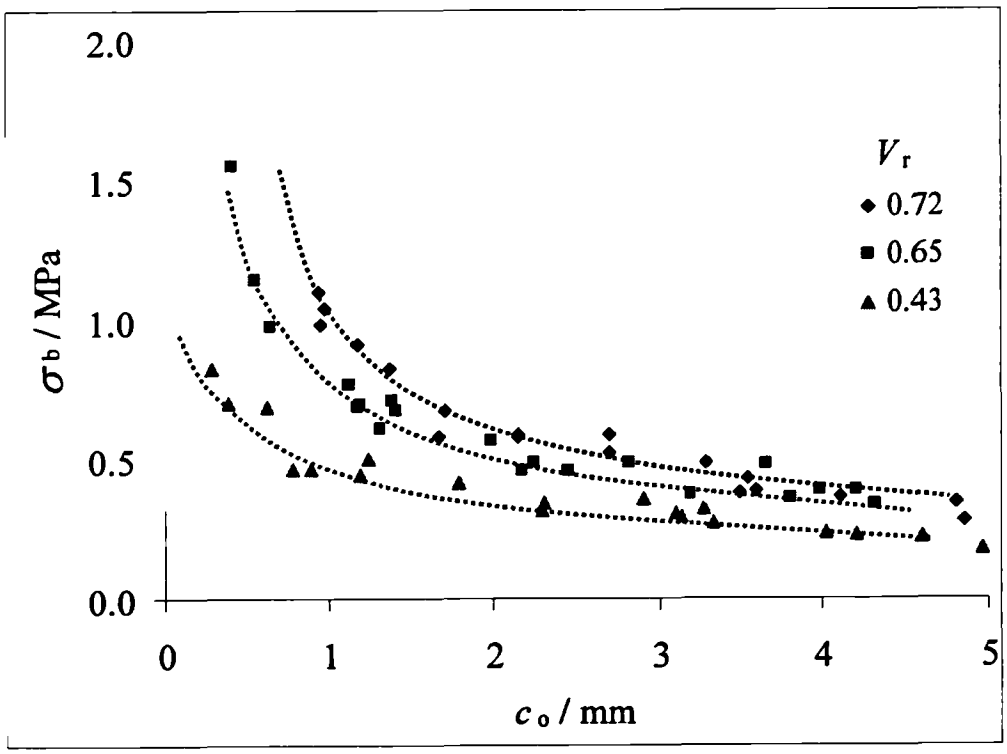

Figure 7-4(b). The tensile strength, σ_b, as a function of initial crack size for NR (NR00-S1) over a wide range of volume fraction of rubber, V_r.

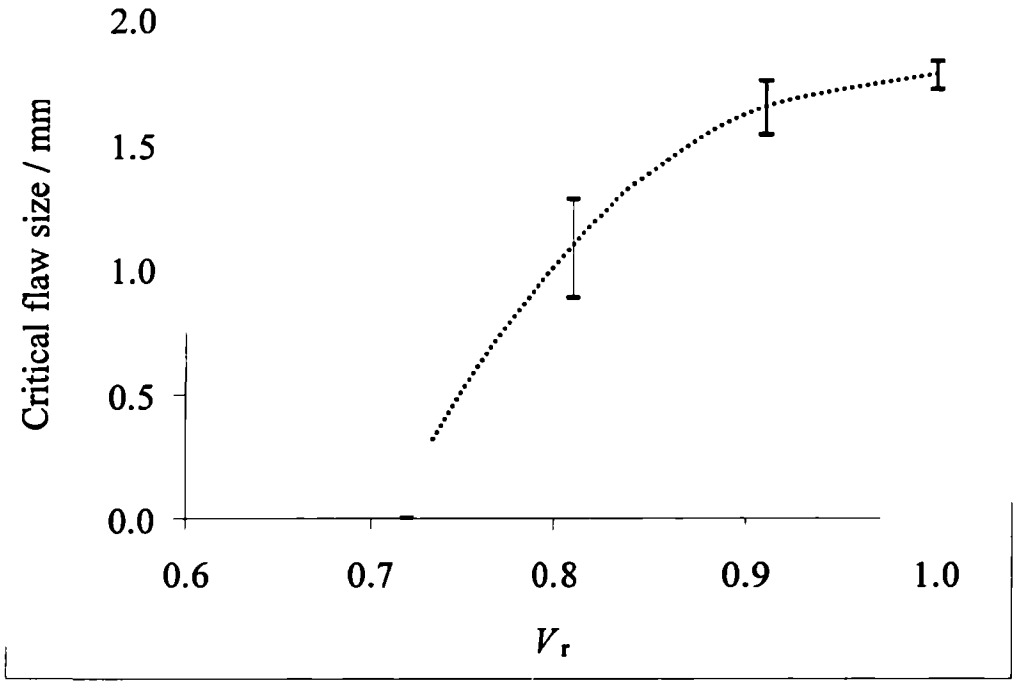

Figure 7-5. The measured critical crack size as a function of volume fraction of rubber for NR (NR00-S1) swollen by DBA.

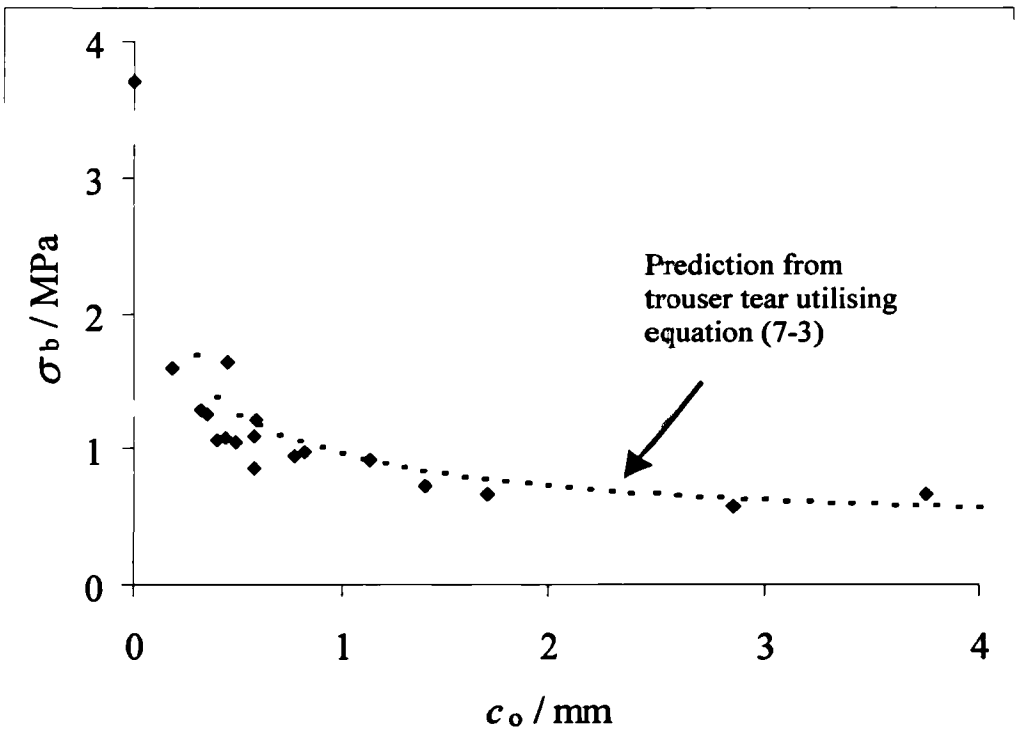

Figure 7-6. The tensile strength, σ_b, as a function of initial crack size for SBR (SBR00-S3). The dashed line represents the predicted σ_b utilising equation (7-3).

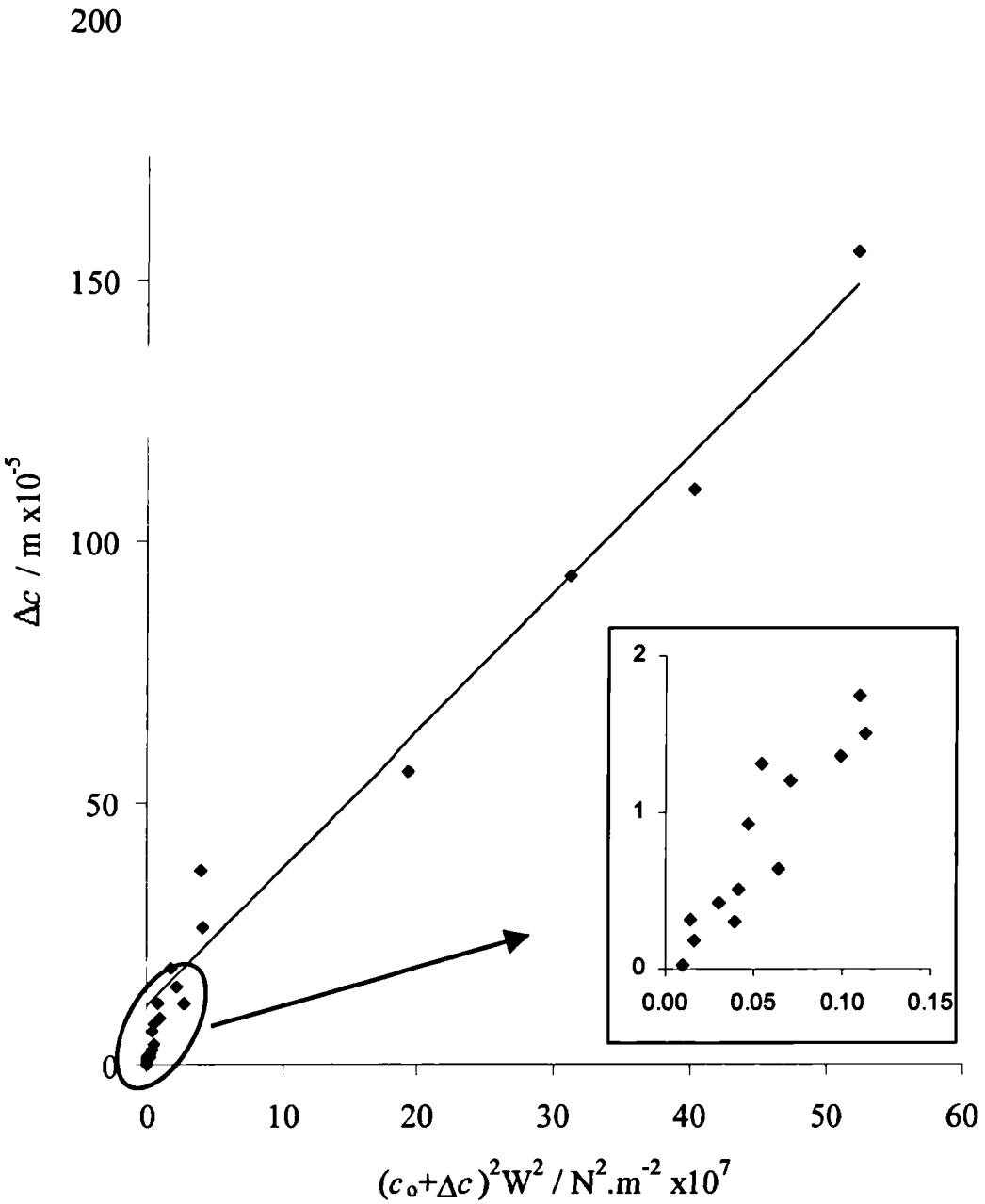

Figure 7-7. The measured Δc as a function of $(c_0+\Delta c)^2W^2$ for NR (NR00-S1) during the cyclic loading measurement. Inset shows the region near the very small scale Δc.

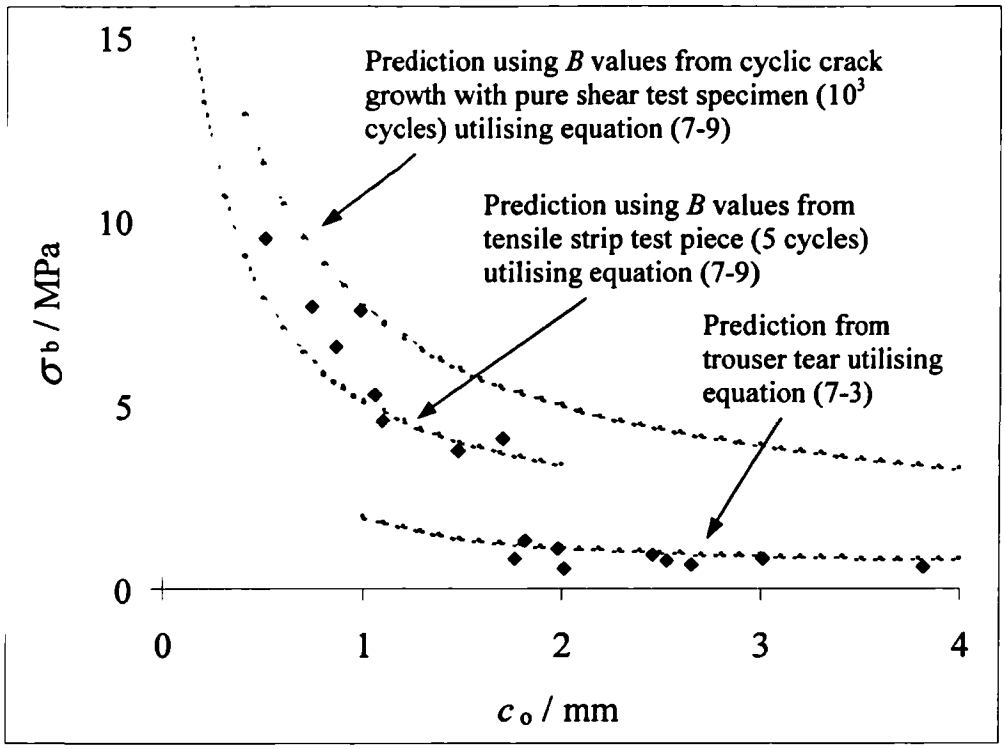

Figure 7-8. The predicted tensile strength for NR (NR00-S1) as a function of initial crack size utilising both equations (7-3) and (7-9).

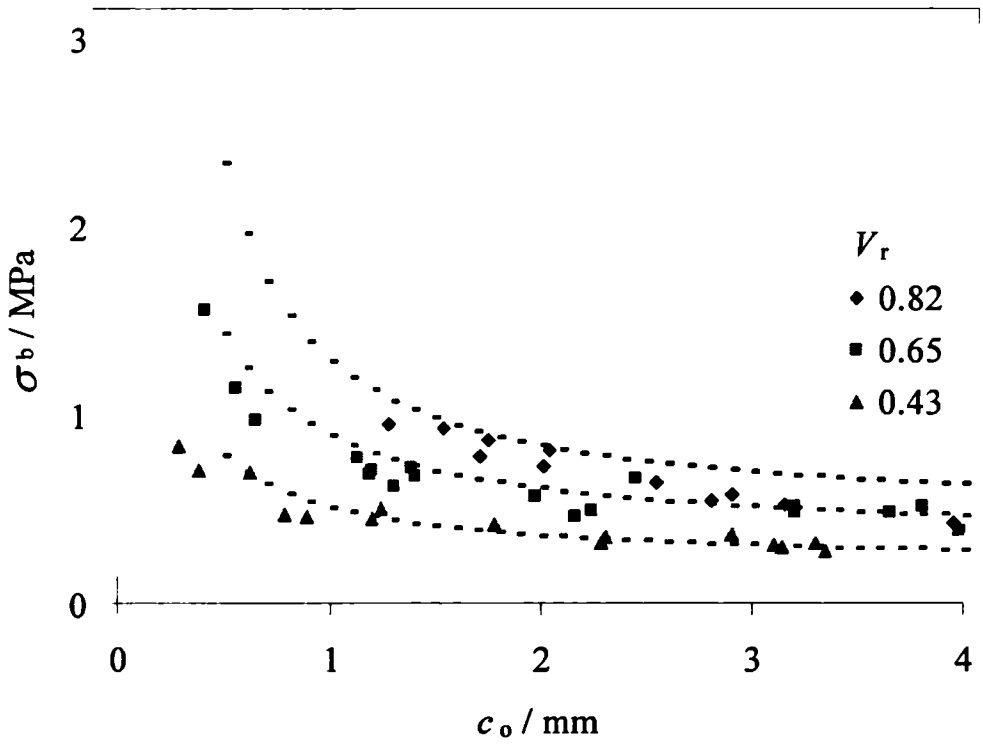

Figure 7-9. The predicted tensile strength for highly swollen NR (NR00-S1) as a function of initial crack size. The dashed line represents the predicted tensile strength utilising equation (7-3).

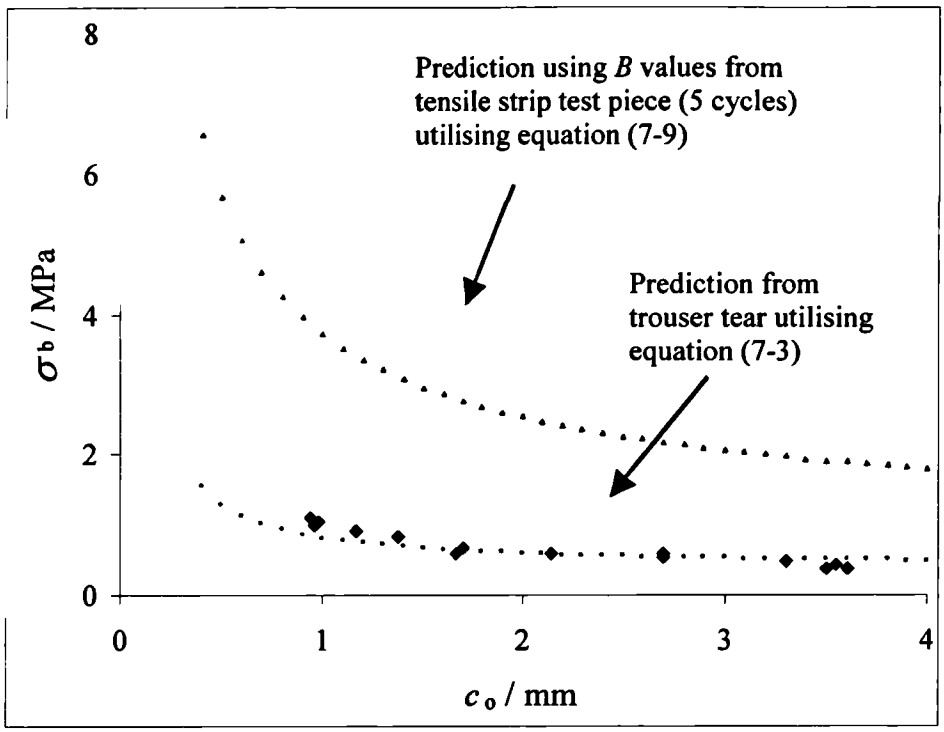

Figure 7-10. The predicted tensile strength for NR (NR00-S1) swollen with DBA to V_r=0.78 as a function of initial crack size utilising both equations (7-3) and (7-9).

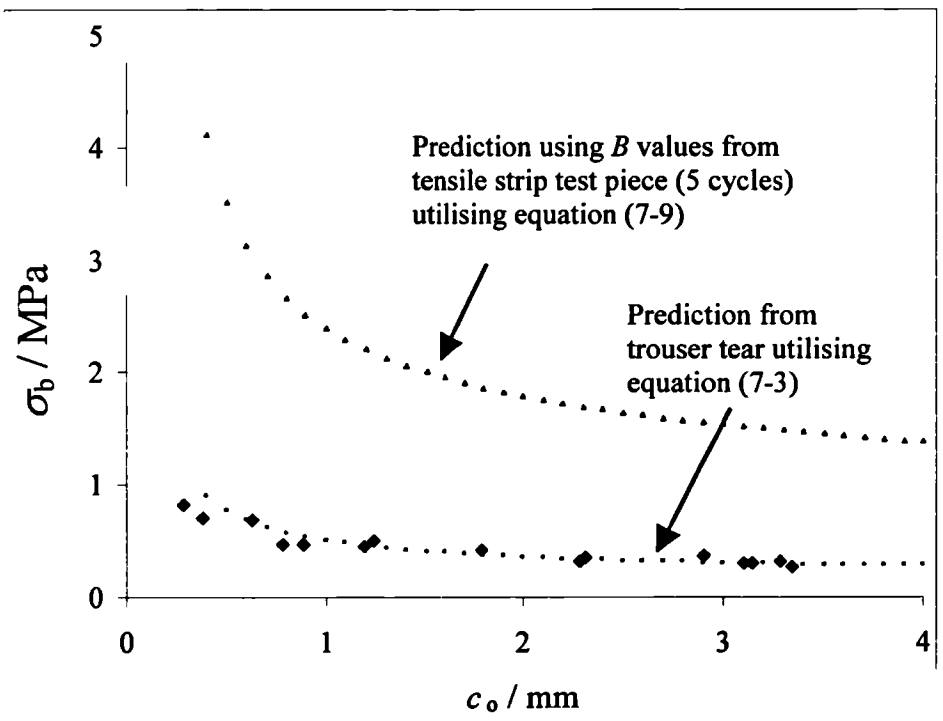

Figure 7-11. The predicted tensile strength for NR (NR00-S1) swollen with DBA to V_r=0.42 as a function of initial crack size utilising both equation (7-3) and (7-9).

Chapter Eight

Summary and suggestions for future work

Static, constant T, crack growth measurements were carried out on rubbers whose visco-elastic properties varied greatly. The variation in visco-elastic behaviour was achieved by a number of different techniques including swelling the test piece in a low viscosity liquid, changing the test temperature, altering the cross-link chemistry and thus changing the average molar mass between cross-links and by the incorporation of different quantities of reinforcing carbon black. Crack growth experiments were also carried out on specimens with different thicknesses. This changed the magnitude of tri-axial stresses ahead of the crack tip and altered the propensity to cavitate. It was found that crack growth in rubber was well described using the tearing energy concept. The magnitude of the tearing energy, T, necessary in the specimen to drive a crack at a given rate was seen to be a function of the visco-elastic losses in the crack tip region and the effective crack tip diameter, d. The typical tearing energy against crack growth rate, r, relationship (T/r relationship) was divided into three regions, which were designated as slow, fast, and stick-slip regions.

In fast crack growth, T scaled with the WLF relationship for both unfilled and carbon black filled SBR and was independent of the specimen thickness. The magnitude of T necessary to drive a crack at a given rate decreased with increasing extent of swelling, decreasing cross-link density, and increasing temperature all of which would result in a reduction in the visco-elastic losses. From this it was concluded that in the fast crack growth region, the magnitude of T necessary to drive a crack at a given rate was determined solely by the amount of the visco-elastic losses at the crack tip and changes in the crack tip diameter were not significant.

Conversely, in the slow crack growth region, changes in T with materials and temperature/rate variables could not be explained by changes in the visco-elastic losses alone. This was because the crack tip profile played an important role in determining the magnitude of T and hence the crack growth behaviour. The proposed mechanisms responsible for the crack tip behaviour were different for unfilled and carbon black filled materials. For unfilled SBR, rough surfaces were observed and it

was postulated that the origin of the roughness might result from cavitation occurring ahead of the crack tip due to tri-axial stresses. In this region the extending crack would intersect with growing cavities causing an increase in the crack tip diameter and hence in the magnitude of T. This hypothesis was supported by the observed effect of specimen thickness on the crack growth behaviour. For the unswollen materials in the slow crack growth region, the magnitude of T necessary to drive a crack at a given rate decreased with decreasing specimen thickness in a manner that would be expected from the decrease in magnitude of the tri-axial stresses and hence propensity to cavitate. For the highly swollen materials, reducing the thickness resulted in a decrease in the magnitude of T and a change from slow to stick-slip or fast crack growth behaviour.

For carbon black filled SBR, the fracture surfaces were not very rough, even at the lowest crack growth rates and there appeared to be no direct effect of specimen thickness on the magnitude of T. Despite the apparent similarity of the fast and slow fracture surfaces, there was still a clear discontinuity in the T/r relationship. Furthermore, it was not possible to converge the temperature/rate data using a WLF relationship suggesting that in the slow crack growth rate region there was still a significant crack tip effect. It was suggested that cavitation did not occur to any significant extent as the elastic modulus and hence the critical tri-axial stresses necessary to inflate the cavities would increase significantly with increasing carbon black content. In the slow crack growth region, a non-planar, groovy cross-section fracture surface profile was observed that was not present in the fast crack growth region for the carbon black filled materials. It was proposed that this might be due to local deviations of the crack growth direction due to the development of strength anisotropy ahead of the advancing crack tip. This would increase the magnitude of the applied T necessary to drive a crack at a given rate as it grows in a different direction to the path that releases the maximum elastic stored energy. The extent of this strength anisotropy depended upon crack growth rate, temperature, cross-link density and carbon black content. At faster crack growth rates, there was insufficient time available to develop strength anisotropy and cracks grew mostly in the horizontal plane in the direction of maximum elastic stored energy release.

Cyclic crack growth measurements were carried out with unswollen, swollen, and carbon black filled SBR. It was found that cyclic crack growth in rubber could

also be described by the tearing energy concept. Two different components of cyclic crack growth behaviour, time dependent and cyclic dependent, were identified. The magnitudes of these two different components responsible for total crack growth per cycle, in SBR, were determined by utilising the crack growth constants from static crack growth measurement and by the measurement of the effect of frequency on the cyclic crack growth behaviour. For unfilled SBR, at the highest tearing energies for the fastest crack growth per cycle, the total cyclic crack growth was dominated by the time dependent component. At low tearing energies and for slow crack growth rates, the total cyclic crack growth was dominated by the cyclic component and was seen to be frequency independent. It was proposed that the cyclic component was associated with quasi strain crystallisation of the butadiene unit of SBR. For the highly swollen SBR cyclic crack growth was totally dominated by the time dependent component and the total cyclic crack growth per cycle was proportional to the reciprocal of the cyclic test frequency. It was presumed that quasi strain crystallisation was not energetically favoured in this highly swollen system. For the 50phr carbon black filled SBR the crack growth per cycle was also independent of cyclic frequency and hence crack growth was dominated by the cyclic component. This probably resulted from the cyclic formation and dissolution of strength anisotropy at the crack tip.

It is clear that a great deal of valuable information on the crack growth behaviour, especially for non-crystallising SBR, was identified during the present study. However, several unanswered questions still exist. Therefore any further investigation should consider researching the following points.

(1) On several occasions the important role of the crack tip diameter was discussed in this study. The magnitude of crack tip diameter was allowed to vary as a consequence of the test conditions. As it is difficult to make *in situ* measurements of the crack tip diameter, an alternative approach would be required. One technique would be to perform cutting experiments with a sharp razor blade. Then a known tip profile could be used during the test to measure the crack growth behaviour at a constant and specified crack tip diameter[16][17]. This cutting experiment could support several of the assumptions presented here.

(2) It was proposed here that crack growth in the slow crack growth region resulted from the intersection of the advancing major crack and growing cavities, generated under the tri-axial stresses ahead of the crack, resulting in rough fracture surfaces for unfilled SBR. If the surface roughness was quantitatively determined accurately, it might be possible to predict the stress field ahead of the crack, with respect to the size and position of any crack cavities and hence predict the crack growth behaviour. The surface roughness should therefore be quantitatively evaluated in an attempt to determine the magnitude of tri-axial stresses generated ahead of the crack tip.

(3) The geometric problem ahead of the crack tip, especially if local cavities were also included would make the analytical solution of the stress field very complex. It would clearly be difficult to precisely determine the magnitude of tri-axial stresses accurately. However, recent improvements to computational techniques such as finite element analysis (FEA) would now enable an estimate of the stress field to be made. One interesting area of study would be to develop a comprehensive model for the crack growth behaviour taking into consideration the tri-axial stresses, cavitation, surface roughness and the magnitude of the tearing energy.

References

1. A.A. Griffith, Phil. Trans. Roy. Soc., A221, 163, 1920
2. E. Orowan, Fracture and Strength of Solids, Reports on Progress in Physics, XII, 185, 1948
3. G.R. Irwin, "Fracture Dynamics, Fracturing of Materials", American Society for Metals, Cleveland, 1948
4. G.R. Irwin, J. Appl.Mech., 24, 361, 1957
5. J.R. Rice, J. Appl. Mech., 35, 379, 1968
6. J.R. Rice, Fracture Ed.by Liebowitz, Academic Press., 2, 191, 1968
7. R.S. Rivlin and A.G. Thomas, J. Polym. Sci., 10, 291, 1953
8. A.G. Thomas, J. Appl. Polym. Sci., 3, 168, 1960
9. G.J. Lake, P.B. Lindley and A.G. Thomas, Proc. 2nd, Int., Conf., of Fracture, Brighton, April, 1969
10. P.B. Lindley, J. Strain Anal., 7 132, 1972
11. A.G. Thomas, J. Polym. Sci., 18, 177, 1955
12. H.W. Greensmith, J. Appl. Polym. Sci., 3, 183, 1960
13. T. Higuchi, H.M. Leeper, and D.S. Davies, Anal. Chem., 20, 1029, 1949
14. A.N. Gent and A.W. Henry, Proc. Int. Rubber Conf., 5th Brighton, 193, 1967
15. G.J. Lake and O.H. Yeoh, Int. J. Fract., 14(5), 509, 1978
16. G.J. Lake and O.H. Yeoh, J. Polym. Sci., Part B, 25, 1157, 1987
17. A.N. Gent, S.M. Lai, C. Nah and C. Wang, Rubber Chem. Thecnol., 67, 610, 1994
18. H.W. Greensmith and A.G. Thomas, J. Polym. Sci., 18, 189, 1955
19. A.G. Thomas, Private Discussion
20. K.K. Mueller and W.G. Knauss, Trans. Soc. Rheol., 15, 217, 1971
21. A. Ahagon and A.N. Gent, J. Polym. Sci., Phys. Ed. 13, 1903, 1975
22. A.N. Gent and R.H. Tobias, J. Polym. Sci, Phys. Ed. 20, 2051, 1982
23. G.J. Lake and A.G. Thomas, Proc. Rubber Soc., London, A300, 108, 1967
24. L.R.G. Treloar, The Physics of Rubber Elasticitty, Oxford; Clarendon Press, 1958
25. H.W. Greensmith, L. Mullins and A.G. Thomas, Trans. Soc. Rheo., 4, 179, 1960

26. M.L. Williams, R.F. Landel and J.D. Ferry, J. American Chem. Soc., 77, P3701, 1955
27. A.K. Doolittle, J. Appl. Phys., 22, 1471, 1951
28. A.K. Doolittle, J. Appl. Phys., 23, 236, 1952
29. J.D. Ferry, Viscoelastic properties of polymers, John Wiley, New York, 314, 1970
30. L. Mullins, Trans. Inst. Rub. Ind. 35, 213, 1981
31. A. Kadir and A.G. Thomas, Rub. Chem. Technol., 54, 15, 1981
32. L. Mullins, Trans. Inst. Rubber Conf., 35, 213, 1959
33. W. Cooper, J. Polym. Sci., 26, 195, 1958
34. P. Brown, M. Porter and A.G. Thomas, Kaut. Gummi. Kunst., 40, 17, 1987
35. A.N. Gent and D.A. Tompkins, J Appl. Phys., 40, 2520, 1969
36. A.N. Gent, In; Science and Technology of Rubber, Ed. By F.R. Eirich, Academic Press, New York Press, 419,1956
37. A.N. Gent and P.B. Lindley, Proc. Roy. Soc., A249, 195, 1959
38. R.L. Dencouer and A.N. Gent, J. Polym. Sci. A2, 6, 1853, 1968
39. A.N. Gent and D.A. Tompkins, J Appl. Phys., 40, 2520, 1969
40. A.E. Oberth and R.S. Bruenner, Trans. Soc. Rheol., 9(2), 165, 1965
41. A. Stevenson and A.G. Thomas, J. Phys., D12, 2101, 1979
42. G.J. Lake, A.G. Thomas and C.C. Lawrence, Polymer, 33, 4069, 1992
43. A.N. Gent, J. Appl. Polym. Sci., 6, 497, 1962
44. P.B. Lindley and A.G. Thomas, Proc. Rubber Technol. Cof. 4th (London), 428, 1962
45. D.G. Young, Rubber Chem. Technol., 59, 819, 1986
46. F. Bueche, J.Appl. Polym. Sci., 7, 1165, 1963
47. A.N. Gent and M. Hindi, Rubber Chem. Technol., 63, 123, 1990
48. A.N. Gent, G.L. Liu and S. Sueyasu, Rubber Chem. Technol., 64, 98, 1991
49. G.J. Lake, Proc. Rubber Technol., 45, 89, 1983
50. A.K. Bhowmick, In "Fractography of rubbery materials", Ed. by A.K. Bhowmick and S.K. De, Elsevier Applied Science, 101, 1991
51. A.N. Gent, P.B. Lindley and A.G. Thomas, J. Appl. Polym. Sci., 8, 455, 1964
52. G.J. Lake and P.B. Lindley, J. Appl. Polym. Sci., 8, 707, 1964
53. D.G. Young, Rubber Chem. Technol., 58, 785, 1985

54. C.J. Derham, G.J. Lake and A.G. Thomas, Rubber Int. Malaysia, 22[2], 191, 1969
55. G.J. Lake, Rubber Chem. Technol., 45, 309, 1972
56. G.J. Lake and P.B. Lindley, J. Appl. Polym. Sci., 9, 1233, 1965
57. H.W. Greensmith, J. Appl. Polym. Sci., 7, 993, 1963
58. G.J. Lake and P.B. Lindley, Rubber J., 146[10], 24, 1964
59. G.J. Lake and P.B. Lindley, Rubber J., 146[11], 30, 1964
60. S.M. Cadwell, R.A. Merrill, C.M. Sloman and F.L.Yost, Ind. Eng. Chem. Anal., 12, 19, 1940
61. A.G. Thomas, in "Deformation and fracture of high polymers" Ed. by H. Kausch, J.A. Hassel and R. Jaffe, Plenum Press, 1974
62. D.G. Young and J.A. Danik, Rubber Chem. Technol., 67, 137, 1993
63. A. Stevenson, Rubber Plast. News, 22, 42, 1988
64. K. Cho, W.J. Jang, D. Lee H. Chun and Y. Chang, Polymer, 41, 179, 2000
65. T.L. Smith, J. Polym. Sci., 32, 99, 1958
66. F. Bueche, J. Appl. Phys., 26, 1133, 1955
67. F. Bueche and J.C. Halpin, J. Appl. Phys., 35, 36, 1964
68. T.L. Smith, J. Polym. Sci., Part A, 1, 3593, 1963
69. T.L. Smith, J. Appl. Phys., 35, 27, 1964
70. T.L. Smith, Polym. Eng. Sci., 5, 270, 1965
71. A. Kadir and A.G. Thomas, In "Elastomers: criteria for engineering design", Ed. by C. Hepburn and R.J.W. Reynolds, Applied Science Publishers, London, 67, 1972
72. A.G. Thomas and J.M. Whittle, Rubber Chem. Technol., 43, 222, 1970
73. B.S.T.T. Boonsta, India Rubber World, 121, 299, 1949
74. G.J. Lake and A.G. Thomas, Kaust. Gum. Kunst. 4, 221, 1967
75. A.G. Thomas, "Physical Basis of Yield and Fracture, conference proceedings", the institute of physics and the physical society, 134, 1964
76. C.L.M. Bell, D. Stinson and A.G. Thomas, Rubber Chem. Technol., 55, 66, 1982
77. T.L. Smoth, In "Reology" Ed. by F.R.Eirich, Vol.5 Ch.4 Academic Press, New York, 1969
78. K.A. Grosch, J.A.C. Hawood and A.R. Payne, Rubber Chem. Technol., 41, 1157, 1968

79. B.A. Dogadkin, D.L. Fedyukin and V.E. Gul, Rubber Chem. Technol., 25, 31, 1952
80. G.R. Taylor and S.R. Darin, J. Polym. Sci., 17, 511, 1955
81. H.W. Greensmith, L. Mullins and A.G. Thomas, In "The Chemistry and Physics of Rubber-Like Substances" Ed. by L. Bateman, Chapter 10, Wiley, New York, 1963
82. L. Mullins, J. Appl. Polym. Sci., 6, 257, 1959
83. P.J. Flory and J. Rehner, J. Chem. Phys., 11, 512, 1943
84. M. Porter, Rubber Chem. Technol., 40, 866, 1967
85. R.S. Rivlin, in "Rheology" ed. by F.R. Eirich, Academic Press, New York, 1959
86. M. Mooney, J. Appl. Phys., 11, 582, 1940
87. K. Akutagawa, "The effect of incorporation of low molar mass liquids on the dynamic mechanical properties of elastomers under strain", Ph.D. thesis, Queen Mary, University of London, 1995
88. C. Deeprasertkul. "Dynamic properties of carbon black filled elastomers containing liquids", Ph.D. thesis, Queen Mary, University of London, 2000
89. L. Mullins, J. Appl. Polym. Sci., 6, 257, 1959
90. R.S. Rivlin, Phil. Trans. Roy. Soc., 39, 36, 1949
91. M. Mooney, L. Appl. Phys., 11, 582, 1940
92. C.C.H. Ratsimba, "Fatigue crack growth of filled elastomers", Ph.D. Thesis, Queen Mary, University of London, 2000
93. A.N. Gent, H.J. Kim, Rubber Chem. Technol., 51, 35, 1978
94. A.B. Samsuri, "Tear strength of filled rubbers", Ph.D. Thesis, University of North London, 1989
95. D.K. De, "The effect of particulate fillers on the strain energy function and crack growth in rubbers", Ph.D. Thesis, Queen Mary, University of London, 1994
96. J. J. C. Busfield, unpublished data
97. R.G. Mancke, J.D. Ferry, Trans. Soc. Rheol., 12, 335, 1968
98. A.G. Thomas, J. Polymer Sci., 31, 467, 1958
99. A.G. Thomas, J. Polymer Sci., 3, 168, 1960

Appendix I

Referred journal papers published by the author as part of this research

Title: Effect of materials variables on the tear behaviour of a non-crystallising elastomer

Authors: K. Tsunoda[1], J.J.C. Busfield, C.K.L. Davies and A.G. Thomas

Department of Materials, Queen Mary, University of London, London E1 4NS.

([1] on leave of absence from Bridgestone Corporation, Japan)

Journal: Journal of Material Science, Vol. 35 (2000) P5187-5198

Abstract: Crack growth rates (r) were measured in pure shear test specimens as a function of strain energy release rate (G) for a non-crystallising SBR elastomer. Measurements were made as a function of, extent of swelling with Dibutyl Adipate, carbon black content and cross-link density. In some cases experiments were carried out over a range of temperatures. In most cases the resulting G versus r plots showed a clear transition from rough to smooth crack surface behaviour with increasing crack growth rate, with an intervening slip/stick region. In the high speed/steady tear /smooth region the value of G necessary to drive a crack at a given rate was determined largely by the magnitude of the visco-elastic losses in the crack tip region, increasing with, decreasing temperature, increasing molar mass between cross-links, decreasing extent of swelling, and increasing carbon black content. However G was independent of specimen thickness in this region suggesting that crack tip effects were minimal. In the low speed/rough region changes in the magnitude of G with materials and temperature/rate variables could not be explained by changes in visco-elastic loss alone. Furthermore the magnitude of G increased significantly with increasing specimen thickness. This suggested that in this region cavitation ahead of the growing crack tip resulting from dilatational stresses determined the crack tip diameter, and hence the magnitude of G.

Title: Contributions of Time Dependent and Cyclic Crack Growth to the Crack Growth Behaviour of Non Strain Crystallising Elastomers

Authors: K. Tsunoda[1], J.J.C. Busfield, C.K.L. Davies and A.G. Thomas

Department of Materials, Queen Mary, University of London, London E1 4NS.

([1] on leave of absence from Bridgestone Corporation, Japan)

Journal: Proceedings, 159th Spring Technical Meeting, Rubber Division, American Chemical Society, Providence, April 24-27, 2001

Abstract: Engineering components are observed to fail more rapidly under cyclic loading than under static loading. This reflects features of the underlying crack growth behaviour. This behaviour is characterised by the relation between the tearing energy, T, and the crack growth per cycle, dc/dn. The increment of crack growth during each cycle may be considered to result from the sum of time dependent and cyclic crack growth components. The time dependent component represents the crack growth behaviour that would be present in a conventional constant T crack growth test. Under repeated stressing additional crack growth, termed the cyclic crack growth component, occurs. For a non-crystallising elastomer, significant effects of frequency have been found on the cyclic crack growth behaviour, reflecting the presence of this cyclic element of crack growth. The cyclic crack growth behaviour over a wide range of frequencies was investigated for unfilled and swollen SBR materials. The time dependent crack growth component was calculated from constant T crack growth tests and the cyclic contribution derived from comparison with the observed cyclic growth. It is shown that decreasing the frequency or increasing the maximum tearing energy during a cycle results in the cyclic crack growth behaviour being dominated by time dependent crack growth. Conversely at high frequency and at low tearing energy, cyclic crack growth is dominated by the cyclic crack growth component. A large effect of frequency on cyclic crack growth behaviour was observed for highly swollen SBR. The cyclic crack growth behaviour was dominated by the time dependent crack growth component over the entire range of tearing energy and/or crack growth rate. The origin of the cyclic component may be the formation/melting of quasi crystals at the crack tip, which is absent at fast crack growth rates in the unswollen SBR and is absent at all rates in the swollen SBR.

Appendix II

Development of the basic equations for the beam oscillation experiment [87]

If the material is perfectly elastic, then the motion of oscillating system can be written as

$$I\frac{\partial^2\theta_D}{\partial t^2}+T_D=0 \qquad \text{(I-1)}$$

where I is the motion of inertia of the beam, θ_D is the angular displacement of the beam, t is the time and T_D is the torque due to the force at the centre of the strained specimens. T_D is given by

$$T_D = f_V r_d = 2k_L r_d{}^2\theta_D \qquad \text{(I-2)}$$

where f_V is the vertical net force on the cross-sectional area of the strained rubber, which is the sum of upward force and downward force, r_D is the length from the rubber strip to the centre of the beam and k_L is the incremental stiffness of the specimen which can be defined as $k_L=\frac{\partial f_V}{\partial l}$. Hence,

$$I\frac{\partial^2\theta_D}{\partial t^2}+2k_L r_d\theta_D=0 \qquad \text{(I-3)}$$

The tensile modulus, E, referred to the actual cross-sectional area of the strained specimen can be defined as

$$E=\frac{\partial\sigma^*}{\partial\varepsilon^*}=\frac{\Delta\sigma^*}{\Delta l\ l_{S1}}=\frac{\Delta\sigma^*}{\Delta l/\lambda l_S}=\lambda\frac{\partial\sigma^*}{\partial\lambda} \qquad \text{(I-4)}$$

where σ^* is the true stress, ε^* is the true strain, l_S is the unstrained half length of the rubber sample, l_{S1} is the strained half length of the rubber sample and λ is the extension ratio equal to $l_{S1}/\ l_S$. If the specimen is perfectly elastic, then the relationship between k_L and E can be given as

$$E=\lambda\frac{\partial\sigma^*}{\partial\lambda}=\lambda\frac{\partial f}{\partial\lambda}\frac{l_S}{A}=\lambda^2\frac{\partial f}{\partial l_{S1}}\frac{l_S}{A_o}=\lambda^2 k\frac{l_S}{A_o} \qquad \text{(I-5)}$$

where A is the strained cross-sectional area of the specimen and A_o is the unstrained cross-sectional area. Hence,

$$k = E\lambda^{-2}\frac{A_o}{l_o} \tag{I-6}$$

From equation (I-3) and (I-6), we have

$$I\frac{\partial^2\theta_D}{\partial t^2} + 2E\lambda^{-2}r_d^{\,2}\frac{A_o}{l_S}\theta_D = 0 \tag{I-7}$$

This equation describes the motion of the system and has the standard solution given by

$$\theta_D = \theta_{Do}\cos(\omega t + \alpha_D) \tag{I-8}$$

where θ_{Do} is the initial angular displacement, ω is the angular velocity of the beam. From equation (I-7) and (I-8), we have

$$\left(2E\lambda^{-2}r_d^{\,2}\frac{A_o}{l_S} - i\omega^2\right)\theta_{Do}\cos(\omega t + \alpha_D) = 0 \tag{I-9}$$

Since $\cos(\omega t + \alpha_D) \neq 0$, hence we have

$$I\omega^2 = 2E\lambda^2 r_d^{\,2}\frac{A_o}{l_S} \tag{I-10}$$

Hence, E is given as

$$E = \frac{I\omega^2}{2r_d^{\,2}}\frac{l_S}{A_o}\lambda^2 \tag{I-11}$$

E of the visco-elastic material can be considered as a complex quantity E^* as

$$E^* = E' + iE'' \tag{I-12}$$

where E' and E'' are the real and imaginary parts of the modulus. For a rubber, where there is no volume change taking place on stretching, then the motion of the system is gives by

$$I\frac{\partial^2\theta_D}{\partial t^2} + p(E' + iE'')\theta_D = 0 \tag{I-13}$$

where p is $2\lambda^{-2}r_d^2\left(\frac{A_o}{l_S}\right)\theta_D$. If this equation is assumed to have a solution

$$\theta_D = \theta_{D_o} e^{-qt} e^{i\omega t} \tag{I-14}$$

where q is the constant. From equations (I-13) and (I-14)

$$\theta_o e^{-qt} e^{i\omega t}\left[\left(q^2-\omega^2\right)I + pE' + \left(pE'' - 2q\omega I\right)i\right] = 0 \tag{I-15}$$

Hence,

$$\left(q^2-\omega^2\right)I + pE' = 0 \tag{I-16}$$

$$\left(pE'' - 2q\omega I\right) = 0 \tag{I-17}$$

From equation (I-16) and (I-17),

$$E' = p^{-1}\left(\omega^2 - q^2\right)I \tag{I-18}$$

$$E'' = 2p^{-1}q\omega I \tag{I-19}$$

$$\tan-\delta = \frac{E''}{E'} = 2q\omega\left(\omega^2-q^2\right)^{-1} \tag{I-20}$$

where tan-δ is the tangent of loss angle. The logarithmic decrement, Λ, is defined as the natural logarithm of the ratio of the amplitude, X_n, of the two successive cycle.

$$\Lambda = \ln\left(\frac{X_n}{X_{n+1}}\right) = \ln\left(\frac{\theta_{D_o} e^{-qt}}{\theta_{D_o} e^{-q(t+2\pi\ \omega)}}\right) = \frac{2\pi}{\omega}q \tag{I-21}$$

where the time period between two successive cycles is defined as $\frac{2\pi}{\omega}$. From equation (I-18) to (I-21),

$$E' = \frac{I\omega^2}{2r_d^2}\frac{l_S}{A_o}\lambda^2\left[1-\left(\frac{\Lambda}{2\pi}\right)^2\right] \approx \frac{I\omega^2}{2r_d^2}\frac{l_S}{A_o}\lambda^2 \tag{I-22}$$

$$E'' = \frac{\Lambda}{\pi}\frac{I\omega^2}{2r_d^2}\frac{l_S}{A_o}\lambda^2 \tag{I-23}$$

$$\tan-\delta = \frac{\Lambda}{\pi}\left[1-\left(\frac{\Lambda}{2\pi}\right)^2\right] = \frac{\Lambda}{\pi} \qquad \text{(I-24)}$$